
Role of the heterotrimeric protein G_q and small GTPase
RhoA in the cholinergic modulation of the slow
afterhyperpolarizing current, sI_{AHP} , in hippocampal
pyramidal neurons

Thesis submitted at UCL

by

Linn Gallasch

For the degree of

Doctor of Philosophy, PhD

Declaration

I, Linn Gallasch confirm that the work presented in this thesis is my own. Where information has been derived from other sources, I confirm that this has been indicated in the thesis.

Abstract

The network activity of the hippocampal formation underlying learning and memory processes is regulated by a number of ionic conductances that determine the neuronal excitability and firing patterns of hippocampal pyramidal neurons. The slow Ca^{2+} -activated K^+ current (sI_{AHP}) and its modulation by acetylcholine (ACh) and glutamate play a crucial role in shaping these intrinsic properties of hippocampal pyramidal neurons. sI_{AHP} follows a train of action potentials and is characterised by its dependency on the rise of intracellular Ca^{2+} and its slow time course, displaying activation kinetics of hundreds of milliseconds and decaying over seconds. It is responsible for spike frequency adaptation that restricts repetitive firing in response to a prolonged stimulus. Hence the suppression of sI_{AHP} by ACh and glutamate, through metabotropic receptors, leads to an enhanced excitability of hippocampal pyramidal neurons. The underlying signal transduction cascade used by ACh and glutamate to inhibit sI_{AHP} is not fully characterised, involving the G-protein subunit $G\alpha_q$, but not its classical signalling pathway via phospholipase C β (PLC β) (Krause et al., 2002). Employing molecular biology and imaging techniques in heterologous expression systems this study establishes that the small GTPase RhoA acts as a signalling partner of $G\alpha_q$, pointing to an involvement of both proteins in a common signalling pathway that mediates the suppression of sI_{AHP} upon the stimulation of G-protein coupled receptors (GPCRs) by cholinergic agonists in hippocampal pyramidal neurons. The introduction of activated and inactivated RhoA mutants into hippocampal pyramidal neurons by viral infection, and subsequent whole-cell patch clamp electrophysiology, showed that constitutively active RhoA-V14 reduces sI_{AHP} significantly, mimicking the inhibitory effect of ACh, whereas sI_{AHP} is unaffected in neurons expressing inactive RhoA-N19. An involvement of RhoA in the regulation of membrane excitability of hippocampal pyramidal neurons and thus in the shaping of neuronal activity on a relatively fast time-scale is a novel function for the small GTPase.

Acknowledgements

First and foremost, I wish to thank my supervisor Martin Stocker for his academic guidance, training and for his support at every stage of my PhD. I am grateful to Paola Pedarzani for her involvement in this project and consistent support over the years. Thank also goes to my second supervisor Julie Pitcher for her assistance in the project and advice.

I am thankful to past and present members of the lab Marisol Sampedro Castaneda, Katie Smith, Marita Gronning Madsen, Hannah Morgan, Anne Boehlen, Agnes Thalhammer, Angelo Tedoldi, Joseph Tebbs-Warner, Simon Bennett and Tim Howe for their technical assistance, their interest in this project and for their contribution to a stimulating lab environment. Thanks also go to Tony Langford and Tina Bashford in their role as lab manager and graduate administrator.

I am ever grateful to my parents, grandparents and brother and to the rest of the family for their unconditional support and encouragement. I am thankful for their advice and guidance throughout the years, and for their patience.

My thanks extend to Mathias Berndt.

To my friends Marisol Sampedro Castaneda and her family, Grit Polewey and Olga Klimecki a sincere thank you for all their kindness and support and for providing welcomed distractions.

Finally, I would also like to thank the BBSRC for providing the funding for my PhD.

Table of Contents

DECLARATION	2
ABSTRACT	3
ACKNOWLEDGEMENTS	4
TABLE OF CONTENTS	5
INDEX OF FIGURES	9
INDEX OF TABLES	10
1 INTRODUCTION	11
1.1 The Hippocampus	12
1.1.1 Hippocampal function, neuroanatomy and circuitry	12
1.1.2 Glutamatergic and cholinergic systems in the hippocampus	13
1.2 Afterhyperpolarizations	16
1.2.1 Fast afterhyperpolarization (fAHP)	17
1.2.2 Medium afterhyperpolarization (mAHP)	18
1.2.3 Slow afterhyperpolarization (sAHP)	23
1.3 GPCRs and G-proteins	28
1.4 Small GTPases	35
1.5 Aims and Objectives	40
2 MATERIALS AND METHODS	41
2.1 Materials	42
2.1.1 DNA constructs	42
2.1.2 Buffers	44
2.1.3 Bacteria media, agar-plates and antibiotic stock solutions	44
2.1.4 Cell culture media	45
2.2 Methods	45
2.2.1 Cell culture	45
2.2.1.1 Coverslip preparation	45
2.2.1.2 Maintenance and splitting of cell lines	46
2.2.1.3 Primary culture of hippocampal neurons	46
2.2.2 Expression	48
2.2.2.1 Transient transfection	48
Lipofectamine 2000	48

FuGene 6	48
2.2.2.2 Microinjection	49
2.2.2.3 Viral infection	49
2.2.3 Lysis preparation	50
2.2.3.1 Lysate preparation from HEK293 cells	50
2.2.3.2 Lysate preparation from rat brain	50
2.2.4 Protein concentration estimation	51
2.2.5 Co-immunoprecipitation	52
2.2.6 SDS-PAGE and Western blotting	52
2.2.6.1 Sodium dodecyl sulfate polyacrylamide gel electrophoresis (SDS-PAGE)	52
2.2.6.2 Transfer and immunodetection	54
2.2.6.3 Coomassie staining of SDS-PAGE gels	56
2.2.7 Glutathione-S-transferase (GST) fusion protein purification	57
2.2.7.1 Electroporation of BL21 (DE3) bacteria	57
2.2.7.2 Purification of GST fusion proteins	57
2.2.7.3 PreScission protease cleaving	59
2.2.8 Binding assays with purified protein	59
2.2.9 <i>In vitro</i> translation and direct binding assays	60
2.2.9.1 <i>In vitro</i> translation	60
2.2.9.2 Direct binding assays with purified RhoA-V14	60
2.2.10 Sindbis virus production	61
2.2.10.1 RNA synthesis	61
2.2.10.2 Transfection of BHK-21 cells and harvesting of virus particles	62
2.2.10.3 Determining the potency of the virus stock	63
2.2.11 Microscopy	64
2.2.11.1 Preparation of cells for microscopy	64
2.2.11.2 Fluorescence resonance energy transfer (FRET)	65
M ₃ muscarinic acetylcholine receptor stimulation	65
Confocal microscopy	65
FRET analysis	66
2.2.11.3 Analysis of stress fibre formation in microinjected or infected cells	66
2.2.11.4 Co-localisation analysis	67
2.2.12 Molecular biology techniques	68
2.2.12.1 Digestion of DNA with restriction enzymes	68
2.2.12.2 Dephosphorylation of vectors	68
2.2.12.3 Agarose gel electrophoresis	69
2.2.12.4 Gel extraction of DNA	69
2.2.12.5 Ligation	69
2.2.12.6 Competent DH5 α bacteria	70
2.2.12.7 Transformation of DH5 α Bacteria	70
2.2.12.8 Isolating DNA from bacteria	71
Isolation of plasmid DNA from small cultures	71
Isolation of plasmid DNA from medium and large cultures	72
Reuse of AX columns	73
2.2.12.9 Amplification of DNA by polymerase chain reaction (PCR)	74
DNA modifications	74

Single colony PCR _____	74
2.2.12.10 Sequencing _____	75
2.2.13 Cloning strategies _____	76
2.2.13.1 pRK5-myc-Venus-RhoA _____	76
2.2.13.2 pcDNA3.1-EE-ECFP-G α_q -Q209L _____	77
2.2.13.3 pSinrep5-RhoA-G14V-EGFP _____	78
2.2.13.4 pSinrep5-RhoA-T19N-EGFP _____	79
2.2.13.5 Restriction enzyme abbreviations _____	80
2.2.14 Electrophysiology _____	80
2.2.14.1 Recordings in primary culture of hippocampal neurons _____	80
2.2.14.2 sI _{AHP} recordings in cultured hippocampal neurons _____	82
2.2.14.3 Data analysis and statistics _____	83
3 RESULTS _____	85
3.1 Investigating the interaction between the G-Protein α subunit Gα_q and the small GTPase RhoA _____	86
3.1.1 The G-Protein α subunit G α_q interacts with the small GTPase RhoA _____	86
3.1.2 Constitutively active G α_q -L209 specifically binds constitutively active RhoA-V14, but not other small GTPases _____	88
3.1.3 Constitutively active RhoA-V14 specifically interacts with constitutively active G α_q -L209 and constitutively active G α_{14} -L205 _____	89
3.1.4 Investigating the interaction between G-protein α subunit G α_q and small GTPase RhoA in rat brain lysates _____	90
3.1.5 Expression and co-localisation of ECFP-tagged G α_q and Venus-tagged RhoA in HEK293 cells _____	92
3.1.6 ECFP-tagged G α_q interacts with Venus-tagged RhoA _____	100
3.1.7 Assessment of the interaction between ECFP-tagged G α_q and Venus-RhoA in HEK293 cells using FRET _____	102
3.1.8 Binding assays between <i>in vitro</i> translated constitutively active G α_q -L209 and purified constitutively active GST-RhoA-V14 _____	109
3.1.9 Summary _____	110
3.2 Purification of mutant RhoA proteins and their intracellular application into hippocampal neurons _____	111
3.2.1 Purification of the fusion proteins GST-RhoA-V14 and GST-RhoA-N19 and the protolytic release of the small GTPases _____	111
3.2.2 Purified mutant GST-RhoA fusion proteins bind to rhophilin and constitutively active G α_q -L209 _____	115
3.2.3 Purified constitutively active RhoA-V14, but not inactive RhoA-N19, causes stress fibre formation in Swiss-3T3 cells _____	116
3.2.4 The effect of intracellularly applied mutant RhoA proteins on sI _{AHP} in acute hippocampal slices _____	120
3.2.5 Summary _____	121
3.3 Assessment of RhoA involvement in the cholinergic modulation of sI_{AHP} in Sindbis virus infected primary hippocampal neurons _____	122

3.3.1	Sindbis virus production and functionality assay _____	122
3.3.1.1	Recombinant Sindbis plasmid construction and RNA synthesis _____	122
3.3.1.2	Production of Sindbis virus particles _____	123
3.3.1.3	Determining the infection capability of the viral stock and the optimal amount of virus needed for infection _____	124
3.3.1.4	Stress fibres formation in constitutively active RhoA-V14 infected BHK-21 cells, but not in inactive RhoA-N19 infected cells _____	126
3.3.2	sl _{AHP} in primary cultured hippocampal neurons _____	127
3.3.2.1	Properties of primary cultured hippocampal pyramidal neurons are not affected by Sindbis virus infection _____	128
3.3.2.2	Unmasking of sl _{AHP} in primary cultured hippocampal neurons _____	129
3.3.2.3	Regulation of sl _{AHP} in cultured hippocampal neurons _____	131
3.3.3	Effects of mutant RhoA virus infection on sl _{AHP} in cultured hippocampal pyramidal neurons _____	134
3.3.3.1	sl _{AHP} in RhoA-N19 and RhoA-V14 infected cultured hippocampal neurons _____	134
3.3.3.2	Cholinergic modulation of sl _{AHP} in EGFP-negative and inactive RhoA-N19 infected cultured hippocampal neurons. _____	135
3.3.4	Summary _____	138
4	DISCUSSION _____	139
4.1	The small GTPase RhoA associates with the heterotrimeric G-protein α subunit $G\alpha_q$ _____	143
4.2	The small GTPase RhoA is involved in the cholinergic suppression of sl_{AHP} _____	151
4.3	Signalling downstream of RhoA _____	153
4.4	Future directions _____	155
	REFERENCES _____	157
	ABBREVIATIONS _____	188
A	APPENDIX _____	191
A.1	List of Materials _____	192
A.1.1	Consumables _____	192
A.1.2	Equipment _____	193
A.1.3	Microscopes _____	194
A.1.4	Kits, reagents and chemicals _____	195
A.1.4.1	Kits _____	195
A.1.4.2	Reagents and chemicals _____	195
A.1.5	Enzymes _____	198
A.1.6	Antibodies and dyes _____	198
A.1.7	DNA and protein molecular weight ladders _____	199
A.1.8	Primers _____	199

Index of Figures

Figure 1.1	The hippocampal formation_____	12
Figure 1.2	Afterhyperpolarizations and the generation of spike frequency adaptation_____	16
Figure 1.3	G α_q signalling_____	29
Figure 1.4	Structure of the heterotrimeric G-protein and its binding to the G-Protein coupled receptors_____	31
Figure 1.5	G-protein activation and deactivation cycle_____	33
Figure 1.6	G α with fluorophore attachment_____	35
Figure 1.7	Structure of small GTPases and conformational change of the switch regions upon GTP binding_____	37
Figure 1.8	Small GTPase activation and deactivation cycle_____	38
Figure 2.1	Amino acid sequence and secondary structure of G α_q _____	43
Figure 2.2	KOD polymerase PCR_____	74
Figure 2.3	Single colony PCR_____	75
Figure 2.4	Sequencing PCR_____	75
Figure 2.5	Cloning strategy of pRK5-myc-Venus-RhoA_____	76
Figure 2.6	Cloning strategy of pcDNA3.1-EE-ECFP-G α_q -Q209L_____	77
Figure 2.7	Cloning strategy of pSinrep5-RhoA-G14V-EGFP_____	78
Figure 2.8	Cloning strategy of pSinrep5-RhoA-T19N-EGFP_____	79
Figure 2.9	Assessing the firing activity of a cell_____	81
Figure 2.10	Measuring passive membrane property of a cell_____	82
Figure 2.11	Example of a sI _{AHP} recording and details of the corresponding stimulation protocol and current measurements_____	83
Figure 3.1	G-Protein α subunit G α_q and constitutively active G α_q -L209 interact with the small GTPase RhoA, constitutively active RhoA-V14 and inactive RhoA-N19_____	87
Figure 3.2	Constitutively active G α_q -L209 specifically interacts with constitutively active RhoA-V14_____	89
Figure 3.3	Constitutively active RhoA-V14 interacts with constitutively active G α_q -L209 and constitutively active G α_{14} -L205_____	90
Figure 3.4	Western blots of brain and HEK293 cell lysates using anti-G $\alpha_{q/11}$ and anti-RhoA antibodies_____	91
Figure 3.5	Localisation of ECFP-tagged G α_q and Venus-tagged RhoA in HEK293 cells_____	93
Figure 3.6	Co-localisation analysis of ECFP-tagged G α_q and Venus-tagged RhoA in HEK293 cells_____	96
Figure 3.7	Co-localisation analysis of ECFP-tagged G α_q and Venus-tagged RhoA in HEK293 cells using intensity correlation analysis_____	99
Figure 3.8	G α_q -ECFP-G α_q and constitutively active G α_q -ECFP-G α_q -L209 interact with Venus-RhoA_____	101
Figure 3.9	Confocal imaging configurations used for FRET experiments prevent cross-talk between G α_q -ECFP-G α_q and Venus-RhoA_____	103
Figure 3.10	FRET in CFP-YFP dimer expressing HEK293 cells_____	104
Figure 3.11	FRET between ECFP-tagged G α_q variants and Venus-RhoA_____	106
Figure 3.12	FRET between G α_q -ECFP-G α_q and Venus-RhoA without and with the stimulation of the mAChR M ₃ _____	108

Figure 3.13	<i>In vitro</i> translated raphilin and constitutively active $G\alpha_q$ -L209 bind directly to purified constitutively active GST-RhoA-V14 _____	109
Figure 3.14	Purification of GST-RhoA-V14 and GST-RhoA-N19 fusion proteins _____	112
Figure 3.15	Purification and proteolytic release of RhoA-V14 and RhoA-N19 proteins _____	114
Figure 3.16	Purified GST-RhoA-V14 and GST-RhoA-N19 bind raphilin and $G\alpha_q$ -L209 _____	115
Figure 3.17	Pull-down experiments of endogenous $G\alpha_q$ using purified GST-RhoA-V14 and GST-RhoA-N19 protein _____	116
Figure 3.18	Transfection of constitutively active RhoA-V14 induces stress fibre formation in Swiss-3T3 cells _____	117
Figure 3.19	Microinjection of purified constitutively active RhoA-V14, but not purified inactive RhoA-N19, into Swiss-3T3 cells stimulates the formation of stress fibres _____	119
Figure 3.20	sl_{AHP} is partially inhibited by the application of purified constitutively active RhoA-V14, but not by inactive RhoA-N19 _____	120
Figure 3.21	RNA synthesis from Sindbis expression and helper constructs _____	123
Figure 3.22	Electroporation of BHK-21 cells with SIN-EGFP RNA using different electroporation systems _____	124
Figure 3.23	Infecting BHK-21 cells with diluted recombinant Sindbis virus to determine the infection capability of the viral stock and the optimal infection conditions for subsequent experiments _____	125
Figure 3.24	Infection with constitutively active RhoA-V14, but not inactive RhoA-N19, Sindbis virus induces stress fibre formation in BHK-21 cells _____	127
Figure 3.25	Properties of hippocampal pyramidal neurons in primary culture _____	129
Figure 3.26	Pharmacological isolation of sl_{AHP} in cultured hippocampal neurons _____	130
Figure 3.27	Removal of extracellular Ca^{2+} abolishes isolated sl_{AHP} _____	131
Figure 3.28	sl_{AHP} is suppressed by CCh and 8CPT-cAMP _____	133
Figure 3.29	sl_{AHP} is present in EGFP-negative and RhoA-N19 infected cultured hippocampal pyramidal neurons, but not in RhoA-V14 infected neurons _____	135
Figure 3.30	The effect of CCh application on sl_{AHP} in EGFP-negative and inactive RhoA-N19 infected cultured hippocampal pyramidal neurons _____	137
Figure 4.1	Signal transduction pathways mediating the suppression of sl_{AHP} _____	141
Figure 4.2	Potential models of $G\alpha_q$ and RhoA interaction _____	145
Figure 4.3	Crystal structure of the $G\alpha_q$ -p63RhoGEF-RhoA protein complex _____	150

Index of Tables

Table 2.1	Preparation of gels for SDS-PAGE, Mini-PROTEAN II (BIO-RAD) _____	53
Table 2.2	Preparation of gels for SDS-PAGE, SE600 (Hoefer) _____	53
Table 3.1	Summary of $G\alpha_q$ and RhoA co-immunoprecipitations experiments _____	88
Table 3.2	Quantitative analysis of the co-localisation of the G-protein α subunit $G\alpha_q$ and the small GTPase RhoA in HEK293 cells _____	100
Table 4.1	Reference list for the signal transduction pathway diagram (Fig. 4.1.) _____	142

1 Introduction

1.1 The Hippocampus

1.1.1 Hippocampal function, neuroanatomy and circuitry

The hippocampal formation (Fig. 1.1A), including dentate gyrus, hippocampus proper (divided into the cornu ammonis (CA) fields 1–3), subicular complex and entorhinal cortex, and the neighbouring structures of perirhinal and parahippocampal cortices are located in the medial temporal lobe and have been extensively studied for their role in memory acquisition and consolidation, spatial awareness and attention control. Furthermore, the hippocampus and associated structures are of interest to researchers as they are prone to generate epileptic seizures and to suffer from ischemic damage, and are greatly damaged in Alzheimer’s disease (Walker et al., 2007). The involvement of medial temporal lobe structures in the formation of declarative memory i.e. the conscious recollection of facts and events has been proposed after the study of patients with brain lesions to this area, the development of animal models and neuroimaging studies (Squire and Zola-Morgan, 1991; Squire et al., 2004). The discovery of place cells in hippocampus and the idea of the formation of cognitive maps have defined the role of the hippocampus in space awareness (O’Keefe and Dostrovsky, 1971; O’Keefe and Nadel, 1978).

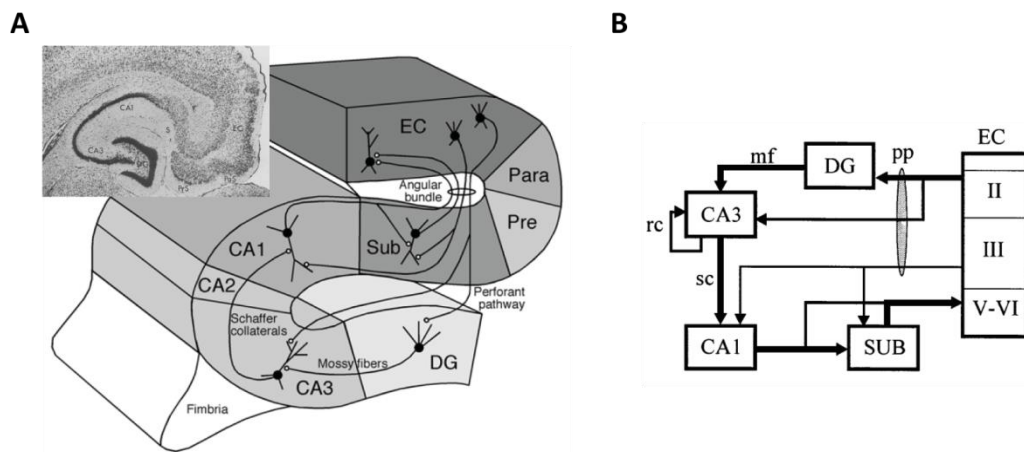


Figure 1.1 The hippocampal formation. (A) Schematic representation of the anatomical regions of the hippocampal formation (from Amaral and Lavenex, 2007). Inset shows a Nissl-stained transverse section of the rat hippocampal formation (from Amaral and Witter, 1989). **(B)** Diagram of the main excitatory connections in the hippocampal circuitry (adapted from Tsien et al., 1996). EC, entorhinal cortex; Para/PaS, parahippocampal cortex; Pre/PrS, perirhinal cortex; Sub/S, subiculum; CA, cornu ammonis; DG, dentate gyrus; pp, perforant pathway; mf, mossy fibres; sc, Schaffer collaterals; rc, recurrent collateral axons

Due to its highly organised neuroanatomy the hippocampal formation and its circuitry has become a well studied area of the brain. At cytoarchitectonic level the hippocampal regions are organised in a laminar fashion. In the CA1–3 fields of the hippocampus proper as well as in the dentate gyrus the principal cells are arranged in tightly packed bands. Principal cells,

pyramidal neurons in the CA fields and granule neurons in the dentate gyrus, make up the majority of cells, while the interneuron population amounts to less than 10 % (Buhl and Whittington, 2007). The regions of the hippocampal formation are connected in a mainly unidirectional manner with the entorhinal cortex serving as the start and end point of the circuit loop, which the hippocampal formation uses to process information (Fig. 1.1B). The majority of neocortical input to the hippocampal formation is received by the entorhinal cortex, whose layer II neurons project, via the perforant pathway, to the dentate gyrus and provide over 80 % of its input (Kobayashi and Amaral, 1999). Via the mossy fibre pathway, the granule cells of the dentate gyrus connect with the pyramidal cells of CA3, which in turn provide the major input, the Schaffer collaterals, to the pyramidal cells of CA1. The loop is closed by projections to the entorhinal cortex from CA1 directly or indirectly via the subiculum. This circuit (Fig. 1.1B) describes the main excitatory connections within the hippocampal formation, but is a simplified version of the real network and additional intrinsic and extrinsic connections to and from various hippocampal fields also contribute. For example, the entorhinal cortex also projects to CA3, CA1 and subiculum directly and both dentate gyrus and the CA fields receive inputs from basal forebrain, hypothalamus and brain stem (Witter and Amaral, 2004; Amaral and Lavenex, 2007). Furthermore, the extensive inhibitory interneuron circuits play a pivotal role in shaping the network activity of the hippocampal formation (Spruston and McBain, 2007). Apart from glutamate as the main excitatory and GABA as the major inhibitory transmitter of the hippocampus formation, others neurotransmitters like ACh and the monoamines noradrenaline, dopamine, serotonin and histamine also contribute to the regulation of the hippocampal network (Kobayashi and Amaral, 1999).

1.1.2 Glutamatergic and cholinergic systems in the hippocampus

As mentioned, glutamate acts as the main excitatory transmitter of the hippocampal formation and is responsible for the excitatory synaptic transmission in the so-called tri-synaptic circuit i.e. projections from entorhinal cortex to dentate gyrus to CA3 and to CA1 described above. Glutamate mediates this transmission by activating ionotropic receptors, AMPA (GluA, nomenclature for proteins according to IUPHAR classification (Collingridge et al., 2009)) as well as NMDA (GluN) receptors, and the opening of these non-selective cation channels causes the postsynaptic neuron to depolarise. The role of kainate (GluK) receptors in synaptic transmission is not well characterised, but their activation by glutamate enhances the excitation of CA3 pyramidal neurons by mossy fibres (Castillo et al., 1997). NMDA receptor activation at Schaffer collateral/CA1 pyramidal neuron synapses and in particular the subsequent influx of Ca^{2+} induces changes in synaptic plasticity that is required for long-term potentiation (LTP) (Bliss and Collingridge, 1993). Ionotropic glutamate receptors are also

localised on inhibitory interneurons and their excitation contributes to the regulation of hippocampal network activity by various feed-forward and feed-backward circuits (Freund and Buzsáki, 1996; Jonas et al., 2004).

On the other hand, glutamate also produces slower responses by acting on metabotropic glutamate receptors (mGluRs), which are coupled to heterotrimeric G-proteins and activate intracellular signalling cascades. Eight mGluR subtypes are known and they are classified into three groups according to sequence similarities and pharmacological and functional profiles: (I) mGlu₁ and mGlu₅, (II) mGlu₂ and mGlu₃ and (III) mGlu₄, mGlu₆, mGlu₇ and mGlu₈; with group (I) coupling to G-proteins of the G_q subfamily and activating PLC β and group (II) and (III) signalling via G-proteins of the G_i subfamily and inhibiting adenylyl cyclase (AC) (Niswender and Conn, 2010). mGluRs are localised mainly outside the pre- and postsynaptic areas and are thus thought to be activated by the spillover of glutamate from the synaptic cleft following high frequency release of glutamate from presynaptic terminals (Lujan et al., 1996; Luján et al., 1997; Shigemoto et al., 1997). The modulatory effects of mGluR activation at presynaptic and postsynaptic sites influence synaptic transmission and neuronal excitability in the hippocampus formation. Furthermore, mGluRs have been linked to synaptic plasticity, since LTP induction has been shown to involve mGluR activation (Bashir et al., 1993; Anwyl, 2009). At the presynaptic neuron group II and III mGluRs inhibit glutamate release from principal neurons by acting as autoreceptors (Scanziani et al., 1997) and also suppress GABA release from interneurons (Semyanov and Kullmann, 2000; Kogo et al., 2004). This modulation of transmitter release by mGluRs is mediated by the suppression of voltage-gated Ca²⁺ (Ca_v) channels as well as by direct inhibition of the machinery involved in transmitter exocytosis (Scanziani et al., 1995; Takahashi et al., 1996; Anwyl, 1999; Cartmell and Schoepp, 2000). At the postsynaptic neuron the activation of the group I mGluRs, mGlu₁ and mGlu₅, causes depolarisation and leads to increased firing (Davies et al., 1995; Mannaioni et al., 2001). These mGluRs increase neuronal excitability by modulating various ion channels including Ca²⁺ channels (Swartz and Bean, 1992; Sahara and Westbrook, 1993), various K⁺ channels (Anwyl, 1999) and non-selective cation channels (Crépel et al., 1994; Guérineau et al., 1995).

In the hippocampal formation, the actions of the neurotransmitter ACh present a powerful system that modulates hippocampal network activity and oscillation state as well as synaptic plasticity by acting on nicotinic and muscarinic receptors. Cholinergic projections to the hippocampal formation originate in the medial septum nucleus and in the nucleus of the diagonal band of Broca and innervate the hippocampus via the fimbria-fornix pathway (Dutar et al., 1995). Cholinergic afferents form synaptic connections with principal cells as well as with interneurons, but also provide diffuse, non-synaptic transmission to the hippocampal

formation so-called volume transmissions (Frotscher and Léránth, 1985; Vizi and Kiss, 1998). A pivotal role of ACh in the hippocampal formation is its regulation of oscillation states such as the hippocampal theta rhythm, which is abolished when septohippocampal projections are damaged (Stewart and Fox, 1990; Buzsáki, 2002; Yoder and Pang, 2005). The synchronous membrane oscillations of 4–10 Hz are thought to constitute the temporal framework for the encoding of information. It allows for the precise firing of cells and influences synaptic plasticity, since LTP induction is known to be enhanced during the peak of theta wave (Huerta and Lisman, 1995).

ACh activates muscarinic acetylcholine receptors (mAChRs) as well as nicotinic acetylcholine receptors (nAChRs). mAChRs (M) are GPCRs, of which five subtypes are known, M_{1-5} . M_1 , M_3 and M_5 couple to G-proteins of the G_q subfamily and activate PLC β , while M_2 and M_4 coupled to G-proteins of the G_i subfamily cause the inhibition of AC (Caulfield and Birdsall, 1998). mAChRs are widely expressed throughout the brain with M_1 being the prevalent receptor subtype, followed by M_2 and M_4 and then by M_3 and M_5 at low levels (Levey et al., 1991; Reever et al., 1997; van der Zee and Luiten, 1999). In the hippocampal formation M_1 and M_3 receptors are predominantly located in principal cells (pyramidal neurons and granule cells), while M_2 and M_4 are found mainly in interneurons; the weak expression of M_5 prevents a clear characterisation (Levey et al., 1995; van der Zee and Luiten, 1999; Volpicelli and Levey, 2004). The overall effect of postsynaptically located mAChRs is the increase in excitability of principal neurons caused by the modulation of various ionic conductance including several K^+ , mixed cation as well as Ca^{2+} currents (Cobb and Davies, 2005). mAChRs activation is also known to enhance the NMDA response of a hippocampal pyramidal neuron (Markram and Segal, 1990; Marino et al., 1998). On interneurons mAChRs cause depolarisation, but also mediate the inhibition of GABA release when located at synaptic terminals and thus have a strong regulatory control over hippocampal network activity (Pitler and Alger, 1992; Behrends and ten Bruggencate, 1993). This effect of presynaptic localised mAChRs is also observed on glutamatergic and, as autoreceptors, on cholinergic terminals (Raiteri et al., 1990; Rouse et al., 1999).

The second type of receptors activated by ACh is the group of nAChRs, which are ionotropic receptors permeable to Na^+ , K^+ and Ca^{2+} . In the hippocampus formation several nAChR subtypes are expressed presynaptically and postsynaptically, namely $\alpha 7$, $\alpha 4\beta 2$ and $\alpha 3\beta 4$ (Alkondon and Albuquerque, 2004; Drever et al., 2011). Alpha7, the prevailing subtype and highly permeable to Ca^{2+} , is also found at glutamatergic and GABAergic terminals, where it increases transmitter release and thus modulates synaptic transmission (Séguéla et al., 1993; Wonnacott, 1997; Fabian-Fine et al., 2001). Postsynaptically, the opening of nAChRs causes

depolarisation and increases intracellular Ca^{2+} levels. nAChRs are strongly expressed on GABAergic interneurons and their activation influences overall hippocampal network activity by modulating the excitability of hippocampal circuits and thus synaptic plasticity (Ji et al., 2001; Drever et al., 2011).

1.2 Afterhyperpolarizations

Hippocampal network activity is regulated by a number of processes and various ionic conductances determine neuronal excitability and firing patterns of hippocampal pyramidal neurons, which in turn contributes to the encoding of information. K^+ conductances, for example, have a major influence on these intrinsic neuronal properties and underlie afterhyperpolarization (AHP) that follows single or trains of action potentials. AHP controls the firing frequency of neurons and generates spike frequency adaptation. It consists of three distinct phases with fast (f), medium (m) and slow (s) kinetics (Fig. 1.2A; Alger and Nicoll, 1980; Hotson and Prince, 1980; Lancaster and Nicoll, 1987; Storm, 1987a and 1989), which are mediated by the opening of Ca^{2+} -activated as well as voltage-gated K^+ channels. While fAHP contributes to action potential repolarisation, mAHP is responsible for early and sAHP for late spike frequency adaptation i.e. the slowing down or termination of firing in response to a prolonged stimulus (Fig. 1.2B; Storm, 1990). AHP and its modulation play a crucial role in shaping neuronal excitability.

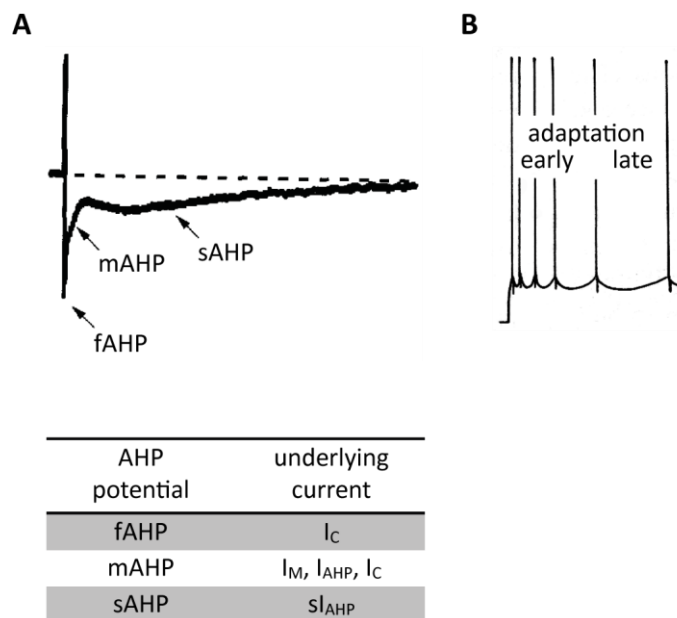


Figure 1.2 Afterhyperpolarizations and the generation of spike frequency adaptation. **(A)** Afterhyperpolarizing potentials of fast (fAHP), medium (mAHP) and slow (sAHP) kinetics (from Sah, 1996). The current I_C is underlying fAHP, I_M , I_{AHP} and I_C are underlying mAHP and sI_{AHP} underlies sAHP (table). **(B)** The adaptation of the firing pattern in response to a prolonged stimulus is generated by mAHP, responsible for early spike frequency adaptation, and sAHP, underlying late spike frequency adaptation (adapted from Storm, 1990).

1.2.1 Fast afterhyperpolarization (fAHP)

fAHP can be observed following a single action potential and the current underlying fAHP has been identified as I_C , which displays rapid activation (1–2 ms) and deactivation kinetics (within tens of milliseconds), is sensitive to submillimolar concentrations of tetraethylammonium (TEA) and is mediated by the opening of large-conductance potassium (BK) channels ($K_{Ca1.1}$) (Brown et al., 1990; Storm, 1990). $K_{Ca1.1}$ channels are K^+ channels that display a single-channel conductance of 100–250 pS (Gribkoff et al., 2001). $K_{Ca1.1}$ channels are voltage- and Ca^{2+} -dependent and thus activate in response to both membrane depolarisation and a rise of intracellular Ca^{2+} , as is the situation during action potential generation. Both stimuli act allosterically to increase the open probability of the channel: Ca^{2+} sensitivity is increased at more depolarised potentials, just as high intracellular Ca^{2+} levels allow the channel to activate at more negative potentials (McManus, 1991; Cui et al., 2009). The opening of $K_{Ca1.1}$ channels contributes to spike repolarisation and hyperpolarisation, and acts as a feed-back mechanism to limit the activity of voltage-gated Ca^{2+} channels (Ca_v), with which they are closely associated (Berkefeld et al., 2006), and thus participates in the control of neuronal excitability.

$K_{Ca1.1}$ channels consist of a pore-forming α subunit tetramer (Shen et al., 1994) and associated β subunits, of which four subunits ($\beta 1$ –4) are known (Orio et al., 2002). $K_{Ca1.1}$ channel α subunits have seven transmembrane segments (S0–6), an extracellular amino-terminus and a large intracellular carboxyl-terminus, and segments S1–6 show similarity to voltage-gated potassium (K_v) channels in that S1–4 constitute the voltage sensor domain and S5–6 the pore-forming domain (Meera et al., 1997). Unlike K_v channels, voltage sensitivity is not predominantly conveyed by S4, but to a large extent also by residues on S2 and S3 (Ma et al., 2006; Pantazis et al., 2010). The large carboxyl-terminus of the α subunit, around two-thirds of the total protein, contains the segments S7–10, two tandem RCK (regulator of K^+ conductance) domains that constitute the channel's gating ring and a highly conserved section of aspartate residues termed the “ Ca^{2+} bowl” (Latorre et al., 2010). Partial deletions or point mutations of the Ca^{2+} bowl results in a reduction in Ca^{2+} sensitivity (Schreiber and Salkoff, 1997; Latorre and Brauchi, 2006). Ca^{2+} sensitivity is, however, not completely abolished, hence $K_{Ca1.1}$ channels must contain more than one Ca^{2+} sensor (Bao et al., 2002; Xia et al., 2002). Crystallography has verified the two tandem RCK domains and has established that the Ca^{2+} bowl is part of the second RCK, but no further Ca^{2+} sensing domains have been identified (Yuan et al., 2010).

Despite being functional on their own, most α subunit tetramers associate with β subunits, which perform modulatory functions by influencing the $K_{Ca1.1}$ channels' Ca^{2+} - and voltage sensitivity, kinetics as well as pharmacological profile (Orio et al., 2002). The β subunits consist of two transmembrane segments and have intracellular amino- and carboxyl-termini.

Functional coupling of the β subunits with α is achieved by contact of the first transmembrane segment of the β subunit with S1 and S2 of the α subunit and of the second transmembrane segment of the β subunit with S0 of the α subunit (Liu et al., 2010; Wu et al., 2013). β 1 is mainly expressed in smooth muscles, β 2 and β 3 are found more widespread, but show limited expression in brain, while β 4 is predominately expressed in neuronal tissue (Berkefeld et al., 2010). Depending on subunit type, the assembly of β with α subunits can produce $K_{Ca1.1}$ channels with diverse profiles. β 1 co-assembly enhances Ca^{2+} sensitivity, which allows the channel to open at more negative potentials and to display greater open probabilities as well as slower activation and deactivation kinetics (Knaus et al., 1994; Bao and Cox, 2005). $K_{Ca1.1}$ channels tend to be non-inactivating, whereas β 2 association causes them to inactivate completely (Bentrop et al., 2001) and β 3 association incompletely (Lingle et al., 2001). $K_{Ca1.1}$ channels containing the β 4 subunit display activation and deactivation kinetics that are modulated in a Ca^{2+} -dependent manner (Brenner et al., 2000; Ha et al., 2004). $K_{Ca1.1}$ channels are blocked by submillimolar concentrations of TEA and by several toxins like charybdotoxin and iberiotoxin (Shen et al., 1994; Kaczorowski et al., 1996). Their pharmacological profile is influenced by the β subunits, for example, β 2–4 association mediates a reduction in charybdotoxin sensitivity with β 4 displaying the lowest affinity, while β 1 association produces high affinity for charybdotoxin (Hanner et al., 1997; Meera et al., 2000; Berkefeld et al., 2010).

In line with the properties of $K_{Ca1.1}$ channels, the generated current I_C is abolished when Ca^{2+} is removed, either extracellularly or by the Ca^{2+} chelator BAPTA (Lancaster and Nicoll, 1987; Storm, 1987a and b). EGTA, another Ca^{2+} chelator, does not bind Ca^{2+} fast enough to prevent $K_{Ca1.1}$ channel activation (Lancaster and Nicoll, 1987; Storm, 1987b; Berkefeld et al., 2006). This indicates the close proximity of $K_{Ca1.1}$ and Ca_v channels, estimated to be <30 nm for $K_{Ca1.1}$ and $Ca_v2.2/N$ -type in hippocampal pyramidal neurons (Marrion and Tavalin, 1998). Furthermore, I_C is not modulated by neurotransmitters such as noradrenaline or the cholinergic agonist carbachol (CCh) (Brown and Griffith, 1983; Lancaster and Adams, 1986; Lancaster and Nicoll, 1987; Madison et al., 1987). Elimination of I_C , either by the removal of Ca^{2+} or the application of TEA or other $K_{Ca1.1}$ channel blockers (charybdotoxin and iberiotoxin) causes an increase in action potential duration and the abolition of fAHP (Storm, 1987a) thus confirming the role of I_C in spike repolarisation and as the underlying current for fAHP.

1.2.2 Medium afterhyperpolarization (mAHP)

Single as well as bursts of action potentials are followed by fAHP and then by an afterhyperpolarization with medium kinetics (mAHP), displaying an activation time of <5 ms and a decay phase lasting hundreds of milliseconds (Gustafsson and Wigström, 1981; Storm, 1989). These kinetic properties and its influence on membrane repolarisation allow mAHP to

control interspike frequency and make it responsible for the early phase of spike frequency adaptation (Fig. 1.2B; Stocker et al., 1999; Shah et al., 2006). At hyperpolarized potentials mAHP is generated by I_h , a Cs^+ -sensitive, mixed cation (K^+ and Na^+) current mediated by hyperpolarization-activated cyclic nucleotide-regulated (HCN) channels (Halliwell and Adams, 1982; Storm, 1989; Gu et al., 2005). Four subtypes (HCN1–4) are known and HCN channels are tetramers with each subunit consisting of six transmembrane segments (S1–6) and intracellular amino- and carboxyl-termini. S4 functions as the voltage sensor and the pore forming region is located between S5 and S6. Activation of HCN channels is caused by hyperpolarization and is facilitated by the interaction with cyclic nucleotides (especially cyclic adenosine monophosphate; cAMP), which cause the channel to open faster (Biel et al., 2009).

The currents underlying mAHP are I_M , mediated by voltage-gated K^+ channels (KCNQ (K_V7)), I_{AHP} , generated by Ca^{2+} -activated small conductance K^+ channels (SK (K_{Ca2})) and to a small extent I_C , which is caused by BK channels ($\text{K}_{Ca1.1}$). The contribution of I_C is supported by the description of a fast Ca^{2+} -dependent component of the mAHP as well as a reduction in early spike frequency adaptation upon blocking of $\text{K}_{Ca1.1}$ channels (Lancaster and Nicoll, 1987; Storm, 1989).

KCNQ channels (K_V7), responsible for I_M (classically known as M-current), are activated by depolarisations exceeding -60 mV, display slow activation kinetics and deactivate over ~ 50 ms, and do not inactivate (Brown and Adams, 1980; Storm, 1990). The K_V7 channel family comprises five members, of which $\text{K}_V7.1$ is found predominantly in heart (Wang et al., 1996), while the other four, $\text{K}_V7.2$ – 7.5 , are expressed in the nervous system (Wang, H-S et al., 1998; Kubisch et al., 1999; Lerche et al., 2000; Schroeder et al., 2000). K_V7 channels are formed by four subunits, which arrange around a central pore and each have six transmembrane segments (S1–6) and intracellular amino- and carboxyl-termini (Robbins, 2001; Howard et al., 2007; Nakajo et al., 2010). The pore forming region of the subunits is located between S5 and S6, while the positively charged S4 serves as the voltage sensor. Unlike other K_V channels, for which the T1 domain of the amino-terminus is responsible for tetramerization, the assembly of K_V7 channels is mediated by their carboxyl-terminus (Haitin and Attali, 2008). The carboxyl-terminus of K_V7 channels is particularly long (300–500 residues) and its distal part contains a conserved region, the A-domain that comprises two coiled coil motifs (the A-domain head, also called tetramerizing coiled coil 1, and the A-domain tail (tetramerizing coiled coil 2)) and is crucial for channel assembly, tetramerization and trafficking (Schmitt et al., 2000; Schwake et al., 2000; Maljevic et al., 2003; Schwake et al., 2003; Howard et al., 2007). The proximal part of the carboxyl-terminus possesses two conserved motifs that constitute the binding site for the Ca^{2+} sensor calmodulin (CaM) (Wen and Levitan, 2002; Yus-Najera et al., 2002; Gamper and

Shapiro, 2003). CaM binds to K_v7 channels constitutively, with or without Ca²⁺ being present, and is essential for channel function as well as being implicated in the assembly and gating of some K_v7 channels (Wen and Levitan, 2002; Shamgar et al., 2006). CaM mediates the Ca²⁺ sensitivity of K_v7 channels and is responsible for the inhibition of K_v7 channels upon the rise of intracellular Ca²⁺ (Gamper and Shapiro, 2003). However, this CaM-mediated inhibition varies between different K_v7 subunits with K_v7.2, K_v7.4 and K_v7.5 channels being affected, while K_v7.1 and K_v7.3 are not (Gamper et al., 2005).

In heterologous expression systems, all K_v7 subunits are able to assemble as homomultimers and in certain combinations as heteromultimers, whereas under physiological conditions channels are thought to be mainly heteromultimers consisting of either K_v7.2, K_v7.4 or K_v7.5 subunits in combination with K_v7.3 at equal stoichiometry, with K_v7.2/7.3 being the predominant combination (Wang, H-S et al., 1998; Kubisch et al., 1999; Jentsch, 2000; Schroeder et al., 2000; Shah et al., 2002; Hadley et al., 2003; Bal et al., 2008). Furthermore, K_v7.1 channels associate with members of the KCNE family, which encompasses five members (KCNE1–5) that act as auxiliary subunits for several K_v channels and consist of one transmembrane segment with an extracellular amino-terminus and a cytosolic carboxyl-terminus (Barhanin et al., 1996; Sanguinetti et al., 1996; McCrossan and Abbott, 2004). K_v7.1/KCNE channels are proposed to consist of two KCNE β subunits assembled with four K_v7.1 α subunits (Chen et al., 2003; Morin and Kobertz, 2008), although a variable stoichiometry of up to four KCNE subunits per K_v7.1 tetramer has also been suggested (Wang, W et al., 1998; Nakajo et al., 2010). While K_v7.1 channels produce fast activating currents, the association with KCNE1 β subunits results in slower activation kinetics and increased current amplitudes (McCrossan and Abbott, 2004). In the heart K_v7.1/KCNE1 channels are responsible for I_{Ks}, the slow delayed rectifier current crucial for cardiac action potential repolarisation (Barhanin et al., 1996; Sanguinetti et al., 1996).

I_M resembles currents generated by K_v7.2/7.3 channels (Wang, H-S et al., 1998), but it can also be produced by other combinations of neuronally expressed channels and thus, depending on neuron type, K_v7 channels of different subunit compositions are likely to generate I_M (Schroeder et al., 2000; Selyanko et al., 2000; Shah et al., 2002; Tzingounis and Nicoll, 2008; Brown and Passmore, 2009). In the hippocampus K_v7.2/7.3 as well as K_v7.3/7.5 channels along with some contribution of homomeric K_v7.2 and K_v7.5 channels are suggested to underlie I_M (Shah et al., 2002; Peters et al., 2005; Tzingounis et al., 2010). I_M is inhibited by mAChR agonists such as ACh and muscarine and its suppression can be reversed by the mAChR antagonist atropine (Halliwell and Adams, 1982; Storm, 1989). K_v7 channels are also blocked by linopirdine (IC₅₀: 3.7–>200 μM) and XE991 (IC₅₀: 0.7–70 μM) as well as by TEA (IC₅₀: 0.3–

>30 mM); sensitivity of K_V7 subunits to the blockers is variable and the order for example with TEA is $K_V7.2 > K_V7.4 = K_V7.1 > K_V7.5 > K_V7.3$ (Storm, 1989; Hadley et al., 2000; Schroeder et al., 2000; Robbins, 2001). The activation of M_1 , mAChRs coupled to the pertussis toxin-insensitive G-proteins of the G_q family, mediates the inhibition of I_M (Caulfield et al., 1994; Selyanko et al., 2000) by decreasing the level of membrane phosphatidylinositol 4,5-bisphosphate (PIP_2), which is required for K_V7 channels to open (Zhang et al., 2003; Brown et al., 2007; Hernandez et al., 2008).

Small conductance potassium (SK) channels (K_{Ca2}), which generate I_{AHP} , are Ca^{2+} -activated K^+ channels that have a single channel conductance of ~ 10 pS and display activation kinetics of 5–15 ms and deactivate over ~ 50 ms (Köhler et al., 1996; Xia et al., 1998; Stocker, 2004). The K_{Ca2} family encompasses three members ($K_{Ca2.1-2.3}$) that are expressed throughout the nervous system and each display a characteristic expression pattern that, in the case of $K_{Ca2.1}$ and $K_{Ca2.2}$, overlaps in some brain areas such as CA1–3 of hippocampus (Köhler et al., 1996; Stocker and Pedarzani, 2000; Sailer et al., 2002). Each subunit of the tetrameric channel comprises six transmembrane segments (S1–6) with a pore domain between S5 and S6 and cytosolic amino- and carboxyl-termini. Compared to K_V channels, K_{Ca2} channels have less positively charged residues in S4, which renders them voltage insensitive (Köhler et al., 1996; Stocker, 2004). K_{Ca2} channels are activated by intracellular Ca^{2+} , towards which they display high sensitivity (EC_{50} : 0.3–0.7 μM ; (Köhler et al., 1996; Hirschberg et al., 1998; Xia et al., 1998; Hirschberg et al., 1999). However, instead of having an intrinsic Ca^{2+} binding motif, activation of K_{Ca2} channels is mediated by the Ca^{2+} sensor CaM, which constitutively binds to each of the four channel subunits (Xia et al., 1998; but see Halling et al., 2014). The CaM binding domain is located in the carboxyl-terminus of the K_{Ca2} channel subunit, directly neighbouring S6, and the constitutive association of CaM with the CaM binding domain is mediated by amino acids in the carboxyl-terminal half of CaM, while two EF hand motifs at the amino-terminus of CaM are responsible for Ca^{2+} binding and channel gating (Keen et al., 1999). Crystallization studies have shown that when Ca^{2+} is bound, the amino-terminus of CaM is associated with the CaM binding domain of a second K_{Ca2} subunit (dimerization; Schumacher et al., 2001). This is thought to cause conformational changes that are conveyed to S6 of the K_{Ca2} channel subunits and result in channel opening. Because of the constitutive association between CaM and the K_{Ca2} channel, changes to the intracellular Ca^{2+} level are rapidly transduced to the channel. The Ca^{2+} sensitivity of K_{Ca2} channels is modulated by additional binding partners to the K_{Ca2} channel/CaM complex, namely protein kinase CK2 and protein phosphatase 2A, which counterbalance each other: CK2 phosphorylates CaM when the channel is in the closed state and thus reduces Ca^{2+} sensitivity, while the dephosphorylation of CaM by protein phosphatase

2A occurs only when the channel is open and results in an increase in Ca^{2+} sensitivity (Bildl et al., 2004; Allen et al., 2007). Apart from conveying Ca^{2+} sensitivity to the $\text{K}_{\text{Ca}2}$ channel, CaM binding has also been implicated in the trafficking of the channel to the plasma membrane (Lee et al., 2003). In hippocampus, small conductance Ca^{2+} -activated K^+ channels, thought to be $\text{K}_{\text{Ca}2}$ channels, are localised in close proximity (50–150 nm) to Ca_v channels ($\text{Ca}_v1.2$ and $\text{Ca}_v1.3/\text{L-type } \text{Ca}^{2+}$ channels), which open during action potentials and causes the increase in intracellular Ca^{2+} that activates these K^+ channels (Marrion and Tavalin, 1998). Other Ca^{2+} sources such as Ca^{2+} release from intracellular stores and the influx of Ca^{2+} through ligand-gated ion channels (NMDARs and nAChRs) and $\text{Ca}_v2.3$ channels (R-type Ca^{2+} channels) have also been shown to activate $\text{K}_{\text{Ca}2}$ channels (Adelman et al., 2012).

Although heteromeric $\text{K}_{\text{Ca}2}$ channels are formed in heterologous expression systems ($\text{K}_{\text{Ca}2.1/2.2}$, Ishii et al, 1997; $\text{K}_{\text{Ca}2.1/2.3}$ and $\text{K}_{\text{Ca}2.2/2.3}$, Monaghan et al., 2004), their existence in native tissue is not well defined or has been excluded (no assembly between $\text{K}_{\text{Ca}2.2}$ and $\text{K}_{\text{Ca}2.3}$, Sailer et al., 2002). Members of the $\text{K}_{\text{Ca}2}$ channel family display different levels of sensitivity to the specific $\text{K}_{\text{Ca}2}$ channel blocker apamin, with $\text{K}_{\text{Ca}2.2}$ being the most sensitive (IC_{50} : 27–140 pM), followed by $\text{K}_{\text{Ca}2.3}$ (IC_{50} : 0.6–4.0 nM) and $\text{K}_{\text{Ca}2.1}$ (IC_{50} : 0.7–12 nM) (Pedarzani and Stocker, 2008). At first, $\text{K}_{\text{Ca}2.1}$ was described as being apamin-insensitive (Köhler et al., 1996; Ishii et al., 1997), but later studies determined its low apamin sensitivity (Shah and Haylett, 2000a; Strøbaek et al., 2000). Other toxins and compounds that inhibit $\text{K}_{\text{Ca}2}$ channels include scyllatoxin, tamapin, d-Tubocurarine (dTC), bicuculline and high millimolar concentrations of TEA (Pedarzani and Stocker, 2008). The modulation of $\text{K}_{\text{Ca}2}$ channels by neurotransmitters is not well established, but noradrenaline (Maingret et al., 2008) and ACh (Buchanan et al., 2010; Giessel and Sabatini, 2010) are suggested to inhibit $\text{K}_{\text{Ca}2}$ channels via associated kinases, namely protein kinase CK2 or protein kinase C (PKC). A role of glutamate and protein kinase A (PKA) in the modulation of $\text{K}_{\text{Ca}2}$ channels has also been suggested (Pedarzani and Stocker, 2008).

In hippocampus, the existence of I_{AHP} and its contribution to mAHP has been shown through its inhibition by apamin, which therefore establishes $\text{K}_{\text{Ca}2}$ channels as the channels generating this Ca^{2+} -activated current (Stocker et al., 1999; Sailer et al., 2002). Moreover, $\text{K}_{\text{Ca}2}$ channel expression in hippocampus (Stocker et al., 1999; Stocker and Pedarzani, 2000; Sailer et al., 2002) matches the reported distribution of apamin binding sites (Mourre et al., 1986; Gehlert and Gackenhaimer, 1993). The most apamin-sensitive $\text{K}_{\text{Ca}2}$ channel subunit $\text{K}_{\text{Ca}2.2}$ is highly expressed, especially in CA1 and CA3, and is suggested to underlie I_{AHP} , while $\text{K}_{\text{Ca}2.1}$, which is localised in the same regions, is not believed to play a role due to its lower apamin sensitivity, however, the contribution of heteromeric $\text{K}_{\text{Ca}2.1/2.2}$ channels to I_{AHP} cannot be excluded

(Stocker and Pedarzani, 2000; Sailer et al., 2002). Studies of K_{Ca2} channel knock-out mice have revealed the responsibility of $K_{Ca2.2}$ underlying I_{AHP} , whereas the current is not affected in $K_{Ca2.1}$ and $K_{Ca2.3}$ knock-out mice, nevertheless a role of heteromeric $K_{Ca2.1/2.2}$ channels can also not be ruled out completely (Bond et al., 2004). The contribution of I_{AHP} to mAHP in hippocampus is, however, contested by studies, which show an apamin-insensitive mAHP and suggest that only I_M , I_C and I_h underlie mAHP (Gu et al., 2005 and 2008).

1.2.3 Slow afterhyperpolarization (sAHP)

sAHP is observed after a train of action potentials and is characterised by its slow kinetics, its Ca^{2+} dependency as well as by its modulation by various neurotransmitters (Storm, 1990; Sah, 1996). It is responsible for the late phase of spike frequency adaptation and thus restricts the repetitive firing of action potentials and contributes greatly to the control of neuronal excitability (Fig. 1.2B; Alger and Nicoll, 1980; Hotson and Prince, 1980; Madison and Nicoll, 1982 and 1984; Lancaster and Nicoll, 1987). sAHP has been described in pyramidal neurons in CA1–3 of hippocampus as well as in the cortex and several other areas of brain, but is not as widely seen as mAHP (Stocker et al., 2004). sAHP activates over several hundreds of milliseconds and decays over seconds (Hotson and Prince, 1980; Lancaster and Adams, 1986; Sah and Clements, 1999; Gerlach et al., 2004), thus presents very slow kinetics compared to fAHP and mAHP. sAHP kinetics are highly temperature dependent, an increase in temperature results in faster activation and decay (Thompson et al., 1985; Lancaster and Adams, 1986).

The K^+ current underlying sAHP has been named sI_{AHP} and its properties include voltage insensitivity, activation by Ca^{2+} and a single channel conductance of 2–5 pS (Hotson and Prince, 1980; Lancaster and Adams, 1986; Sah and Isaacson, 1995). The search for the channel mediating sI_{AHP} is hampered by the lack of specific blockers, since it is insensitive to non-selective K^+ channel blockers like TEA or 4-aminopyridine (4-AP) as well as the toxin apamin (Lancaster and Adams, 1986; Lancaster and Nicoll, 1987; Storm, 1989; Stocker et al., 1999). Reports proposing a block of the channel generating sI_{AHP} by the clotrimazole analogues, UCL2027 and UCL2077, is the only exception (Shah et al., 2001 and 2006; Soh and Tzingounis, 2010).

The activation of sI_{AHP} depends on intracellular Ca^{2+} concentration (threshold at $[Ca^{2+}]_i = 160$ nM) (Abel et al., 2004) and can be eliminated by the removal of extracellular Ca^{2+} , the application of Ca^{2+} channels blockers like cadmium or the intracellular application of Ca^{2+} chelators such as EGTA and BAPTA (Schwartzkroin and Stafstrom, 1980; Madison and Nicoll, 1982 and 1984; Lancaster and Adams, 1986; Zhang et al., 1995). The extracellular source of Ca^{2+} to activate sI_{AHP} is via Ca_v channels, which open during action potential firing and the

involvement of Ca_v1 channels (L-type) has been determined by specific channel inhibitors such as isradipine and nifedipine, which suppress sI_{AHP} (Tanabe et al., 1998; Shah and Haylett, 2000b; Lima and Marrion, 2007). In contrast, inhibition of $\text{Ca}_v2.1$ (P/Q-type) and $\text{Ca}_v2.2$ (N-type) channels does not suppress sI_{AHP} (Tanabe et al., 1998; Lima and Marrion, 2007; but see Shah and Haylett, 2000b). Of the two main neuronal Ca_v1 channel subtypes the deletion of $\text{Ca}_v1.3$, but not $\text{Ca}_v1.2$, reduces sAHP (Gamelli et al., 2011). In addition to its direct action, Ca^{2+} entering the cell through Ca_v channels also causes Ca^{2+} -induced Ca^{2+} release. Such a process contributes to the activation of sI_{AHP} , since sI_{AHP} is diminished when intracellular Ca^{2+} stores are depleted by Ca^{2+} ATPase inhibitors or when Ca^{2+} release from stores is inhibited by the block of ryanodine receptors (RyR3) (Tanabe et al., 1998; Shah and Haylett, 2000b; van de Vrede et al., 2007; but see Zhang et al., 1995). sI_{AHP} amplitude is directly related to the amount of Ca^{2+} entering the cell; increasing the duration and intensity of the depolarising step (or of the current pulses when recording sAHP) augments sI_{AHP} amplitude with peak values being reached when $[\text{Ca}^{2+}]_i$ reaches 250–350 nM (Abel et al., 2004), while changing Ca^{2+} does not affect sI_{AHP} kinetics (Hotson and Prince, 1980; Gustafsson and Wigström, 1981; Madison and Nicoll, 1984; Lancaster and Adams, 1986; Gerlach et al., 2004).

A key characteristic of sI_{AHP} is its susceptibility to neurotransmitter modulation, which presents a way to control cell excitability and firing properties. sI_{AHP} is suppressed by the monoamine neurotransmitters dopamine (Benardo and Prince, 1982; Pedarzani and Storm, 1995), histamine (Haas and Konnerth, 1983; Pedarzani and Storm, 1993), noradrenaline (Madison and Nicoll, 1982; Haas and Konnerth, 1983; Lancaster and Adams, 1986; Madison and Nicoll, 1986a; Pedarzani and Storm, 1993; Blitzer et al., 1994) and serotonin (Andrade and Nicoll, 1987; Colino and Halliwell, 1987; Pedarzani and Storm, 1993; Torres et al., 1995). Other neurotransmitters like glutamate (Chapak et al., 1990) and ACh (Cole and Nicoll, 1983; Madison et al., 1987) also suppress sI_{AHP} . sI_{AHP} modulation by neurotransmitter is not caused by changes to the Ca^{2+} influx into the cell given that Ca^{2+} spikes are not affected when sI_{AHP} is blocked (Cole and Nicoll, 1983; Madison and Nicoll, 1986a; Knöpfel et al., 1990; Pedarzani and Storm, 1995). Monoamine neurotransmitters inhibit sI_{AHP} by acting on GPCRs coupled to G-proteins of the G_s family and thus via the second messenger cAMP, which is derived from ATP by $G\alpha_s$ stimulated AC and causes activation of PKA (Madison and Nicoll, 1986b; Pedarzani and Storm, 1993 and 1995; Torres et al., 1995). The suppression of sI_{AHP} by monoamine neurotransmitters is prevented when PKA is blocked by the intracellular application of the PKA inhibitors, Rp-adenosine-3',5'-cyclic monophosphorothioate (Rp-cAMPs) and Walsh peptide (PKI) (Pedarzani and Storm, 1993 and 1995). In contrast the application of either forskolin, which activates AC and thus increases cAMP levels, or cAMP analogues 8-bromoadenosine

3',5'-monophosphate (8-Br cAMP) and 8-(4-chlorophenylthio) adenosine 3',5'-cyclic monophosphate (8CPT-cAMP), suppress sI_{AHP} and so behave like monoamine neurotransmitters (Madison and Nicoll, 1986b; Pedarzani and Storm, 1993; Torres et al., 1995). Thus inhibition of sI_{AHP} seems to involve a phosphorylation step that alters the channel generating sI_{AHP} either directly or via intermediate proteins (Nicoll, 1988; Pedarzani and Storm, 1993). In contrast the signalling pathways to suppress sI_{AHP} used by glutamate and ACh are not well identified. Both neurotransmitters activate GPCRs, mGluRs (Charpak et al., 1990) and mAChRs (Cole and Nicoll, 1983 and 1984), coupled to pertussis toxin-insensitive G-proteins (Dutar and Nicoll, 1988; Gerber et al., 1992). Unlike monoamine neurotransmitters, the suppression of sI_{AHP} by glutamatergic and cholinergic agonists is not altered in the presence of PKA inhibitors, so neither glutamate nor ACh mediated signalling involves PKA (Gerber et al., 1992; Pedarzani and Storm, 1993; Blitzer et al., 1994; Pedarzani and Storm, 1996). Furthermore, the modulatory effect of ACh and glutamate on sI_{AHP} is not mediated by PKC either as PKC inhibitors do not affect sI_{AHP} suppression (Gerber et al., 1992; Sim et al., 1992; Engisch et al., 1996). The suppression of sI_{AHP} by ACh, but not by glutamate, is, however, reduced when CamKII is inhibited (Müller et al., 1992; Pedarzani and Storm, 1996).

Ca^{2+} entering the cell during action potentials acts as an important signalling molecule before being sequestered (Berridge et al., 2003). The slow time course of sI_{AHP} activation does not match the kinetics of the rise of intracellular Ca^{2+} during action potentials (Sah and Clements, 1999). This discrepancy between sI_{AHP} kinetics and Ca^{2+} signalling has led to a range of proposals for the underlying mechanism determining sI_{AHP} kinetics. The first proposal suggests that once Ca^{2+} enters the cell it directly binds and activates the channel generating sI_{AHP} and explains the slow time scale of sI_{AHP} with a channel location distant from the site of Ca^{2+} entry (Lancaster and Nicoll, 1987; Lancaster and Zucker, 1994). However, such a proposal for channel activation has been questioned, since the activation kinetics of sI_{AHP} do not change in response to higher levels of intracellular Ca^{2+} (Gerlach et al., 2004) and the increase in sI_{AHP} kinetics due to higher temperatures is too large to be explained by the simple diffusion of Ca^{2+} (Lee et al., 2005). The second proposal suggests that opening of the channel generating sI_{AHP} might be the reason for the slow kinetics of sI_{AHP} . The kinetics of sI_{AHP} have been examined in response to the rapid rise or fall of intracellular Ca^{2+} following the photolysis of caged Ca^{2+} or Ca^{2+} buffers. One study reports a quick response of sI_{AHP} to increasing and decreasing Ca^{2+} concentrations, which would indicate an underlying channel with fast kinetics and a prominent role of Ca^{2+} diffusion and buffering for sI_{AHP} kinetics (Lancaster and Zucker, 1994). In contrast, another study depicts a channel generating sI_{AHP} with slow gating mechanisms, unaffected by rapid Ca^{2+} level changes, and proposes the direct binding of Ca^{2+} to the channel (Sah and

Clements, 1999). However, increasing the Ca^{2+} influx into the cell results in the shortening of activation times and thus questions the idea of intrinsically slow channel kinetics (Gerlach et al., 2004). One mechanism that might result in the slow activation of sI_{AHP} , albeit an underlying channel with fast kinetics, is the delayed facilitation of Ca_v1 channels, which has been observed in response to a depolarising pulse or a train of action potentials at negative potentials (-20 – -60 mV) (Cloues et al., 1997; Bowden et al., 2001). A third proposal for the slow kinetics of sI_{AHP} is its activation by Ca^{2+} -induced Ca^{2+} release, which would prolong the time until the channel is activated. However, it has been shown that Ca^{2+} -induced Ca^{2+} release is not the sole mediator of sI_{AHP} in hippocampus, but only contributed to its activation (Tanabe et al., 1998; Shah and Haylett, 2000b; van de Vrede et al., 2007). Lastly, the slow kinetics and temperature sensitivity of sI_{AHP} have led to the proposal of a second messenger system and hippocalcin, a family member of the neuronal Ca^{2+} sensor proteins strongly expressed in hippocampus (Saitoh et al., 1994), as potential Ca^{2+} sensor for sI_{AHP} (Tzingounis et al., 2007). Upon Ca^{2+} binding hippocalcin translocates to the cell membrane (Markova et al., 2008), where it is thought to gate the channel generating sI_{AHP} given that this current is reduced in hippocalcin knock-out mice (Tzingounis et al., 2007). The absence of a Ca^{2+} sensing domain on the channel could explain the slow time course of sI_{AHP} . Nevertheless sI_{AHP} is not completely suppressed in hippocalcin knock-out mice and maybe hippocalcin is not the only Ca^{2+} sensing protein mediating sI_{AHP} activation upon the rise of intracellular Ca^{2+} . Other neuronal Ca^{2+} sensor proteins are also expressed in hippocampus as well as in other brain areas that display sI_{AHP} and could contribute to its activation (Paterlini et al., 2000). For example, hippocalcin expression in cortex is much lower than in hippocampus and neurocalcin δ , another neuronal Ca^{2+} sensor protein, has been shown to perform a comparable role in cortex and could act alongside hippocalcin in activating sI_{AHP} (Villalobos and Andrade, 2010).

Finding the channel generating sI_{AHP} has been the focus of many studies since the early description of sI_{AHP} . The channel underlying I_c was suggested to also be responsible for generating sI_{AHP} and the distinct time courses of the two currents were explained by different channel locations in relation to the site of Ca^{2+} entry i.e. channels generating I_c being located close to Ca_v channels and the channels for sI_{AHP} further away (Lancaster and Adams, 1986). However, it is accepted that $\text{K}_{\text{Ca}1.1}$ channels are responsible for I_c and their characteristics, such as voltage and TEA sensitivity, fast kinetics and big conductance (section 1.2.1), do not match the profile of sI_{AHP} . Another group of channel candidates for sI_{AHP} emerged with the identification of $\text{K}_{\text{Ca}2}$ channels. Because they are voltage-independent and activated by Ca^{2+} , have smaller conductances than $\text{K}_{\text{Ca}1.1}$ channels and are sensitive to TEA only at high millimolar concentrations (section 1.2.2), they have been proposed to generate sI_{AHP} (Lancaster

et al., 1991; Köhler et al., 1996; Marrion and Tavalin, 1998; Stocker et al., 1999; Bowden et al., 2001). However, the apamin sensitivity of K_{Ca2} channels complicates the picture: on the one hand it identified K_{Ca2} channels as being responsible for apamin-sensitive I_{AHP} (Stocker et al., 1999), on the other hand K_{Ca2} channels continued to be advocated as the ones generating apamin-insensitive sI_{AHP} . This was mainly because the $K_{Ca2.1}$ subunit was initially described as apamin-insensitive and its expression overlapped with neurons displaying sI_{AHP} (Köhler et al., 1996; Ishii et al., 1997), but was eventually determined to be apamin-sensitive (Shah and Haylett, 2000a; Strøbaek et al., 2000). Additionally, heteromeric K_{Ca2} channels with intermediate apamin sensitivity, such as $K_{Ca2.1/2.2}$ in heterologous expression system (Ishii et al., 1997), were thought to account for the different pharmacological and kinetic profiles of I_{AHP} and sI_{AHP} (Stocker et al., 1999), but their existence in native tissue has not been shown. In contrast, sI_{AHP} has been recorded in all three K_{Ca2} channel knock-out mice (Bond et al., 2004). Additionally, K_{Ca2} channel can be discounted as the channel responsible for sI_{AHP} as it displays much faster kinetics than seen for sI_{AHP} and are thought to be closely located to Ca_v channels (Marrion and Tavalin, 1998) and thus to restricted domains of Ca^{2+} , while sI_{AHP} is activated by an increase in bulk intracellular Ca^{2+} (Abel et al., 2004).

Furthermore, K_v7 channels have recently been linked with the generation of sI_{AHP} in dentate gyrus and CA3, because sI_{AHP} is reduced in mice deficient in either $K_v7.2$, $K_v7.3$ or $K_v7.5$ (Tzingounis and Nicoll, 2008; Tzingounis et al., 2010). In addition K_v7 channels, especially $K_v7.1$ and $K_v7.2$, are blocked by UCL2077, which has been shown to inhibit $sAHP$ (Shah et al., 2006), and are therefore implicated in underlying sI_{AHP} (Soh and Tzingounis, 2010). Retigabine, an activator of K_v7 channels, increases the rate of sI_{AHP} activation (Kim et al., 2012). But questions remain on how a voltage-gated K_v7 channel should be responsible for a current characterised as voltage-independent, activated by Ca^{2+} and insensitive to K^+ channel blockers. A proposed mechanism for the activation of sI_{AHP} involves PIP_2 , its expression level at the plasma membrane is known to be raised by Ca^{2+} and its participation in K_v7 channel gating (Zhang et al., 2003; Hernandez et al., 2008) could promote their opening at more negative potentials (Andrade et al., 2012). Over-expression of phosphatidylinositol 4 phosphate 5-kinase (PIP5K), the phospholipid kinase catalysing the production of PIP_2 , enhances the Ca^{2+} sensitivity of sI_{AHP} , which suggests a common signalling pathway of Ca^{2+} and PIP_2 to activate sI_{AHP} (Villalobos et al., 2011). Furthermore, the inhibition of PIP5K, for example by PKA (Park et al., 2001), would reduce available PIP_2 and thus hinder K_v7 channel activation, and could present the mechanism by which monoamine neurotransmitter suppress sI_{AHP} (Andrade et al., 2012). K_v7 channels are also known to bind CaM, which in response to a rise in intracellular Ca^{2+} mediates their inhibition, albeit to different degrees (Delmas and Brown, 2005).

1.3 GPCRs and G-proteins

Cholinergic and glutamatergic innervations of the hippocampus formation as well as the modulatory effect of ACh and glutamate on sI_{AHP} have been outlined earlier (section 1.1.2 and 1.2.3), but the mechanisms by which sI_{AHP} is suppressed by these neurotransmitters are not fully identified. ACh and Glutamate exert their action on sI_{AHP} via GPCRs, since agonists of mAChRs and mGluRs mimic and antagonists prevent the suppression of sI_{AHP} by ACh and glutamate, while the modulation of sI_{AHP} is unchanged in the presence of nicotinic acetylcholine receptor and ionotropic glutamate receptor blockers (Cole and Nicoll, 1983 and 1984; Charpak et al., 1990; Ito et al., 1992; Davies et al., 1995). The two groups of GPCRs are subdivided into M_{1-5} (mAChR) and $mGlu_{1-8}$ (mGluR) and various approaches have been used to determine the receptor subtypes mediating the actions of ACh and glutamate on sI_{AHP} . In the case of ACh, both M_1 and M_3 are expressed in the principal cells of the hippocampus (Levey et al., 1995) and thus represent good candidates. M_1 is the prevailing receptor subtype, but cholinergic agonists continue to suppress sI_{AHP} when M_1 is blocked by the M_1 antagonist pirenzepin, the M_1 toxin or by gene deletion (Rouse et al., 2000). The exclusion of M_1 , establishes a role of M_3 in the modulation of sI_{AHP} , which is supported by earlier pharmacological findings showing that the application of the M_3 antagonist 4-DAMP prevents the cholinergic agonist-induced suppression of sI_{AHP} (Pitler and Alger, 1990). An involvement of other mAChRs is unlikely on the basis of their expression and localisation (section 1.1.2) and results of pharmacological studies, in which the suppression of sI_{AHP} by cholinergic agonists is maintained in the presence of M_2 receptor antagonists (Dutar and Nicoll, 1988; Pitler and Alger, 1990). mGluRs are divided into three groups (I) $mGlu_1$ and $mGlu_5$, (II) $mGlu_2$ and $mGlu_3$ and (III) $mGlu_4$, $mGlu_6$, $mGlu_7$ and $mGlu_8$, but only group (I) antagonists prevent the suppression of sI_{AHP} by glutamatergic agonists (Davies et al., 1995; Gereau and Conn, 1995). $mGlu_5$ is the prevailing subtype of the group (I) receptors expressed in CA1 pyramidal neurons (Shigemoto et al., 1992; Fotuhi et al., 1994; Romano et al., 1995) and specific $mGlu_5$, but not $mGlu_1$, antagonists block the suppression of sI_{AHP} by glutamatergic agonists (Mannaioni et al., 2001).

The involvement of M_3 and $mGlu_5$ agrees with findings that the modulation of sI_{AHP} by ACh and glutamate is mediated by GPCRs coupled to pertussis toxin-insensitive G-proteins of the G_q family (Dutar and Nicoll, 1988; Gerber et al., 1992; Offermanns et al., 1994; Blin et al., 1995; Pin and Duvoisin, 1995; Abdul-Ghani et al., 1996). Experiments in knock-out mice have shown that $G\alpha_q$, but not $G\alpha_{11}$, mediates the suppression of sI_{AHP} by ACh and glutamate (Krause et al., 2002). The activation of GPCRs coupled to $G\alpha_q$ stimulates $PLC\beta$ (Fig. 1.3; Smrcka et al., 1991; Arkininstall et al., 1995) leading to the hydrolysis of PIP_2 to produce the second messengers

inositol 1,4,5-triphosphate (IP₃), which causes the release of Ca²⁺ from intracellular stores, and diacylglycerol (DAG), which in turn activates PKC (McLaughlin et al., 2002; Rhee, 2001). Both mAChRs (M_{1/3/5}) as well as group (I) mGluRs (mGlu_{1/5}) have been shown to couple to this second messenger system (Peralta et al., 1988; Abe et al., 1992; Berstein et al., 1992; Schoepp et al., 1999). However, this classical signalling pathway of GPCRs coupled to Gα_q is not mediating the suppression of sI_{AHP} by ACh and glutamate, since their modulatory effect on sI_{AHP} is maintained in the presence of PLC inhibitors as well as in PLCβ knock-out mice (Krause and Pedarzani, 2000; Young et al., 2004). Additionally, the cholinergic and glutamatergic modulation of sI_{AHP} is unchanged when IP₃-sensitive stores are blocked by IP₃ receptor antagonists (Krause and Pedarzani, 2000) or when PKC inhibitors are applied (Gerber et al., 1992; Sim et al., 1992; Engisch et al., 1996).

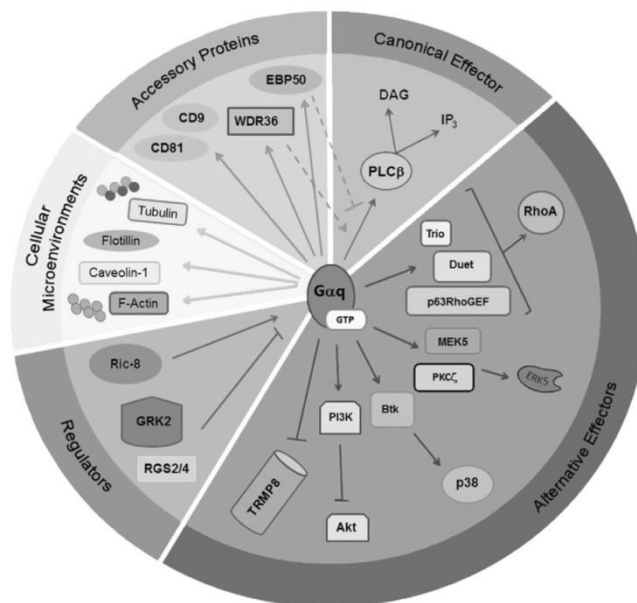


Figure 1.3 Gα_q signalling. Following the activation by GPCRs, Gα_q stimulates its canonical effector phospholipase C β, which leads to the production of the second messengers inositol 1,4,5-triphosphate and diacylglycerol. Apart from this classical signalling pathway, Gα_q also signals via alternative effectors and is involved in controlling cellular microenvironments such as the cytoskeleton. Gα_q signalling is assisted by accessory proteins, which for example support the coupling of Gα_q with GPCRs, and is controlled by various regulators that for instance accelerate the intrinsic GTPase activity of Gα_q. (from Sanchez-Fernandes et al, 2014)

Since the ACh- and glutamate-induced suppression of sI_{AHP} involves the GPCRs, M₃ and mGlu₅, and the G_q-protein, but not their principal signalling pathway, the G_q-protein must mediate the regulation of neuronal excitability in conjunction with other downstream effectors (Fig. 1.3). This question is central to this thesis and thus functions and properties of G-proteins will be examined closely. As seen above, G-proteins are coupled to GPCRs and link extracellular stimuli, which activate the receptors at the cell surface, to intracellular signalling cascades and thus determine a cell's response. G-proteins belong to the superfamily of GTPases and are

heterotrimeric guanine nucleotide-binding proteins, which consist of α , β and γ subunits (Fung et al., 1981; Sternweis and Robishaw, 1984; Hamm and Gilchrist, 1996) and function as molecular switches alternating between inactive (GDP-bound) and active (GTP-bound) states. They are defined by their α subunit, whose sequence similarities and functional characteristics subdivide G-proteins into four families G_s , G_i , G_q and G_{12} (Simon et al., 1991; Wilkie et al., 1992). Principally, G-protein α subunits ($G\alpha$) of the G_s ($G\alpha_s$ and $G\alpha_{olf}$) and G_i ($G\alpha_i$, $G\alpha_o$, $G\alpha_z$, but not $G\alpha_t$ and $G\alpha_{gust}$ (cGMP phosphodiesterase)) families target AC, which is either stimulated (G_s) or inhibited (G_i), with therefore opposite effects on intracellular cAMP levels. Alpha subunits of the G_q family ($G\alpha_q$, $G\alpha_{11}$, $G\alpha_{14}$, $G\alpha_{15/16}$) activate PLC β and cause the formation of second messengers IP $_3$ and DAG (Fig. 1.3), while members of the G_{12} -protein family ($G\alpha_{12}$, $G\alpha_{13}$) activate small GTPases of the Rho family (McCudden et al., 2005). In addition to the diversity of $G\alpha$, multiple subtypes of G-protein β ($G\beta$) and γ ($G\gamma$) subunits have also been identified ($G\beta_{1-5}$, $G\gamma_{1-12}$; Ray et al., 1995; McCudden et al., 2005) and unlike initial assumptions the $G\beta\gamma$ dimer does not only assist $G\alpha$ coupling to GPCRs, but has its own array of cellular targets including ion channels like GIRK (K $_{ir}$ 3) and Ca $_v$ channels, PLC β , AC, mitogen-activated protein kinases (MAPKs) and G-protein-coupled receptor kinases (GRKs) as well as small GTPases (Clapham and Neer, 1997; McCudden et al., 2005).

Structurally, $G\alpha$ consists of two domains that create a nucleotide-binding pocket: an α -helical domain and a Ras-like GTPase domain composed of α helices as well as β sheets (Fig. 1.4A and Fig. 2.1; Lambright et al., 1994). The Ras-like GTPase domain is conserved throughout the superfamily of GTPases, is responsible for the binding of the nucleotide and includes three flexible switch regions that mediate the conformational change of $G\alpha$ depending on whether GDP or GTP is bound (Sprang, 1997). $G\beta$ is composed of seven β -sheet repeats (WD40 repeats) that arrange in a propeller-like structure and interact with $G\alpha$, and of an α -helical amino-terminus forming a coiled coil with the amino-terminal α -helix of $G\gamma$ at its entire length and thus explains the high affinity of $G\beta$ and $G\gamma$ that lets them act as a dimer at all times (Fig. 1.4A; Wall et al., 1995; Sondek et al., 1996; Clapham and Neer, 1997).

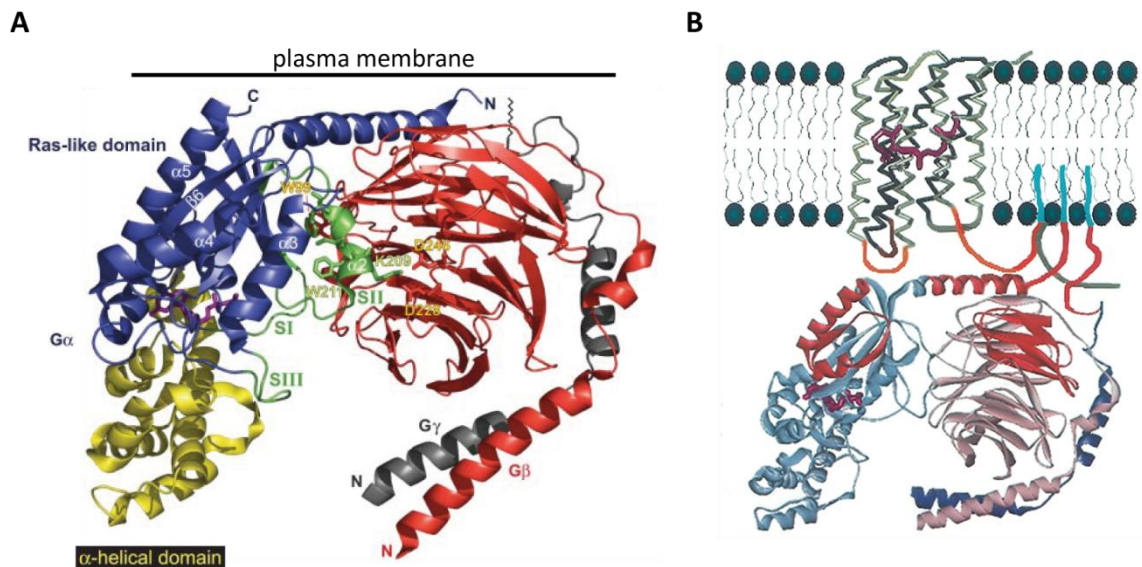


Figure 1.4 Structure of the heterotrimeric G-protein and its binding to the G-protein coupled receptor. (A) The heterotrimeric G-protein consist of $G\alpha$ and the $G\beta\gamma$ dimer. $G\alpha$ is composed of an α -helical domain (yellow) and a Ras-like GTPase domain (blue). The flexible switch regions (SI–III) of $G\alpha$ are shown in green and bound GDP in magenta. The dimer is formed of $G\beta$ (red) and $G\gamma$ (grey), whose prenylated carboxyl-terminus is depicted as a saw-tooth wave. Important residues of $G\alpha$ and $G\beta$ that interact at the switch region/ $G\beta$ contact site are indicated. (adapted from Johnston and Siderovski, 2007) (B) The seven transmembrane G-protein coupled receptor is depicted in green with transmembrane segments 1, 5, 6 and 7 (light green) at the front and segments 2, 3 and 4 (dark green) at the back. The receptor couples to the G-protein via the second (brown) and third (orange) intracellular loops and the carboxyl-terminus (orange) that leads to the palmitoylation site (cyan). Lipid modifications on the G-protein are also depicted (cyan). Several regions (red) of the G-protein bind to the G-protein coupled receptor including the amino- and carboxyl-termini and the $\alpha 4$ - $\beta 6$ loop of $G\alpha$ and the carboxyl-terminus and the sixth β -sheet repeat of $G\beta$ as well as the carboxyl-terminus of $G\gamma$. (from Hamm, 1998)

In contrast to their separate functions and signalling pathways in the active state, $G\alpha$ and the $G\beta\gamma$ dimer form a complex, when G-proteins are inactive i.e. GDP-bound (Fig. 1.5). The association between $G\alpha$ and $G\beta\gamma$ requires an intact $G\alpha$ amino-terminus (Neer et al., 1988), whose residues are responsible for interaction with $G\beta$ (Fig. 1.4A and Fig. 2.1; Wall et al., 1995; Lambright et al., 1996). $G\beta$ also binds the switch II region of $G\alpha$ and thus stabilizes the inactive G-protein preventing the release of GDP from $G\alpha$ (Fig. 1.4A and Fig. 2.1; Wall et al., 1995; Lambright et al., 1996). In the case of G_{s^-} , G_{q^-} and G_{12^-} -protein families the $G\beta\gamma$ dimer is also responsible for the plasma membrane targeting of $G\alpha$ (Evanko et al., 2000 and 2001). G-proteins attach to the plasma membrane by lipid modifications and the $G\beta\gamma$ dimer is anchored to the plasma membrane following prenylation at the carboxyl-terminus of $G\gamma$ (Fig. 1.4B; Simonds et al., 1991; Muntz et al., 1992). For $G\alpha$ a two-signal model is proposed: firstly plasma membrane targeting either by myristoylation at the amino-terminus of α subunits of the G_T -protein family or by $G\beta\gamma$ interaction of α subunits of the $G_{s/q/12^-}$ -protein families and secondly stable attachment to the plasma membrane by palmitoylation at the amino-terminus of all α subunits (Fig. 1.4B and Fig. 2.1; Evanko et al., 2000; Chen and Manning, 2001).

Membrane attachment and complex formation of G α and G $\beta\gamma$ are essential for the binding of G-proteins to GPCRs and their subsequent activation. The carboxyl-terminus as well as regions of the amino-terminus and the α 4- β 6 loop of G α have been established as sites of contact with GPCRs (Fig. 1.4B; Hamm et al., 1988; Conklin and Bourne, 1993; Onrust et al., 1997; Oldham and Hamm, 2008; Hu et al., 2010), with the last amino acids of the carboxyl-terminus being critical for GPCR specificity (Martin et al., 1996; Kostenis et al., 1997). G α primarily contacts the seven transmembrane GPCRs at the third intracellular loop that itself mediates the coupling to a specific G α (Fig. 1.4B; Taylor et al., 1994; Kostenis et al., 1997; Bourne, 1997), but also at the second intracellular loop and at the intracellular carboxyl-terminus of GPCRs (Fig. 1.4B; Conklin and Bourne, 1993). Additionally, the carboxyl-terminus and the sixth β -sheet repeat of G β bind to the third intracellular loop and the carboxyl-terminus of the GPCR (Fig. 1.4B; Taylor et al., 1994 and 1996; Bourne, 1997; Wu et al., 1998 and 2000; Hou et al., 2001; Mahon et al., 2006), while the carboxyl-terminus of G γ contributes to GPCR binding (at the carboxyl-terminus) as well as to receptor specificity (Fig. 1.4B; Yasuda et al., 1996; Bourne, 1997; Hou et al., 2000). Furthermore, point mutations in G β at regions contacting the switch II region and the amino-terminus of G α prevent the exchange of GDP to GTP at G α and thus show the importance of complex formation for G-protein activation (Ford et al., 1998).

GPCR and G-protein interaction occurs rapidly (< 100 ms; Hein et al., 2005 and 2006), but whether G-protein coupling to GPCRs is established before ligand-binding to the receptor (pre-coupled model) or requires an activated GPCR (collision model) is not fully characterised (Oldham and Hamm, 2008). Some studies have reported G-protein binding to inactive GPCRs (Nobles et al., 2005; Galés et al., 2005 and 2006). But others have shown that GPCR activation produces a conformational change in the receptor, in particular a rearrangement of the third and sixth transmembrane segments, which in turn reveals the binding domain for the carboxyl-terminus of G α (Gether et al., 1995; Farrens et al., 1996; Janz and Farrens, 2004; Park et al., 2008; Scheerer et al., 2008). In either case, activated receptor-induced structural changes are relayed to the G-protein and cause the release of GDP by perturbing the receptor-bound carboxyl-terminus and α 4- β 6 loop of the Ras-like GTPase domain of G α , which are both linked to the β 6- α 5 loop containing a conserved nucleotide-binding motif (TCAT) (Fig. 1.4A and Fig. 2.1; Sprang, 1997; Kisselev et al., 1998; Oldham et al., 2006; Johnston and Siderovski, 2007; Oldham and Hamm, 2008). Mutations in this motif have been shown to considerably decrease GDP affinity (Thomas et al., 1993). The tight coupling of G α and GDP slows the release of GDP upon receptor activation and constitutes the rate-limiting step in the signalling cascade of GPCRs (Ferguson et al., 1986). Rates for G-protein activation to be completed range from a few hundreds of milliseconds to seconds (Bünemann et al., 2003; Hein et al., 2006; Nikolaev et al.,

2006; Adjobo-Hermans et al., 2011), which is substantially slower than GPCR activation and receptor association with the G-protein (Villardaga et al., 2003; Lohse et al., 2008). Following GDP release, GTP, which is present in excess over GDP, binds to a conserved nucleotide-binding motif (DVGGQ) in the Ras-like GTPase domain of $G\alpha$ that partly overlaps with the switch II region (Fig. 2.1; Bourne et al., 1991; Sprang, 1997; Johnston and Siderovski, 2007). GTP binding causes the flexible switch regions of $G\alpha$ to undergo a dramatic movement that separates the G-protein complex into $G\alpha$ and $G\beta\gamma$ dimer and both dissociate from the GPCR (Fig. 1.5; Noel et al., 1993; Coleman et al., 1994; Lambright et al., 1994; Wall et al., 1995). Activated $G\alpha$ and the now uninhibited $G\beta\gamma$ dimer engage in the regulation of their various effectors described above. The innate GTPase activity of $G\alpha$ is responsible for the termination of $G\alpha$ signalling by hydrolysing the γ phosphate of GTP, leaving $G\alpha$ bound to GDP (Fig. 1.5; Hamm and Gilchrist, 1996). Three residues of the switch regions have been shown to be essential for GTP hydrolysis (R183, T186 and Q209 in $G\alpha_q$; Noel et al., 1993; Coleman et al., 1994; Sondek et al., 1994; Johnston and Siderovski, 2007). The reversal of the conformational changes caused by GTP binding restores the affinity of $G\alpha$ for the $G\beta\gamma$ dimer and re-establishes the trimeric complex that G-protein adopt in their inactive state, thus completing the G-protein cycle (Fig. 1.5).

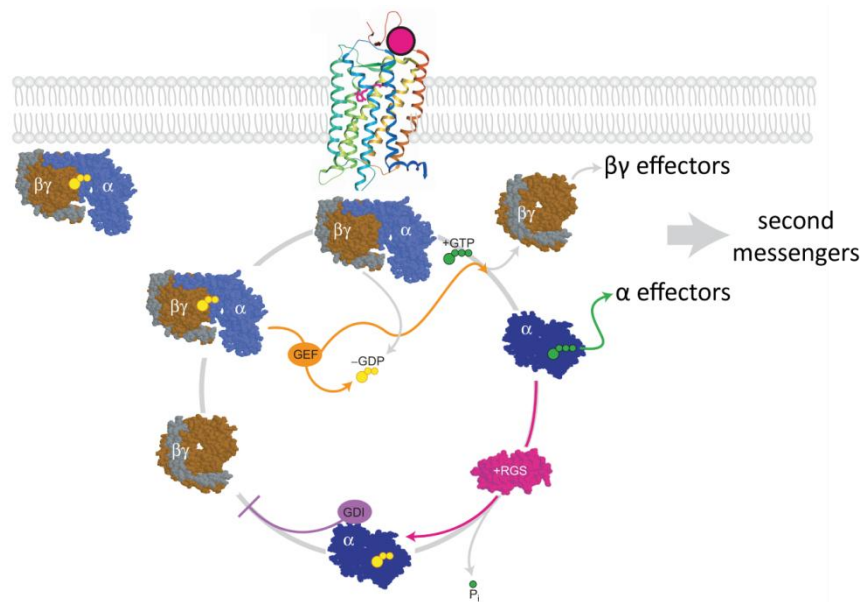


Figure 1.5 G-protein activation and deactivation cycle. The activated G-protein coupled receptor couples to the heterotrimeric G-protein consisting of $G\alpha$ (blue), $G\beta$ (brown) and $G\gamma$ (grey). The receptor acts as a guanine nucleotide exchange factor (orange) and facilitates GDP (yellow, the small circles depict the two phosphates) release from $G\alpha$. Subsequent GTP (green, the small circles depict the three phosphates) binding causes the G-protein to activate and separate into $G\alpha$ and the $G\beta\gamma$ dimer, which in turn signal to their downstream effectors. GTPase accelerating proteins such as regulators of G-protein signalling (magenta) accelerate the intrinsic GTPase activity of $G\alpha$ that terminates $G\alpha$ signalling and results in GDP-bound $G\alpha$. Guanine nucleotide dissociation inhibitors (purple) bind inactive $G\alpha$ and hinder the release of GDP as well as re-assembly of $G\alpha$ with the $G\beta\gamma$ dimer. (from Preininger and Hamm, 2004)

The cycle of G-protein activation and deactivation is additionally controlled by various regulators that influence each step in the sequence. For example, GPCRs act as guanine nucleotide exchange factors (GEFs), since they facilitate the GDP/GTP exchange on $G\alpha$ and thus catalyse G-protein activation (Fig. 1.5). Active GPCRs are themselves objects of regulation by GRKs, which phosphorylate the receptor causing its desensitization and enable the binding of β -arrestins that initiate GPCR internalization (Pitcher et al., 1998). The signalling of activated $G\alpha$ is restricted by its intrinsic GTPase activity, whose rate of GTP hydrolysis is dramatically enhanced by GTPase accelerating proteins (GAPs) such as members of the regulator of G-protein signalling (RGS) family (Fig. 1.5; Druey et al., 1996; Watson et al., 1996; Ross and Wilkie, 2000). RGS interact with activated $G\alpha$ and catalyse its GTPase activity not by directly engaging in the GTP hydrolysis processes, but by stabilizing the switch regions of the GTP-bound $G\alpha$ (Berman et al., 1996; Tesmer et al., 1997). In the case of $G\alpha_q$ the GAP RGS4 accelerated GTP hydrolysis to < 100 ms (Mukhopadhyay and Ross, 1999). With $G\alpha$ returned to the GDP-bound state, guanine nucleotide dissociation inhibitors (GDIs) such as GoLoco motif-containing proteins assert their effect by binding to inactive $G\alpha$ and inhibiting the release of GDP (Willard et al., 2004). This renders $G\alpha$ ineffective and presents a mechanism to control $G\alpha$ signalling. Because their binding sites are overlapping, GDIs can also prevent the association of $G\alpha$ with the $G\beta\gamma$ dimer (Fig. 1.5; Preininger and Hamm, 2004). Once the heterotrimeric G-protein complex is restored, the $G\beta\gamma$ dimer also acts as a GDI given that it stabilizes the GDP-bound $G\alpha$ by sequestering its switch regions as described before.

$G\alpha$ becomes constitutively active by mutating residues in the switch regions that are essential for its intrinsic GTPase activity (Fig. 2.1; Noel et al., 1993; Coleman et al., 1994; Sonddek et al., 1994; Johnston and Siderovski, 2007). Mutating these key residues results in the inability of $G\alpha$ to hydrolyse bound GTP and thus creates a $G\alpha$ that remains in the active state and which in turn constitutively activates its effectors (Graziano and Gilman, 1989; Landis et al., 1989; Wong et al., 1991; Gupta et al., 1992). In the case of $G\alpha_q$ the mutation of residue arginine (R)183 to cystine (C) or glutamine (Q)209 to leucine (L) results in constitutively active $G\alpha_q$ (Fig. 2.1; Conklin et al., 1992; De Vivo et al., 1992; Kalinec et al., 1992; Wu et al., 1992; Qian et al., 1993). On the other hand, many GTP-binding proteins are rendered inactive by preventing the binding of GTP through a mutation of aspartate (D) into asparagine (N) in the conserved motif (NKXD; Fig. 2.1), which results in the binding of xanthine nucleotides instead of guanine nucleotides (Yu et al., 1997). However, in the case of $G\alpha$ subunits this single mutation is insufficient and a double mutation is necessary to convey the xanthine nucleotide binding preference to $G\alpha$ (Q209 to L and D277 to N in $G\alpha_q$; Fig. 2.1; Yu et al., 1997; Yu and Simon, 1998). Furthermore, $G\alpha_q$ has been studied using fluorescence microscopy techniques by

attaching fluorophores, such as green fluorescent protein (GFP) or enhanced cyan fluorescent protein (ECFP), to its carboxyl-terminus or in a loop of the α -helical domain (between residues 124 and 125; Fig. 1.6 and Fig. 2.1) (Hughes et al., 2001; Witherow et al., 2003).

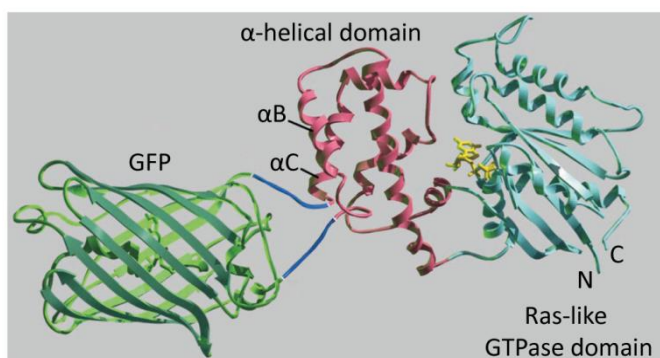


Figure 1.6 **G α with fluorophore attachment.** Green fluorescent protein (green) inserted in a loop of the α -helical domain of the G α subunit. (from Hughes et al., 2001)

1.4 Small GTPases

Since sl_{AHP} suppression by ACh and glutamate through the metabotropic receptors M₃ and mGlu₅ and the G_q-protein does not involve the classical signal transduction pathway of G α_q (section 1.2.3 and 1.3), the inhibitory effect of ACh and glutamate must be conveyed by other downstream effectors of G α_q . Small GTPases have emerged as mediators of GPCR signalling (van Biesen et al., 1996; Seasholtz et al., 1999; Sah et al., 2000; Marinissen and Gutkind, 2001; Bhattacharya et al., 2004). Due to their expression in the hippocampus (Olenik et al., 1997; O’Kane et al., 2003), reports of them being effectors of GPCRs coupled to G-proteins of the G_q family (Mitchell et al., 1998; Sagi et al., 2001; Booden et al., 2002; Chikumi et al., 2002; Dutt et al., 2002) and their ability to modulate ion channel activity (Wilk-Blaszczak et al., 1997; Cachero et al., 1998; Storey et al., 2002; Staruschenko et al., 2004; Yatani et al., 2005; Rossignol and Jones, 2006; Pochynyuk et al., 2007) small GTPases represent potential candidates in the signal transduction cascade leading to the suppression of sl_{AHP} by ACh and glutamate.

Small GTPases are monomeric G-proteins, with molecular weights of 20–40 kDa and their extensive superfamily comprises five subgroups: Ras, Rho, Rab, Sar1/Arf and Ran (Takai et al., 2001). Like heterotrimeric G-proteins they act as molecular switches cycling between an inactive GDP-bound and an active GTP-bound state. Small GTPases signal to a multitude of effectors and regulate a variety of cellular processes including cell cycle progression, gene transcription, microtubule organization, intracellular vesicular and nucleocytoplasmic transport, regulation of cell growth and motility (Takai et al., 2001; Jaffe and Hall, 2005). Members of the Rho-GTPase subfamily are primarily known for their regulation of the actin

cytoskeleton (Machesky and Hall, 1996; Hall, 1998; Aspenström et al., 2004). For example, Rac causes the formation of the actin filament mesh found in membrane ruffles and lamellipodia and Cdc42 produces actin spikes known as filopodia, both associated with cell motility and process outgrowth, while Rho is responsible for the formation of focal adhesions and long actin filament bundles known as stress fibres and causes cell rounding and process retraction (Paterson et al., 1990; Ridley and Hall, 1992; Ridley et al., 1992; Kozma et al., 1995; Nobes and Hall, 1995; Katoh et al., 1998; Luo, 2000). In hippocampal pyramidal neurons Rho-GTPases are also associated with the outgrowth or retraction of dendritic spines (Nakayama et al., 2000).

Cellular processes regulated by Rho-GTPases involve signalling pathways downstream of GPCRs (Buhl et al., 1995; Gohla et al., 1998; Katoh et al., 1998; Kjøller and Hall, 1999; Seasholtz et al., 1999). The signal transduction of activated GPCRs is mediated through the interaction of their associated G-protein α subunit ($G\alpha$) with GEFs, which serve as activators of small GTPases (Hart et al., 1998; Kozasa et al., 1998; Fukuhara et al., 1999 and 2000; Booden et al., 2002; Lutz et al., 2005). Downstream targets of the small GTPase RhoA include serine/threonine kinases like Rho-kinase (ROCK; Leung et al., 1995; Kimura et al., 1996; Matsui et al., 1996) and citron (Madaule et al., 1995) and protein kinase N (PKN; Amano et al., 1996; Watanabe et al., 1996), myosin-binding subunit of myosin light chain phosphatase (Kimura et al., 1998) as well as RhoA-binding proteins such as rhophilin (Watanabe et al., 1996), rhotekin (Reid et al., 1996) and mDia (Watanabe et al., 1997).

Structurally, like all members of the superfamily of GTPases including the α subunit of heterotrimeric G-proteins, small GTPases contain a conserved domain consisting of α helices, β sheets and connecting loops (G1–5) that convey their guanine nucleotide-binding capacity as well as their GTPase activity (Bourne et al., 1991). Guanine nucleotide-binding occurs at conserved motifs of small GTPases with the guanine base being recognised by the (N/T)KXD motif in G4 and by the (T/G/C)(C/S)A motif in G5, while the β phosphate interacts with the GXXXXGK(S/T) motif in G1/P-loop (phosphate-binding loop; Sprang, 1997; Paduch et al., 2001; Vetter and Wittinghofer, 2001). Depending on whether small GTPases are bound to GDP or GTP, a conformational change mediated by the flexible switch regions I and II occurs (Fig. 1.7; Milburn et al., 1990; Wei et al., 1997; Ihara et al., 1998). The γ phosphate of GTP interacts with the conserved threonine in the XTX motif in G2/switch I and with the DXXG motif in G3/switch II of small GTPases and causes the structural change, which is reversed once GTP is hydrolysed (Sprang, 1997; Paduch et al., 2001; Vetter and Wittinghofer, 2001). The switch regions of small GTPases are critical for effector binding and the conformational change of switch I and II in the active GTP-bound state uncovers numerous binding sites, many of them overlapping (Corbett and Alber, 2001; Vetter and Wittinghofer, 2001; Biou and Cherfils, 2004).

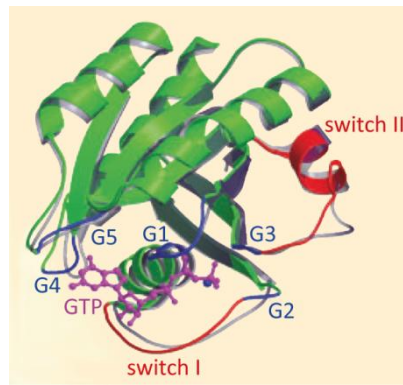


Figure 1.7 Structure of small GTPases and conformational change of the switch regions upon GTP binding. Small GTPase bound to GTP is shown in green (α helices and β sheets), red (switch regions), blue (loops G1–5) and magenta (GTP). The structure of the small GTPase bound to GDP is displayed in grey. (from Wennerberg et al., 2005)

The activated state is terminated by hydrolysis of the γ phosphate of the bound GTP and the small GTPase returns to its inactive GDP-bound state. The intrinsic GTPase activity of small GTPases, $k_{\text{cat}} 0.02 \text{ min}^{-1}$, is much lower than that of G-protein α subunits, $k_{\text{cat}} 3\text{--}5 \text{ min}^{-1}$ (Bourne et al., 1991). Akin to heterotrimeric G-protein α subunits, a conserved glutamine (Q63 in RhoA; equivalent to Q209 in $G\alpha_q$) in G3/switch II plays a central role in the hydrolysis of GTP in small GTPases (Pai et al., 1990; Bourne et al., 1991; Sprang, 1997). Mutating this residue renders small GTPases deficient in their ability to hydrolyse GTP, which results in small GTPases that are constitutively active (Der et al., 1986). Furthermore, an arginine (R), which in $G\alpha$ (R183 in $G\alpha_q$) interacts with the γ phosphate of GTP and is essential in GTP hydrolysis (Noel et al., 1993), is absent in small GTPases and contributes to the lower GTPase activity of small GTPases (Paduch et al., 2001). Small GTPases rely on GAPs (Fig. 1.8; Trahey and McCormick, 1987) to provide the missing arginine (also called the arginine finger; Ahmadian et al., 1997; Li et al., 1997; Scheffzek et al., 1997; Nassar et al., 1998) and to catalyse GTP hydrolysis to $k_{\text{cat}} 32\text{--}72 \text{ min}^{-1}$ (Zhang et al., 1998). GAPs are subfamily-specific, but their mechanism to promote GTP hydrolysis is similar (Gamblin and Smerdon, 1998; Scheffzek et al., 1998). GAP binding stabilizes the switch regions of the small GTPase and ensures the proper alignment of the conserved glutamine (Q63 in RhoA) allowing it to perform its GTPase activity (Resat et al., 2001; Moon and Zheng, 2003). Small GTPases in their inactive GDP-bound state can then be reactivated by the release of GDP and subsequent binding of GTP.

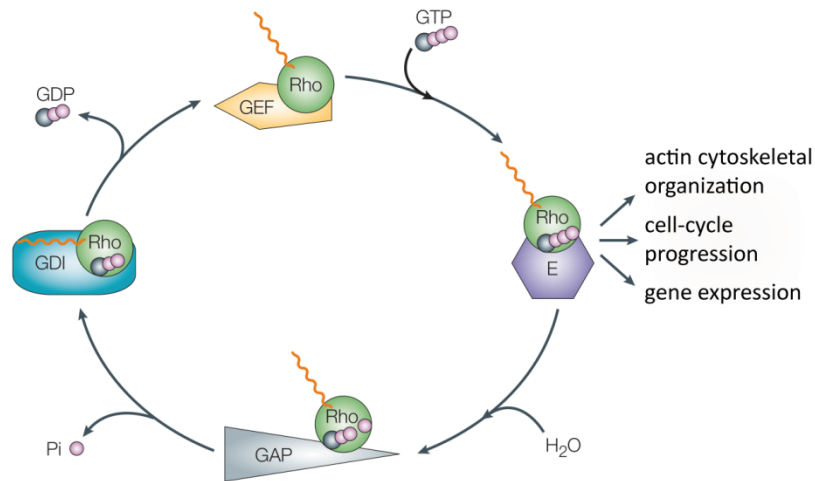


Figure 1.8 Small GTPase activation and deactivation cycle. Rho-GTPases (green) are molecular switches that cycle between an inactive GDP-bound state and an active GTP-bound state (GDP and GTP, blue circle with small purple circles depicting the phosphates). These two conditions are regulated by guanine nucleotide dissociation inhibitors (blue) that hinder GDP release and keep small GTPases inactive, by guanine nucleotide exchange factor (yellow) that promote the activation of small GTPases by accelerating exchange of GDP to GTP and by GTPase accelerating proteins (grey) that facilitate GTPase activity. Membrane association of Rho-GTPases is conveyed by a hydrophobic moiety (orange wavy line) at the carboxyl-terminus, which in the inactive state is shielded by GDI and thus ensures the cytosolic localisation of Rho-GTPase. Bound to their effectors (purple) Rho-GTPases are responsible for numerous cellular processes including the regulation of the actin cytoskeleton, cell-cycle progression and gene expression. (from Rossman et al., 2005)

The activation and deactivation cycle of small GTPase is not only assisted by the aforementioned GAPs, but also by two other classes of regulators namely GEFs, which activate small GTPases by promoting the exchange of GDP to GTP, and GDIs, which keep small GTPases inactive by preventing GDP release (Fig. 1.8; Boguski and McCormick, 1993). In their inactive state small GTPases are bound to GDP and in the case of Rho- and Rab-GTPases this conformation is stabilized by subfamily-specific GDIs, which inhibit nucleotide exchange and thus the activation of these small GTPases (Vetter and Wittinghofer, 2001). Rho-GTPases are prenylated at the conserved CAAX motif of the carboxyl terminus and this lipid modification, mainly through geranylgeranylation, mediates their attachment to membranes (Adamson et al., 1992a; Wennerberg and Der, 2004). The linkage of a geranylgeranyl isoprenoid group makes Rho-GTPases more hydrophobic than, for example, the farnesylated Ras-GTPases (Seabra, 1998). GDIs are able to extract Rho-GTPases from membranes and sequester them in the cytoplasm by shielding the prenyl group in a hydrophobic pocket of their carboxyl-terminus and the amino-terminus of GDIs binds to the switch regions of the small GTPases hindering the association of GEFs and thereby the release of GDP (Gosser et al., 1997; Hoffman et al., 2000; Scheffzek et al., 2000). In the cell the concentration of Rho-GDI and Rho-GTPases is similar, suggesting that the majority of Rho-GTPases is associated with GDIs and therefore

inactive (Michaelson et al., 2001). The release of GDP presents the rate-limiting step of the signalling cascade of any small GTPase and its intrinsic rate is slow, $k_{\text{diss}} 0.001\text{--}0.01 \text{ min}^{-1}$, however, GDP release is facilitated by GEFs that accelerate the activation of small GTPases up to 10^5 -fold (Klebe et al., 1995; Lenzen et al., 1998; Hutchinson and Eccleston, 2000). GEF association causes a structural disturbance of the nucleotide-binding pocket of small GTPases and as a result GDP-binding becomes unstable (Renault et al., 2001; Hoffman and Cerione, 2002). Small GTPase-interacting GEFs are subfamily specific, for example RasGEFs are characterised by a Cdc25 homology domain (Boguski and McCormick, 1993; Chardin et al., 1993) and the majority of RhoGEFs contain a Dbl homology (DH) domain usually in combination with a pleckstrin homology (PH) domain (Cerione and Zheng, 1996; Schmidt and Hall, 2002; Rossman et al., 2005), while another group of RhoGEFs contain a Dock homology region (DHR) domain (Côté and Vuori, 2002). Following the release of GDP, the small GTPase, still in complex with a GEF, transiently exists in a nucleotide-free state, before GTP binding and the subsequent separation from the GEF allows the now active small GTPase to interact with its downstream targets (Vetter and Wittinghofer, 2001).

Small GTPases become constitutively active through the mutation of residues involved in GTP hydrolysis (Barbacid, 1987). As described before a glutamine (Q63 in RhoA) of switch II is essential for GTPase activity and its mutation into leucine (L) results in the inability of small GTPases to hydrolyse GTP (Der et al., 1986). Furthermore, constitutively active small GTPases are also generated by mutating the P-loop residue glycine (G14 in RhoA) into valine (V) (Seeburg et al., 1984; Garrett et al., 1989). Since this residue of the P-loop is not affected by the conformational change following GTP binding, the inhibitory effect on GTPases activity of the valine substitution (V14 in RhoA) cannot be caused by a direct involvement in GTP hydrolysis (Krengel et al., 1990; Milburn et al., 1990). Instead, the valine side chain perturbs the space and thus the orientation of the glutamine (Q63 in RhoA) of switch II, which hinders its ability to hydrolyse GTP (Krengel et al., 1990; Milburn et al., 1990). On the other hand, inactive small GTPases show a reduced affinity for GTP and have initially been described for Ras-GTPases displaying a serine (S) to asparagine (N) mutation at residue 17 (Feig and Cooper, 1988); the corresponding mutation in RhoA is a threonine (T) to asparagine (N) substitution at residue 19 (Qiu et al., 1995). These inactive mutants have an increased affinity for GEFs and this competitive binding prevents the interaction of GEFs with endogenous small GTPases (Feig, 1999). Inactive small GTPases are neither bound to GDP nor to GTP i.e. exist in a nucleotide-free state that in the normal cycle is only transitional, which prevents the interaction with downstream effectors and thus disrupts the signal transduction pathway (Feig, 1999; Strassheim et al., 2000).

Since small GTPases are able to mediate GPCR signalling, the potential participation of small GTPases in the transduction pathway used by ACh and glutamate to suppress sI_{AHP} was investigated in the laboratory of one of my supervisors. Whole-cell patch clamp recordings of sI_{AHP} in hippocampal pyramidal neurons in the presence of a RhoA inhibitory peptide showed a reduction in the cholinergic inhibition of sI_{AHP} (P. Pedarzani, personal communication). Furthermore, the intracellular application of C3-exoenzyme, which inhibits RhoA by ADP-ribosylation (Narumiya et al., 1988; Aktories and Hall, 1989; Sekine et al., 1989), reduces the inhibitory effect of cholinergic as well as glutamatergic agonist on sI_{AHP} (P. Pedarzani, personal communication). This indicates that RhoA is part of the signalling pathway mediating the suppression of sI_{AHP} by ACh and glutamate.

1.5 Aims and Objectives

The slow afterhyperpolarizing current (sI_{AHP}), which is activated by Ca^{2+} and follows a train of action potentials, contributes to the regulation of neuronal excitability and firing properties of hippocampal pyramidal neurons by being responsible for spike frequency adaptation i.e. the cessation of firing in response to a prolonged stimulus. sI_{AHP} is suppressed by various neurotransmitters and thus presents a point of convergence allowing separate signalling pathways to influence neuronal excitability. While the signalling cascade of monoamine transmitters to suppress sI_{AHP} is established, the pathway used by ACh and glutamate is not well characterised. The aim of this study was to investigate the nature of the signal transduction pathway mediating the suppression of sI_{AHP} following the cholinergic activation of GPCRs. The mAChR M_3 couples to the heterotrimeric G_q -protein and the participation of the G_q -protein α subunit ($G\alpha_q$) in sI_{AHP} suppression by cholinergic agonists has been shown (Krause et al., 2002). The involvement of the small GTPase RhoA in this signalling pathway and its role as a downstream effector of $G\alpha_q$ was to be investigated by the work undertaken in this study. The potential protein-protein interaction of $G\alpha_q$ and RhoA was studied by performing co-immunoprecipitation and fluorescence resonance energy transfer (FRET) experiments in heterologous expression system. The ability of the small GTPase RhoA to associate with $G\alpha_q$ would indicate that both proteins could also be part of a common signal transduction pathway that is responsible for the inhibitory effect of ACh on sI_{AHP} observed in hippocampal pyramidal neurons. In order to identify a RhoA involvement in the suppression of sI_{AHP} , constitutively active or inactive RhoA mutants were introduced into hippocampal pyramidal neurons either by the intracellularly application of purified RhoA protein or by Sindbis virus infection and the effect of mutant RhoA on sI_{AHP} was studied by whole-cell patch clamp electrophysiology.

2 Materials and Methods

2.1 Materials

2.1.1 DNA constructs

The following DNA constructs were used in this thesis and were either obtained from other researchers or constructed by myself (section 2.2.13). Plasmid DNA was prepared by transforming bacteria (section 2.2.12.7) followed by the growth of bacteria cultures and the isolation of plasmid DNA (section 2.2.12.8). The DNA was used to transfect cells (section 2.2.2.1), which were subsequently used to prepare cell lysates for Western blotting (section 2.2.3.1) or to perform microscopy experiments (section 2.2.11). The pGex plasmids were used to perform protein purifications (section 2.2.7). The pSinrep5 and Sindbis helper plasmids were used to produce Sindbis virus (section 2.2.10) that was used to infect cells and cultured hippocampal neurons (section 2.2.2.3).

Construct name	Plasmids	Researcher
<i>Small GTPase RhoA</i>		
RhoA	pRK5-myc-RhoA	J. Pitcher
RhoA-V14	pRK5-myc-RhoA-G14V	J. Pitcher
RhoA-N19	pRK5-myc-RhoA-T19N	J. Pitcher
Venus-RhoA	pRK5-myc-Venus-RhoA	L. Gallasch
VP16-RhoA-V14	pVP16-4-RhoA-G14V	M. Stocker
<i>G-protein Gα_q</i>		
Gα _q	pcDNA3.1-EE-Gα _q	J. Pitcher
Gα _q -L209	pcDNA3.1-EE-Gα _q -Q209L	J. Pitcher
Gα _q -L209/N277	pcDNA3.1-EE-Gα _q -Q209L-D277N	J. Pitcher
Gα _q -ECFP	pECFP-N1-Gα _q (COOH-terminus tag)	G. Willars
Gα _q -ECFP- Gα _q	pECFP-N1-Gα _q (loop tag)	G. Willars
Gα _q -ECFP-Gα _q -C183	pcDNA1-ECFP-Gα _q -R183C (loop tag)	L. Scarlata
Gα _q -ECFP-Gα _q -L209	pcDNA3.1-EE-ECFP-Gα _q -Q209L (loop tag)	L. Gallasch
<i>Protein purification</i>		
GST-RhoA-V14	pGEX-6P-1-RhoA-G14V	J. Pitcher
GST-RhoA-N19	pGEX-6P-1-RhoA-T19N	J. Pitcher
GST	pGEX-4T	M. Stocker
GST	pGEX-6P-1	J. Pitcher
<i>Sindbis virus</i>		
EGFP control	pSinrep5-EGFP	A. Jeromin
RhoA-V14	pSinrep5-RhoA-G14V-EGFP	L. Gallasch
RhoA-N19	pSinrep5-RhoA-T19N-EGFP	L. Gallasch
Helper	pHelper-DH-BB (tRNA/TE12)	A. Jeromin
<i>Others</i>		
CFP-YFP	pECFP-N1-EYFP	A. Tinker
M ₃	pCD-HA-M3	J. Wess
mRFP	pRK7-mRFP	R. Schoepfer
Na _v 1.2	pRII-2A	M. Stocker
Raichu	pCAGGS-Raichu1298X	Y. Goda
Rhopilin	pRK5-myc-Rhopilin	J. Pitcher

		α N			β 1	
MTLESIMACC	LSEEAKEARR	INDEIERQLR	RDKRDARREL	KLLLL	GTGES	50
α 1		α A				
GKSTFIQMR	IHGSYSDE	DKRGFTKLVY	QNIFTAMQAM	IRAMDTLKIP		100
α B		ECFP	α C		α D	
YKYEHKAHA	QLVREVDVEK	VSAFENPYVD	AIKSLWNDPG	IQECYDRRRE		150
α E		α F		β 2		
YQLSDSTKY	LNDLDRVADP	EYMPTEQDVL	RVCVPTTGII	EYPFDLQSVI		200
β 3	α 2		β 4			
FRMV	DVGGLR	SERRKWIHCF	ENVTSIMFLV	ALSEYDQVLV	ESDNENRMEE	250
α 3		β 5		α G		
SKALFRTIIT	YPWFQNSSVI	LFL	NKKV	LLE	EKIMYSHLVD	YFPEYDGPQR
α 4		β 6		α 5		
DAQAAREFIL	KMFVDLNPDS	DKIYSHF	TC	AT	DTENIRFV	FAAVKDTILQ

LNLKEYNLV.

- α -helix, in Ras-like domain
- α -helix, in α -helical domain
- β -sheet, in Ras-like domain
- switch regions
- palmitoylation sites
- residues that contact G β
- mutation sites
- GTP hydrolysis sites
- nucleotide binding motifs
- EE-tag
- ECFP fluorophore insertion site

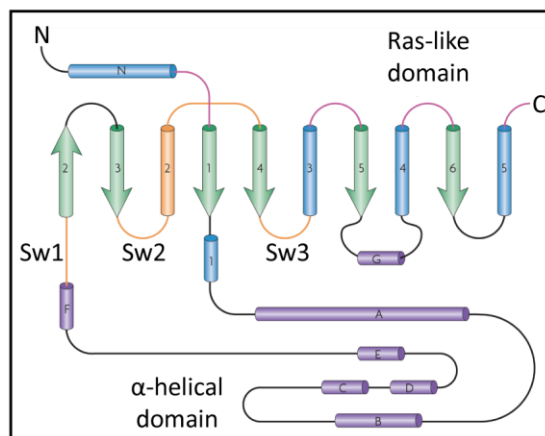


Figure 2.1 Amino acid sequence and secondary structure of G α q. Conserved motifs such as nucleotide binding motifs (highlighted in red) and sites involved in GTP hydrolysis (highlighted in yellow) are indicated in the amino acid sequence. The mutation sites of the G α q constructs used in this thesis are indicated (bold and underlined amino acids): the constitutively active mutations R183C or Q209L and the inactive double mutation Q209L/D277N. Attachment of G α q to the plasma membrane is achieved through palmitoylation of two cysteine residues (C9 and C10, black bar) at the amino-terminus as well as through complex formation with G $\beta\gamma$, with G γ being prenylated at the carboxyl terminus. Contact sites of G α q with G $\beta\gamma$ are indicated by black dots above the amino acid sequence. Features of the secondary structure of G α q, α -helices (blue and magenta boxes) and β -sheets (green arrows), are shown below the amino acid sequence. (adapted from Johnston and Siderovski, 2007) The inset displays the secondary structure of G α q distinguishing the α -helical domain and the Ras-like GTPase domain of G α q. (adapted from Oldham and Hamm, 2008)

2.1.2 Buffers

10x PBS	1.3 M	NaCl
	70 mM	Na ₂ HPO ₄
	30 mM	NaH ₂ PO ₄
		pH 7.3, autoclave
10x TBS	1.4 M	NaCl
	200 mM	Tris Base
		pH 7.5, autoclave
2x Laemmli Buffer	120 mM	Tris-HCl pH 6.8
	4 %	SDS
	20 %	Glycerol
	0.016 %	Bromphenol Blue
	5 %	β-Mercaptoethanol
6x Laemmli Buffer	300 mM	Tris-HCl pH 6.8
	12 %	SDS
	20 %	Glycerol
	0.6 %	Bromphenol Blue
	600 mM	DTT

2.1.3 Bacteria media, agar-plates and antibiotic stock solutions

Miller's Luria Broth (LB medium)	25 g/l	Miller's Luria Broth base autoclave
LB Plates	500 ml	LB Medium
	7.5 g	Select Agar autoclave
LB-ampicillin/kanamycin Plates	500 ml	LB Medium
	7.5 g	Select Agar autoclave, cool to 50°C and add
	2.5 ml	Ampicillin Stock Solution (C _{Final} 50 µg/ml)
	or 5 ml	Ampicillin Stock Solution (C _{Final} 100 µg/ml)
	or 1.5 ml	Kanamycin Stock Solution (C _{Final} 30 µg/ml)
Antibiotics Stock Solutions	10 mg/ml	Ampicillin
	10 mg/ml	Kanamycin
	10 mg/ml	Carbenicillin

2.1.4 Cell culture media

BHK-21 Starvation Medium		MEM alpha
	2 mM	L-Glutamine
	100 U/ml	Penicillin
	100 µg/ml	Streptomycin

BHK-21 Complete Medium

BHK-21 Starvation Medium supplemented with 5 % FBS

BHK-21 Low Serum Medium

BHK-21 Starvation Medium supplemented with 1 % FBS

BHK-21 Virus Production Medium		MEM alpha with Ultraglutamine and nucleosides
	5 %	FBS
	100 U/ml	Penicillin
	100 µg/ml	Streptomycin

HEK293 Complete Medium

	10 %	FBS
	2 mM	L-Glutamine
	100 U/ml	Penicillin
	100 µg/ml	Streptomycin

HEK293 FuGene 6 Transfection Medium

		DMEM/F-12
	2 mM	L-Glutamine

Swiss-3T3 Starvation Medium

		DMEM
	2 mM	L-Glutamine
	100 U/ml	Penicillin
	100 µg/ml	Streptomycin

Swiss-3T3 Complete Medium

Swiss-3T3 Starvation Medium supplemented with 10 % FBS

2.2 Methods

2.2.1 Cell culture

2.2.1.1 Coverslip preparation

Glass coverslips, 10 mm Ø for primary cell culture and 22 x 22 mm for experiments with cell lines, were washed with 100 % IMS for 1 h, then rinsed three times with 75 % IMS and sterilized by baking at 200 °C for a minimum of 6 h. Before use coverslips were coated with poly-D-lysine (100 µg/ml); the 10 mm Ø coverslips were incubated at 37 °C for 3–24 h and the 22 x 22 mm coverslips at 37 °C for 10 min–3 h. Poly-D-lysine treatment was followed by three

rinses (5 min each) with dH₂O and coverslips were either used immediately or stored at 37 °C in water or medium.

2.2.1.2 Maintenance and splitting of cell lines

Human embryonic kidney (HEK293) and Swiss-3T3 cell lines were grown in their respective complete medium (section 2.1.4) in T25 flasks in the incubator at 37 °C and 5 % CO₂. Cells were split when they reached 80–90 % confluency. The medium was aspirated and the cells were washed with 3 ml PBS (Gibco). 1 ml of 0.05 % Trypsin/EDTA solution was added to the flask and gently distributed to coat the cell layer. Surplus trypsin solution was removed and the cells were incubated 1–2 min at 37 °C. Detached cells were resuspended in 3 ml complete medium. To maintain cell lines 500 µl of this cell suspension plus 4.5 ml of complete medium was placed back into a flask and returned to the incubator. The remaining cells were plated for experiments such as lysate preparation for Western blotting and co-immunoprecipitation (section 3.1.1 and 3.1.6) and other binding assays (section 3.2.2), FRET experiments (section 3.1.7) or stress fibre formation assessments (section 3.2.3).

Baby hamster kidney (BHK-21) cells were maintained in BHK-21 complete medium (section 2.1.4) in T75 flasks in the incubator (37 °C, 5 % CO₂) and split when 80-90 % confluent. The medium was aspirated and cells were rinsed twice with 5 ml PBS (Gibco). 3 ml of 0.05 % Trypsin/EDTA solution was added to the flask, evenly distributed and then removed. Cells were incubated at 37 °C for 3 min and resuspended in 5 ml BHK-21 complete medium. To maintain the cell line 5 x 10⁵ cells (counted in a Neubauer chamber) were placed into a T75 flask, complete medium was added to a total volume of 15 ml and the flask was returned to the incubator. The remaining cells were used for experiments during Sindbis virus production (section 3.3.1).

2.2.1.3 Primary culture of hippocampal neurons

All procedures were carried out according to regulations of the Home Office Animal (Scientific Procedures) Act of 1986. Three P0 (newborn) Sprague Dawley rats were sacrificed by decapitation and the brains dissected. Both brain hemispheres were transferred to a dish containing cold dissection medium, the meninges were removed and the hippocampus isolated. In a separate dish containing fresh dissection medium, the hippocampus was cut into small pieces and transferred to a 15 ml tube. The tissue was left to settle in the bottom of the tube and the dissection medium was replaced with 0.25 % trypsin (Gibco, 2.5 %) solution, diluted in 2 ml dissection medium. Digestion occurred at 37 °C for 10 min after which the tissue was transferred to a new tube, allowed to settle and the remaining trypsin solution was aspirated. The tissue pellet was rinsed twice with fresh dissection medium (~7 ml) and twice

with attachment medium (~7 ml) to completely remove the trypsin; the tissue was allowed to settle in the bottom of the tube between each wash. To obtain a homogeneous solution the tissue was dissociated mechanically by pipetting up and down with fire-polished glass Pasteur pipettes of decreasing tip. Briefly, after the last wash 3 ml of attachment medium was added and the tissue was triturated (~10x) with a wide-opening glass Pasteur pipette. Tissue that was not dissociated was allowed to settle and the supernatant was recovered and transferred to a new 15 ml tube. 2 ml attachment medium were added and trituration was repeated with a narrow-opening glass Pasteur pipette (10x). Remaining tissue was left to settle at the bottom of the tube and the supernatant was recovered and centrifuged (Heraeus) at 200 x g for 3 min. The cell pellet was resuspended in 3 ml attachment medium and a sample of the cell suspension was stained with 10 % Trypan Blue. Using a Neubauer chamber viable cell numbers were determined; on average 1.65×10^6 cells/ 3 P0 rats. Cells were plated on poly-D-lysine coated coverslips (4.5×10^4 /well) in a total volume of 500 μ l attachment medium, which was replaced with maintenance medium 6–24 h later. Cells were kept in the incubator (37 °C, 5 % CO₂) and half of the maintenance medium was replaced with fresh maintenance medium every five days. The replaced medium (conditioned maintenance medium) was kept at 4 °C and used in subsequent experiments (section 2.2.2.3). Day *in vitro* (DIV) 1 corresponded to the day the culture was made. Primary cultured hippocampal neurons were used to perform whole-cell patch clamp recordings (section 3.3.2 and 3.3.3).

Dissection Medium		1x HBSS
	10 mM	HEPES
Attachment Medium		MEM
	10 %	Horse Serum
	0.6 %	Glucose
	2 mM	Glutamine
	1 mM	Sodium Pyruvate
Maintenance Medium		Neurobasal
	1 x	B27
	0.6 %	Glucose
	2 mM	Glutamine
	100 U/ml	Penicillin
	100 μ g/ml	Streptomycin

2.2.2 Expression

2.2.2.1 Transient transfection

Lipofectamine 2000

HEK293 cells ($1\text{--}1.3 \times 10^6/3.5\text{ cm } \emptyset$ well and $3 \times 10^6/6\text{ cm } \emptyset$ well) were plated 24 h before transfection in HEK293 complete medium (section 2.1.4). Cells were transfected with Lipofectamine 2000 when grown to 85–95 % confluency. At a ratio of 1:2.5, DNA and Lipofectamine 2000 ($1.2\text{--}7\text{ }\mu\text{g DNA}:3\text{--}17.5\text{ }\mu\text{l Lipofectamine 2000}$) were separately diluted in Opti-MEM ($50\text{--}250\text{ }\mu\text{l}$) and incubated at room temperature for 15 min. Diluted DNA and Lipofectamine 2000 were combined, mixed gently and incubated for another 15 min at room temperature. Cells were removed from the incubator and the medium was replaced with enough Opti-MEM to cover the cells ($300\text{--}750\text{ }\mu\text{l}/3.5\text{--}6\text{ cm } \emptyset$ well). The transfection complex was added to the cells, mixed gently, and incubated at 37 °C for 3–5 h. After incubation, the transfection complex/Opti-MEM mix was removed and replaced with HEK293 complete medium without antibiotics (section 2.1.4). Cells were returned to the incubator for 24 h before being used for experiments such as cell lysate preparation for Western blotting and co-immunoprecipitation (section 3.1.1 and 3.1.6) as well as other binding assays (section 3.2.2) or FRET experiments (section 3.1.7).

Swiss-3T3 cells ($0.5 \times 10^4/3.5\text{ cm } \emptyset$ well) were plated on poly-D-lysine coverslips in Swiss-3T3 complete medium (section 2.1.4) and allowed to grow for three days before being washed twice with 2 ml PBS (Gibco) and kept in Swiss-3T3 starvation medium (section 2.1.4) for two days before transfection. Transfections with Lipofectamine 2000 were performed as described above and cells were kept in Swiss-3T3 starvation medium without antibiotics (section 2.1.4) in the incubator for 24 h before being used in stress fibre formation assessments (section 3.2.3).

FuGene 6

HEK293 cells were plated 24–48 h before transfection in HEK293 complete medium (section 2.1.4) in 10 cm \emptyset dishes. Transfections with FuGene 6 were carried out when cells reached 30–50 % confluency. At a FuGene 6 to DNA ratio of 3:1, FuGene 6 was diluted in HEK293 FuGene 6 transfection medium (section 2.1.4) and incubated at room temperature for 5 min. Diluted FuGene 6 was added to the DNA ($2\text{ }\mu\text{g RhoA}$, $5\text{ }\mu\text{g G}\alpha_q$) and incubated at room temperature for 30 min. Cells were removed from incubator and the transfection complex was gently added. Cells were incubated at 37 °C for 48 h before cell lysates were prepared for Western blotting and co-immunoprecipitation experiments (section 3.1.1 and 3.1.6).

2.2.2.2 Microinjection

Swiss-3T3 cells ($6-9 \times 10^4/3.5 \text{ cm } \emptyset$ well) were plated on poly-D-lysine coated coverslips in Swiss-3T3 complete medium (section 2.1.4) and allowed to attach (min 6 h). Cells were rinsed twice with 2 ml PBS (Gibco) and Swiss-3T3 starvation medium (section 2.1.4) was added. Cells were starved for two to three days before microinjection took place. Microinjections were performed using a FemtoJet microinjector (Eppendorf) and a 5171 micromanipulator (Eppendorf). Long tapered needles were pulled on a horizontal P-97 Flaming/Brown puller (Sutter) from Borosilicate glass capillaries (Harvard). Before use, all solutions were filtered using VectaSpin Micro centrifuge filters (Eppendorf, 9,400 x g, 4 min). The dish containing the cells was removed from the incubator and placed on a microscope (Axiovert 135M, Zeiss, section A.1.3) stage enclosed in a Perspex chamber. The FemtoJet microinjector settings were adjusted to: injection pressure (pi) of 120 hPa, injection time (ti) of 0.3 s and compensation pressure (pc) of 60 hPa. Microinjections were carried out in semi-automatic mode with defined Z-plane limits and a set injection time or manually by touching the cell membrane with the tip of the needle and retracting the needle once a slight shiver and enlargement of the cell was observed. Manual injection was the method most often used as it gave fine control over the entire injection process. Experiments were performed with two concentrations of purified RhoA protein (0.15 $\mu\text{g}/\mu\text{l}$ and 0.3 $\mu\text{g}/\mu\text{l}$, in adapted intracellular solution; section 2.2.7.2). Purified RhoA-V14 or RhoA-N19 protein was injected into the cytoplasm of the cells. To detect injected cells, tetramethylrhodamine isothiocyanate (TRITC; 5–12.5 mg/ml) was microinjected together with the purified protein at all times. As a control TRITC (8–10 mg/ml, in microinjection buffer) was also injected on its own. Microinjections lasted no longer than 30 min after which the cells were returned to the incubator and allowed to recover (max 1.5 h). Cells were fixed and prepared for microscopy (section 2.2.11.1) in order to assess stress fibre formation (section 3.2.3).

Microinjection Buffer	154 mM	NaCl
	5 mM	HEPES
	2.5 mM	KCl
	0.5 mM	MgCl ₂
		pH 7.4

2.2.2.3 Viral infection

BHK-21 cells ($2 \times 10^5/3.5 \text{ cm } \emptyset$ well) were plated on poly-D-lysine coated coverslips in BHK-21 complete medium (section 2.1.4). The next day cells were rinsed twice with 2 ml PBS (Gibco) and BHK-21 starvation medium (section 2.1.4) was added. Infections with Sindbis virus took place 24 h later. The virus was diluted in BHK-21 starvation medium (EGFP control 1:5000,

RhoA-N19 1:1000 and RhoA-V14 1:100) and 100 µl of the diluted virus was added to the cells, which had been covered with 900 µl fresh BHK-21 starvation medium. After 4 h of incubation at 37 °C another 1 ml of BHK-21 starvation medium was added to the cells without removing the virus. Cells were left to incubate for 24 h before being fixed and stained (section 2.2.11.1) for stress fibre formation assessment (section 3.3.1.4).

Cultured hippocampal neurons (DIV 9–16) were infected with Sindbis virus. The virus was diluted (EGFP control 1:5000; RhoA-N19 1:1000 or 1:2000; RhoA-V14 1:100 or 1:500) in conditioned maintenance medium (section 2.2.1.3). 100 µl of virus dilution was mixed with 100 µl of medium from the wells and added to the neurons, from which the remaining medium had been removed. The removed medium was used to enrich fresh maintenance medium (50:50). After an incubation of 2 h at 37 °C the virus was removed from the neurons and 500 µl of enriched maintenance medium was added to each well. Neurons were returned to the incubator and used for whole-cell patch clamp experiments 24–48 h later (section 3.3.3).

2.2.3 Lysis preparation

2.2.3.1 Lysate preparation from HEK293 cells

Transiently transfected (Lipofectamine 2000 or FuGene 6) HEK293 cells were lysed 24 h after transfection. Dishes containing the cells were removed from the incubator, placed on ice and cells were rinsed twice with ice-cold 1x PBS (section 2.1.2). GTPase lysis buffer was added to each dish (0.5–1 ml/6–10 cm Ø dish), cells were scraped off and transferred to a 1.5 ml tube. The lysate was sonicated using a SonoPuls sonicator (Bandelin) at 15 % intensity and 40 % pulse at 4 °C for 30 s and centrifuged (Eppendorf) at 16,100 x g and 4 °C for 5 min. The supernatant was transferred to a fresh 1.5 ml tube and an aliquot was taken for protein estimation (section 2.2.4) before samples were frozen at -20 °C. Cell lysates were used in Western blotting and co-immunoprecipitation experiments (section 3.1.1 and 3.1.6) and in other binding assays (section 3.2.2).

GTPase Lysis Buffer	50 mM	Tris-HCl pH 8.0
	150 mM	NaCl
	10 %	Glycerol
	2 mM	EDTA
	1 %	Triton X-100
	1 mM	Benzamidine
	0.23 mM	PMSF

2.2.3.2 Lysate preparation from rat brain

All procedures were carried out according to Schedule One of the 1986 Home Office Animal (Scientific Procedures) Act. P23 Sprague Dawley rats were sacrificed by dislocation of the neck

and the brains dissected. Working on ice, cortex and hippocampus were isolated and cut into small pieces. Tissue pieces were suspended in cold homogenisation buffer A at a tissue to medium ratio of 5–10 % (w/v) and homogenised with 15 strokes using a pre-chilled glass homogeniser (Glas-Col). The homogenate was transferred to a Greiner tube and centrifuged (Heraeus) at 1,400 x g and 4 °C for 10 min. The supernatant (S1) was collected and stored on ice, while the pellet was resuspended in homogenisation buffer A and centrifuged as before. The resulting pellet (P1) was resuspended in homogenisation buffer B and aliquoted. The supernatant (S1') was combined with S1 (small aliquots were taken) and centrifuged (Beckman, JA-17) at 13,800 x g and 4 °C for 10 min. The supernatant (S2) was collected and aliquoted. The pellet (P2) was resuspended in homogenisation buffer B and aliquoted. All aliquots were snap-frozen in liquid nitrogen and stored at -80 °C. Before use Triton X-100, to a final concentration of 0.5 %, was added to the samples and small aliquots were taken to estimate the protein concentration. 20 mM DTT (final concentration) was added and samples were rotated at 4 °C for 30 min. Brain lysates were used in Western blotting and co-immunoprecipitation experiments (section 3.1.4) and in other binding assays (section 3.2.2).

Homogenisation Buffer A	320 mM	Sucrose
	10 mM	Tris-HCl pH 8.0
	0.1 mM	EDTA
	0.1 mM	PMSF
	1 µg/ul	Aprotinin
	1 µM	Leupeptin
	1 µM	Pepstatin
Homogenisation Buffer B	20 mM	Tris-HCl pH 8.0
	0.1 mM	EDTA
	0.1 mM	PMSF
	1 µg/ul	Aprotinin
	1 µM	Leupeptin
	1 µM	Pepstatin

2.2.4 Protein concentration estimation

The protein concentration of HEK293 lysates was estimated using a Bradford assay. Protein standards (0, 2, 4, 6 µg bovine serum albumin; BSA) were set up in 1.5 ml tubes, to which 2.5 µl of GTPase lysis buffer (section 2.2.3.1) had been added. 2.5 µl of each sample lysate was added to separate 1.5 ml tubes. The Bradford stock solution (BIO-RAD) was diluted 1:5 with water and 1 ml of diluted Bradford solution was added to every standard and sample tube. Vortexed briefly, all were transferred to disposable cuvettes and incubated at room temperature for 5 min. Optical density (OD) values were read at 595 nm and protein concentrations were

estimated using a spectrophotometer (SmartSpec Plus, BIO-RAD). Protein concentrations of brain lysates were estimated in the same way as HEK293 lysates. Homogenisation buffer B (section 2.2.3.2) was used to set up the BSA protein standards.

The Bradford assay was also used to estimate protein concentrations of cleaved purified proteins (section 2.2.7.3). The assay was scaled down and a Nanodrop 1000 spectrophotometer (Labtech International) was used to read OD values and estimate the protein concentration of the samples. BSA protein standard dilutions (0, 0.1, 0.2, 0.4, 0.6 $\mu\text{g}/\mu\text{l}$) were set up in adapted intracellular solution (section 2.2.7.2). 4 μl of these dilutions and of the purified protein samples were transferred to 1.5 ml tubes and 200 μl of Bradford working solution (1:5 dilution of Bradford stock solution) was added to each. After 5 min incubation at room temperature, OD values were read at 595 nm and protein concentrations estimated.

2.2.5 Co-immunoprecipitation

250 μg of lysate from HEK293 cells or rat brain (P2 fraction) was incubated with 1–2 μg of antibody (anti-myc, anti-RhoA or anti- $\text{G}\alpha_{q/11}$ (Millipore and Santa Cruz)) and rotated at 4 °C for 1 h. Protein A/G agarose (20–30 μl of 50 % slurry) was washed once with 1 ml cold GTPase lysis buffer (section 2.2.3.1). The samples were added to the washed beads and rotated at 4 °C for a further hour. Samples were centrifuged (Eppendorf) at 200 x g for 2 min and beads were rinsed three times with 1 ml cold GTPase lysis buffer. After the last wash beads were transferred to new 1.5 ml tubes, the GTPase lysis buffer was aspirated and 20 μl of 1x Laemmli buffer (diluted from 6x Laemmli buffer with 1x PBS, section 2.1.2) was added. The samples were denatured at 60 °C for 30 min before being analysed by Western blotting.

2.2.6 SDS-PAGE and Western blotting

2.2.6.1 Sodium dodecyl sulfate polyacrylamide gel electrophoresis (SDS-PAGE)

SDS-PAGE was carried out using either a mini-PROTEAN II (BIO-RAD) or a SE600 (Hoefer) system. Discontinuous polyacrylamide gels consisting of a 3 or 4 % stacking gel and a 10–15 % separating gel were used to separate proteins. Gels were cast at room temperature between glass plates using the provided casting stands. Polyacrylamide (AA/BA) polymerisation was initiated by ammonium persulfate (APS) and catalysed by TEMED.

Mini-PROTEAN II (BIO-RAD)

For 2 gels	10 %	12 %	15 %	Stacking Gel, 3 %
30 % AA/BA, ml	3.33	4.0	5	0.5
Lower Tris, ml	2.5	2.5	2.5	-
Upper Tris, ml	-	-	-	1.25
APS (10 %), ul	70	70	70	30
TEMED, ul	10	10	10	10
dH ₂ O, ml	4.09	3.42	2.42	3.21
Total, ml	10	10	10	5

Table 2.1 Preparation of gels for SDS-PAGE, Mini-PROTEAN II (BIO-RAD).

Upper Tris	0.4 % 0.5 M	SDS Tris-HCl, pH 8.8
Lower Tris	0.4 % 1.5 M	SDS Tris-HCl, pH 6.8

SE600 (Hoefer)

For 2 gels	11 %	12.5 %	Stacking Gel, 4 %
30 % AA/BA, ml	13.75	15.625	2.6
Tris-HCl, pH 8.8, ml	18.75	18.75	-
Tris-HCl, pH 6.8, ml	-	-	3.3
SDS (10 %), ul	375	375	200
APS (10 %), ml	2	2	1.4
TEMED, ul	25	25	20
dH ₂ O, ml	2.6	0.725	12.5
Total, ml	37.5	37.5	20

Table 2.2 Preparation of gels for SDS-PAGE, SE600 (Hoefer).

Indicated amounts of HEK293 and brain samples were prepared for SDS-PAGE by mixing the lysate with 1x PBS (section 2.1.2) and 6x Laemmli buffer (section 2.1.2; 1x final concentration) to a minimum final volume of 18 μ l and denatured at 60 °C for 30 min for G α_q samples and at 95 °C for 5 min for RhoA samples (section 3.1.6). Co-immunoprecipitation samples were denatured at 60 °C for 30 min, and protein purification samples at 95 °C for 10 min. Denaturing conditions for the various binding assay are specified in the individual sections in the results

chapter. To bring down condensation or to pellet beads, samples were centrifuged (Eppendorf) at 200 x g for up to 3 min before being loaded onto the gel. Protein markers (All Blue PrecisionPlus or Low Range, BIO-RAD or High-Range Rainbow, GE) were loaded alongside the samples. SDS-PAGE was carried out in 1x running buffer and gels were run at 80 V constant voltage through the stacking gel and 18 mA constant current through the separating gel (mini-PROTEAN II , BIO-RAD) or at 300 V constant voltage (SE600 , Hoefer) until the Bromphenol Blue dye had run out of the gel.

1x Running Buffer	192 mM	Glycine
	25 mM	Tris
	0.1 %	SDS

2.2.6.2 Transfer and immunodetection

Following SDS-PAGE proteins were transferred onto nitrocellulose membranes (Protran BA83, Whatman or Hybond ECL, GE) either by tank (mini Trans-Blot, BIO-RAD) or semi-dry blotting (V20-SDB, Scie-Plas).

For tank blotting, the gel was equilibrated in cold 1x tank transfer buffer for 5 min and the nitrocellulose membrane was pre-soaked in dH₂O and 1x tank transfer buffer. The transfer cassette was assembled by placing the gel together with the nitrocellulose membrane in between two pieces of blotting paper and two fibre pads; all soaked in 1x tank transfer buffer. The transfer cassette was placed into the tank; the black/gel side of the cassette facing the cathode (negative, black) and the clear/membrane side of the cassette facing the anode (positive, red). An ice-pack and stirring bar were also placed into the tank and it was filled with cold 1x tank transfer buffer. In the cold-room (4 °C) the tank was placed on a magnetic stirrer and transfer was performed at 100 V constant voltage for 50 min.

1x Tank Transfer Buffer	192 mM	Glycine
	25 mM	Tris
	20 %	Methanol

For semi-dry transfer, the gel and six pieces of blotting paper were soaked in 1x Semi-Dry transfer buffer and the transfer was assembled in the following order: three pieces of blotting paper were placed onto the anode (positive) plate, followed by the nitrocellulose membrane, the gel and three further pieces of blotting paper; the stack was then covered with the cathode (negative) plate. Transfer was performed at a constant current of 0.8 mA/cm² for 1 h 50 min.

1x Semi-Dry Transfer Buffer	40 mM	Glycine
	50 mM	Tris
	0.3 %	SDS
	20 %	methanol

The two systems, BIO-RAD and Hoefer/Scie-Plas, used gels and membranes that differed in size and thus volumes of solutions in the immunodetection experiments had to vary. Volumes in the text refer to experiments that used the BIO-RAD system; volumes in brackets were used with the Hoefer/Scie-Plas system.

Blots were processed directly or stored overnight, in 1x TBS (section 2.1.2) at 4 °C or dried at room temperature. The dried membrane was soaked for 10 min in dH₂O and 10 min in 1x TBS before use. Membranes were blocked at room temperature on an orbital shaker for 40 min–1 h in 15 ml (50 ml) blocking solution. Primary antibodies were diluted in 1 ml (20 ml) blocking solution and membranes were incubated in primary antibody solutions in a plastic pouch (in a box) at room temperature for 3 h or at 4 °C overnight, continuously rotating or shaking. Membranes were washed three times with 12 ml blocking solution and three times with 12 ml TBST for 5 min each (6x with 50 ml TBST, 5 min each) and then incubated with horseradish peroxidase (HRP)-conjugated secondary antibodies, diluted in 10 ml (25 ml) blocking solution, at room temperature on an orbital shaker for 1 h. Washes in blocking solution and TBST were repeated as before. For each blot 1 ml SuperSignal West Pico (Pierce) (25 ml ECL, GE) detection reagent was used; the luminal and enhancer solutions were mixed in equal amounts. Detection solution was added to the blots, which were placed on a glass plate (in a box), and incubated for 5 min (1 min) at room temperature. Membranes were drained off excess detection solution, covered with an acetate sheet and placed into a developing cassette. Emitted signals were detected by exposing the blots to films (Hyperfilm ECL, GE or BioMax MR-1, Kodak) for up to 30 min and developing the films in an automatic film processor (RG II, Fuji). At times signals were detected digitally using a CCD-camera based imager (ImageQuant LAS4000 mini, GE). In this case, blots were placed on a tray, covered in 1.5 ml SuperSignal West Pico detection solution, which remained on the blot during imaging, and placed inside the ImageQuant machine. Exposure conditions and times were set using the ImageQuant LAS4000 control software.

At times membranes were stripped of antibody and re-probed. Membranes were submerged in stripping buffer and incubated at 60 °C for 30 min, after which they were extensively rinsed in TBST (~30 min). Membranes were incubated in blocking solution and probed with a different primary antibody following the procedure as described before.

Primary Antibodies

RhoA	anti-mouse	Santa Cruz	0.2 mg/ml	1:200-1:1000
	anti-rabbit	Santa Cruz	0.2 mg/ml	1:200
G $\alpha_{q/11}$	anti-rabbit	Santa Cruz	0.2 mg/ml	1:200-1:1000
G α_q	anti-rabbit	Santa Cruz	0.2 mg/ml	1:1000
Myc	anti-mouse	Roche	0.4 mg/ml	1:400
	anti-mouse	Millipore	1 mg/ml	1:1000
	anti-rabbit	Santa Cruz	0.2 mg/ml	1:400-1:1000
EE	anti-rabbit	Abcam	0.2 mg/ml	1:500

Secondary Antibodies

Goat anti-mouse HRP	BioRad	1:5000
Sheep anti-mouse HRP	GE	1:2500
Goat anti-rabbit HRP	BioRad	1:5000
Donkey anti-rabbit HRP	GE	1:2500

Blocking Solution	1 x	TBS
	5 %	Milk powder
	5 %	NGS
	0.1 %	Tween-20

TBST	1 x	TBS
	0.1 %	Tween-20

Stripping Buffer	62.5 mM	Tris-HCl pH 6.8
	2 %	SDS
	100 mM	β -Mercaptoethanol

2.2.6.3 Coomassie staining of SDS-PAGE gels

SDS-PAGE gels were stained with Coomassie Blue to document the stages of protein purification and to estimate purified protein concentrations (section 2.2.7 and 3.2.1) or to evaluate transfer efficiency during Western blotting experiments. Gels were stained with Coomassie solution at room temperature on an orbital shaker for 10–20 min. The Coomassie solution was removed and gels were rinsed with dH₂O before being destained in Fast Destain solution for 15 min and Slow Destain solution at room temperature overnight. Gels were soaked in drying solution and dried between cellophane sheets (Novex).

Coomassie Solution	0.2 %	Coomassie Brilliant Blue R250
	7.5 %	Acetic Acid
	50 %	Methanol

Fast Destain Solution	45 %	Methanol
	7.5 %	Acetic Acid

Slow Destain Solution	10 %	Methanol
	7.5 %	Acetic Acid
Drying Solution	2 %	Glycerol
	0.01 %	Na-Azide

2.2.7 Glutathione-S-transferase (GST) fusion protein purification

RhoA-V14 and RhoA-N19 were purified as recombinant GST fusion proteins. For binding assay experiments (section 3.2.2) purified GST-RhoA-V14 and GST-RhoA-N19 were used bound to glutathione agarose beads. In electrophysiological experiments (section 3.2.4) RhoA-V14 and RhoA-N19 cleaved off the GST fusion protein were added to the intracellular solution.

2.2.7.1 Electroporation of BL21 (DE3) bacteria

Electroporation cuvettes (1 mm, BTX model 610, Harvard Apparatus) were cooled on ice. 1 µg of DNA (pGEX-6P-1-RhoA-V14, pGEX-6P-1-RhoA-N19) was gently mixed with 25 µl electrocompetent BL21 (DE3) bacteria and then added to the cuvettes before being electroporated at 129 Ω, 50 µF, 1.5 kV (ECM 600, BTX). Bacteria were transferred to a Falcon tube with 1 ml of LB medium (section 2.1.3; 37 °C) and incubated at 37 °C and 120 rpm for 40 min. Bacteria were harvested by centrifugation (Heraeus, 2,000 x g, 1 min), resuspended in 100 µl LB medium and spread on LB-ampicillin plates (section 2.1.3; 100 µg/ml). Plates were incubated at 37 °C overnight.

2.2.7.2 Purification of GST fusion proteins

This description of the purification of GST fusion proteins is also illustrated by a flow diagram (Fig. 3.14A) in the results section. As a starter culture, 20 ml LB medium (section 2.1.3; 100 µg/ml Ampicillin) was inoculated with a single colony picked from the LB-ampicillin plate and incubated, shaking at 200 rpm, at 37 °C overnight. 5 ml starter culture was diluted (1:50) in 250 ml LB medium (100 µg/ml Ampicillin) and grown at 200 rpm until an OD₆₀₀ of 0.4–0.5 was reached; incubation took place at 37 °C for ~1 h before the culture was cooled down to 22 °C. An aliquot (pre-induction) of the culture was taken, the bacteria pelleted (Eppendorf, 13,500 x g, 5 min) and resuspended in 2x Laemmli buffer (section 2.1.2); so as not to overload the gel 2x Laemmli buffer was added in proportion to the OD₆₀₀ according to the following formula: (ml of culture taken x OD₆₀₀ / 0.035) x 10. Protein expression was induced by adding 0.05 mM isopropyl β-D-thiogalactopyranoside (IPTG), which causes transcription of the cloned genes controlled by the *lac* operon, to the culture and the culture was incubated at 200 rpm, at 22 °C for 3 h. An aliquot (post-induction) was taken, centrifuged and resuspended as described for the pre-induction aliquot. Bacteria were harvested by centrifugation (Beckman, JA-14 rotor, 3,100 x g, 4 °C, 10 min). On ice, the pellet was washed with 10 ml cold GST fusion

protein lysis buffer (without DTT and PMSF) and transferred to a 15 ml tube. After centrifugation (Heraeus) at 3,200 x g and 4 °C for 10 min the pellet was resuspended in 5 ml cold GST fusion protein lysis buffer (without DTT and PMSF). 0.5 mg/ml lysozyme was added and incubated on ice for 15 min. PMSF and DTT were added to a final concentration of 1 mM and the lysate was sonicated (Bandelin, 25 % intensity, continuous, 1min, on ice). To precipitate DNA, 0.5 ml of a 30 % streptomycin sulphate solution was added and rotated at 4 °C for 10 min. The lysate was centrifuged (Beckman, JA-17 rotor) in polycarbonate tubes at 27,000 x g and 4 °C for 15 min. An aliquot of the supernatant was taken and 2x Laemmli buffer was added according to the following formula: μl of supernatant taken x OD600 (post induction) / 0.35. Glutathione agarose beads (Sigma, 100 μl of 25 % slurry i.e. 25 μl of packed beads/250 ml culture) were prepared by three washes with 150 μl GST fusion protein lysis buffer (without DTT and PMSF) and were transferred to a 15 ml tube. The supernatant was added to the prepared glutathione agarose beads and rotated at 4 °C for 1 h. After incubation beads were pelleted (Heraeus, 98 x g, 4 °C, 10 min), transferred to a 1.5 ml tube and centrifuged (Eppendorf) at 200 x g and 4 °C for 3 min. Depending on use, beads were then washed three times with 250 μl GST fusion protein lysis buffer (without PMSF, for binding assay experiments) or in 250 μl adapted intracellular solution (for electrophysiology). Beads were resuspended in their corresponding buffers to a total volume of 100 μl (25 % slurry). An aliquot (2 μl) was taken and 10 μl of 2x Laemmli buffer was added. For binding assay experiments GST-RhoA-V14 and GST-RhoA-N19 bound glutathione agarose beads were aliquoted, snap-frozen and stored in liquid nitrogen. For electrophysiology purified RhoA-V14 and RhoA-N19 proteins were cleaved off the GST fusion protein (section 2.2.7.3). The aliquots taken at various stages of the purification process were denatured at 95 °C for 10 min and subjected to SDS-PAGE as described before (section 2.2.6.1). A 1 μg BSA sample was loaded onto the gel alongside the samples and used to estimate the concentration of purified GST-RhoA-V14 and GST-RhoA-N19 protein bound to the glutathione agarose beads by Coomassie staining of the gel (section 2.2.6.3). GST, expressed from pGEX-6P-1, was purified as described for RhoA and used as a control for direct binding assays (section 2.2.9.2).

GST Fusion Protein Lysis Buffer	50 mM	Tris-HCl pH 7.5
	50 mM	NaCl
	5 mM	MgCl ₂
	1 mM	DTT
	1 mM	PMSF

Adapted Intracellular Solution	135 mM	KGluc
	10 mM	KCl
	10 mM	HEPES
	1 mM	MgCl ₂
	1 mM	DTT
		pH 7.2–7.3
		osmolarity 270–290

2.2.7.3 PreScission protease cleaving

For electrophysiological experiments (section 3.2.4) purified RhoA-V14 and RhoA-N19 were cleaved off their GST-fusion part with PreScission protease (GE) to ensure the intracellular application of only the protein of interest and to limit the size of the protein having to be introduced to the neuron through the patch pipette. The process of PreScission protease cleaving is also illustrated by a flow diagram (Fig. 3.15A) in the results section. 1 U of PreScission protease was added to the GST-RhoA-V14 or GST-RhoA-N19 glutathione agarose beads (resuspended in adapted intracellular solution, section 2.2.7.2) and rotated at 4 °C for 2 h. Beads were pelleted by centrifugation (Eppendorf, 200 x g, 4 °C, 3 min), the supernatant was saved and the beads were resuspended to a total volume of 100 µl with GST fusion protein lysis buffer (section 2.2.7.2). Aliquots (2 µl) of the supernatant and beads were taken and 10 µl of 2x Laemmli buffer (section 2.1.2) was added to each. Any excess PreScission protease, a GST-fusion protein itself, was removed from the supernatant by adding the supernatant to a fresh set of glutathione agarose beads (100 µl of 25% slurry, washed three times with 150 µl adapted intracellular solution) and rotating at 4 °C for 30 min. Beads were pelleted as before and the supernatant was aliquoted. The supernatant was either used directly or snap-frozen and stored in liquid nitrogen. The protein concentration of the cleaved purified protein was estimated using a Bradford assay as described before (section 2.2.4). The aliquots taken at various stages of the purification and cleaving process were denatured at 95 °C for 10 min and subjected to SDS-PAGE and stained with Coomassie (section 2.2.6). As a control for electrophysiology recordings GST, expressed from pGEX-4T, was mock purified and cleaved in the same way.

2.2.8 Binding assays with purified protein

Purified GST-RhoA-V14 and GST-RhoA-N19 bound to glutathione agarose beads (section 2.2.7.2) were incubated with HEK293 lysates or brain lysates. As a control, GST protein (25 µg) was bound to glutathione agarose beads (20 µl of 25 % slurry), which had been washed three times with 150 µl GTPase lysis buffer (without PMSF and Benzamidine; section 2.2.3.1), by rotating at 4 °C for 1 h in 100 µl GTPase lysis buffer. After incubation GST bound beads were rinsed three times with 150 µl GTPase lysis buffer and resuspended in a total volume of 20 µl

with GTPase lysis buffer. The amount of purified GST-RhoA-V14 and GST-RhoA-N19 bound to glutathione agarose beads was estimated as described (section 2.2.7.2) and the binding assay experiments were performed using 40 µg purified GST-RhoA protein. GST bound control beads, GST-RhoA-V14 and GST-RhoA-N19 bound beads were incubated with Gα_q HEK293 lysate (50 µg) or brain lysate (250–1500 µg), and as control with raphilin HEK293 lysate (25 µg). Beads, lysates and 100 µl of cold GTPase lysis buffer (+5 mM MgCl₂) were mixed in a 1.5 ml tube and rotated at 4 °C for 1 h. Beads were pelleted (Eppendorf) at 200 x g and 4 °C for 3 min, rinsed three times with cold 500 µl GTPase lysis buffer and transferred to a new 1.5 ml tube. 20 µl of 1x Laemmli buffer (diluted from 6x Laemmli buffer with 1x PBS, section 2.1.2) was added and the samples were denatured at 95 °C for 10 min or at 60 °C for 20 min. Samples were analysed by SDS-PAGE and Western blotting (section 2.2.6).

2.2.9 *In vitro* translation and direct binding assays

2.2.9.1 *In vitro* translation

The TNT coupled transcription/translation system (Promega) was used to *in vitro* translate raphilin and Gα_q-L209. *In vitro* translation reactions were performed according to manufacturer's instructions. Briefly, 1 µg of sample DNA was mixed with 25 µl of TNT rabbit reticulocyte lysate, 2 µl TNT reaction buffer, 1 µl TNT RNA polymerase, 1 µl amino acid mixture (without methionine) and 1 µl RNasin Ribonuclease inhibitor or with 40 µl of TNT quick master mix. 2 µl [³⁵S] methionine was added and the reaction brought to a total volume of 50 µl with nuclease-free water before being incubated at 30 °C for 90 min. Synthesised proteins were analysed by running 1–2 µl of the radioactive translation products on SDS-PAGE and exposing the dried gel to films as described below (section 2.2.9.2). *In vitro* translation reactions in the absence of DNA were carried out and served as controls in direct binding assays (section 3.1.8).

2.2.9.2 Direct binding assays with purified RhoA-V14

20 µl of *in vitro* [³⁵S] translation product (raphilin, Gα_q-L209 or control) was added to 10 µg purified GST-RhoA-V14 or GST protein bound to glutathione agarose beads (section 2.2.7.2). 200 µl of NP-40 buffer was added and samples were rotated at 4 °C for 1 h. Beads were washed three times with 1 ml NP-40 buffer and transferred into a new 1.5 ml tube. Beads were resuspended in 25 µl 1x Laemmli buffer (diluted from 6x Laemmli buffer with 1x PBS, section 2.1.2) and denatured at 70 °C for 5 min. Samples were analysed by electrophoresis as described (section 2.2.6.1). Gels were fixed in fixation solution for 15 min, rinsed with dH₂O and soaked in Autofluor enhancer solution (National Diagnostics) at room temperature for 1 h. Gels were dried on a gel dryer (BIO-RAD) at 80 °C for 2 h and exposed to films (BioMax MR-1, Kodak) at -80 °C for 48 h. Films were developed using an automatic film processor (RG II, Fuji).

NP-40 Buffer	50 mM	Tris-HCl pH 7.5
	100 mM	NaCl
	10 mM	MgCl ₂
	0.5 %	NP-40
Fixation Solution	7 %	Methanol
	7 %	Acetic Acid

2.2.10 Sindbis virus production

2.2.10.1 RNA synthesis

RhoA-V14 and RhoA-N19 were cloned into pSinRep5-EGFP (section 2.2.13) generously provided by A. Jeromin (Jeromin et al., 2003). The Sindbis plasmid contained the nonstructural protein (nsP) 2 mutation (P726S) that has been described (Dryga et al., 1997) and expressed enhanced green fluorescent protein (EGFP) under control of a second genomic promoter. Plasmid DNA (pSinrep5-EGFP, pSinrep5-RhoA-V14-EGFP, pSinrep5-RhoA-N19-EGFP and pHelper-DH-BB (tRNA/TE12)) was linearized by digesting 3 µg of DNA with the appropriate amount of restriction enzyme and its respective buffer (Roche or NEB) in a total reaction volume of 40 µl at 37 °C for 1–4 h. pSIN vectors were digested with *PacI* for 4 h and the helper plasmid with *XhoI* for 1 h. 1 µl aliquots of the digests were taken for analysis. Linearized plasmids were purified by phenol/chloroform extraction. Briefly, digests were taken up to 100 µl with diethyl pyrocarbonate (DEPC)-dH₂O and 100 µl phenol (pH 7.5) and 50 µl chloroform were added. Samples were vortexed for 10 s and centrifuged (Eppendorf) at 16,100 x g and 4 °C for 5 min. The upper phase was transferred to a new 1.5 ml tube and 1 volume chloroform was added; samples were vortexed and centrifuged as before. The upper phase was transferred into a new 1.5 ml tube and 300 mM NaAc (pH 5.2) and 2.5 volumes 100 % EtOH added; DNA was precipitated at -20 °C overnight. The DNA was pelleted (Eppendorf) at 16,100 x g and 4 °C for 15 min and washed with 500 µl 80 % EtOH. The sample was centrifuged again under the same conditions for 5 min and the supernatant was aspirated. The pellet was air-dried for 35 min and dissolved in 5 µl DEPC-dH₂O. A 0.5 µl aliquot was 1:20 diluted in DEPC-dH₂O, of which 3 µl was analysed on a DNA agarose gel (section 2.2.12.3) alongside the corresponding samples taken before purification.

RNA was synthesised using the mMessage mMachinE SP6 kit (Ambion). The reaction was performed according to manufacturer's instructions. In 20 µl total volume, 2.5–4.5 µl of linearized DNA (0.5–1 µg) was combined with 5 mM of each ATP, CTP and UTP, 1–2 mM GTP, 4 mM CAP analog (m⁷G(5')ppp(5')G), 1x reaction buffer and 1x enzyme mix (including RNase inhibitor). The amount of GTP added to the reaction depended on the length of the synthesised transcripts; for larger transcripts (pSIN-EGFP, 9 kb; pSIN-RhoA-V14-EGFP and pSIN-

RhoA-N19-EGFP, 9.5 kb) 2 mM GTP was added. Additional GTP will decrease the amount of capped RNA, but is necessary to synthesise full-length transcripts. According to the mMessage mMachine manual a ratio of 4:1 (CAP:GTP) results in 80 % of the synthesised transcripts being capped, while the 2:1 ratio used for larger transcripts produces transcripts of which 67 % are capped. Transcription was performed at 37 °C for 2 h and was followed by DNase treatment. 2 U TURBO DNase (provided with the mMessage mMachine SP6 kit) was added to the reaction and incubated at 37 °C for 15 min. 0.5 µl aliquots were taken for analysis and the remaining RNA was stored at -20 °C before being used in the Sindbis virus production (section 3.3.1).

RNA samples, alongside a sample of isolated RNA from HEK293 cells (1 µg), were analysed by formaldehyde agarose gel electrophoresis. 0.5 µl of RNA sample was combined with 2.5 µl DEPC-dH₂O and 5 volumes of RNA loading buffer, and incubated at 65 °C for 15 min. 1 µl of ethidium bromide (1mg/ml) was added and the samples were loaded onto a 1 % formaldehyde agarose gel (pre-run at 50 V constant voltage at 4 °C for 30 min). Electrophoresis was performed at 50 V constant voltage at 4 °C for 2 h. The RNA was visualized under UV light and the gels documented as prints.

10x MOPS/EDTA	200 mM	MOPS
	50 mM	NaAC
	10 mM	EDTA
		pH 7.0
Formaldehyde Agarose Gel	1 %	SeaKem LE agarose
	1 x	MOPS/EDTA
	0.63 M	Formaldehyde
1x RNA Gel Running Buffer	1 x	MOPS/EDTA
	0.63 M	Formaldehyde
RNA Loading Buffer	750 µl	Formamid
	150 µl	10x MOPS/EDTA
	240 µl	37 % Formaldehyde
	100 µl	Glycerol
	60 µl	H ₂ O
	20 µl	Bromphenol Blue stock
	20 µl	Xylene Cyanol stock

2.2.10.2 Transfection of BHK-21 cells and harvesting of virus particles

BHK-21 cells were transfected with the synthesised RNA by electroporation. BHK-21 cells were harvested by trypsinisation as described (section 2.2.1.2). Trypsinised cells were resuspended in 5 ml BHK-21 complete medium (section 2.1.4) and pipetted up and down to obtain a single

cell suspension. After centrifugation (Heraeus) at 200 x g for 5 min, cells were rinsed with 10 ml ice-cold PBS (Gibco, without cations) and counted in a Neubauer chamber. Cells were centrifuged (Heraeus, 200 x g, 5 min) and resuspended in ice-cold PBS at 1×10^7 cells/ml. For each electroporation 5×10^6 cells (500 μ l) were transferred to a pre-cooled electroporation cuvette (4 mm, BTX model 640, Harvard Apparatus, cooled on ice for ~ 40 min). 7.5 μ l (3.75–10 μ g RNA) each of synthesised Sindbis (SIN-RhoA-V14-EGFP, SIN-RhoA-N19-EGFP or SIN-EGFP) and helper RNA were mixed with the cells. Electroporation was performed on a GenePulser XCell electroporator (BIO-RAD) using the time constant protocol to deliver an exponential pulse with a specified pulse length of 7 ms and voltage of 500 V. Capacitor and resistor settings were selected automatically to produce the requested pulse. Pulses were delivered to the cells twice. Following electroporation cells were allowed to recover on ice for 5 min. They were then transferred to 15 ml tubes containing 9.5 ml BHK-21 virus production medium (with nucleosides; section 2.1.4) and the cuvettes were rinsed several times to collect all cells. Cells were plated in 10 cm \varnothing dishes and returned to the incubator for 24 h. The medium containing the virus particles was collected and centrifuged (Eppendorf, 2,000 x g, 10 min) to remove any detached cells. The supernatant was aliquoted and stored at -80°C and subsequently used for the infection of BHK-21 cells (section 3.3.1) and primary cultured hippocampal neurons (section 3.3.3).

2.2.10.3 Determining the potency of the virus stock

The potency of the harvested virus stock and the optimal amounts of virus needed for infection were determined empirically by infecting BHK-21 cells with various dilutions of the virus stock and using EGFP expression as an indicator for the number of virions (section 3.3.1.3). BHK-21 cells (2×10^5 /3.5 cm \varnothing well) were plated 24 h prior to infection in BHK-21 complete medium (section 2.1.4). Dilutions of the virus (1:10, 1:100, 1:500, 1: 1000, 1:2500 and 1:5000) were prepared in BHK-21 low serum medium (1 % FBS; section 2.1.4). Cells were removed from the incubator and the medium aspirated. 100 μ l of the dilutions was mixed with 300 μ l of BHK-21 low serum medium and added to the cells. Cells were incubated at 4°C for 1 h, during which the dishes were tilted every 15 min to make sure the cells remained covered in solution. 2 ml of BHK-21 low serum medium was added and cells were placed in the incubator for 24 h. Cells were rinsed twice with 2 ml PBS (Gibco) and 2 ml of fresh BHK-21 low serum medium was added. Cells were examined using an inverted microscope (DM IBR, Leica, section A.1.3) equipped with a 20x objective and an eyepiece grid micrometer (10 x 10 grid, 0.25 mm² with 20x objective). EGFP-positive (infected) cells were counted in the 10 x 10 grid in several areas of the dish and used to calculate the potency of the virus stock; on average 10^8 – 10^9 virions/ml.

$$\text{Virions/ml} = \frac{\text{Average number of infected cells in } 10 \times 10 \text{ grid} \times 3,520 \times \text{dilution factor}}{\text{volume of viral dilution used (ml)}}$$

$$3,520 = 3.5 \text{ cm } \varnothing \text{ dish (880 mm}^2\text{)} / 10 \times 10 \text{ grid (0.25 mm}^2\text{)}$$

$$1 \text{ infected cell} = 1 \text{ virion}$$

2.2.11 Microscopy

2.2.11.1 Preparation of cells for microscopy

Transiently transfected, microinjected and infected cells were prepared for microscopy by fixation with paraformaldehyde followed in some cases by immunocytochemistry or cell staining. Transfected cells (HEK293 or Swiss-3T3) were fixed in 4 % PFA/PBS. For microinjected (Swiss-3T3) and infected (BHK-21) cells the 4 % PFA/PBS fixation solution also contained 10 % sucrose. HEK293 cells, transfected with Lipofectamine 2000 in 3.5 cm \varnothing dishes, were split onto poly-D-lysine coated 22 x 22 mm coverslips (8×10^4 - 1×10^5 cells/well) 24 h before fixation. Swiss-3T3 and BHK-21 cells were plated on poly-D-lysine coverslips from the start of an experiment.

Transiently transfected HEK293 and Swiss-3T3 cells were removed from the incubator, the medium was aspirated and the cells were rinsed three times with 2 ml 1x PBS (section 2.1.2). Cells were fixed in 1 ml 4 % PFA/PBS at room temperature for 10 min and then washed twice with 2 ml 1x PBS. For FRET experiments, HEK293 cells were mounted onto glass slides (BDH) with Mowiol mounting medium. Microinjected Swiss-3T3 cells and infected BHK-21 cells were fixed by adding 300 μ l of 4 % PFA/PBS (also containing 10 % sucrose) to the medium and incubating at room temperature for 30 min. Cells were then rinsed twice with 2 ml 1x PBS. For immunocytochemistry and cell staining, fixed HEK293, Swiss-3T3 and BHK-21 cells were permeabilized in 750 μ l 0.2 % Triton X-100 for 2 min and rinsed four times 5 min with 2 ml 1x PBS. Coverslips were transferred into a humidified chamber and 200 μ l of blocking solution was added to each coverslip. The humidified chamber was placed into an incubator (37 $^{\circ}$ C) for 30 min. For cell staining experiments of Swiss-3T3 and BHK-21 cells, the blocking solution was replaced with Alexa Fluor 488 or 594 phalloidin conjugate (0.25 U) diluted in 200 μ l blocking solution and incubated in the humidified chamber at 37 $^{\circ}$ C for 30 min. After incubation the solution was drained off the coverslips and coverslips were rinsed by dipping them 5x in a beaker filled with 30 ml 1x PBS and then by washing them three times 5 min with 10 ml 1x PBS. Coverslips were mounted onto glass slides using ProLong Antifade (Molecular Probes) mounting medium. For immunocytochemistry experiments of HEK293 cells, the blocking solution was removed and 200 μ l of primary antibody dilution (anti-HA 1:100, in blocking solution) was added to the coverslips. Incubation was performed in the humidified chamber at

37 °C for 1h and coverslips were then washed with 1x PBS as described for cell staining experiments. Cells were incubated with secondary antibodies (anti-mouse Cy5 conjugated 1:600, in 200 µl of blocking solution) in the humidified chamber at 37 °C for 30 min. Coverslips were washed as before and mounted onto glass slides with ProLong Antifade mounting medium. Protected from light, slides were kept at room temperature overnight to allow the mounting medium to harden. Coverslips were fixed firmly to the slides by sealing the edges with nail polish. Slides were examined and images acquired with an Axiophot (Zeiss) microscope and Micropublisher CCD camera (QImaging) or with a TCS SP5 confocal (Leica) microscope and corresponding LAS AF software (Leica) (section A.1.3). Images were analysed and processed with ImageJ (version 1.44p, Java 1.6.0_20) and Adobe Photoshop CS.

4 % PFA/PBS	1 x	PBS
	4 %	PFA pH 7.3
0.2 % Triton X-100	1 x	PBS pH 7.3
	0.2 %	Triton X-100
Blocking Solution	1 x	PBS
	10 %	FBS
	2 %	BSA
Mowiol Mounting Medium	100 mM	Tris-HCl pH 8.5
	10 %	Mowiol 4-88
	25 %	Glycerol

2.2.11.2 Fluorescence resonance energy transfer (FRET)

M₃ muscarinic acetylcholine receptor stimulation

Muscarinic acetylcholine receptor M₃ transfected HEK293 cells for FRET experiments (section 3.1.7) were stimulated with CCh (10 µM) before fixation. Cells were removed from the incubator and washed once with 2 ml 1x PBS (section 2.1.2). The dilution of CCh was prepared in 1x PBS and added to the cells for 3 min at room temperature. Cells were fixed in 4 % PFA/PBS containing CCh (10 µM) for 10 min. Cells were washed four times with 2 ml 1x PBS before being mounted onto glass slides (BDH) with Mowiol mounting medium.

Confocal microscopy

FRET experiments (section 3.1.7) were performed on a TCS SP5 Leica confocal microscope fitted with a 63x/1.4 NA oil-immersion objective (section A.1.3). Confocal images were acquired at 8 bit intensity resolution over 512 x 512 pixels and with a scan speed of 100 Hz of

the 100 mW Argon laser (set to 20%). Cyan fluorescent protein (CFP) and its derivatives were excited using the 458 nm laser line (at 20–30% intensity) and detected at 462–500 nm, and yellow fluorescent protein (YFP) and its derivatives were excited with the 514 nm laser line (at 20–30% intensity) and detected at 520–600 nm. No cross talk was observed under these conditions. FRET was assessed by acceptor photobleaching and was performed using Leica's LAS AF software acceptor photobleaching wizard. Bleaching experiments were performed as follows: first sequential scans of the donor and acceptor were acquired, secondly a defined region of interest (ROI) of the acceptor was bleached by increasing the intensity of the 514 nm laser line (to 50 %) to destroy the YFP fluorophores, and thirdly the sequential scan of the donor and acceptor was repeated.

FRET analysis

The ImageJ plug-in AccPbFRET (Roszik et al., 2008) was used. Following the subtraction of the background fluorescence of a cell-free area from the overall fluorescence intensity and the registration of before and after photobleaching images, FRET image analysis was performed. The mean fluorescence intensities of ROIs at the membrane (for cells expressing $G\alpha_q$ -ECFP- $G\alpha_q$) or in the cytoplasm (for cells expressing CFP-YFP, $G\alpha_q$ -ECFP, $G\alpha_q$ -ECFP- $G\alpha_q$ -L209 or $G\alpha_q$ -ECFP- $G\alpha_q$ -C183) were measured in before and after bleaching donor images and used to calculate FRET efficiency (E) according to the following formula:

$$E = 1 - (I_{DA}/I_D)$$

I_{DA} describes the normalized fluorescence intensity of the donor in presence of the acceptor (i.e. before acceptor photobleaching) and I_D the normalized fluorescence intensity of the donor after acceptor photobleaching. The average of three ROI FRET efficiency measurements was taken to determine a cell's overall FRET efficiency.

Mean acceptor fluorescence after bleaching was calculated as percentage left (with 100% corresponding to the acceptor fluorescence intensity before photobleaching) by measuring YFP fluorescence intensity of three ROIs in before and after photobleaching images.

2.2.11.3 Analysis of stress fibre formation in microinjected or infected cells

Mean fluorescence intensity was used as a measure to impartially assess the level of stress fibre formation in control, RhoA-V14 and RhoA-N19 microinjected and infected cells (section 3.2.3 and 3.3.1.4). Cells injected with TRITC alone were used as control in microinjection experiments, while the effect of RhoA-V14 and RhoA-N19 infections was compared to EGFP infected cells. TRITC and EGFP also served to identify microinjected and infected cells. Actin was stained with Alexa Fluor 488 phalloidin conjugate or Alexa Fluor 594 phalloidin conjugate

and its image was analysed together with its reporter image (TRITC or EGFP) in ImageJ. The reporter image was enhanced and the threshold (Image -> Adjust -> Threshold -> select over/under) adjusted in a way that only the injected/infected cell was spared from being masked in blue. Using the wand tool the cell was selected and its outline displayed by a yellow line. This cell outline was saved as a ROI in the ROI manager (Analyse -> Tools -> ROI Manager) and used to select the same area in the corresponding actin stain image. The mean fluorescence intensity of the actin stained cell was measured using the ROI manager. This procedure was repeated for all control, RhoA-V14 or RhoA-N19 injected. Results are shown as mean \pm SEM and statistical analysis was performed in GraphPad Prism 4.0 (GraphPad software). For statistical comparison one-way ANOVA (including a post-hoc Bonferroni's multiple comparison test) was used and significance was defined as $P < 0.05$.

2.2.11.4 Co-localisation analysis

Co-localisation between ECFP-tagged $G\alpha_q$ and Venus-RhoA (section 3.1.5) was analysed using the ImageJ plug-ins: Just Another Co-localisation plug-in (JACoP; plug-in authors S. Bolte and F. Cordelières; Bolte and Cordelières, 2006) and the intensity correlation analysis plug-in (plug-in authors T. Collins and E. Stanley; Li et al., 2004). The Pearson's coefficient, overlap coefficient and Manders' co-localisation coefficients were calculated using the JACoP plug-in and the intensity correlation quotient (ICQ) was calculated using the intensity correlation analysis plug-in. Confocal images were aligned and background subtracted before co-localisation analysis. For the analysis of the plasma membrane region, a membrane-only ROI was drawn in ImageJ with the $G\alpha_q$ -ECFP- $G\alpha_q$ image as a template. The equal number of objects in each channel is a requirement for the overlap coefficient, so ratios between channel A (ECFP-tagged $G\alpha_q$) and channel B (Venus-RhoA) were determined using the intensity correlation analysis plug-in. The normalized intensity scatter plots were drawn using the ECFP-tagged $G\alpha_q$ and Venus-RhoA intensity value pairs obtain with the intensity correlation analysis plug-in. For the intensity correlation analysis graphs the product of the difference of the mean (PDM) values were plotted against the normalized fluorescence intensity of ECFP-tagged $G\alpha_q$ or Venus-RhoA intensity; all values were obtained using the intensity correlation analysis plug-in. Whether the calculated ICQ was significantly different from zero, was assessed by performing a sign test using Excel.

The following formulas refer to the pixel intensity values of channel A (ECFP-tagged $G\alpha_q$) as A_i and of channel B (Venus-RhoA) as B_i , corresponding mean intensity values are represented as a and b . $N_{+ve\ PDM}$ is defined as the number of positive PDM values obtained and N_{total} refers to the total number of pixel pairs tested.

Pearson's Coefficient

$$r_p = \frac{\sum_i (A_i - a) \times (B_i - b)}{\sqrt{\sum_i (A_i - a)^2 \times \sum_i (B_i - b)^2}}$$

Overlap Coefficient

$$r = \frac{\sum_i A_i \times B_i}{\sqrt{\sum_i A_i^2 \times \sum_i B_i^2}}$$

Manders' Colocalisation Coefficients

$$M_1 = \frac{\sum_i A_{i,coloc}}{\sum A_i} \quad \text{with} \quad A_{i,coloc} = A_i, \text{ if } B_i > 0$$

$$M_2 = \frac{\sum_i B_{i,coloc}}{\sum B_i} \quad \text{with} \quad B_{i,coloc} = B_i, \text{ if } A_i > 0$$

Intensity Correlation Quotient

$$ICQ = \left(\frac{N_{+ve PDM}}{N_{total}} \right) - 0.5 \quad \text{with} \quad PDM = (A_i - a) \times (B_i - b)$$

2.2.12 Molecular biology techniques

2.2.12.1 Digestion of DNA with restriction enzymes

DNA was mixed with the appropriate amount of restriction enzymes, their corresponding buffer (Roche, GE or NEB) and dH₂O in 1.5 ml tubes and digested at 37 °C for 1–4 h. Analytical digests were performed in a total volume of 15 µl containing 40–1000 ng DNA. For preparative digests and digestions of vectors 1–3.6 µg DNA was digested in a volume of 40 µl. 5x DNA sample buffer was added to the digests to stop the reaction. Samples were analysed on an agarose gel.

5x DNA Sample Buffer	20 %	Ficoll 400
	100 mM	EDTA
	0.25 %	Bromphenol Blue
	0.25 %	Xylene Cyanol

2.2.12.2 Dephosphorylation of vectors

After linearization by restriction enzyme digestion, vectors were treated with alkaline phosphatase to prevent self-ligation. 2 U of alkaline phosphatase (Roche) and corresponding 10x dephosphorylation buffer was added to the digestion reaction and incubated at 37 °C for 1 h. Reactions were stopped with the addition of 5x DNA sample buffer (section 2.2.12.1).

2.2.12.3 Agarose gel electrophoresis

DNA fragments were separated by horizontal agarose gel electrophoresis. Depending on fragment size separation was performed on 0.5 %, 0.7 %, 1.0 % or 1.3 % agarose gels. TAE (National Diagnostics) buffer was used for preparative gels; TBE buffer was used for analytical gels. The necessary amount of agarose was added to 1x TAE or 1x TBE buffer in 40 ml or 70 ml and dissolved by heating in the microwave. After cooling ethidium bromide was added to a final concentration of 0.4 µg/ml, which was identical to the amount of ethidium bromide in the 1x TAE or 1x TBE running buffer, and the gel was poured. Samples were loaded alongside DNA molecular weight markers (100 bp and 1 kb DNA ladders, Invitrogen) and electrophoresis was performed at 50–100 V for 30 min–2 h. The DNA was visualized under UV light (365 nm for preparative gels, 254 nm for analytical gels) and the gels documented as prints.

5x TBE	445 mM	Tris Base
	445 mM	Boric Acid
	10 mM	EDTA

2.2.12.4 Gel extraction of DNA

DNA was extracted from gels with the Nucleobond Extract kit (Macherey-Nagel) according to manufacturer's instructions. The required DNA fragment was excised from the gel with a scalpel and the gel slice was dissolved in NT1 buffer (300 µl buffer/100 mg gel) at 65 °C for 5–10 min. The DNA was isolated by loading the sample onto a DNA binding column (silica membrane adsorption), followed by two washes with NT3 buffer (600 µl and 200 µl) and elution with 30 µl NE buffer. To increase the yield the elution was run over the column a second time.

2.2.12.5 Ligation

Dephosphorylated vector was mixed with 3 molar excess of DNA insert, 1 U T4 ligase and 5x ligation buffer and dH₂O to a final volume of 20 µl. Ligation reactions were carried out in a water bath at 14 °C for 2 h. 10 µl of the ligation mix was used to transform DH5α bacteria (section 2.2.12.7). The remaining reaction was continued to be incubated overnight and used in case the transformation of the 2 h ligation product did not result in sufficient numbers of colonies.

5x Ligation Buffer	100 mM	Tris-HCl pH 7.5
	50 mM	MgCl ₂
	50 mM	DTT
	5 mM	ATP

2.2.12.6 Competent DH5 α bacteria

DH5 α bacteria were made competent for transformation using the Okayama method (Inoue et al, 1990). DH5 α bacteria were spread onto LB plates (section 2.1.3) and incubated at 37 °C overnight. A single colony was picked the next morning, inoculated in 25 ml of SOB medium and incubated at 37 °C and 220 rpm for 6-8 h. Of this starter culture 8 ml, 6 ml and 3 ml were used to start three cultures of 125 ml SOB medium each. Incubation was carried out at 18 °C and 150 rpm overnight. Once one of the cultures reached an OD₆₀₀ of 0.55 it was transferred to an ice water bath for 10 min; the other two cultures were discarded. Bacteria were harvested by centrifugation (Beckman, JA-14 rotor) at 2,500 x g and 4 °C for 10 min, resuspended in 38 ml ice-cold TB buffer and incubated in the ice water bath for 10 min. Bacteria were pelleted (Beckman, JA-14 rotor, 2,500 x g, 4 °C, 10 min) and resuspended in 10 ml ice-cold TB buffer. Keeping the bacteria suspension in the ice water bath and swirling it gently 750 μ l of DMSO was added drop-wise. Bacteria were incubated in the ice water bath for 10 min before being aliquoted (~110 μ l/ aliquot) and immediately snap-frozen in liquid nitrogen. Competent DH5 α bacteria were stored at -80 °C and had a transformation efficiency of $\geq 3 \times 10^7$.

SOB Medium	20 g/l	Tryptone
	5 g/l	Yeast Extract
	10 mM	NaCl
	5 mM	KCl
		pH 7.0, autoclave
	10 mM	MgCl ₂ , sterile-filtered
	10 mM	MgSO ₄ , sterile-filtered
TB Buffer	10 mM	MOPS
	15 mM	CaCl ₂
	250 mM	KCl
		pH 6.7
	55 mM	MnCl ₂ sterilized by filtration

2.2.12.7 Transformation of DH5 α Bacteria

Transformation of DH5 α bacteria with DNA was performed according to one of the following protocols.

In the short protocol, 100 μ l of competent bacteria were added to plasmid DNA, which had been diluted in 10 μ l dH₂O, and mixed gently. Depending on selection criterion, transformed bacteria were spread either on LB-ampicillin plates (section 2.1.3; 100 μ g/ml) or on LB-kanamycin plates (section 2.1.3; 30 μ g/ml) and incubated at 37 °C overnight to allow colonies to grow.

The standard protocol was mainly used following ligations. 10 µl of the ligation product was mixed with 100 µl bacteria and incubated on ice for 15 min. The bacteria were heat-shocked by placing them on a heat block at 37 °C for 5 min. 110 µl of pre-warmed LB medium (section 2.1.3) was added to the bacteria, mixed gently, and the bacteria were further incubated at 37 °C for 15 min. Transformed bacteria were plated on LB-ampicillin plates (100 µg/ml) and incubated at 37 °C overnight.

The gentle protocol was used to transform DH5α bacteria with Sindbis plasmid DNA (pSIN-EGFP, pSIN-RhoA-V14-EGFP and pSIN-RhoA-N19-EGFP) and its helper pHelper-DH-BB (tRNA/TE12). Bacteria were thawed on ice, mixed with DNA (diluted in 10 µl dH₂O) or 5 µl of ligation product in pre-cooled 1.5 ml tubes and incubated on ice for 30 min. The heat-shock was performed by transferring bacteria to a heat block at 37 °C for 5 min. 1 ml pre-warmed SOC medium was added and bacteria were incubated at 37 °C and 120 rpm for 45 min. Bacteria were harvested by centrifugation (Eppendorf) at 2,500 x g for 6 min and resuspended in 110 µl SOC medium. Transformed bacteria were spread on LB-ampicillin plates (50 µg/ml) and incubated at 37 °C overnight.

SOC Medium	20 g/l	Tryptone
	5 g/l	Yeast Extract
	10 mM	NaCl
	2.5 mM	KCl
		pH 7.0, autoclave
	20 mM	Glucose, sterile-filtered
	10 mM	MgCl ₂ , sterile-filtered
	10 mM	MgSO ₄ , sterile-filtered

2.2.12.8 Isolating DNA from bacteria

Isolation of plasmid DNA from small cultures

A single colony was picked from a LB-ampicillin or LB-kanamycin plate and used to inoculate 4.5 ml LB medium (section 2.1.3) containing the appropriate antibiotic (75–100 µg/ml ampicillin or 20 µg/ml kanamycin). The culture was incubated in 14 ml Falcon tubes with snap-caps at 37 °C and 200 rpm overnight. Plasmid DNA was isolated using the NucleoSpin Plasmid kit (Macherey-Nagel) according to manufacturer's instruction. Bacteria were harvested by centrifugation (Heraeus) at 3,200 x g for 5 min and the pellet was resuspended in 250 µl A1 buffer and transferred to a 1.5 ml tube. 250 µl of A2 lysis buffer was added and gently mixed by inverting. 300 µl of A3 neutralization buffer was added, mixed and the lysate was clarified by centrifugation (Eppendorf) at 16,100 x g for 5 min. The DNA was bound by loading the supernatant onto the NucleoSpin Plasmid column (silica membrane adsorption) (Eppendorf,

11,000 x g, 1 min) and washed by adding 600 µl A4 wash buffer (Eppendorf, 11,000 x g, 1 min). The column membrane was dried by centrifugation (Eppendorf) at 11,000 x g for 2 min. The DNA was eluted by addition of 50 µl pre-warmed AE elution buffer (70 °C), incubation for 1 min and centrifugation (Eppendorf) at 11,000 x g for 1 min.

Isolation of plasmid DNA from medium and large cultures

Plasmid DNA was isolated using the NucleoBond PC100 or PC500 kits (Macherey-Nagel) according to manufacturer's instructions. Midi-preparations (PC100) were prepared from 40 ml cultures (high-copy plasmid protocol) or 70 ml cultures (adapted low-copy plasmid protocol) bacterial cultures; maxi-preparations (PC500) from 120 ml cultures (high-copy plasmid protocol) or 210 ml cultures (adapted low-copy plasmid protocol).

40 ml of LB medium (section 2.1.3) containing the appropriate antibiotic (100 µg/ml ampicillin or 20 µg/ml kanamycin) was inoculated with a single colony picked from a LB-ampicillin or LB-kanamycin plate and incubated at 37 °C and 200 rpm overnight. Bacteria were harvested by centrifugation (Heraeus) at 3,200 x g and 4 °C for 10 min and resuspended in 4 ml cold S1 buffer. Cells were lysed by adding 4 ml of S2 buffer and the suspension was gently mixed by inverting. 4 ml S3 buffer was added, gently mixed and incubated on ice for 5 min. The lysate was clarified by centrifugation (Heraeus, 3,200 x g, 4 °C, 5 min) and filtration of the supernatant through a paper filter. The supernatant was loaded onto an AX100 column (anion-exchange chromatography), which had been pre-equilibrated with 2.5 ml N2 buffer. The cartridge was washed twice with 5 ml N3 buffer and the DNA was eluted with 5 ml N5 buffer. The eluted DNA was precipitated by adding 3.5 ml isopropanol and centrifuging (Beckman, JA-17 rotor) at 12,000 x g and 4 °C for 30 min. The pelleted DNA was washed with 2 ml 75 % ethanol and centrifuged (Beckman, JA-17 rotor, 12,000 x g, 4 °C, 15 min) before being air-dried and dissolved in dH₂O at a final concentration of 1 µg/µl. DNA purity and concentration was determined using a spectrophotometer (SmartSpec Plus, BIO-RAD or NanoDrop 1000, Labtech International).

Sindbis plasmids (pSIN-EGFP, pSIN-RhoA-V14-EGFP and pSIN-RhoA-N19-EGFP) were purified from 70 ml bacterial cultures. LB medium containing 75 µg/ml carbenicillin was inoculated with a single colony or with 5 µl of a starter-culture (a single colony grown in 5 ml LB medium (75 µg/ml carbenicillin) at 37 °C and 200 rpm for 7 h) and grown at 37 °C and 200 rpm overnight. Bacteria were harvested (Heraeus, 3,200 x g, 4 °C, 10 min), resuspended in 8 ml S1 buffer containing 2 mg/ml lysozyme and incubated on ice for 10 min. Purification was continued as described above, using 8 ml of S2 and S3 buffers. Column-bound DNA was washed three times with 4 ml N3 wash buffer and elution of DNA was carried out using 5 ml

pre-warmed N5 (50 °C). DNA was precipitated, washed and dissolved following the above protocol exactly.

For DNA purifications using the NucleoBond PC500 kit (Macherey-Nagel) and the high-copy plasmid protocol, 120 ml of LB medium (100 µg/ml ampicillin) was inoculated with a single colony picked from a LB-ampicillin plate and grown at 37 °C and 200 rpm overnight. DNA purification was performed as described for 40 ml bacterial culture preparations. It differed only in the use of larger amounts of buffers (12 ml of S1, S2 and S3) and the removal of cell debris by a centrifugation of 15 min (Heraeus, 3,200 x g, 4 °C) instead of 5 min. An AX500 column, equilibrated with 6 ml N2 buffer, was used to bind the DNA and bound DNA was washed twice with 16 ml N3 buffer. 15 ml of N5 buffer was used to elute DNA, which was precipitated by addition of 11 ml of isopropanol and centrifugation (Beckman, JA-17 rotor, 12,000 x g, 4 °C, 30 min). DNA pellets were washed and dissolved as described above.

Maxi-preparations of the Sindbis helper plasmid (pHelper-DH-BB (tRNA/TE12)) were performed using the adapted low-copy plasmid protocol described above for 70 ml cultures. Briefly, a 5 ml starter culture (LB medium, 75 µg/ml carbenicillin) was inoculated with a single colony and grown at 37 °C and 200 rpm for 7 h. 5 µl of the starter culture was used to inoculate 210 ml LB medium (75 µg/ml carbenicillin) and grown at 37 °C and 200 rpm overnight. Bacteria were harvested (Beckman, JA-14) at 3,200 x g and 4 °C for 10 min and the pellet was resuspended in 24 ml S1 buffer containing 2 mg/ml lysozyme and incubated on ice for 10 min. Purification was continued as described for 120 ml high-copy plasmid purifications, using 24 ml of S2 and S3 buffers. DNA bound to the AX500 column was washed twice with 18 ml N3 buffer. Elution and precipitation of DNA was performed as described for maxi-preparations and the DNA was dissolved in dH₂O.

Reuse of AX columns

At times AX100 and AX500 columns were reused. Cross contamination was avoided by always using a cartridge for only one plasmid DNA. For direct reuse the cartridge was re-equilibrated with the appropriate amount of N2 buffer (2.5 ml for AX100 and 6 ml for AX500). For long term storage the cartridge was washed twice with dH₂O and then once with 50 % ethanol; the cartridge was filled all the way to the top and allowed to completely run out. The cartridge was carefully wrapped in Parafilm and stored in its original plastic packaging at 4 °C. The cartridge was prepared for reuse by one rinse with dH₂O and equilibration with N2 buffer as described above.

2.2.12.9 Amplification of DNA by polymerase chain reaction (PCR)

DNA modifications

DNA was amplified by PCR with KOD hot start polymerase (Novagen). In 0.2 ml PCR tubes, DNA was mixed with 1 pmol/ μ l of each of the two primers, 0.2 mM dNTPs, 1.5 mM MgSO₄, 1x KOD hot start buffer and 1 U KOD hot start polymerase in a total volume of 50 μ l. In a thermal cycler (2720, Applied Biosystems) the PCR was performed as follows: an initial denaturing step at 94 °C for 5 min was followed by 15 cycles of denaturing at 94 °C for 30 s, annealing at 45 °C for 30 s and elongation at 72 °C for 1 min, and concluded by an elongation at 72 °C for 10 min. The reaction was kept in the thermal cycler at 4 °C until use.

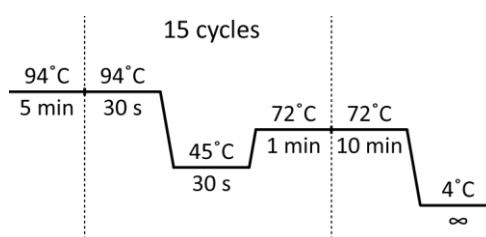


Figure 2.2 KOD polymerase PCR. Schematic representation of the reaction conditions used to perform DNA modifications.

PCR products were separated by agarose gel electrophoresis and extracted from the gel (section 2.2.12.3 and 2.2.12.4). Amplified DNA products were digested with appropriate restriction enzymes (section 2.2.12.1) and prepared for ligation by agarose electrophoresis and gel extraction as before.

Single colony PCR

Following ligations of RhoA-V14 or RhoA-N19 into pSIN-EGFP single colony PCR was performed to screen for recombinant plasmids. Single colonies were picked from LB-ampicillin plates and dissolved in 10 μ l dH₂O. In 0.2 ml PCR tubes, 5 μ l of the dissolved colony was mixed with 1 pmol/ μ l primers (P2137 and P2222), 0.2 mM dNTPs, 1.5 mM MgCl₂, 1x Taq buffer and 0.15 U Taq polymerase (Invitrogen) in a total volume of 15 μ l. PCR was performed with the following settings: an initial denaturing step at 95 °C for 10 min was followed by 25 cycles of denaturing at 94 °C for 30 s, annealing at 65 °C for 30 s and elongation at 72 °C for 1 min, and was completed by an elongation at 70 °C for 7 min. Reactions were kept at 4 °C in the thermal cycler until use. PCR products were analysed by agarose gel electrophoresis (section 2.2.12.3).

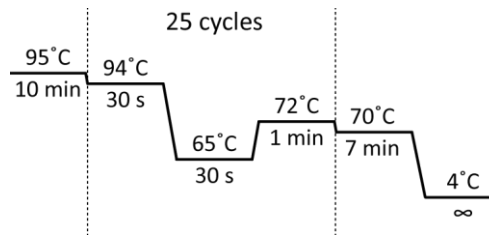


Figure 2.3 Single colony PCR. Schematic representation of the reaction conditions used to carry out single colony PCR.

2.2.12.10 Sequencing

For sequencing reactions, 400 ng of DNA was mixed with 4 μ l BigDye terminator v2.0 (Applied Biosystems) and 3.5 pmol of the sequencing primer and brought to a total volume of 20 μ l with dH₂O. The PCR was run with the following settings in a 2720 thermal cycler (Applied Biosystems): an initial denaturing step at 94 °C for 30 s was followed by 25 cycles of denaturing at 94 °C for 30 s, annealing at 50 °C for 15 s and elongation at 60 °C for 4 min; reactions were then kept at 4 °C in the thermal cycler or at -20 °C until processed.

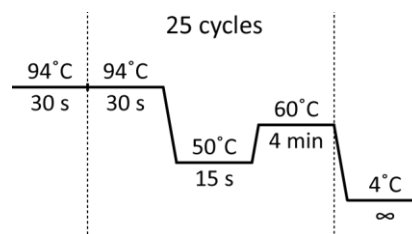


Figure 2.4 Sequencing PCR. Schematic representation illustrating the reaction settings used to sequence DNA.

Sequencing PCR products were precipitated with the addition of 2 μ l NaAc (pH 4.6, 3 M) mixed with 50 μ l EtOH absolute and incubation on ice for 10 min. Precipitated DNA was collected by centrifugation (Eppendorf) at 14,000 x g and 4 °C for 15 min, the supernatant was aspirated and the pellet was washed with 250 μ l EtOH (75 %) and centrifuged as before. All liquid was aspirated and the pellet air-dried before being sent for sequencing (3100-Avant, Applied Biosystems). Analysis was performed with DNASTar Software (Lasergene).

2.2.13 Cloning strategies

2.2.13.1 pRK5-myc-Venus-RhoA

The fluorescent fusion protein Venus-RhoA, used for FRET experiments (section 3.1.7), was constructed by inserting the YFP derivative Venus into pRK5-myc-RhoA using the *Bam* HI site. Employing this cloning strategy leaves the carboxyl-terminus of RhoA, which contains a CAAX motif essential for plasma membrane attachment, intact.

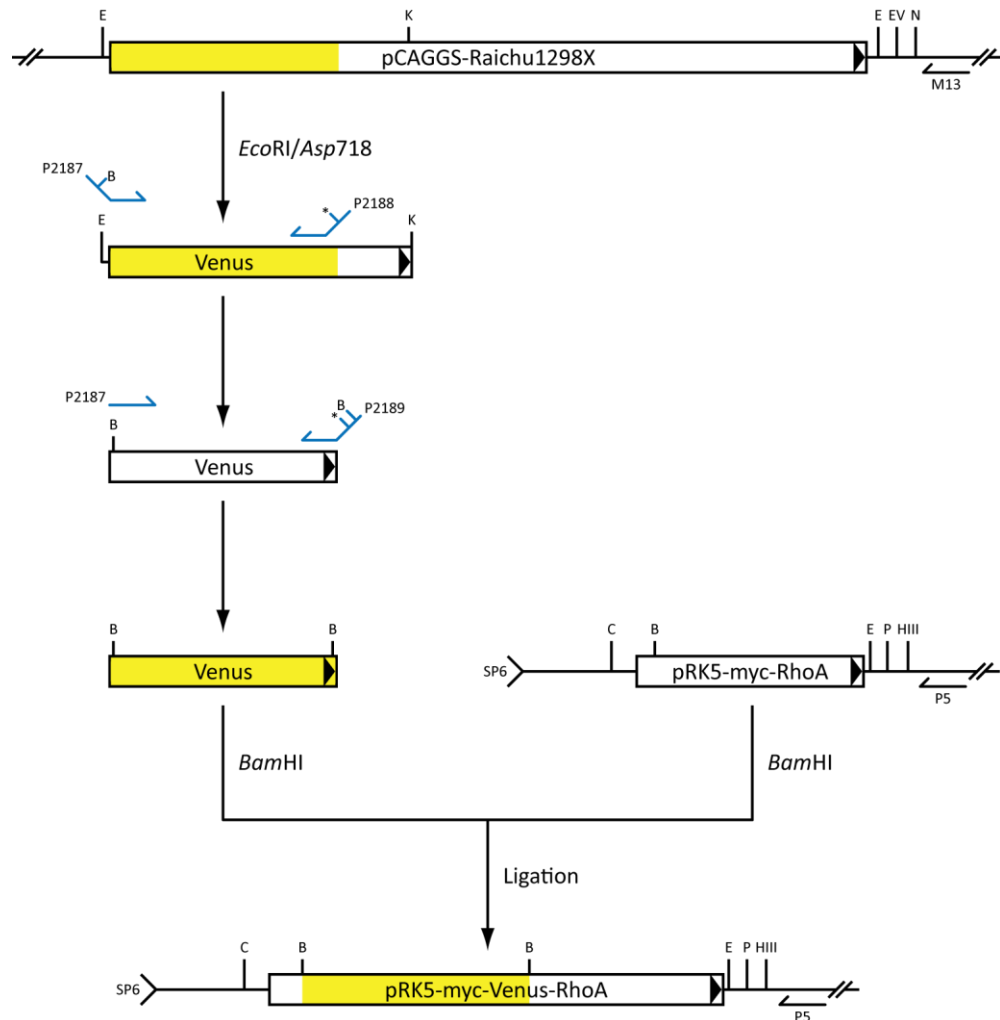


Figure 2.5 Cloning strategy of pRK5-myc-Venus-RhoA. The fluorophore Venus, a YFP derivative, was inserted between the Myc-tag and the amino-terminus of RhoA.

2.2.13.2 pcDNA3.1-EE-ECFP-G α_q -Q209L

The fluorescent fusion protein G α_q -ECFP-G α_q -L209, used for FRET experiments (section 3.1.7), was constructed by inserting a section of G α_q that was tagged with the fluorophore ECFP between residues 124 and 125 into pcDNA3.1-EE-G α_q -Q209L using the *Hind* III and *Nde* I sites. The strategy to insert ECFP into an internal loop of G α_q was chosen to leave the amino-terminus of G α_q intact, because these residues are essential for palmitoylation and G $\beta\gamma$ binding (Evanko et al., 2000; Chen and Manning, 2001), and are required so as to prevent cytosolic localization of a carboxyl-terminal tagged G α_q (Witherow et al., 2003).

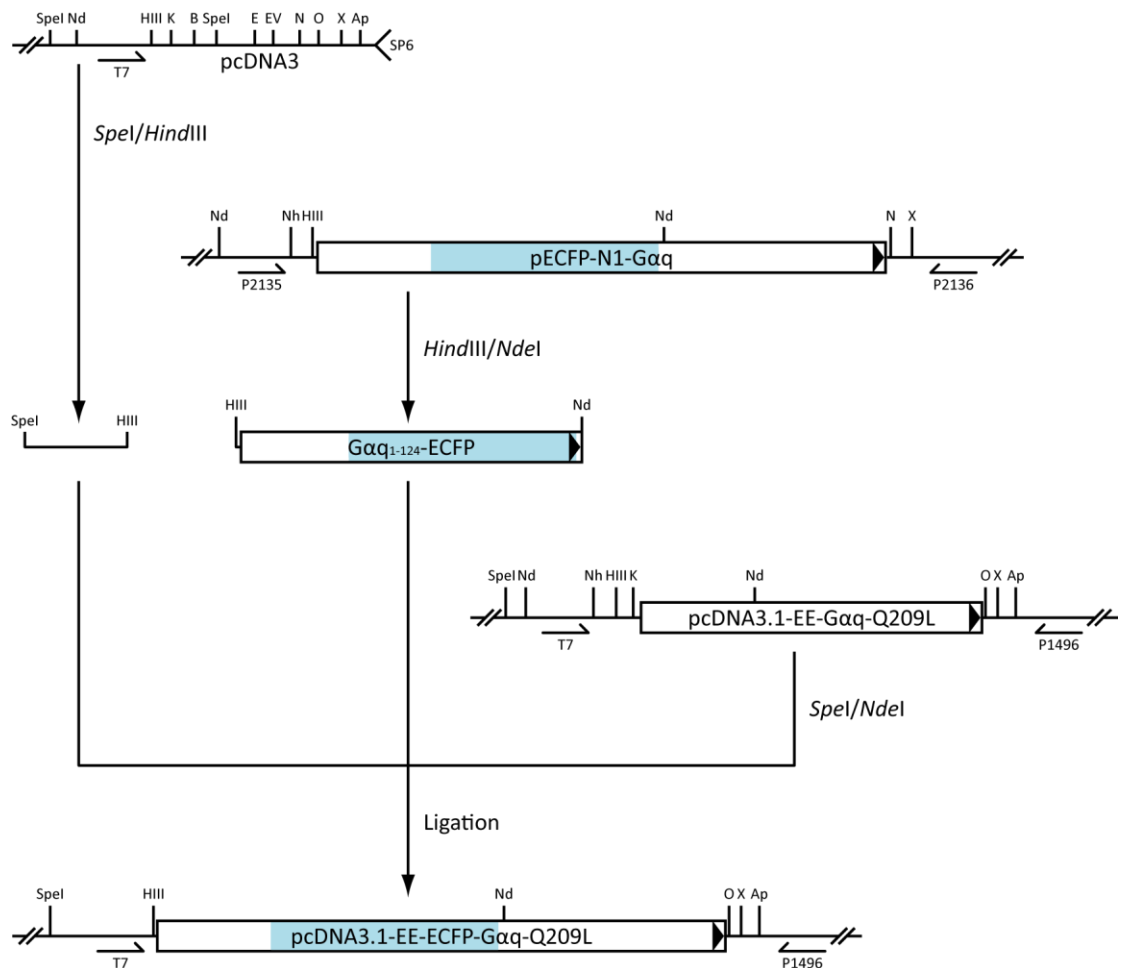


Figure 2.6 Cloning strategy of pcDNA3.1-EE-ECFP-G α_q -Q209L. Construction of constitutively active G α_q -ECFP-G α_q -L209 with ECFP placed between residues 124 and 125 of G α_q .

2.2.13.3 pSinrep5-RhoA-G14V-EGFP

RhoA-V14 Sindbis virus, used to infect cultured hippocampal pyramidal neurons (section 3.3.3), was constructed by inserting constitutively active RhoA-V14 into pSinrep5-EGFP using the *Xba* I site.

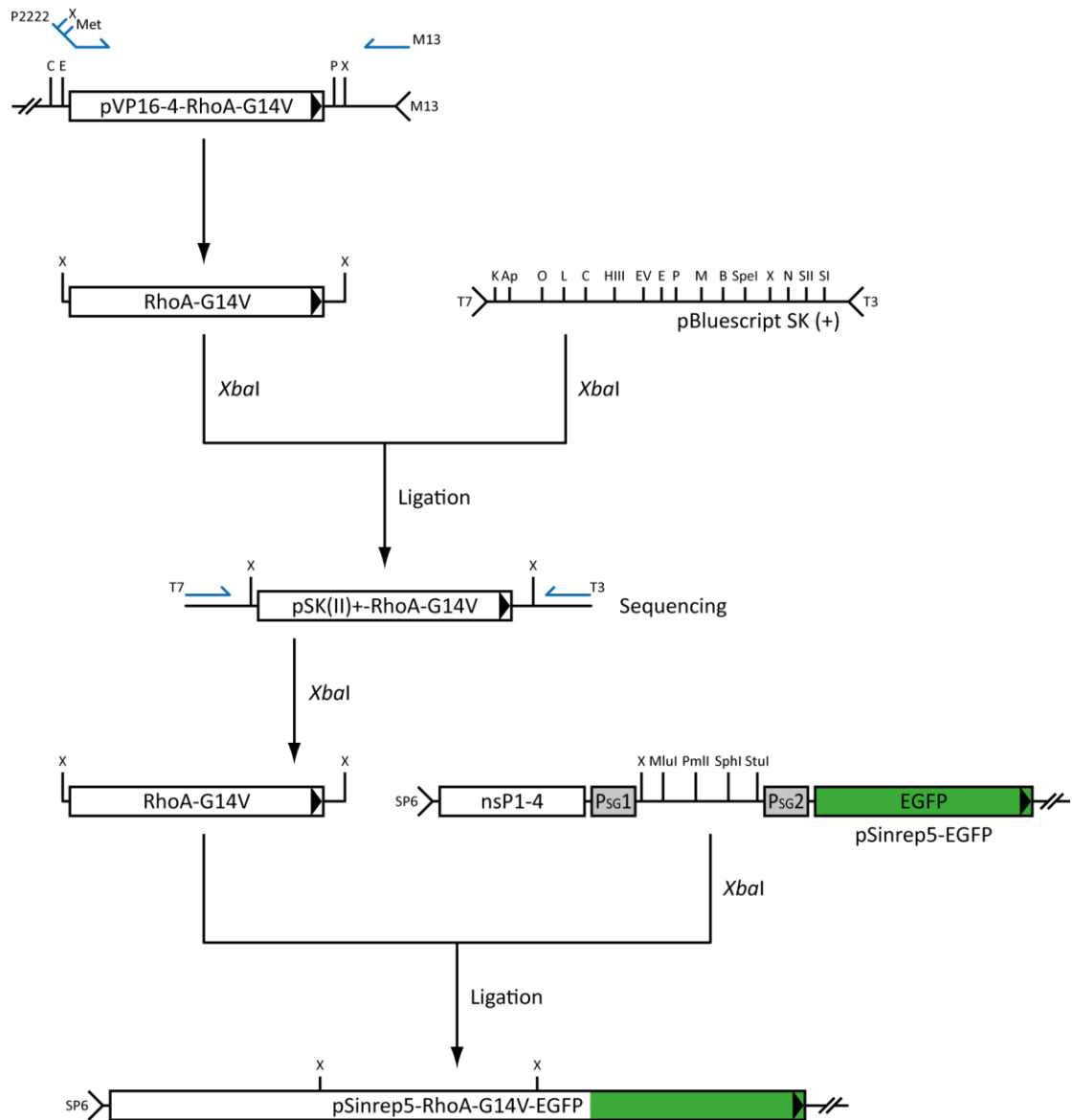


Figure 2.7 Cloning strategy of pSinrep5-RhoA-G14V-EGFP. Constitutively active RhoA-V14 was cloned into the Sindbis virus expression vector. nsP, nonstructural protein; P_{SG}, subgenomic promoter

2.2.13.4 pSinrep5-RhoA-T19N-EGFP

RhoA-N19 Sindbis virus, used to infect cultured hippocampal pyramidal neurons (section 3.3.3), was constructed by inserting inactive RhoA-N19 into pSinrep5-EGFP using the *Xba* I site.

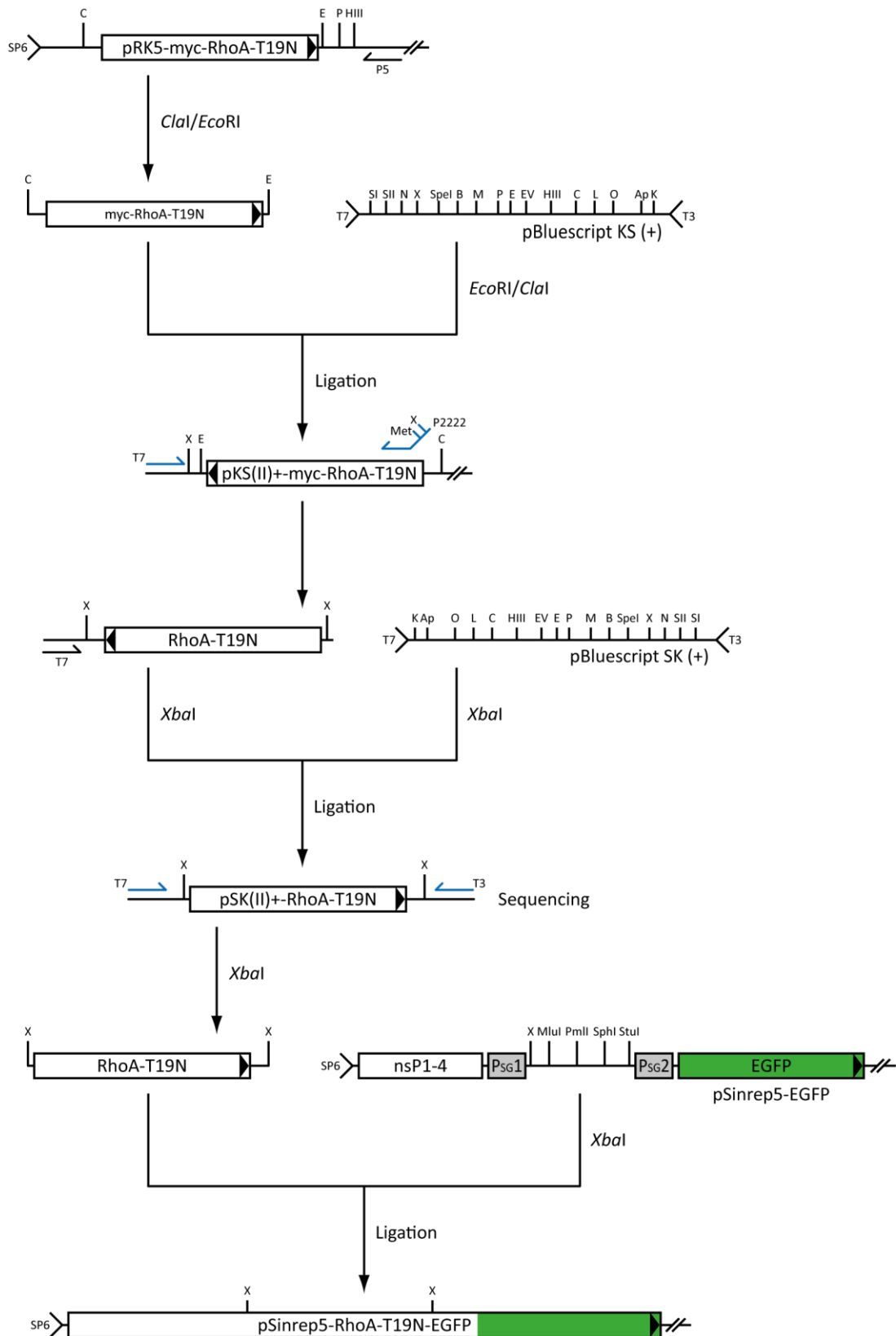


Figure 2.8 Cloning strategy of pSinrep5-RhoA-T19N-EGFP. Inactive RhoA-N19 was cloned into the Sindbis virus expression vector. nsP, nonstructural protein; P_{SG}, subgenomic promoter

2.2.13.5 Restriction enzyme abbreviations

<i>Apa</i> I	Ap	<i>Nhe</i> I	Nh
<i>Asp</i> 718	K	<i>Not</i> I	N
<i>Bam</i> HI	B	<i>Pst</i> I	P
<i>Cla</i> I	C	<i>Sal</i> I	L
<i>Eco</i> RI	E	<i>Sma</i> I	M
<i>Eco</i> RV	EV	<i>Sst</i> I	SI
<i>Hind</i> III	HIII	<i>Xba</i> I	X
<i>Ksp</i> I	SII	<i>Xho</i> I	O
<i>Nde</i> I	Nd		

2.2.14 Electrophysiology

2.2.14.1 Recordings in primary culture of hippocampal neurons

3.8–5.0 M Ω borosilicate glass pipettes were pulled with a L/M-3P-A vertical puller (List Medical) and filled with a potassium methylsulphate (KMeSO₄)-based intracellular solution. Whole-cell gigaseal recordings (Hamill et al., 1981) were obtained from pyramidal neurons in hippocampal cultures (DIV 9–16; section 3.3.2 and 3.3.3) prepared as described above (section 2.2.1.3). Using an EPC10 patch clamp amplifier (HEKA Elektronik) and the Pulse v8.8 software (HEKA Elektronik) recordings were performed under visual control (Axiovert 200, Zeiss, section A.1.3) and pyramidal neurons were identified by their morphology. Cells, infected with RhoA-V14 or RhoA-N19 Sindbis virus, were identified by their EGFP expression. Recordings from uninfected neurons served as control. Recordings were carried out at room temperature and cells were constantly superfused with extracellular solution (1 ml/min). In these recordings the liquid junction potential was 9.5 mV and not corrected. D-(-)-2-amino-5-phosphonopentanoic acid (APV, 25 μ M), blocking NMDA receptors, and 2,3-dioxo-6-nitro-1,2,3,4-tetrahydrobenzo(f) quinoxaline-7-sulfonamide (NBQX, 5 μ M), blocking AMPA receptors, were added to the extracellular solution at all times to suppress excitatory network activity of the neurons.

Intracellular Solution	135 mM	KMeSO ₄
	10 mM	KCl
	10 mM	HEPES
	1 mM	MgCl ₂
	2 mM	ATP-Na
	0.4 mM	GTP-Na
		pH 7.25–7.3
		osmolarity 290–300

Extracellular Solution	140 mM	NaCl
	3.5 mM	KCl
	10 mM	HEPES
	16 mM	Glucose
	2 mM	CaCl ₂
	1.5 mM	MgCl ₂
		pH 7.4 osmolarity 305–310
Ca ²⁺ -free Extracellular Solution	140 mM	NaCl
	3.5 mM	KCl
	10 mM	HEPES
	16 mM	Glucose
	5 mM	MgCl ₂
		pH 7.4
		osmolarity 305–310

Once whole-cell configuration was established, the membrane resting potential of a cell was read off immediately by switching to current clamp mode (without injecting any current). Only cells with a membrane resting potential of $V_{rest} \leq -50$ mV were included in the analysis. In current clamp mode the firing activity of a cell was examined by delivering current injections in 50 pA steps (starting with 50 pA) that lasted 1 s (Fig. 2.9). Current injections were delivered every 10 s and acquired traces were filtered at 2.8 kHz.

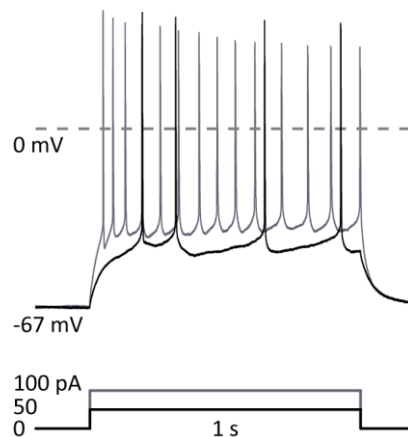


Figure 2.9 Assessing the firing activity of a cell. The firing behaviour of a cell (top) was examined using a stimulation protocol (bottom) that delivered increasing current injections, in 50 pA steps, every 10 s with each injecting of current lasting 1 s. In this example of a recording, only current injections of 50 pA and 100 pA were delivered.

The cell was then switched to voltage clamp mode and held at a holding potential of -50 mV. In whole-cell configuration the current will flow through a series of resistors. The resistances (series resistance, R_s and membrane resistance, R_{in}) present were calculated from the current response of the cell to a 5 mV hyperpolarizing step from the holding potential of -50 mV that

lasted 100 ms (Fig. 2.10). Traces were acquired at intervals of 4 s and were filtered at 5 kHz. Only cells with a series resistance of $R_s < 30 \text{ M}\Omega$ and a membrane resistance of $R_{in} > 100 \text{ M}\Omega$ were included in the analysis.

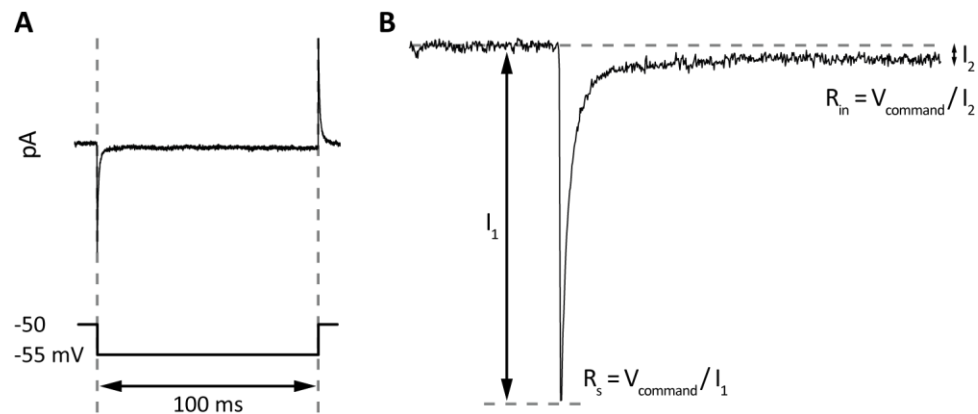


Figure 2.10 Measuring passive membrane property of a cell. (A) The hyperpolarizing voltage step from -50 mV to -55 mV (V_{command} , bottom) resulted in the current trace shown (top). **(B)** This current response was used to calculate the series resistance (R_s) and the membrane resistance (R_{in}) using Ohm's law. R_s was calculated by dividing the V_{command} step by the amplitude of the capacitive transient, I_1 . For R_{in} the V_{command} step was divided by the amplitude of the current (after reaching steady state), I_2 .

2.2.14.2 sI_{AHP} recordings in cultured hippocampal neurons

Cells were voltage-clamped at -50 mV and sI_{AHP} was activated by applying a depolarizing step to +30 mV that lasted 200 ms (Fig. 2.11A). This caused a rise in intracellular Ca^{2+} , which was elicited by the opening of voltage-gated Ca^{2+} channels (Ca_v). Changes to the series resistance were monitored throughout by delivering a 100 ms long 5 mV hyperpolarizing step to the cell at the beginning of each protocol (Fig. 2.11A). This stimulating protocol was delivered at 30 s intervals and traces were filtered at 250 Hz. Ca^{2+} influx into the cells was maximized by adding the voltage-gated Na^+ channel blocker tetrodotoxin (TTX, 0.5 μM) and the voltage-gated K^+ channel blocker TEA (1 mM) to the bath solution. The addition of dTC (50–100 μM) to the extracellular solution isolated sI_{AHP} by blocking $\text{K}_{\text{Ca}2}$ channels that underlie I_{AHP} . sI_{AHP} was suppressed by the application of the cyclic AMP analogue 8CPT-cAMP (100 μM , in bath solution) or the cholinergic agonist CCh (2.5 μM , in bath solution).

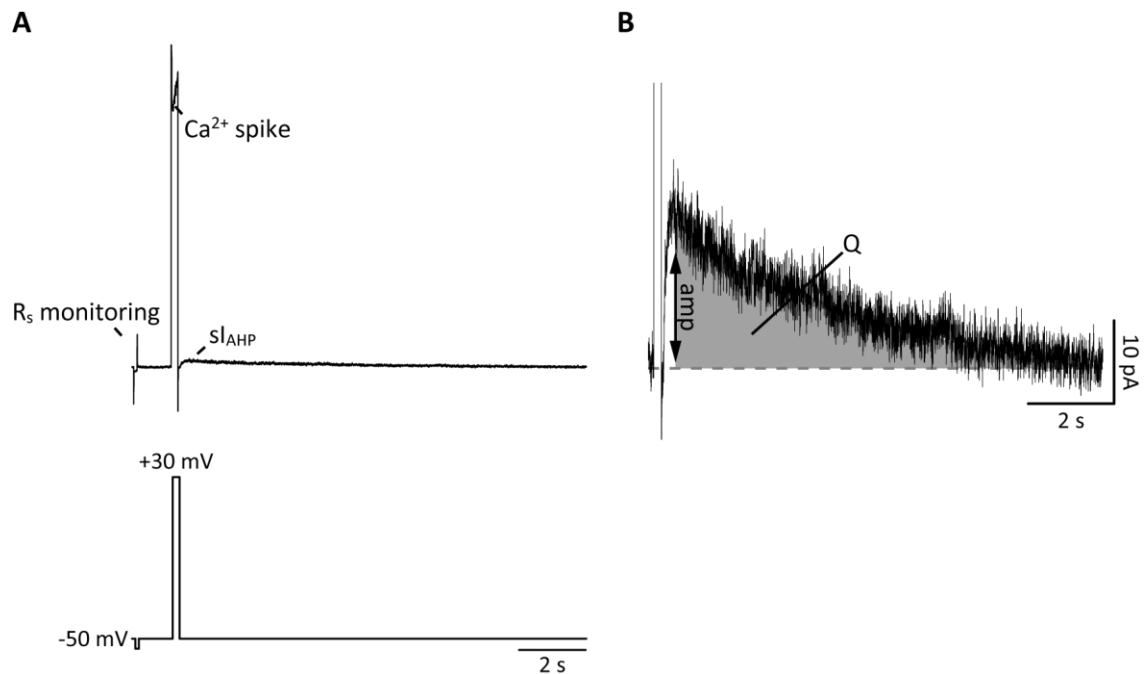


Figure 2.11 Example of a sI_{AHP} recording and details of the corresponding stimulation protocol and current measurements. (A) Current trace (top) recorded upon delivery of the voltage clamp protocol shown (bottom). The protocol commenced with a hyperpolarizing step (to -55 mV for 100 ms) that was used to monitor series resistance (R_s), while the depolarizing step (to $+30$ mV for 200 ms) caused an influx of Ca^{2+} through Ca_v channels and activated Ca^{2+} -dependent sI_{AHP} . **(B)** Enlarged sI_{AHP} current trace indicating the measurements that were taken: amplitude (amp, mean amplitude value at the peak of sI_{AHP}) and charge transfer (Q, area under the curve measured from the peak to the end of the trace). The dashed grey line indicates zero current. The recording was performed in the presence of $25 \mu\text{M}$ D-(-)-2-amino-5-phosphonopentanoic acid, $5 \mu\text{M}$ 2,3-dioxo-6-nitro-1,2,3,4-tetrahydrobenzo(f) quinoxaline-7-sulfonamide, $0.5 \mu\text{M}$ tetrodotoxin, 1 mM tetraethylammonium and $50 \mu\text{M}$ d-Tubocurarine.

After reaching a stable baseline, recorded sI_{AHP} current traces were analysed by taking the following measurements: amplitude (amp; Fig. 2.11B, mean current value measured at the peak of the sI_{AHP} trace (0.7–1.0 s after the end of the depolarisation step)) and charge transfer (Q; Fig. 2.11B, area under curve measured from the peak to the end of the sI_{AHP} current trace). Occasionally I_{AHP} current traces were analysed (Fig. 3.26) and mean I_{AHP} amplitude values were measured ~ 0.1 s after termination of the depolarisation step. Stock solution of 8CPT-cAMP (50 mM), APV (50 mM), CCh (10 mM), dTC (20 mM), NBQX (5 mM), TEA (1 M) and TTX (0.2 mM) were prepared in dH_2O . TEA and TTX stock solutions were stored at $+4^\circ\text{C}$ and all other stock solutions at -20°C .

2.2.14.3 Data analysis and statistics

Electrophysiological data were analysed using Igor Pro 6.2 (WaveMetrics) and statistical analysis was performed in GraphPad Prism 4.0 (GraphPad software). Results are shown as mean \pm SEM. For statistical comparison paired and unpaired two-tailed Student's t-tests and

one-way ANOVA (including a post-hoc Bonferroni's multiple comparison test) were used and significance was defined as $P < 0.05$.

3 Results

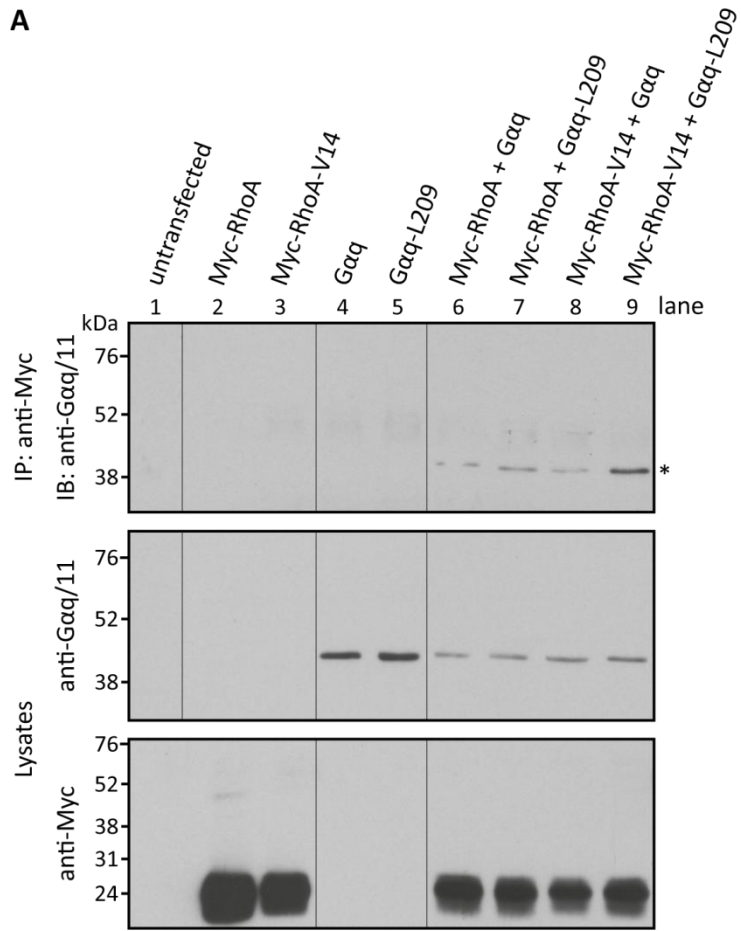
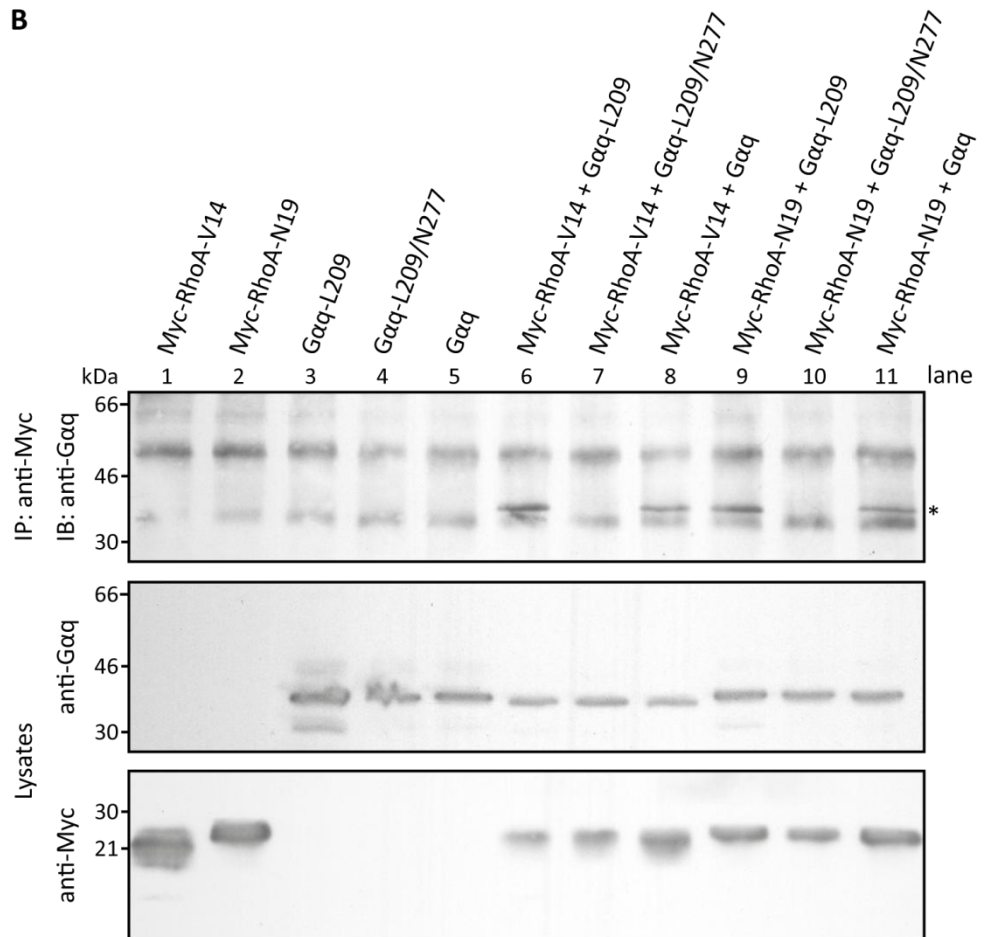
3.1 Investigating the interaction between the G-Protein α subunit $G\alpha_q$ and the small GTPase RhoA

The signalling pathway mediating the suppression of sI_{AHP} by cholinergic and glutamatergic agonists has been shown to involve the G-protein α subunit $G\alpha_q$ (Krause et al., 2002), but not via the classical pathway involving activation of $PLC\beta$ and Ca^{2+} release from IP_3 -sensitive stores or activation of PKC (Krause and Pedarzani, 2000; Sim et al., 1992). Thus this thesis examined whether sI_{AHP} suppression was conveyed by other downstream effectors of $G\alpha_q$, for example through members of the family of small GTPases (section 1.4). It focuses on the involvement of the small GTPase RhoA in the signalling pathway responsible for the inhibition of sI_{AHP} by cholinergic and glutamatergic agonists and its association with $G\alpha_q$.

3.1.1 The G-Protein α subunit $G\alpha_q$ interacts with the small GTPase RhoA

The hypothesized interaction of the G-protein α subunit $G\alpha_q$ and the small GTPase RhoA was assessed by conducting co-immunoprecipitation experiments. G-proteins and small GTPases cycle between GTP-bound (active) and GDP-bound (inactive) states and co-immunoprecipitations were performed using active and inactive mutants as well as native $G\alpha_q$ and RhoA (section 2.1.1 and Fig. 2.1). Native $G\alpha_q$, constitutively active $G\alpha_q$ -L209 and inactive $G\alpha_q$ -L209/N277 were transiently transfected into HEK293 or COS7 cells together with native RhoA, constitutively active RhoA-V14 or inactive RhoA-N19, all three were Myc-tagged at the amino terminus (section 2.1.1). $G\alpha_q$, $G\alpha_q$ -L209, $G\alpha_q$ -L209/N277, RhoA, RhoA-V14 and RhoA-N19 transfected on their own served as controls as did untransfected HEK293 cells. Protein expression was assessed by Western blotting using anti- $G\alpha_{q/11}$, anti-Gaq and anti-Myc antibodies and the detected bands at ~ 40 kDa for $G\alpha_q$ and at ~ 23 kDa for Myc-tagged RhoA matched their predicted molecular weights (Fig. 3.1A and B, middle and lower panels (lysates)).

Figure 3.1 **G-Protein α subunit $G\alpha_q$ and constitutively active $G\alpha_q$ -L209 interact with the small GTPase RhoA, constitutively active RhoA-V14 and inactive RhoA-N19.** HEK293 cells **(A)** and COS7 cells **(B)** were transiently transfected with the various RhoA and $G\alpha_q$ constructs as indicated (section 2.1.1 for construct details). Untransfected HEK293 cells were used as control (A, lane 1). Protein expression was analysed by Western blotting (lysates (15 μ g), middle and lower panels (A and B)) using anti- $G\alpha_{q/11}$, anti- $G\alpha_q$ and anti-Myc (targeting Myc-tagged RhoA) antibodies at a dilution of 1:1000. For co-immunoprecipitations (A and B, upper panels), 250 μ g of the lysates were incubated with 1–2 μ g anti-Myc antibody (Millipore (A) or Santa Cruz (B)) and RhoA was immunoprecipitated (IP). Proteins were separated on 12.5 % polyacrylamide gels, transferred to nitrocellulose membranes and immunoblotting (IB) was performed using anti- $G\alpha_{q/11}$ (A, upper panel) or anti- $G\alpha_q$ (B, upper panel) antibodies at a dilution of 1:1000. (A) Representative result, n=6. The vertical grey lines show where the digital image of the blot was cut into sections in order to present the data of this experiment in two different figures. (B) Experiments were performed by J. Pitcher and a different antibody (anti- $G\alpha_q$, Santa Cruz) and molecular weight marker was used. The anti- $G\alpha_q$ antibody generally resulted in high background signals and because the two antibodies (anti-Myc and anti- $G\alpha_q$, both Santa Cruz) were raised in the same species, antibody chain bands (~50 kDa, upper panel) were detected. The star in the upper panels indicate co-immunoprecipitated $G\alpha_q$.

A**B**

The small GTPase RhoA was immunoprecipitated using an anti-Myc antibody and co-immunoprecipitation of $G\alpha_q$ was tested by probing with anti- $G\alpha_{q/11}$ or anti- $G\alpha_q$ antibody (Fig. 3.1A and B, upper panels). Two different $G\alpha_q$ antibodies (anti- $G\alpha_{q/11}$ and anti- $G\alpha_q$; section A.1.6) were tested in the co-immunoprecipitation experiments presented in this thesis. The anti- $G\alpha_q$ antibody resulted in high background signals and thus the anti- $G\alpha_{q/11}$ antibody was preferentially used. Co-immunoprecipitations of untransfected HEK293 cell lysates and lysates transfected with the various constructs of RhoA or $G\alpha_q$ on their own did not result in the detection of bands when probed with anti- $G\alpha_{q/11}$ antibody (Fig. 3.1A, upper panel, lanes 1–5) or anti- $G\alpha_q$ antibody (Fig. 3.1B, upper panel, lanes 1–5). In lysates expressing both proteins, $G\alpha_q$ and constitutively active $G\alpha_q$ -L209 were able to associate with RhoA and constitutively active RhoA-V14 as seen by the detection of bands at ~40 kDa (Fig. 3.1A, upper panel, lane 6–9). $G\alpha_q$ and constitutively active $G\alpha_q$ -L209 also interacted with inactive RhoA-N19 (Fig. 3.1B, upper panel, lanes 9 and 11). Inactive $G\alpha_q$ -L209/N277 failed to associate with constitutively active RhoA-V14 as well as with inactive RhoA-N19 (Fig. 3.1B, upper panel, lanes 7 and 10). It was thus shown that, in a heterologous expression system, the G-protein α subunit $G\alpha_q$ interacts with the small GTPase RhoA and that this interaction relies on $G\alpha_q$ being active.

	RhoA	active RhoA-V14	inactive RhoA-N19
$G\alpha_q$	✓	✓	✓
active $G\alpha_q$ -L209	✓	✓	✓
inactive $G\alpha_q$ -L209/N277		X	X

Table 3.1 Summary of $G\alpha_q$ and RhoA co-immunoprecipitations experiments. Co-immunoprecipitations of the G-Protein α subunit $G\alpha_q$ and the small GTPase RhoA have shown that $G\alpha_q$ and constitutively active $G\alpha_q$ -L209 interact with RhoA, constitutively active RhoA-V14 and inactive RhoA-N19, while inactive $G\alpha_q$ -L209/N277 binds neither constitutively active RhoA-V14 nor inactive RhoA-N19.

3.1.2 Constitutively active $G\alpha_q$ -L209 specifically binds constitutively active RhoA-V14, but not other small GTPases

To test whether the interaction of the G-Protein α subunit $G\alpha_q$ with the small GTPase RhoA was specific, co-immunoprecipitations of constitutively active $G\alpha_q$ -L209 with other small GTPases were performed. COS7 cells were transiently transfected with constitutively active $G\alpha_q$ -L209 on its own or together with RhoA-V14, Rac-V12, Cdc42-V12, RalA-L61 or Arf6-L67, all of which were constitutively active mutants and Myc-tagged at the amino-terminus. Protein expression was tested by Western blotting using anti- $G\alpha_{q/11}$ and anti-Myc antibodies and bands were detected at ~40 kDa for $G\alpha_q$ -L209 and ~21 kDa for the small GTPases (Fig. 3.2, middle and lower panels (lysates)). Small GTPases were immunoprecipitated using an anti-Myc antibody and co-immunoprecipitation of $G\alpha_q$ -L209 was assessed by probing with an anti- $G\alpha_{q/11}$

antibody. $G\alpha_q$ -L209 associated specifically with RhoA-V14 and bound none of the other small GTPases tested (Fig. 3.2, upper panel, lane 3).

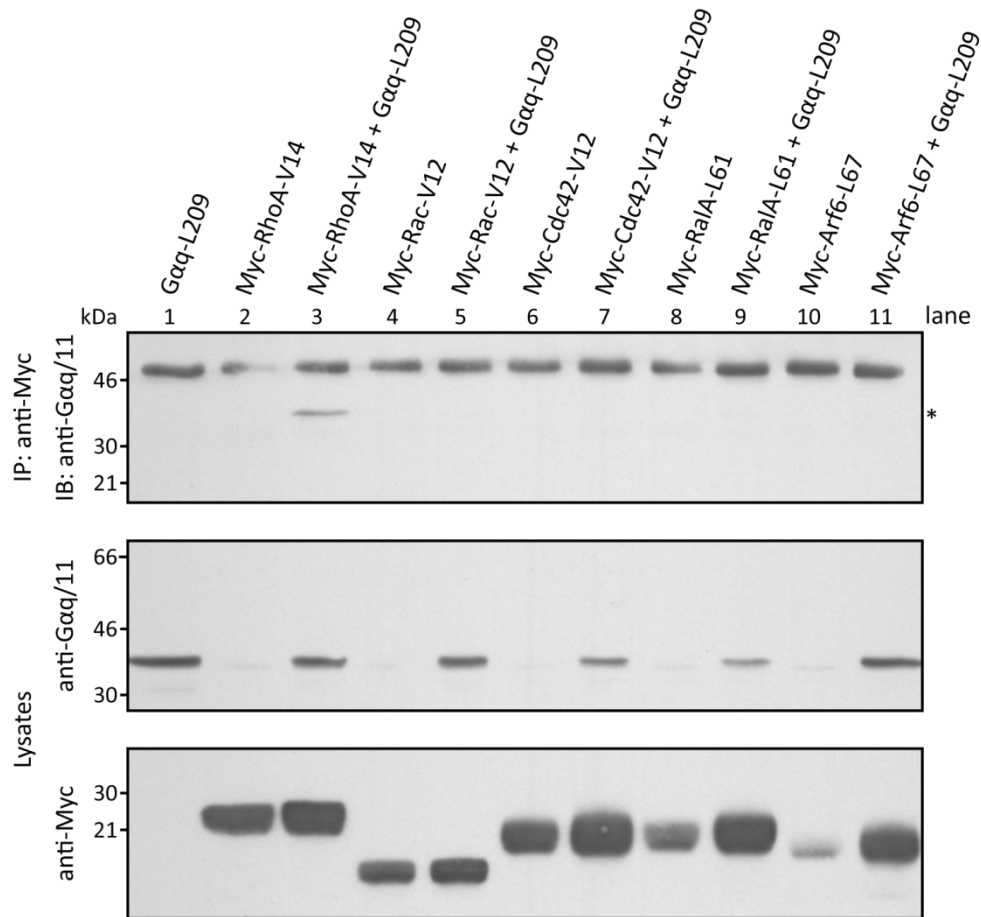


Figure 3.2 **Constitutively active $G\alpha_q$ -L209 specifically interacts with constitutively active RhoA-V14.** COS7 cells were transiently transfected with constitutively active $G\alpha_q$ -L209 and constitutively active small GTPases as indicated. 15 μ g of the lysates were used to test for protein expression by Western blotting with anti- $G\alpha_{q/11}$ (middle panel) and anti-Myc (lower panel) antibodies at a dilution of 1:1000. To immunoprecipitate (IP) Myc-tagged small GTPases 250 μ g of the lysates were incubated with 1 μ g anti-Myc antibody (Santa Cruz), before being probed (IB) for associated $G\alpha_q$ -L209 using the anti- $G\alpha_{q/11}$ antibody (upper panel) at a dilution of 1:1000. Proteins were separated on 12.5 % polyacrylamide gels. Antibody chain bands (\sim 50 kDa, upper panel) were detected, as the two antibodies (anti-Myc and anti- $G\alpha_q$, both Santa Cruz) used in this co-immunoprecipitation experiment were raised in the same species. The star indicates co-immunoprecipitated $G\alpha_q$. Experiments were performed by J. Pitcher.

3.1.3 Constitutively active RhoA-V14 specifically interacts with constitutively active $G\alpha_q$ -L209 and constitutively active $G\alpha_{14}$ -L205

$G\alpha_q$ has been shown to specifically bind RhoA and this interaction led to the investigation of whether RhoA can also associate with other $G\alpha$ subunits. To perform these co-immunoprecipitations COS7 cells were transiently transfected with constitutively active RhoA-V14 and constitutively active, Glu Glu (EE) epitope-tagged $G\alpha_q$ -L209 (Fig. 2.1), $G\alpha_{11}$ -L209, $G\alpha_{14}$ -L205, $G\alpha_{15}$ -L212, $G\alpha_{12}$ -L231 or $G\alpha_{13}$ -L226. Expression of the proteins was assessed by Western blotting using anti-Myc and anti-EE antibodies and bands of the expected molecular weights

were detected (Fig. 3.3, middle and lower panels (lysates)). Constitutively active RhoA-V14 was immunoprecipitated with anti-Myc antibody and its interaction with constitutively active $G\alpha_q$ -L209 as well as constitutively active $G\alpha_{14}$ -L205 was determined after probing with an anti-EE antibody (Fig. 3.3, upper panel, lane 3 and 7).

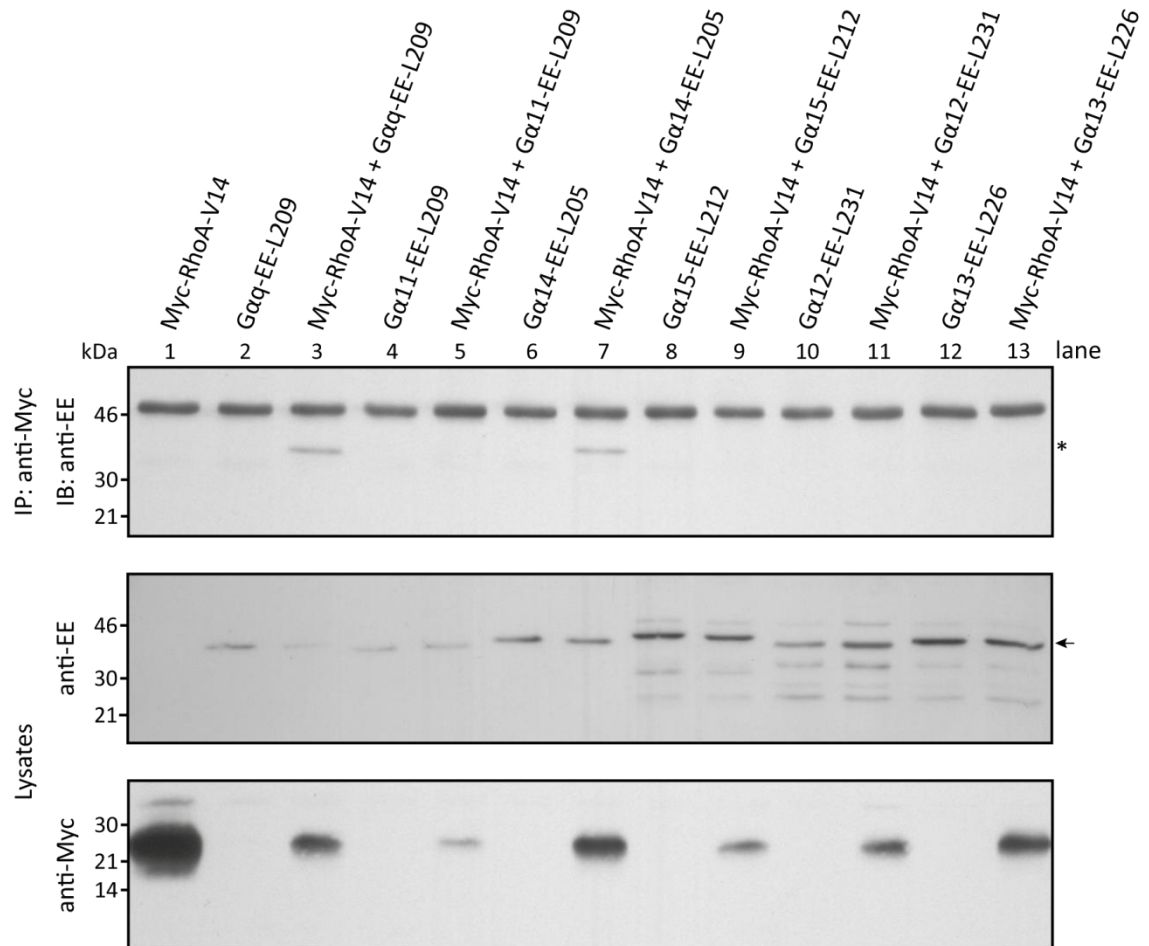


Figure 3.3 Constitutively active RhoA-V14 interacts with constitutively active $G\alpha_q$ -L209 and constitutively active $G\alpha_{14}$ -L205. COS7 cells were transiently transfected with RhoA-V14 and $G\alpha$ subunits as indicated and Western blotting using anti-Myc and anti-EE antibodies at a dilution of 1:1000 assessed the expression of the proteins (lysates (15 μ g), middle and lower panels). To immunoprecipitate (IP) Myc-tagged RhoA-V14 250 μ g of the lysates were incubated with 1 μ g anti-Myc antibody (Santa Cruz). Associated $G\alpha$ subunits were detected by probing (IB) with an anti-EE antibody at a dilution of 1:1000 (upper panel). Proteins were separated on 12.5 % polyacrylamide gels. Antibody chain bands (~50 kDa, upper panel) were detected, as the two antibodies (anti-Myc and anti- $G\alpha_q$, both Santa Cruz) used in this co-immunoprecipitation experiment were raised in the same species. The star indicates co-immunoprecipitated $G\alpha_q$ and the arrow the correct molecular weight of $G\alpha$ subunits (40 kDa). Experiments were performed by J. Pitcher.

3.1.4 Investigating the interaction between G-protein α subunit $G\alpha_q$ and small GTPase RhoA in rat brain lysates

Following the successful co-immunoprecipitation of G-Protein α subunit $G\alpha_q$ with the small GTPase RhoA in a heterologous expression system, their interaction was studied in native tissue. Lysates of rat brain were prepared and the presence of endogenous proteins was

assessed by Western blotting. Western blots of brain lysate were probed with anti-G $\alpha_{q/11}$ antibody and showed a band at ~40 kDa being similar to the band of G α_q -L209 expressed in HEK293 cells and the known molecular weight of G α_q (Fig. 3.4A). The anti-RhoA antibody was shown to detect RhoA expressed in HEK293 cells just like the anti-Myc antibody did (compare Fig. 3.4B, right panel to Fig. 3.1A). When it was used to probe for endogenous RhoA in brain lysates it detected a band at ~21 kDa corresponding with the molecular weight of RhoA (Fig. 3.4B, left panel). But, while endogenous G α_q was readily detected by the anti-G $\alpha_{q/11}$ antibody, the detection of RhoA with anti-RhoA antibody required the use of far greater amounts of brain lysate (Fig. 3.4).

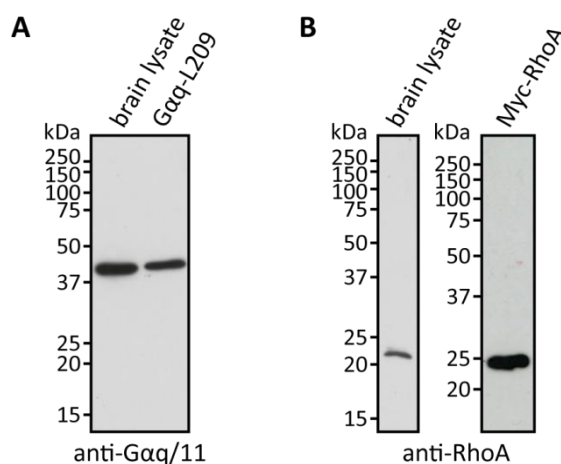


Figure 3.4 Western blots of brain and HEK293 cell lysates using anti-G $\alpha_{q/11}$ and anti-RhoA antibodies. Cell lysates were separated on 12 % polyacrylamide gels, transferred to nitrocellulose membranes and probed with either anti-G $\alpha_{q/11}$ (A) or anti-RhoA antibodies (B). **(A)** 30 μ g of brain lysate and 15 μ g of HEK293 cell lysate expressing G α_q -L209 were separated by SDS-PAGE and immunoblotting was performed using anti-G $\alpha_{q/11}$ antibody at a dilution of 1:500. **(B)** Western blots of RhoA used 110 μ g of brain lysate and 15 μ g of HEK293 cell lysate expressing RhoA and were probed using anti-RhoA antibody at a dilution of 1:200. Western blots are representative of at least three separate experiments.

Co-immunoprecipitations of endogenous G α_q and RhoA were performed by incubating brain lysate with anti-RhoA antibody before probing for G α_q using the anti-G $\alpha_{q/11}$ antibody. No bands were detected at ~40 kDa, indicating that G α_q was probably not associated with RhoA (data not shown). Co-immunoprecipitations were repeated using anti-G $\alpha_{q/11}$ antibody to precipitate G α_q and probing for bound RhoA with anti-RhoA antibody, but no band was detected at the expected molecular weight of RhoA at ~21 kDa (data not shown). To test the effectiveness of the anti-RhoA antibody in co-immunoprecipitation experiments, both versions of co-immunoprecipitations described above for brain lysates were also performed with HEK293 cell lysates co-expressing G α_q and RhoA. Once more, no bands were detected at the expected molecular weights in either experiment (data not shown). To test whether RhoA was precipitated in the first place, immunoprecipitations of RhoA were probed with anti-RhoA antibody and the absence of bands established that the anti-RhoA antibody could not

immunoprecipitate RhoA (data not shown). Thus, due to the unavailability of an anti-RhoA antibody with sufficient avidity, the interaction of the G-protein α subunit $G\alpha_q$ and the small GTPase RhoA shown in heterologous expression systems could not be verified in native tissue.

3.1.5 Expression and co-localisation of ECFP-tagged $G\alpha_q$ and Venus-tagged RhoA in HEK293 cells

To study the interaction of the G-Protein α subunit $G\alpha_q$ and the small GTPase RhoA by FRET, fluorescent fusion proteins were constructed. The choice for the generation of fluorescent fusion proteins was based on our experience with CFP/YFP tags in FRET experiments (Kerschensteiner et al., 2005) and on the fact that the anti-RhoA antibody was found to be too insensitive in previous experiments. $G\alpha_q$ and RhoA were tagged with GFP variants and in the case of $G\alpha_q$ several ECFP-tagged fusion proteins were constructed. The ECFP-tag was placed either at the carboxyl-terminus of $G\alpha_q$ (Witherow et al., 2003) or between residues 124 and 125 in a loop of the α -helical domain (Fig. 1.6 and Fig. 2.1) (Hughes et al., 2001; Witherow et al., 2003). The reason to insert ECFP into an internal loop of $G\alpha_q$ was due to reports of a cytosolic localisation of the carboxyl-terminal tagged $G\alpha_q$ (Witherow et al., 2003). In addition to the native $G\alpha_q$ fusion proteins, two constitutively active $G\alpha_q$ constructs containing the ECFP-tag between residues 124 and 125 were constructed ($G\alpha_q$ -ECFP- $G\alpha_q$ -L209; section 2.2.13 and $G\alpha_q$ -ECFP- $G\alpha_q$ -C183; Dowal et al., 2006).

RhoA contains a CAAX motif at the carboxyl-terminus, which is prenylated and the lipid modification allows the small GTPase to anchor to the plasma membranes (Wennerberg and Der, 2004). Given the importance of an intact carboxyl-terminus for the plasma membrane localisation of RhoA (Adamson et al., 1992b; Robertson et al., 1995), the RhoA fusion protein was constructed by inserting the fluorophore Venus, a YFP-derivative, between the Myc-tag and the amino-terminus of RhoA (section 2.2.13). A constitutively active Venus-tagged RhoA construct was not constructed, since the over-expression of active RhoA was expected to lead to gross morphological changes like cell rounding and blebbing (Paterson et al., 1990).

To assess their expression and localisation the constructed $G\alpha_q$ and RhoA fusion-proteins were transiently transfected into HEK293 cells. In addition to the confocal image, panels A–E of Fig. 3.5 show a graph underneath plotting the fluorescence intensity along the line indicated in the image. Carboxyl-terminal tagged $G\alpha$ -ECFP was evenly distributed throughout the cytoplasm of HEK293 cells, which can also be seen in the line plot (Fig. 3.5A). This cytosolic localisation of $G\alpha_q$ -ECFP resembles the distribution previously reported (Witherow et al., 2003). Loop-tagged $G\alpha_q$ -ECFP- $G\alpha_q$ was localised almost exclusively at the cell membrane with only limited expression in the cytoplasm, as clearly illustrated by the distribution plot

(Fig. 3.5B). In contrast, the constitutively active $G\alpha_q$ -ECFP- $G\alpha_q$ -L209 and $G\alpha_q$ -ECFP- $G\alpha_q$ -C183 were localised throughout the cytoplasm, even though they were both loop-tagged (Fig. 3.5C and D). Thus the position of the ECFP-tag was not the only factor influencing the localisation of $G\alpha_q$. Any potential membrane signal in cells expressing $G\alpha_q$ -ECFP- $G\alpha_q$ -L209 or $G\alpha_q$ -ECFP- $G\alpha_q$ -C183 was not distinguishable from the expression in the cytoplasm. HEK293 cells expressing $G\alpha_q$ -ECFP- $G\alpha_q$ -C183 displayed clusters of higher fluorescence intensity (Fig. 3.5D) that were not observed in $G\alpha_q$ -ECFP- $G\alpha_q$ -L209 expressing cells (Fig. 3.5C). There was hardly any signal above background noise in the nucleus in any of the ECFP-tagged $G\alpha_q$ transfected cells.

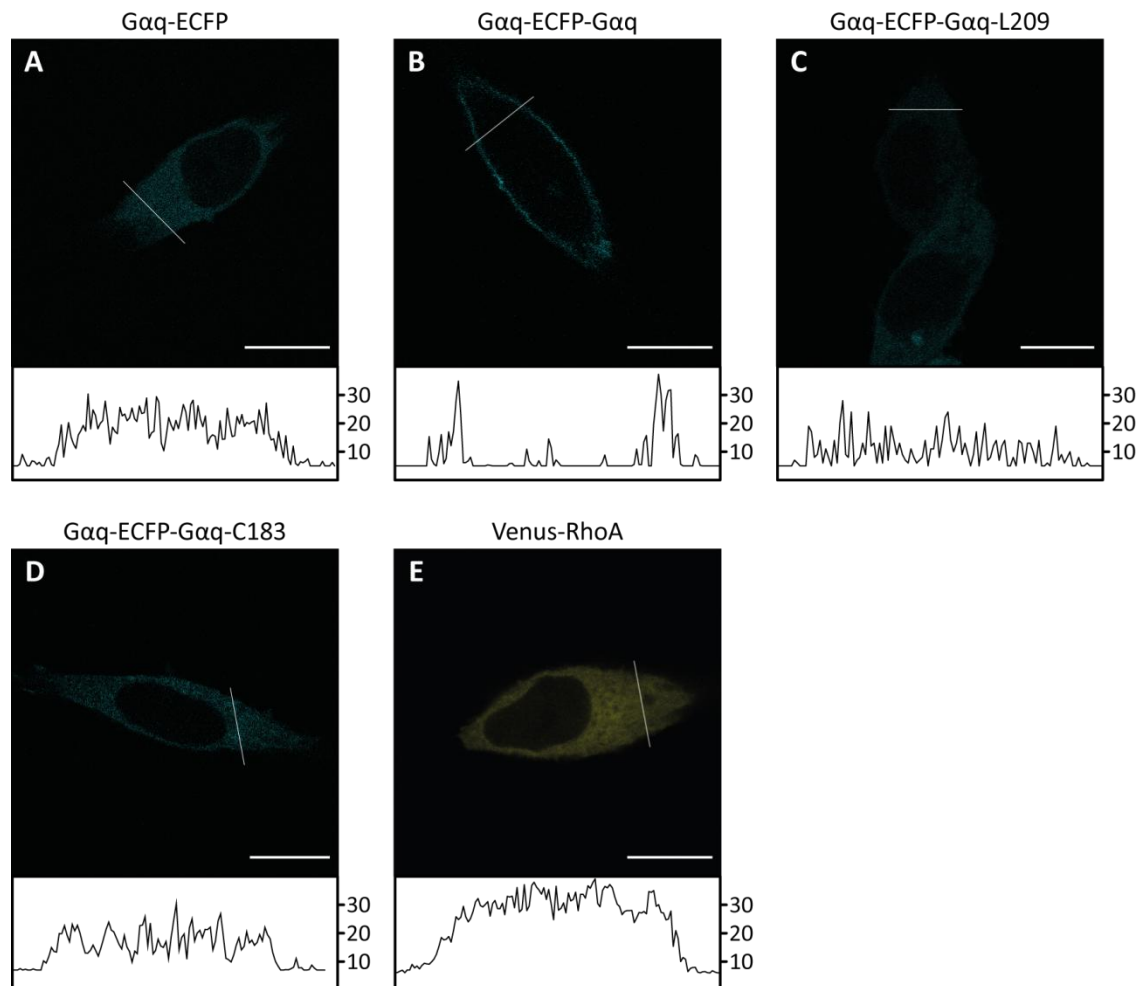


Figure 3.5 Localisation of ECFP-tagged $G\alpha_q$ and Venus-tagged RhoA in HEK293 cells. HEK293 cells were transfected with ECFP-tagged $G\alpha_q$ or Venus RhoA as indicated. Confocal images and line scans of representative cells are shown. Carboxyl-terminal tagged $G\alpha_q$ -ECFP was distributed throughout the cytoplasm (A), while the loop-tagged $G\alpha_q$ -ECFP- $G\alpha_q$ was localised at the cell membrane (B). Both constitutively active and loop-tagged $G\alpha_q$, $G\alpha_q$ -ECFP- $G\alpha_q$ -L209 (C) and $G\alpha_q$ -ECFP- $G\alpha_q$ -C183 (D), were localised in the cytoplasm with no distinguishable membrane signal. Venus-RhoA was distributed throughout the cytoplasm (E). The fluorescence intensity plots below the images represent line scans through the cells along the indicated bars; the x-axis corresponds to 10 μm and the y-axis represents fluorescence intensity. Scale bars 10 μm .

HEK293 cells expressing Venus-RhoA showed a distribution throughout the cytoplasm with no distinguishable signal at the cell membrane or expression in the nucleus, which is supported by the line plot (Fig. 3.5E). This predominantly cytosolic expression of RhoA was reported previously (Adamson et al., 1992b; Michaelson et al., 2001) and demonstrates that a Venus tag at the amino-terminus does not interfere with the localisation of RhoA.

Confocal images of $G\alpha_q$ and RhoA expressing HEK293 cells were also used to study the co-distribution of their signals by performing co-localisation analysis. Co-localisation of ECFP-tagged $G\alpha_q$ and Venus-RhoA was assessed in HEK293 cells transiently transfected with $G\alpha_q$ -ECFP, $G\alpha_q$ -ECFP- $G\alpha_q$, $G\alpha_q$ -ECFP- $G\alpha_q$ -L209 or $G\alpha_q$ -ECFP- $G\alpha_q$ -C183 in combination with Venus-RhoA. The distribution of the expressed fusion proteins was not influenced by the co-transfection. $G\alpha_q$ -ECFP was distributed throughout the cytoplasm (Fig. 3.6A) and $G\alpha_q$ -ECFP- $G\alpha_q$ displayed membrane localisation (Fig. 3.6D), while constitutively active $G\alpha_q$ -ECFP- $G\alpha_q$ -L209 (Fig. 3.6G) and $G\alpha_q$ -ECFP- $G\alpha_q$ -C183 (Fig. 3.6J) localised in the cytoplasm. Expression of Venus-RhoA was observed throughout the cytoplasm (Fig. 3.6B, E, H and K). Co-localisation of $G\alpha_q$ and RhoA was analysed using the Just Another Co-localisation Plug-in (JACoP) and the intensity correlation analysis plug-in in ImageJ. Co-localisation was quantified by calculating the Pearson's coefficient (Manders et al., 1992), the overlap coefficient and Manders' M1 and M2 coefficients (Manders et al., 1993) and the more recently developed ICQ (Li et al., 2004) (Table 3.2). Scatter plots (Fig. 3.6C, F, I and L) were used to study co-localisation graphically by plotting the intensity value of a pixel in one channel against the intensity of the corresponding pixel in the other channel. A pixel's x-coordinate corresponds to its intensity value in channel A (ECFP-tagged $G\alpha_q$), while its intensity value in channel B (Venus-RhoA) is used as the y-coordinate. Complete co-localisation would be represented by a diagonal line, while exclusion would result in a scatter plot displaying two distinct dot clouds along the x- and y-axes. Thus while scatter plots can give some insight into the degree of co-localisation of two proteins, only the use of co-localisation coefficients allow its quantification.

The Pearson's coefficient uses the intensity values of the pixels in a dual-colour image, as displayed in the scatter plot, to estimate the strength of their association. It ranges from -1 to 1, with -1 being complete negative correlation, 0 indicating absence of correlation and 1 complete positive correlation, while conclusions from mid-range values (-0.5 – 0.5) cannot be drawn. The scatter plots of $G\alpha_q$ -ECFP and $G\alpha_q$ -ECFP- $G\alpha_q$ -L209 with Venus-RhoA show dot clouds that display a good percentage of co-localised pixels along the diagonal (Fig. 3.6C and I). This observation was substantiated by a Pearson's coefficient of 0.791 for $G\alpha_q$ -ECFP and Venus-RhoA (Fig. 3.6A, B) and 0.725 for $G\alpha_q$ -ECFP- $G\alpha_q$ -L209 and Venus-RhoA (Fig. 3.6G, H) indicating strong correlation. The scatter plot of $G\alpha_q$ -ECFP- $G\alpha_q$ -C183 with Venus-RhoA

(Fig. 3.6L) implied a weaker correlation, which was confirmed by a Pearson's coefficient of 0.578 (Fig. 3.6J, K). In cells expressing $G\alpha_q$ -ECFP- $G\alpha_q$ with Venus-RhoA (Fig. 3.6D, E) the cytosolic signal of Venus-RhoA led to a dot cloud along the y-axis of the scatter plot (Fig. 3.6F) and a weak Pearson's coefficient of 0.470. Therefore analysis of these cells was restricted to a membrane-only region, for which a ROI (membrane-only) was created in ImageJ using the $G\alpha_q$ -ECFP- $G\alpha_q$ image as a template. In the scatter plot of the membrane region (Fig. 3.6f) the deflection towards the y-axis was reduced displaying more co-localised pixels along the diagonal and a Pearson's coefficient of 0.778 indicated strong correlation (Fig. 3.6d, e).

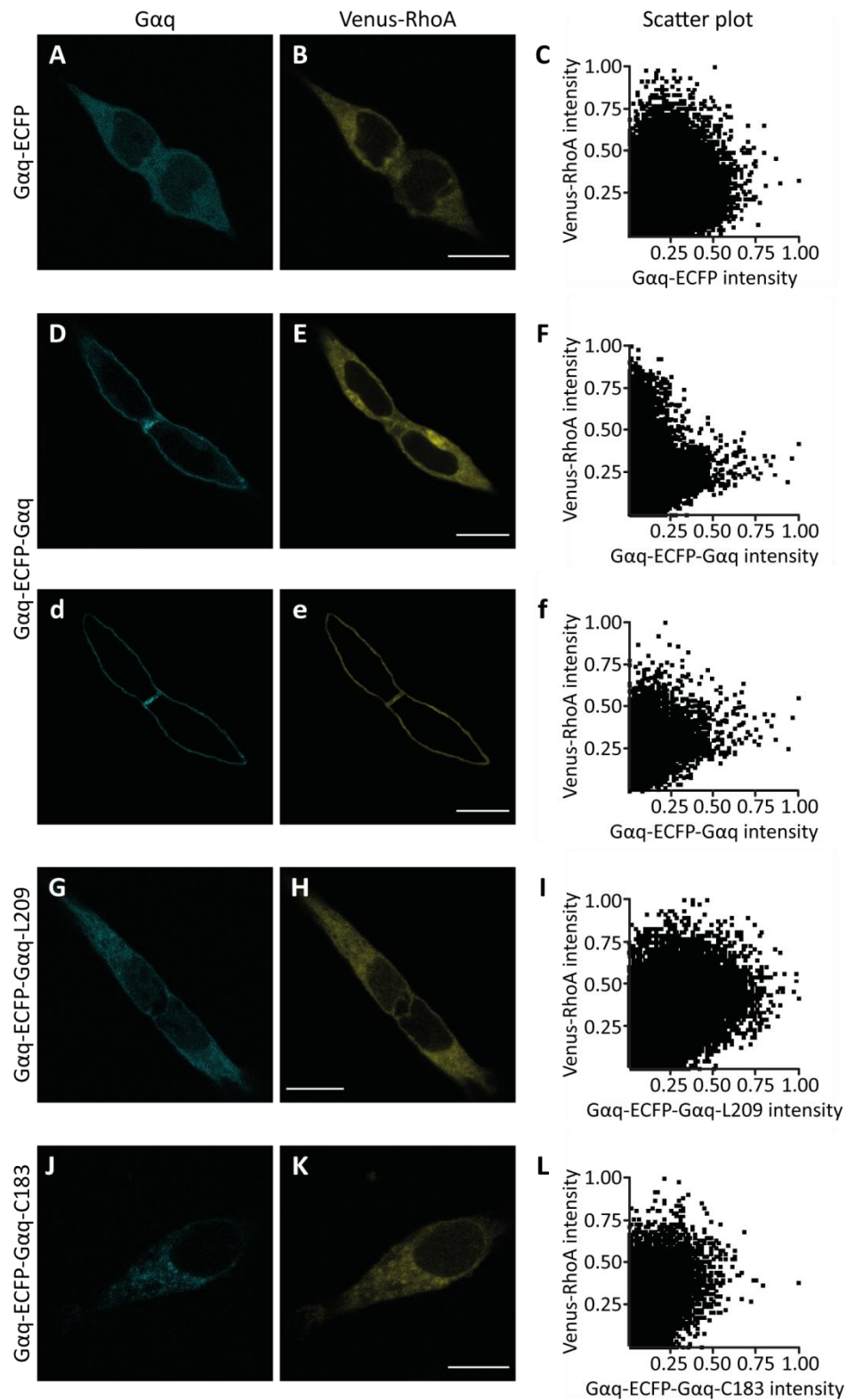


Figure 3.6 Co-localisation analysis of ECFP-tagged $G\alpha_q$ and Venus-tagged RhoA in HEK293 cells. Representative confocal images of HEK293 cells co-transfected with $G\alpha_q$ -ECFP and Venus-RhoA (**A, B**), $G\alpha_q$ -ECFP- $G\alpha_q$ and Venus-RhoA (**D, E**), $G\alpha_q$ -ECFP- $G\alpha_q$ -L209 and Venus-RhoA (**G, H**) or $G\alpha_q$ -ECFP- $G\alpha_q$ -C183 and Venus-RhoA (**J, K**) are shown. Cells expressing $G\alpha_q$ -ECFP- $G\alpha_q$ and Venus-RhoA the membrane-only region was analysed separately (**d, e**). Normalized scatter plots displaying the pixel intensity values of both channels plotted against one another (**C, F, I and L**), representing a method of visualising the degree of correlation between two proteins, in which a diagonal line would represent complete co-localisation. Scale bars 10 μ m.

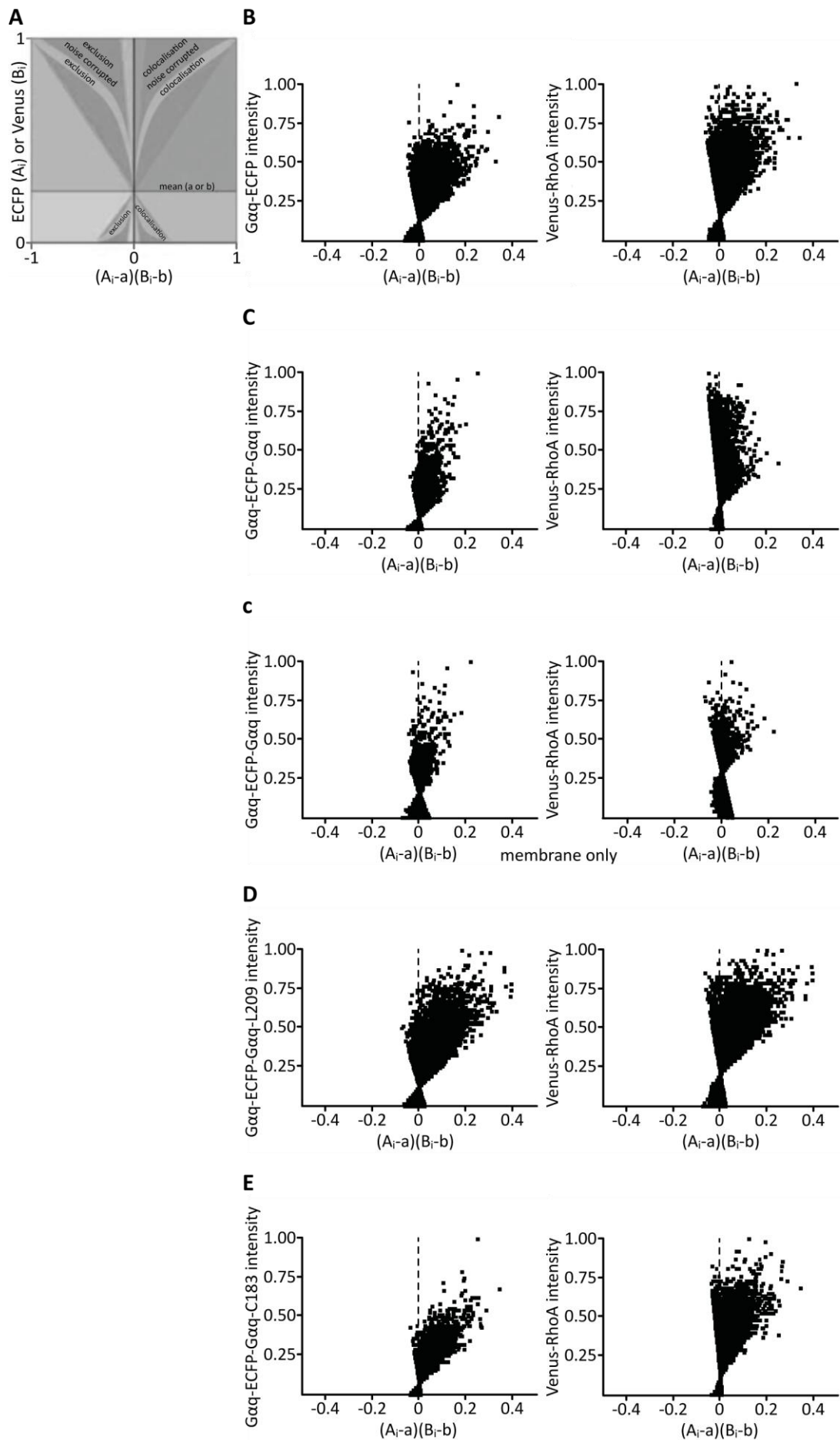
The Pearson's coefficient provides information about the correlation of intensity values but the degree of overlapping signals is more reliably described by the overlap coefficient. It is based on Pearson's coefficient but the mean intensities are removed from the equation (section 2.2.11.4). The overlap coefficient ranges from 0 (no overlap) to 1 (complete co-localisation) and therefore gives the percentage of overlapping pixels. However, results from the overlap coefficient only provide valuable information when the number of objects in each channel is equal (i.e. a channel A (ECFP-tagged $G\alpha_q$):channel B (Venus-RhoA) ratio of one). The overlap coefficient of $G\alpha_q$ -ECFP with Venus-RhoA (Fig. 3.6A, B) was 0.814 indicating co-localisation of the two proteins, in agreement with the results obtained from the Pearson's coefficient. However, the channel A:channel B ratio of 0.775 limited the validity of the calculated overlap coefficient. The same was observed with other $G\alpha_q$ and RhoA combinations: the overlap coefficient of $G\alpha_q$ -ECFP- $G\alpha_q$ with Venus-RhoA was 0.521 (Fig. 3.6D, E; channel A:channel B ratio of 0.739), of $G\alpha_q$ -ECFP- $G\alpha_q$ -L209 with Venus-RhoA 0.752 (Fig. 3.6G, H; ratio 0.662) and of $G\alpha_q$ -ECFP- $G\alpha_q$ -C183 with Venus-RhoA 0.634 (Fig. 3.6J, K; ratio 0.801). Only the analysis of the membrane-only ROI for $G\alpha_q$ -ECFP- $G\alpha_q$ with Venus-RhoA resulted in an equal channel A:channel B ratio (Fig. 3.6d, e; 0.938) and therefore allowed the use of the overlap coefficient, which was 0.781 and supported the co-localisation indicated by Pearson's coefficient.

Manders' coefficients M1 and M2, ranging from 0 (no overlap) to 1 (complete co-localisation), quantify the proportion of signals in one channel that coincide with above zero intensity signals in the second channel. Manders' coefficients M1 and M2 are thus suitable for quantifying co-localisation in images displaying unequal number of particles in the two channels. The analysis of $G\alpha_q$ -ECFP with Venus-RhoA (Fig. 3.6A, B) resulted in M1 (the amount of $G\alpha_q$ overlapping RhoA) and M2 (the amount of RhoA overlapping $G\alpha_q$) coefficients of 0.919 and 0.933 and thus indicated co-localisation of the two proteins. A similarly strong correlation was observed for $G\alpha_q$ -ECFP- $G\alpha_q$ -L209 with Venus-RhoA (Fig. 3.6G, H) with M1 and M2 coefficients of 0.895. On the other hand, the weaker correlation between $G\alpha_q$ -ECFP- $G\alpha_q$ -C183 and Venus-RhoA (Fig. 3.6J, K) was indicated by M1 and M2 coefficients of 0.718 and 0.662. M1 and M2 coefficients calculated for $G\alpha_q$ -ECFP- $G\alpha_q$ with Venus-RhoA (Fig. 3.6D, E) were 0.790 and 0.704, while the analysis of its membrane-only ROI (Fig. 3.6d, e) produced M1 and M2 coefficients of 0.996 and 0.948 indicating almost complete co-localisation of both proteins at the membrane.

The intensity correlation analysis is based on the assumption that if two proteins co-localise their signal intensities would deviate from the mean intensity in synchrony, but would change in opposite directions if they do not. In a dual-channel image the signal intensity of each pixel

pair is tested for its deviation from the mean and the ICQ is calculated by dividing the number of pairs, whose PDM was positive, by the total number of pixel pairs (section 2.2.11.4; Li et al., 2004). 0.5 is subtracted from this value to produce an ICQ ranging from -0.5 to 0.5, with -0.5 corresponding to exclusion and 0.5 to co-localisation. Plotting the normalized channels' intensity against the PDM produces a graph that allows the identification of co-localisation (Fig. 3.7). Dots on the right side ($x > 0$) of the graph represent co-localisation, while pixels on the left ($x < 0$) indicate exclusion (Fig. 3.7A). The ICQ of $G\alpha_q$ -ECFP with Venus-RhoA was 0.364 ($P_{\text{sign test}} < 0.001$; the sign test was used to assess if PDM values were significantly different from zero (Li et al., 2004)) and that of $G\alpha_q$ -ECFP- $G\alpha_q$ -L209 with Venus-RhoA was 0.302 ($P_{\text{sign test}} < 0.001$), which corresponded with the strong correlation determined by the other co-localisation coefficients and was also seen in the intensity correlation analysis graphs (Fig. 3.7B and D). An ICQ of 0.265 ($P_{\text{sign test}} < 0.001$) was calculated for $G\alpha_q$ -ECFP- $G\alpha_q$ -C183 with Venus-RhoA (Fig. 3.7E), which still indicates a strong covariance of the channels' signal intensities and thus co-localisation. Co-localisation was also determined in the case of $G\alpha_q$ -ECFP- $G\alpha_q$ with Venus-RhoA (the calculated ICQ was 0.256 ($P_{\text{sign test}} < 0.001$); Fig. 3.7C), while the analysis of its membrane-only ROI produced an ICQ of 0.090 ($P_{\text{sign test}} < 0.001$; Fig. 3.7c) indicating only moderate covariance (Khanna et al., 2006).

Figure 3.7 Co-localisation analysis of ECFP-tagged $G\alpha_q$ and Venus-tagged RhoA in HEK293 cells using intensity correlation analysis. **(A)** The graph was adapted from Bolte and Cordelieres, 2006 and gives details on how to interpret results obtained with the intensity correlation analysis. A dot cloud on the positive side of the x-axis ($x>0$) signifies co-localisation, while pixels on the negative side ($x<0$) stand for exclusion. The representations of **(B)** $G\alpha_q$ -ECFP with Venus-RhoA, **(D)** $G\alpha_q$ -ECFP- $G\alpha_q$ -L209 with Venus-RhoA and **(E)** $G\alpha_q$ -ECFP- $G\alpha_q$ -C183 with Venus-RhoA display the majority of pixels on the right side of the $x=0$ line indicating the co-localisation of $G\alpha_q$ and RhoA. **(C)** Due to the localisation of the two proteins (see Fig. 3.6D and E) the case of $G\alpha_q$ -ECFP- $G\alpha_q$ with Venus-RhoA is more complex. The pixel cloud representing $G\alpha_q$ -ECFP- $G\alpha_q$ is situated mainly on the positive side of the x-axis, while the Venus-RhoA cloud also displayed dots on the left side of the graph representing pixels that are not co-localised. **(c)** The analysis of the membrane-only $G\alpha_q$ -ECFP- $G\alpha_q$ with Venus-RhoA resulted in dot clouds being concentrated around the centre of the graph with some deflection towards the positive side of the x-axis.



A summary of the co-localisation analysis is displayed in Table 3.2.

	Pearson's Coefficient	Manders' Overlap Coefficient	Channel A: Channel B ratio	Manders' M1 Coefficient - ECFP	Manders' M2 Coefficient - Venus	Intensity Correlation Quotient (ICQ)
G α_q -ECFP + Venus-RhoA	0.791 ± 0.025	0.814 ± 0.025	0.775 ± 0.084	0.919 ± 0.016	0.933 ± 0.020	0.364 ± 0.024
G α_q -ECFP-G α_q + Venus-RhoA	0.470 ± 0.060	0.521 ± 0.045	0.739 ± 0.078	0.790 ± 0.056	0.704 ± 0.082	0.256 ± 0.028
G α_q -ECFP-G α_q + Venus-RhoA (membrane-only)	0.778 ± 0.032	0.781 ± 0.031	0.938 ± 0.023	0.996 ± 0.003	0.948 ± 0.023	0.090 ± 0.015
G α_q -ECFP-G α_q -L209 + Venus-RhoA	0.725 ± 0.028	0.752 ± 0.026	0.662 ± 0.078	0.895 ± 0.047	0.895 ± 0.023	0.302 ± 0.026
G α_q -ECFP-G α_q -C183 + Venus-RhoA	0.578 ± 0.044	0.634 ± 0.030	0.801 ± 0.046	0.718 ± 0.035	0.662 ± 0.021	0.265 ± 0.017

Table 3.2 Quantitative analysis of the co-localisation of the G-protein α subunit G α_q and the small GTPase RhoA in HEK293 cells. The expression of each ECFP-tagged G α_q in combination with Venus-RhoA was analysed for co-localisation by calculating the Pearson's r , overlap r , Manders' M1 and M2 coefficients and the intensity correlation quotient using the JACoP and intensity correlation analysis plug-ins in ImageJ (section 2.2.11.4). For cells expressing G α_q -ECFP-G α_q and Venus-RhoA a membrane-only ROI was also analysed. Results from the overlap coefficient analysis are reported, however, only G α_q -ECFP-G α_q and Venus-RhoA (membrane-only) displayed an equal number of particles in both channels, while the ratio in all other cases was ≤ 0.800 . Mean values \pm SEM are presented, n=5 (number of cells analysed from multiple transfections).

3.1.6 ECFP-tagged G α_q interacts with Venus-tagged RhoA

Whether the fusion proteins ECFP-tagged G α_q and Venus-tagged RhoA retained their ability to interact was tested by co-immunoprecipitations. HEK293 cells were transiently transfected with G α_q -ECFP-G α_q or constitutively active G α_q -ECFP-G α_q -L209 in combination with Venus-RhoA, which was also Myc-tagged (section 2.1.1). G α_q -ECFP-G α_q , G α_q -ECFP-G α_q -L209 and Venus-RhoA transfected on their own served as controls. Protein expression was assessed by Western blotting using anti-G $\alpha_{q/11}$ and anti-Myc antibodies, which detected bands at the expected molecular weights of ~ 67 kDa for G α_q -ECFP-G α_q and G α_q -ECFP-G α_q -L209 (Fig. 3.8, middle panel (lysates), lanes 3–6) and of ~ 49 kDa for Venus-RhoA (Fig. 3.8, lower panel (lysates), lanes 2, 5 and 6). The detection of multiple bands in lysates expressing Venus-RhoA (Fig. 3.8, lower panel (lysates), lanes 2, 5 and 6) was reduced by denaturing the protein at 95 °C for 5 min (instead of 60 °C for 30 min), but continued to be observed especially in lysates co-expressing Venus-RhoA and G α_q -ECFP-G α_q -L209. Multiple bands were also detected in G α_q -ECFP-G α_q -L209 lysate and to a lesser extent in G α_q -ECFP-G α_q (Fig. 3.8, middle panel (lysates), lanes 3–6), but were independent of denaturing conditions. Co-immunoprecipitations were performed using an anti-Myc antibody to immunoprecipitate Venus-RhoA and Western blots

were probed with anti-G $\alpha_{q/11}$ antibody. As expected, no bands were detected in immunoprecipitations of lysates of untransfected HEK293 cells or lysates expressing Venus-RhoA, G α_q -ECFP-G α_q or G α_q -ECFP-G α_q -L209 on their own (Fig. 3.8, upper panel, lanes 1–4). Immunoprecipitations of lysates co-expressing both proteins showed that G α_q -ECFP-G α_q and G α_q -ECFP-G α_q -L209 were co-immunoprecipitated with Venus-RhoA (Fig. 3.8, upper panel, lanes 5 and 6). This shows that the interaction between the G-Protein α subunit G α_q and the small GTPase RhoA was not hindered by tagging the proteins with GFP variants.

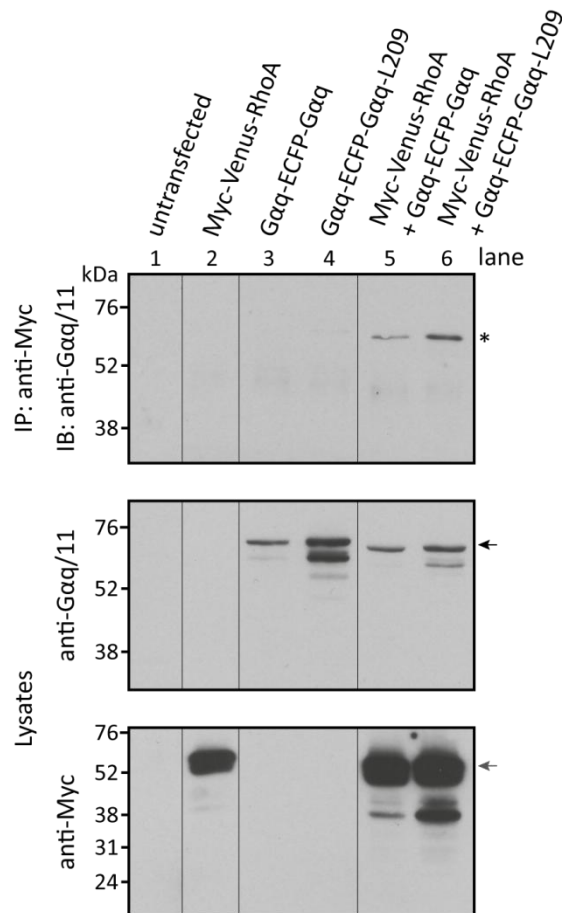


Figure 3.8 G α_q -ECFP-G α_q and constitutively active G α_q -ECFP-G α_q -L209 interact with Venus-RhoA. HEK293 cells were transiently transfected with Venus-tagged RhoA and ECFP-tagged G α_q as indicated (see section 2.1.1 for construct details). Untransfected HEK293 cells were used as control (lane 1). Protein expression was analysed by Western blotting (lysates (15 μ g), middle and lower panels) using anti-G $\alpha_{q/11}$ and anti-Myc (targeting Myc-tagged RhoA) antibodies at a dilution of 1:1000. For co-immunoprecipitations (upper panel), 250 μ g of the lysates were incubated with 1–2 μ g anti-Myc antibody (Millipore (this presented experiment) or Santa Cruz) and Venus-RhoA was immunoprecipitated (IP). Proteins were separated on 12.5% polyacrylamide gels, transferred to nitrocellulose membranes and immunoblotting (IB) was performed using anti-G $\alpha_{q/11}$ antibody at a dilution of 1:1000. The vertical grey lines show where the digital image of the blot was cut into sections in order to present the data of this experiment in two different figures. The star indicates co-immunoprecipitated G α_q and the arrows specify the correct molecular weights of G α_q -ECFP-G α_q , G α_q -ECFP-G α_q -L209, and Venus-RhoA. Representative result, n=6.

3.1.7 Assessment of the interaction between ECFP-tagged $G\alpha_q$ and Venus-RhoA in HEK293 cells using FRET

Results from the co-localisation studies and co-immunoprecipitation experiments indicate an interaction between the small GTPase RhoA and the G-protein α subunit $G\alpha_q$, potentially involving them in a common signalling pathway leading to the suppression of sl_{AHP} . In order to obtain an additional line of evidence to support this interaction, FRET experiments were performed. FRET occurs only when donor and acceptor fluorophores are located in close proximity (<10 nm), thus operating over a distance the size of proteins. The detection of a FRET signal is considered equivalent to direct protein interaction. FRET is the non-radiative transfer of energy from a donor fluorophore to an acceptor fluorophore such that excitation of a donor fluorophore leads to the emission of acceptor fluorescence. For FRET to occur certain requirements must be met. First the emission spectrum of the donor must overlap with the absorption spectrum of the acceptor, secondly the fluorophore dipoles have to be orientated parallel to one another and thirdly donor and acceptor must be no more than 10 nm apart (Vogel et al., 2006). Acceptor photobleaching is a widely accepted method to measure FRET, and examines the donor fluorescence before and after bleaching of the acceptor using conventional confocal microscopy without the need for additional equipment (fluorescence lifetime imaging microscopy (FLIM)-FRET) or extensive controls to account for potential cross-talk and image processing (Sensitized Emission). In acceptor photobleaching FRET is present when the donor fluorophore shows an increase in fluorescence upon the destruction of the acceptor fluorophore (de-quenching), since the donor-acceptor energy transfer can no longer take place.

First the acquisition settings of the confocal microscope were established to ensure that ECFP-tagged $G\alpha_q$ and Venus-RhoA were properly visible and to prevent potential cross-talk between the two channels. HEK293 cells were either transfected with $G\alpha_q$ -ECFP- $G\alpha_q$ (Fig. 3.9A and B) or Venus-RhoA on their own (Fig. 3.9C and D) or together (Fig. 3.9E and F) and images were acquired using the same laser levels and photomultiplier tube (PMT) settings used during FRET experiments. In the CFP channel, CFP was excited with the 458 nm laser line and the PMT set to collect CFP emission between 462–500 nm, while the YFP channel uses the 514 nm laser line to excite of YFP/Venus with the PMT being set to 520–600 nm (section 2.2.11.2 and A.1.3). With these settings the chance of cross-talk was minimized, because the slight excitation of Venus/YFP by the 458 nm laser line (< 10 % of peak excitation efficiency) is minimally collected (< 5 %) by the CFP PMT and the excitation of CFP by the 514 nm laser line is low (< 1 %) in the first place (Karpova et al., 2003). Cells expressing $G\alpha_q$ -ECFP- $G\alpha_q$ alone were visible in the CFP channel (Fig. 3.9A), but not in the YFP channel (Fig. 3.9B). On the other hand Venus-RhoA was

only detected in the YFP channel, but not in the CFP channel (Fig. 3.9C and D). HEK293 cells expressing both proteins were clearly visible in both channels (Fig. 3.9E and F).

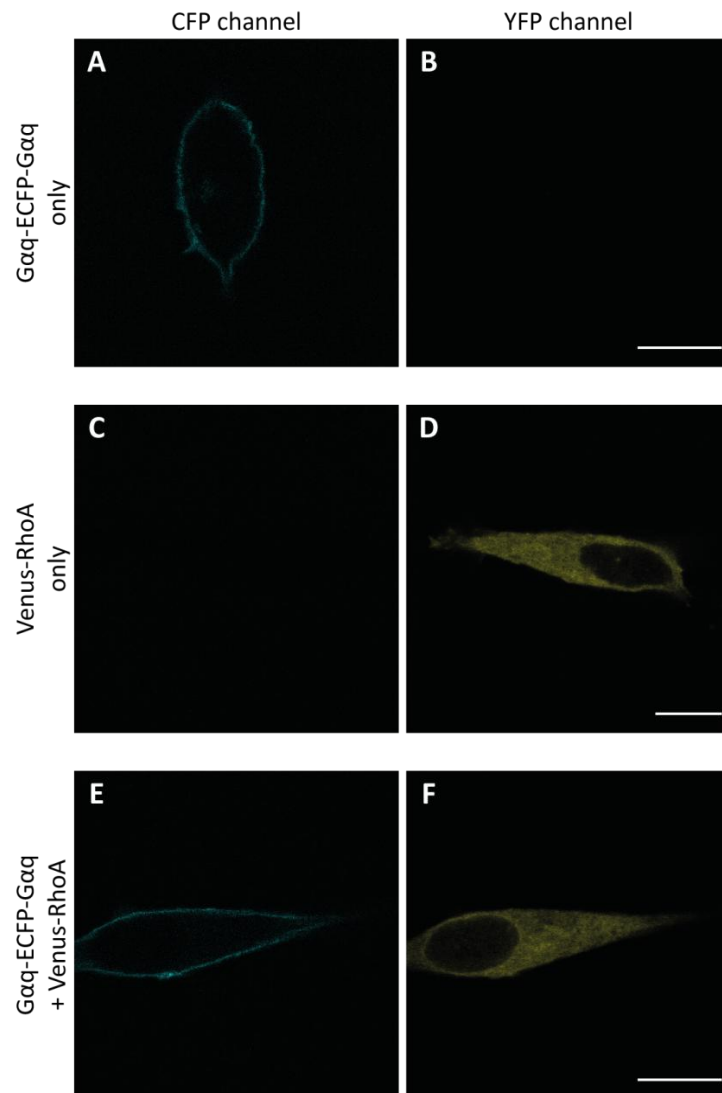


Figure 3.9 Confocal imaging configurations used for FRET experiments prevent cross-talk between $G\alpha_q$ -ECFP- $G\alpha_q$ and Venus-RhoA. HEK293 cells were transfected with $G\alpha_q$ -ECFP- $G\alpha_q$ (A and B), with Venus-RhoA (C and D) or were co-transfected with both constructs (E and F). Confocal images were acquired using the same settings and protocol as for FRET experiments. Cells expressing only $G\alpha_q$ -ECFP- $G\alpha_q$ are visible in the CFP channel (A) without any cross-talk in the YFP channel (B). The same was true for Venus-RhoA expressing cells, which were visible in the YFP channel (D), but not in the CFP channel (C). Cells expressing $G\alpha_q$ -ECFP- $G\alpha_q$ as well as Venus-RhoA were detected in both channels (E and F). Scale bars 10 μ m.

Control FRET experiments were performed in HEK293 cells transfected with a CFP-YFP dimer (section 2.1.1). The dimer was constructed by inserting enhanced YFP (EYFP) into pECFP-N1 using the XhoI and BamHI sites of the multiple cloning site, yielding a CFP-YFP fusion protein (Benians et al., 2005). FRET experiments were carried out using Leica's LAS AF software acceptor photobleaching wizard (section 2.2.11.2). Sequential scans of CFP (donor) and YFP (acceptor) were acquired before the acceptor was bleached by repeated scans with increased

laser power at 514 nm. The bleaching phase was followed by a second sequential scan of CFP and YFP. Confocal images of a HEK293 cell expressing the CFP-YFP dimer are presented before and after photobleaching (Fig. 3.10A). Acceptor photobleaching was performed in the area indicated by the square (Fig. 3.10A, upper right panel) and the destruction of the YFP fluorophore was demonstrated by plotting YFP fluorescence intensity against bleaching steps (Fig. 3.10B). YFP fluorescence intensity was plotted as percentage left with 100 % corresponding to the intensity measured at the first bleaching step. Mean acceptor fluorescence after photobleaching was 9.8 ± 1.1 %. To calculate FRET efficiencies CFP fluorescence intensities in before and after photobleaching images were measured in three cytosolic ROIs in each cell; the average of which accounted for a cell's overall FRET efficiency. The detected FRET of the CFP-YFP fusion protein expressed in HEK293 cells amounted to $E = 21.0 \pm 1.4$ %, $n=20$ (Fig. 3.10C).

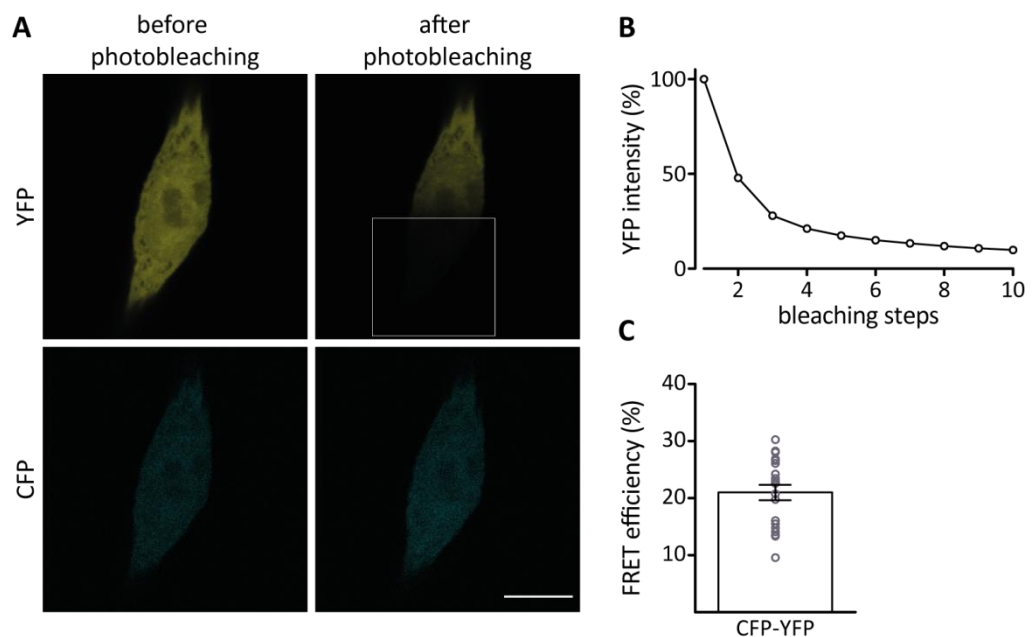


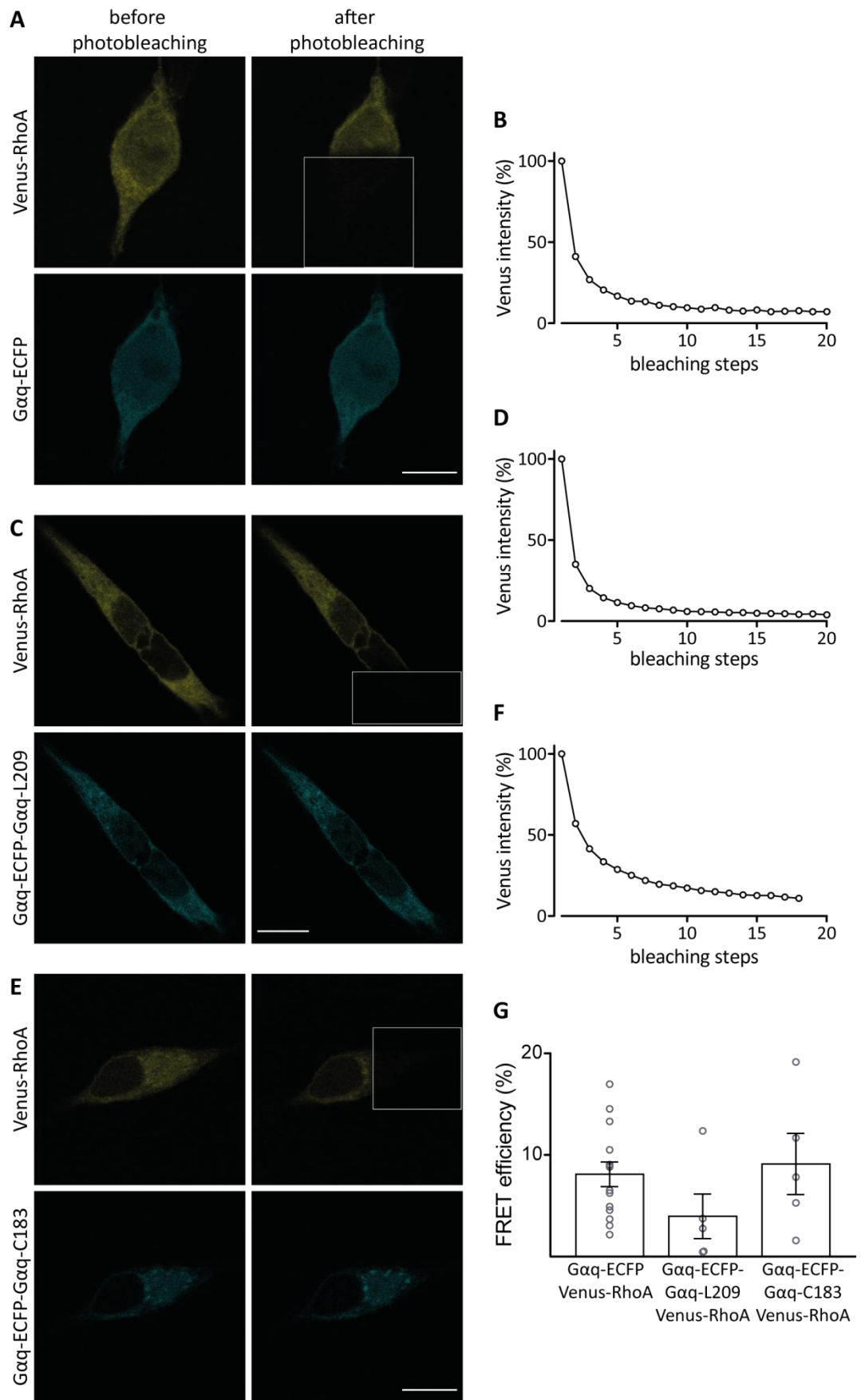
Figure 3.10 FRET in CFP-YFP dimer expressing HEK293 cells. As control, HEK293 cells were transfected with CFP-YFP and FRET was assessed by performing acceptor photobleaching experiments. **(A)** Confocal images of a representative cell expressing YFP (upper panels) and CFP (lower panels) before and after photobleaching. Acceptor photobleaching was carried out in the area of the cell indicated by the square. Scale bar 10 μ m. **(B)** Bleaching of the acceptor was achieved by repeatedly scanning the defined area with high laser power at 514 nm. Plotting the YFP fluorescence intensity of this area against the bleaching steps illustrates the destruction of the YFP fluorophores. **(C)** FRET efficiency (E) was calculated using the CFP fluorescence intensities, measured in three cytosolic regions of interest in each cell, before (I_{DA}) and after (I_D) acceptor photobleaching according to the following formula: $E = 1 - (I_{DA}/I_D)$ (section 2.2.11.2). FRET detected with the CFP-YFP dimer was $E = 21.0 \pm 1.4$ %, $n=20$ (number of cells analysed from multiple transfections). Mean values \pm SEM are presented.

Interaction between ECFP-tagged $G\alpha_q$ and Venus-RhoA was examined using the FRET acceptor photobleaching method tested on the CFP-YFP dimer control. HEK293 cells were transfected with $G\alpha_q$ -ECFP, constitutively active $G\alpha_q$ -ECFP- $G\alpha_q$ -L209 or constitutively active $G\alpha_q$ -ECFP- $G\alpha_q$ -

C183 in combination with Venus-RhoA. Confocal images of ECFP-tagged $G\alpha_q$ and Venus-RhoA before and after photobleaching were acquired (Fig. 3.11A, C and E) and the indicated area of the cells was repeatedly scanned to bleach the acceptor fluorophore Venus (Fig. 3.11B, D and F). The application used to perform acceptor photobleaching experiments did not allow for any intervention during the acquisition process and therefore the number of bleaching steps had to be estimated at the start of an experiment. Bleaching iterations varied from 7–20 and mean acceptor fluorescence after bleaching amounted to $10.7 \pm 2.6 \%$ for cells co-expressing $G\alpha_q$ -ECFP and Venus-RhoA (Fig. 3.11A), $27.0 \pm 6.0 \%$ for $G\alpha_q$ -ECFP- $G\alpha_q$ -L209 with Venus-RhoA (Fig. 3.11C) and $11.6 \pm 4.8 \%$ for $G\alpha_q$ -ECFP- $G\alpha_q$ -C183 with Venus RhoA (Fig. 3.11E). FRET efficiencies were calculated from the ECFP fluorescence intensities measured from three cytosolic ROIs per cell in the before and after photobleaching images. In HEK293 cells expressing $G\alpha_q$ -ECFP with Venus-RhoA a FRET efficiency of $E = 8.2 \pm 1.2 \%$, $n=14$ was calculated (Fig. 3.11G). Cells expressing the constitutively active $G\alpha_q$ -ECFP- $G\alpha_q$ -L209 with Venus-RhoA had a FRET efficiency of $E = 4.0 \pm 2.2 \%$, $n=5$ (Fig. 3.11G). The FRET efficiency determined for the constitutively active $G\alpha_q$ -ECFP- $G\alpha_q$ -C183 with Venus-RhoA was $E = 9.2 \pm 3.0 \%$, $n=5$ (Fig. 3.11G).

FRET experiments with ECFP-tagged $G\alpha_q$ variants and Venus-RhoA repeatedly resulted in negative FRET efficiencies (36 % of $G\alpha_q$ -ECFP, 55 % of $G\alpha_q$ -ECFP- $G\alpha_q$ -L209 and 62 % of $G\alpha_q$ -ECFP- $G\alpha_q$ -C183 in combination with Venus-RhoA transfected cells) and were excluded from the analysis. Negative FRET efficiencies occur when the donor's fluorescence intensity before acceptor photobleaching is greater than after, which could be caused by the bleaching of the donor itself during image acquisition or by the cross-excitation of ECFP with the 514 nm laser line (Karpova et al., 2003). What exactly caused this CFP bleaching effect could not be determined and was also observed in cells expressing $G\alpha_q$ -ECFP- $G\alpha_q$ alone (donor only; $E = -6.0 \pm 3.2\%$, $n=3$). Acceptor photobleaching experiments performed under the same conditions and on the same day could produce positive (53 % of cells) as well as negative (47 % of cells) FRET efficiencies. Furthermore, a potential effect of the number of bleaching iterations on FRET efficiency was rejected, since there was overall no correlation between these and the occurrence of negative FRET efficiencies ($r^2=0.16$). It was therefore assumed that CFP bleaching was possible in any experiment and the introduced error to the FRET efficiency calculation was similar.

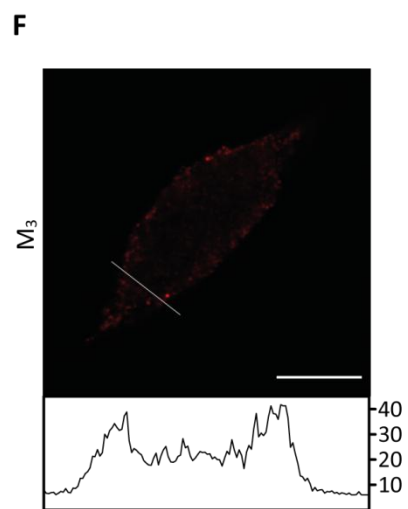
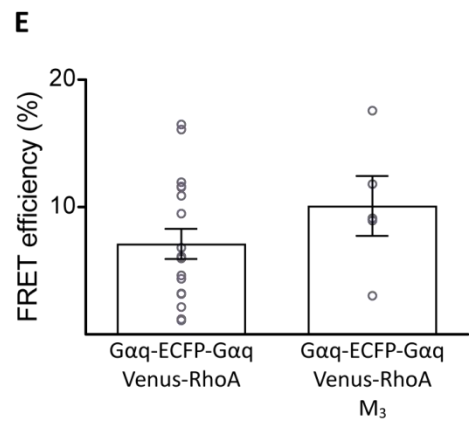
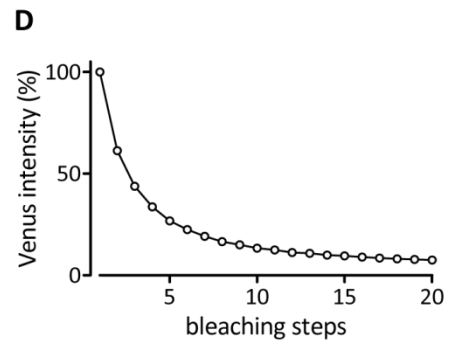
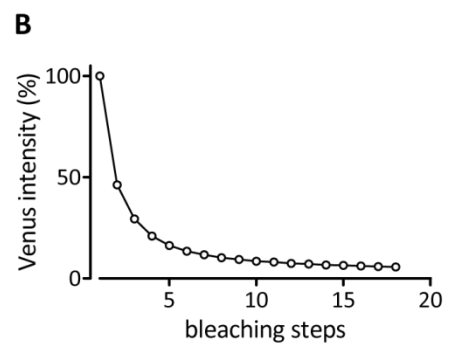
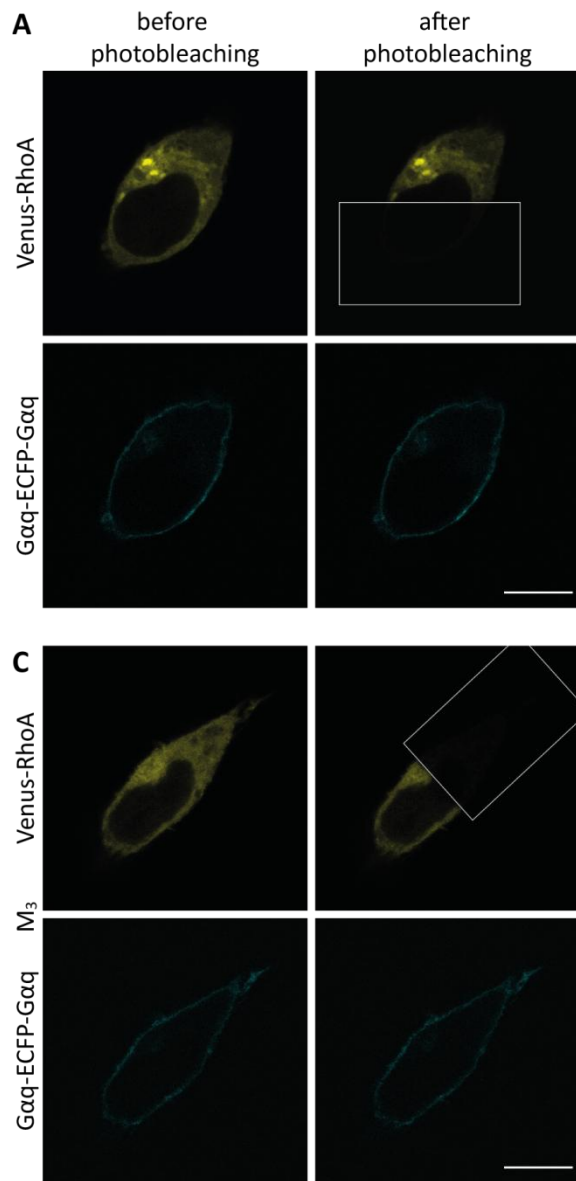
Figure 3.11 FRET between ECFP-tagged $G\alpha_q$ variants and Venus-RhoA. HEK293 cells were co-transfected with $G\alpha_q$ -ECFP and Venus-RhoA **(A)**, constitutively active $G\alpha_q$ -ECFP- $G\alpha_q$ -L209 and Venus-RhoA **(C)** or constitutively active $G\alpha_q$ -ECFP- $G\alpha_q$ -C183 and Venus-RhoA **(E)** and acceptor photobleaching experiments were performed to determine FRET. **(A, C and E)** Confocal images of representative cells display Venus-RhoA (upper panels) and ECFP-tagged $G\alpha_q$ (lower panels) before and after acceptor photobleaching. The area of the cell that was bleached is indicated by the square in the Venus-RhoA after photobleaching images (A, C and E, upper right panels). Scale bars 10 μm . **(B, D and F)** For the cells shown in A, C and E the destruction of the acceptor fluorophores by bleaching was documented by plotting Venus fluorescence intensities against the bleaching iterations. **(G)** ECFP fluorescence intensities in before and after photobleaching images were measured in three cytosolic regions of interest in each cell and used to calculate FRET efficiency (E) (section 2.2.11.2). In cells expressing $G\alpha_q$ -ECFP and Venus-RhoA the calculated FRET efficiency was $E = 8.2 \pm 1.2 \%$, $n=14$, in $G\alpha_q$ -ECFP- $G\alpha_q$ -L209 and Venus-RhoA expressing cells it amounted to $E = 4.0 \pm 2.2 \%$, $n=5$ and in $G\alpha_q$ -ECFP- $G\alpha_q$ -C183 and Venus-RhoA expressing cells to $E = 9.2 \pm 3.0 \%$, $n=5$. Only cells that displayed positive FRET efficiency values were included in the analysis. n numbers refer to the number of cells analysed from multiple transfections and mean values \pm SEM are presented.



The FRET results so far indicate that there is an interaction between the G-protein α subunit $G\alpha_q$ and small GTPase RhoA, although the efficiency values obtained were considerably lower than the ones determined for the optimised CFP-YFP control. In order to assess the effect of $G\alpha_q$ localisation on FRET efficiencies, the acceptor photobleaching experiments were repeated with HEK293 cells expressing $G\alpha_q$ -ECFP- $G\alpha_q$ and Venus-RhoA (Fig. 3.12A), which were shown to co-localise at the membrane. Repeated scans using the 514 nm laser line destroyed the Venus fluorophores (Fig. 3.12A and B; mean acceptor fluorescence after photobleaching was $8.4 \pm 1.5 \%$) and the FRET efficiency detected was $E = 7.1 \pm 1.2 \%$, $n=18$ (Fig. 3.12E; excluding 44 % of the cells because of negative FRET efficiency values). This FRET value was in a similar range as those observed with the previous ECFP-tagged $G\alpha_q$ constructs. In a separate set of experiments, co-expression of mAChR M_3 with $G\alpha_q$ -ECFP- $G\alpha_q$ and Venus-RhoA (Fig. 3.12C) and CCh application (10 μ M) to activate the $G\alpha_q$ signalling cascade, led to a comparable FRET efficiency of $E = 10.1 \pm 2.4 \%$, $n=5$ (Fig. 3.12E; excluding 38 % of the cells). CCh was applied to the cells to stimulate the M_3 receptor and thereby activating $G\alpha_q$ before cells were prepared for microscopy and acceptor photobleaching experiments carried out as described (Fig. 3.12C and D, mean acceptor fluorescence after photobleaching was $5.5 \pm 1.0 \%$). Immunocytochemistry experiments using an anti-HA antibody showed that the M_3 receptor was predominantly located at the membrane with only limited expression in the cytoplasm, which can also be seen in the distribution plot (Fig. 3.12F). Expression of Venus-RhoA and $G\alpha_q$ -ECFP- $G\alpha_q$ was not influenced by the co-transfection of the M_3 receptor (compare Fig. 3.12C to Fig. 3.12A).

The FRET efficiency values determined between the different ECFP-tagged $G\alpha_q$ and Venus-RhoA indicated an interaction of the two proteins, which supports the observations made in co-localisation and co-immunoprecipitation experiments.

Figure 3.12 FRET between $G\alpha_q$ -ECFP- $G\alpha_q$ and Venus-RhoA without and with the stimulation of the mAChR M_3 . HEK293 cells were co-transfected with $G\alpha_q$ -ECFP- $G\alpha_q$ and Venus-RhoA (**A**) or with $G\alpha_q$ -ECFP- $G\alpha_q$, Venus-RhoA and M_3 receptor (**C**). FRET acceptor photobleaching experiments were performed and confocal images of Venus-RhoA (A and C, upper panels) and $G\alpha_q$ -ECFP- $G\alpha_q$ (A and C, lower panels) before and after photobleaching were acquired. (**B and D**) The process of acceptor bleaching of the area indicated in the cells shown in A and C was documented by plotting Venus fluorophore intensity against the bleaching steps. (**E**) ECFP fluorescence intensity measurements in three membrane regions of interest in each cell were taken in before and after photobleaching images and used to calculate FRET efficiency (E) (section 2.2.11.2). Only cells, which displayed positive FRET efficiencies, were included in the analysis. FRET detected in cells expressing $G\alpha_q$ -ECFP- $G\alpha_q$ with Venus-RhoA was $E = 7.1 \pm 1.2 \%$, $n=18$. In cells that also expressed the mAChR M_3 and which were stimulated with CCh ($10 \mu\text{M}$) FRET between $G\alpha_q$ -ECFP- $G\alpha_q$ and Venus-RhoA was $E = 10.1 \pm 2.4 \%$, $n=5$. These efficiencies were not significantly different ($P=0.39$, unpaired t-test). n numbers refer to the number of cells analysed from multiple transfections and mean values \pm SEM are presented. (**F**) Expression of M_3 was studied by immunocytochemistry using an anti-HA antibody (1:100) and a Cy5 secondary antibody (1:600). It was predominantly expressed at the membrane showing only limited expression in the cytoplasm. The plot below the image represents fluorescence intensity along the indicated line with the x-axis representing $10 \mu\text{m}$ and the y-axis fluorescence intensity. Scale bars $10 \mu\text{m}$.



3.1.8 Binding assays between *in vitro* translated constitutively active $G\alpha_q$ -L209 and purified constitutively active GST-RhoA-V14

The co-immunoprecipitation experiments indicate the formation of a complex between two or more proteins. However, a potential direct interaction between the G-protein α subunit $G\alpha_q$ and the small GTPase RhoA can be investigated with a binding assay, in which only the proteins of interest are present. *In vitro* translated constitutively active $G\alpha_q$ -L209 (section 2.2.9.1) was used in pull-down experiments together with purified constitutively active GST-RhoA-V14 (section 2.2.7). The fusion protein GST-RhoA-V14 purified from bacterial lysate was incubated with [³⁵S] methionine-labelled $G\alpha_q$ -L209. *In vitro* translated $G\alpha_q$ -L209 was pulled down by GST-RhoA-V14 (Fig. 3.13A, ~40 kDa), suggesting a direct interaction of the two proteins. Rhophilin, a known binding partner of RhoA (Watanabe et al., 1996), was used as a positive control and was also pulled down by GST-RhoA-V14 (Fig. 3.13B, ~76 kDa), whereas no bands were observed in the absence of *in vitro* translated product (Fig. 3.13C). In all cases unspecific binding was tested by incubating GST beads with *in vitro* translated product. Input lanes of *in vitro* translated $G\alpha_q$ -L209 and rhophilin showed bands of the expected molecular weights, ~40 kDa and ~76 kDa (Fig. 3.13A and B, input) and no bands were detected in the input lane of the control (no DNA) sample (Fig. 3.13C).

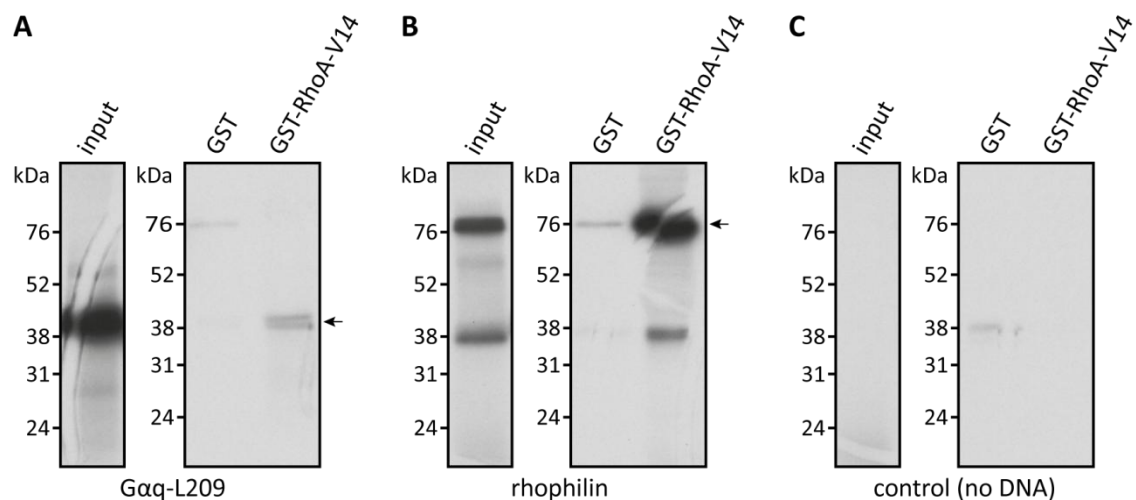


Figure 3.13 *In vitro* translated rhophilin and constitutively active $G\alpha_q$ -L209 bind directly to purified constitutively active GST-RhoA-V14. GST and GST-RhoA-V14 were purified and used to perform pull-down assays with *in vitro* translated [³⁵S] methionine-labelled control (no DNA), rhophilin and $G\alpha_q$ -L209. 10 μ g of GST and GST-Rho-V14 beads were incubated with 20 μ l of *in vitro* translated product. Binding assay samples and 1 μ l of each *in vitro* translated product (input) were separated on an 11 % polyacrylamide gel, which was dried before autoradiography. **(A)** $G\alpha_q$ was *in vitro* translated (~40 kDa, input) and pulled down by GST-Rho-V14 but not by GST. Under these conditions the binding assay was performed once. **(B)** *In vitro* translated rhophilin, band at ~76 kDa (input) was pulled-down by GST-RhoA-V14 and also slightly by GST. The second band, at ~38 kDa, visible in the input as well as GST-RhoA-V14 binding assay lane was repeatedly observed. Rhophilin, but not $G\alpha_q$ -L209, pull-downs with GST-RhoA-V14 were also observed in two other experiments, in which conditions varied as to the type of buffer and to the amount of *in vitro* translated product and beads used. **(C)** Assays performed in the absence of *in vitro* translated product did not show any bands in pull-down assay with GST-RhoA-V14 beads; a faint unspecific band at ~38 kDa was visible with GST.

3.1.9 Summary

The results of co-localisation, co-immunoprecipitation, FRET and binding assays have shown that the small GTPase RhoA is a binding partner of the G-protein α subunit $G\alpha_q$ and could therefore be part of a common signalling pathway that mediates the suppression of sl_{AHP} upon stimulation of GPCRs by cholinergic and glutamatergic agonists. In a heterologous expression system RhoA, the constitutively active RhoA-V14 and the inactive RhoA-N19 were co-immunoprecipitated with $G\alpha_q$ and constitutively active $G\alpha_q$. This co-immunoprecipitation of $G\alpha_q$ and RhoA was not hindered by the attachment of the fluorophore tags, ECFP and Venus. An interaction of endogenous $G\alpha_q$ and RhoA in co-immunoprecipitation experiments using brain lysate could not be shown. A strong correlation between Venus-RhoA and the carboxyl-terminal tagged $G\alpha_q$ -ECFP, the constitutively active, loop-tagged $G\alpha_q$ -ECFP- $G\alpha_q$ -L209 and, at membrane level, also for $G\alpha_q$ -ECFP- $G\alpha_q$ was shown by co-localisation analysis. Complex formation of the G-Protein α subunit $G\alpha_q$ and the small GTPase RhoA was also shown by FRET and binding assays.

3.2 Purification of mutant RhoA proteins and their intracellular application into hippocampal neurons

The involvement of the small GTPase RhoA in the signalling pathways mediating the cholinergic and glutamatergic suppression of sI_{AHP} has been hypothesized from experiments showing the reduced inhibitory effect of the agonists CCh and DHPG following the intracellular application of RhoA inhibitors (section 1.4). The ability to purify RhoA proteins allows for the introduction of RhoA mutants, constitutively active RhoA-V14 and inactive RhoA-N19, directly into the neuron via a patch pipette. Electrophysiological recordings of sI_{AHP} can therefore be performed under the influence of intracellularly applied mutant RhoA proteins. This approach has been used before for small GTPases in heterologous expression system (Storey et al., 2002) and should, in case of Rho-N19 being introduced into the neuron, lead to a reduced suppression of sI_{AHP} by cholinergic and glutamatergic agonists. In contrast, the introduction of RhoA-V14 should lead to the inhibition of sI_{AHP} without the application of cholinergic and glutamatergic agonists.

3.2.1 Purification of the fusion proteins GST-RhoA-V14 and GST-RhoA-N19 and the proteolytic release of the small GTPases

The RhoA mutants, constitutively active RhoA-V14 and inactive RhoA-N19, were purified from bacterial lysates as recombinant GST fusion proteins using glutathione agarose beads (Fig. 3.14A and section 2.2.7). Expression of GST-RhoA-V14 and GST-RhoA-N19 proteins was visible by the additional band at ~47 kDa in the post-induction lanes compared to pre-induction lanes (Fig. 3.14B, indicated by black arrow head). Bacteria were harvested, lysed and the supernatants containing the GST fusion proteins (Fig. 3.14B) were incubated with glutathione agarose beads. Beads were pelleted and the amount of bound GST-RhoA-V14 or GST-RhoA-N19 protein was estimated by comparison with a BSA standard on a polyacrylamide gel (Fig. 3.14B). In addition GST was bound to glutathione beads and used as control in subsequent binding assays (section 2.2.8). Bound GST protein was detected in the Coomassie stained polyacrylamide gel (Fig. 3.14C).

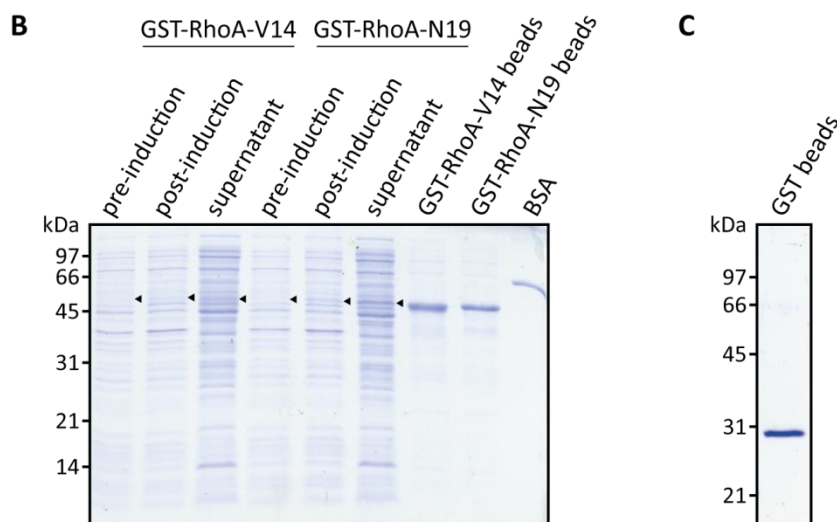
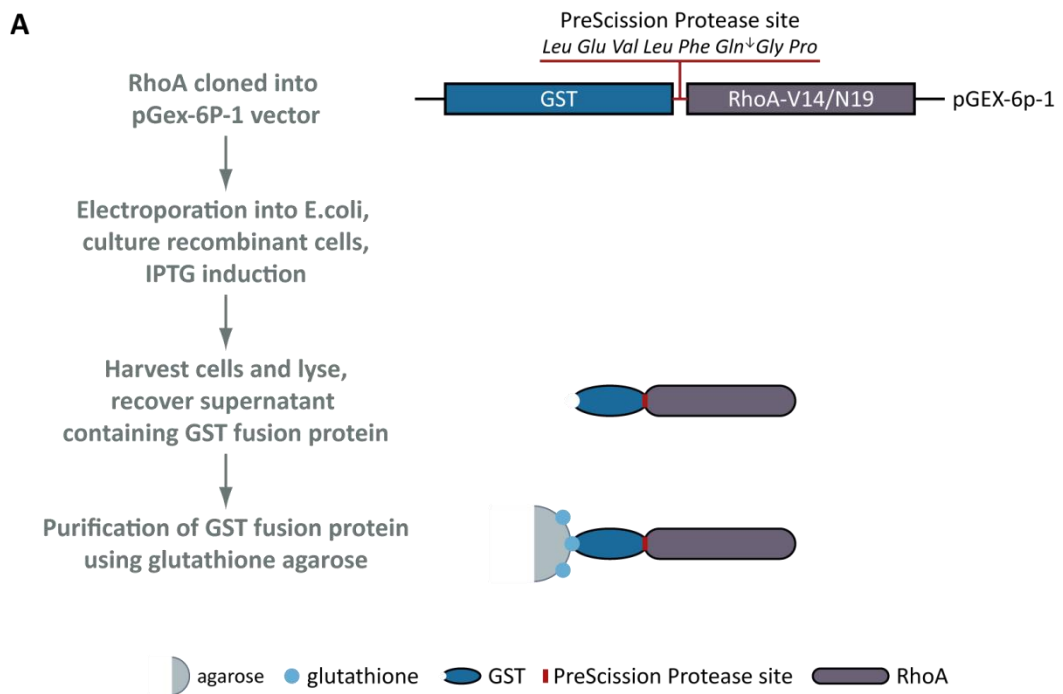


Figure 3.14 Purification of GST-RhoA-V14 and GST-RhoA-N19 fusion proteins. (A) Flow diagram of the steps leading to the purification of GST-RhoA-V14 and GST-RhoA-N19 proteins and details of the construct. **(B)** Samples taken at the various stages of the purification process were separated by SDS-PAGE and the gels were analysed by Coomassie staining. 10 μ l of pre-induction, post-induction and supernatant samples and 2 μ l of GST-RhoA-V14 and GST-RhoA-N19 beads samples alongside a BSA standard (1 μ g) were separated on a 15 % polyacrylamide gel. Expressed GST-RhoA-V14 and GST-RhoA-N19 proteins, at \sim 47 kDa, are indicated by the black arrow head. The Coomassie stained gel documenting the protein purification process is a representative and was run for every purification batch. **(C)** GST protein was bound to glutathione agarose beads and used as control in the binding assay experiments. 10 μ l of GST beads sample was separated on a 12 % polyacrylamide gel and stained with Coomassie. Control GST beads were examined by Coomassie stain once.

For use in electrophysiological experiments, the purified RhoA proteins were cleaved off the glutathione agarose beads. This was achieved by incubating GST-RhoA-V14 and GST-RhoA-N19 beads with PreScission protease, which cleaves the RhoA proteins at its recognition site leaving the GST-tag bound to the glutathione agarose beads (Fig. 3.15A). Cleaved RhoA protein was observed at ~25 kDa (Fig. 3.15B, indicated by the black arrow). A sample of the beads after cleaving was also analysed and three bands were detected: the ~47 kDa band corresponding to uncleaved GST-RhoA-V14 beads (Fig. 3.15B, indicated by the black arrow head), the middle band at ~30 kDa represents GST protein (Fig. 3.15B, indicated by the grey arrow) and the ~25 kDa band matching cleaved RhoA-V14 protein (Fig. 3.15B, indicated by the black arrow). Purified and cleaved RhoA protein was also examined by Western blotting using anti-RhoA antibody and the detected band demonstrated that RhoA was purified (Fig. 3.15C).

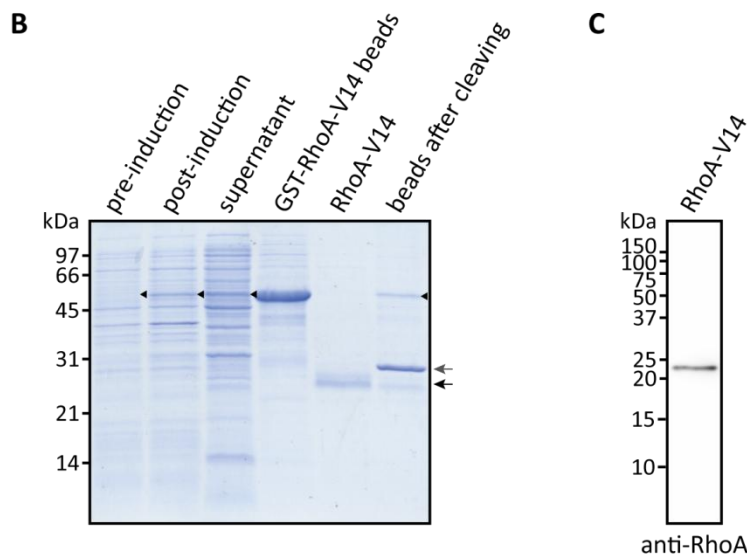
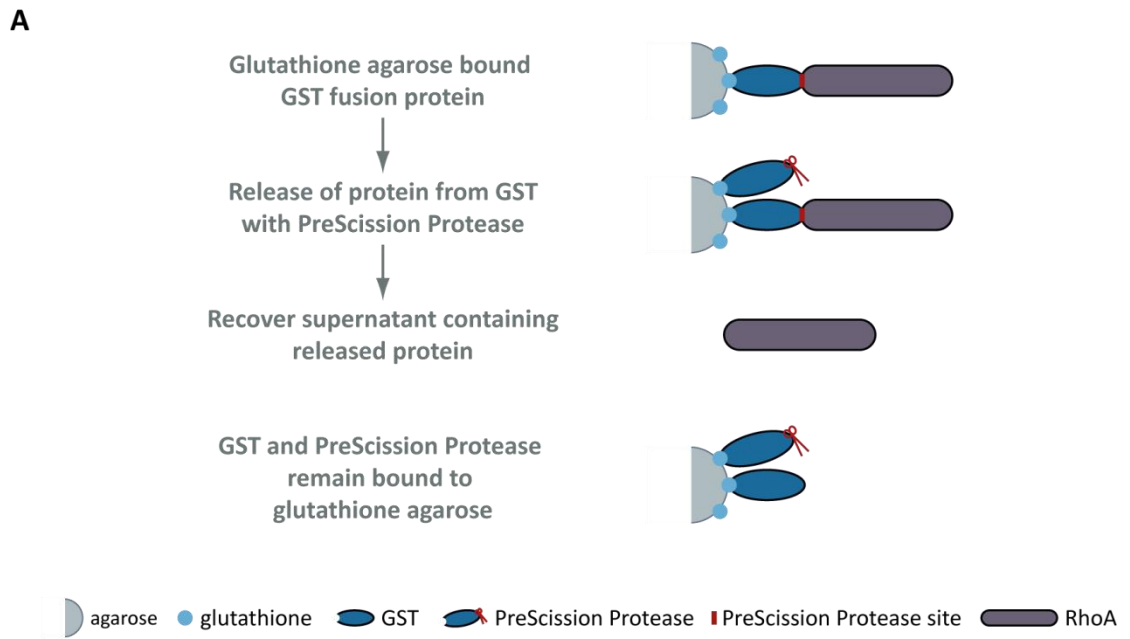


Figure 3.15 Purification and proteolytic release of RhoA-V14 and RhoA-N19 proteins. (A) Flow diagram illustrating the cleaving of purified RhoA off the beads using PreScission protease. (B) Samples taken at the various stages of the purification process were separated by SDS-PAGE and the gels were analysed by Coomassie staining. 10 μ l of pre-induction, post-induction and supernatant samples, 2 μ l of GST-RhoA-V14 beads sample, 2 μ l cleaved RhoA-V14 and 2 μ l of beads after cleaving samples were separated on a 15% polyacrylamide gel, which was stained with Coomassie. GST-RhoA-V14 is indicated by the black arrow head. Cleaved RhoA-V14 is indicated by the black arrow, while the band corresponding to GST protein in the beads after cleaving lane is indicated by the grey arrow. Coomassie stained gel documenting the protein purification and cleaving process is a representative and was run for every purification batch. The same procedure was performed for RhoA-N19. (C) 0.6 μ g of cleaved RhoA-V14 protein was run on a 15% polyacrylamide gel and Western blotting was performed using anti-RhoA antibody at a dilution of 1:500. Western blotting of cleaved RhoA-V14 was performed once.

3.2.2 Purified mutant GST-RhoA fusion proteins bind to raphilin and constitutively active $G\alpha_q$ -L209

Whether purified mutant RhoA proteins retained their binding ability was tested by performing pull-down assays with the known RhoA binding partner raphilin and also with constitutively active $G\alpha_q$ -L209. Binding assays of purified mutant RhoA with $G\alpha_q$ would also verify results obtained in co-immunoprecipitation experiments. Purified mutant GST-RhoA protein used for the pull-down assays was firstly examined by Western blotting and a band at ~47 kDa was detected matching the expected molecular weight of the GST-RhoA fusion protein (Fig. 3.16C). Pull-down experiments were performed by incubating purified GST-RhoA-V14 and GST-RhoA-N19 bound to glutathione agarose beads as well as control GST beads with HEK293 lysate expressing Myc-raphilin or the constitutively active $G\alpha_q$ -L209. The detected bands at ~76 kDa showed that GST-RhoA-V14 as well as GST-RhoA-N19 pulled-down Myc-raphilin (Fig. 3.16A). Pull-down assays were also performed with $G\alpha_q$, and GST-RhoA-V14 as well as GST-RhoA-N19 were able to bind $G\alpha_q$ -L209 as shown by the bands at ~40 kDa (Fig. 3.16B). These results are consistent with the co-immunoprecipitation experiments that reported the ability of constitutively active $G\alpha_q$ -L209 to bind RhoA-V14 as well as with RhoA-N19 (Fig. 3.1).

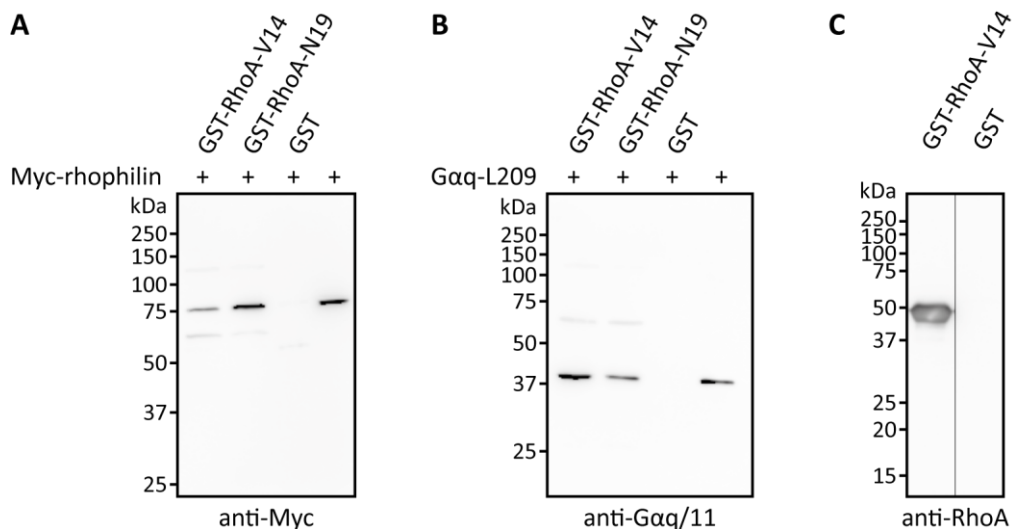


Figure 3.16 Purified GST-RhoA-V14 and GST-RhoA-N19 bind raphilin and $G\alpha_q$ -L209. GST-RhoA-V14, GST-RhoA-N19 and control GST beads were incubated with HEK293 lysate expressing Myc-raphilin or $G\alpha_q$ -L209. Samples were subjected to SDS-PAGE, transferred to nitrocellulose membranes and analysed by Western blotting. **(A)** 25 μ g Myc-raphilin lysate was incubated with 40 μ g GST-RhoA-V14 and GST-RhoA-N19 beads as well as with 25 μ g control GST beads. The pull-down assay samples alongside a 10 μ g Myc-raphilin lysate control were separated on 10 % polyacrylamide gels. Western blotting was performed using anti-myc antibody at a dilution of 1:400. **(B)** 50 μ g $G\alpha_q$ -L209 lysate were incubated with 40 μ g GST-RhoA-V14 and GST-RhoA-N19 beads as well as with 25 μ g control GST beads and the samples, alongside a 2.5 μ g $G\alpha_q$ lysate control, were separated on 10 % polyacrylamide gels. Western blotting was performed using anti- $G\alpha_{q/11}$ antibody at a dilution of 1:500. **(C)** GST-RhoA-V14 was examined by reprobing the membrane of a pull-down experiment, like (A) or (B), using anti-RhoA antibody at a dilution of 1:1000. The grey line indicates a discontinuity of the blot, because for this figure lanes were left out. Western blots of pull-down assays are representative of at least three separate experiments. Western blotting of GST-RhoA-V14 was performed once.

Having shown the ability of purified GST-RhoA-V14 and GST-RhoA-N19 to bind to $G\alpha_q$ -L209 expressed in HEK293 lysates, pull-down assays were repeated using endogenous $G\alpha_q$ from brain lysates. Membranes were probed with anti- $G\alpha_{q/11}$ antibody to detect any associated $G\alpha_q$. $G\alpha_q$ bands at ~40 kDa were detected in both GST-RhoA-V14 and GST-RhoA-N19 binding assays (Fig. 3.17, indicated by the black arrow). However, the detected bands were very faint and experiments using more lysate (up to 1500 μ g) did not result in stronger signals. Although detection in these pull-down experiments was weak, purified mutant GST-RhoA proteins seem to be able to interact with endogenous $G\alpha_q$.

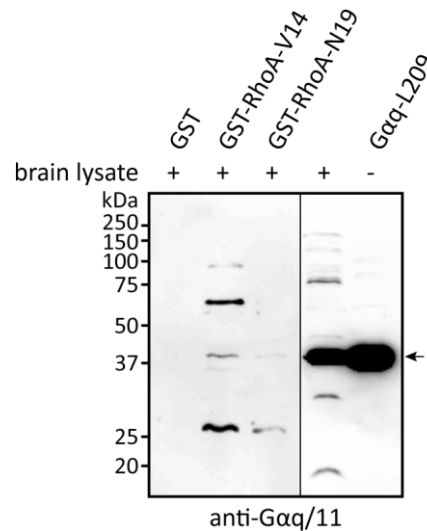


Figure 3.17 Pull-down experiments of endogenous $G\alpha_q$ using purified GST-RhoA-V14 and GST-RhoA-N19 protein. 25 μ g control GST beads and 40 μ g GST-RhoA-V14 and GST-RhoA-N19 were incubated with 700 μ g brain lysate (P2 fraction). Samples, alongside 100 μ g brain lysate and 25 μ g $G\alpha_q$ -L209 HEK293 cell lysate controls, were separated on a 12 % polyacrylamide gel, transferred to nitrocellulose membrane and analysed by Western blotting using anti- $G\alpha_{q/11}$ antibody at a dilution of 1:500. Under this condition (700 μ g brain lysate) the binding assay was performed only once, but was repeated using different amounts of brain lysates (250–1500 μ g), which also resulted in very faint bands.

3.2.3 Purified constitutively active RhoA-V14, but not inactive RhoA-N19, causes stress fibre formation in Swiss-3T3 cells

Before being used in electrophysiology studies, the biological activity of the purified and cleaved mutant RhoA proteins, constitutively active RhoA-V14 and inactive RhoA-N19, was tested by assessing their ability to affect the actin cytoskeleton structure within the cell. RhoA, together with other small GTPases like Rac and Cdc42, is known to be a regulator of the actin cytoskeleton (section 1.4) and microinjection of constitutively active RhoA-V14 has been shown to stimulate the formation of stress fibres in serum-starved Swiss-3T3 cells (Ridley and Hall, 1992). Thus this system was used to test the purified mutant RhoA proteins; RhoA-V14 injected cells should show an increase in stress fibres, whereas RhoA-N19 injected cells should not differ from control cells. The concept of stress fibre formation induced by RhoA-V14 was

first tested by transfecting RhoA-V14 into Swiss-3T3 cells, which were serum-starved since they contain stress fibres in the presence of serum. Monomeric red fluorescent protein (mRFP) was co-transfected with RhoA-V14 to be able to identify transfected cells. Alexa Fluor 488 phalloidin was used to label actin and transfected cells displayed abundant stress fibres compared to untransfected cells (Fig. 3.18A). Like untransfected cells, serum-starved Swiss-3T3 cells that underwent mock transfection did not show the formation of stress fibres (compare Fig. 3.18A and Fig. 3.18B).

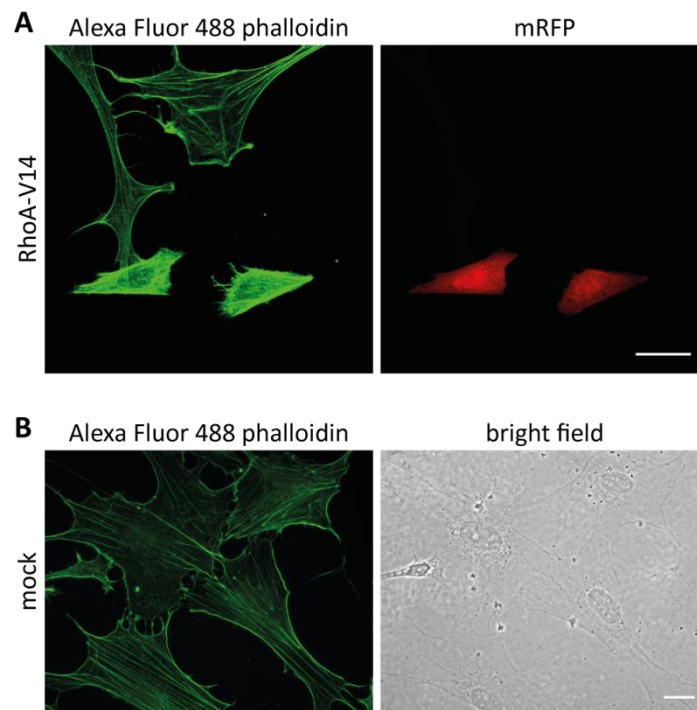
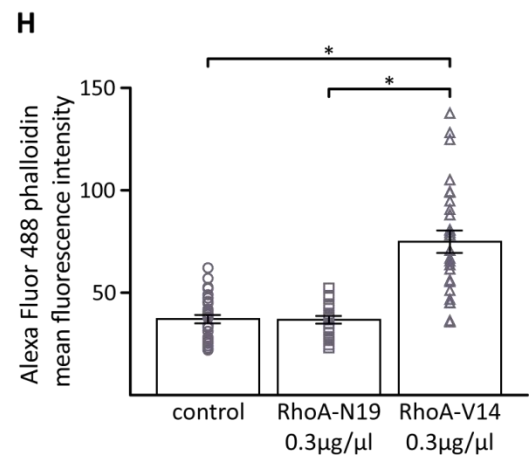
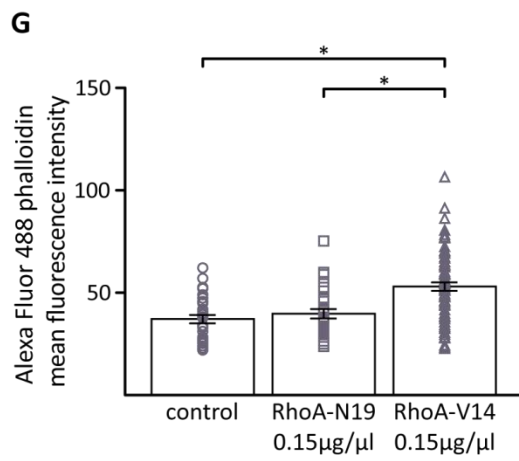
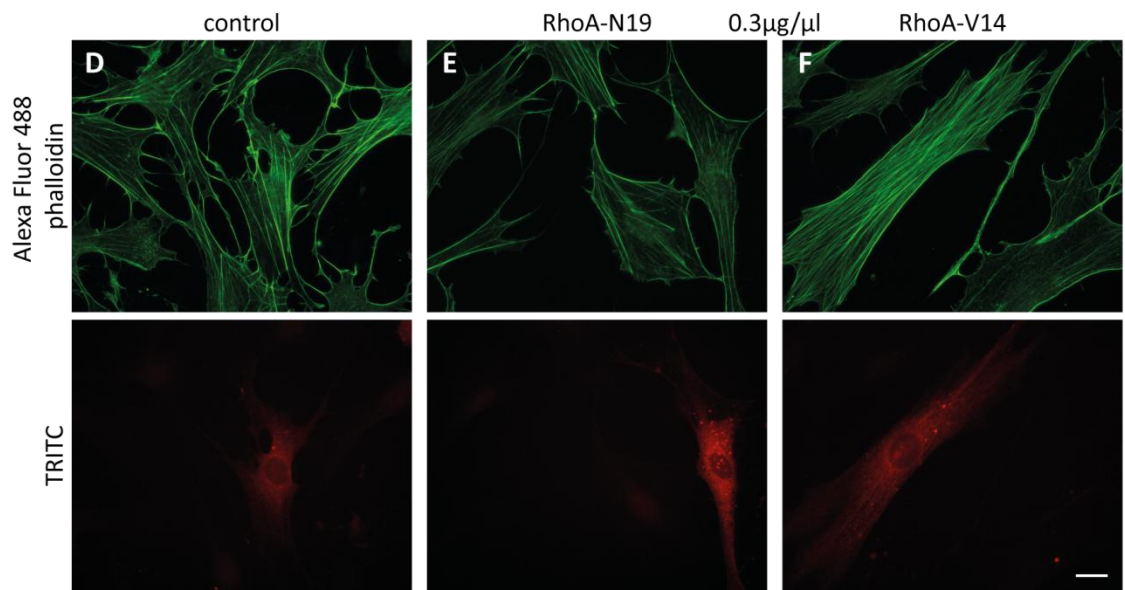
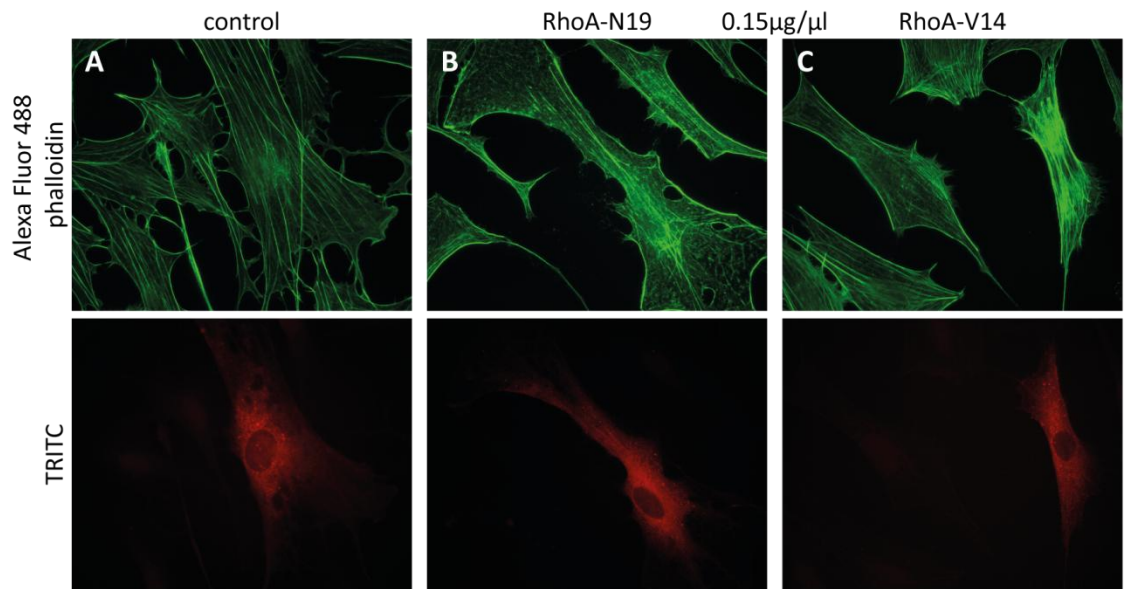


Figure 3.18 Transfection of constitutively active RhoA-V14 induces stress fibre formation in Swiss-3T3 cells. **(A)** Representative images of serum-starved Swiss-3T3 cells, which were co-transfected with RhoA-V14 and monomeric red fluorescent protein. Actin was visualized by labelling the cells with Alexa Fluor 488 phalloidin (0.25 U) and monomeric red fluorescent protein was used to identify transfected cells. **(B)** Mock transfected serum-starved Swiss-3T3 cells were labelled with Alexa Fluor 488 phalloidin (0.25 U). Scale bars 20 μ m.

Transfecting constitutively active RhoA-V14 successfully induced stress fibre assembly in Swiss-3T3 cells, an effect that was subsequently assessed by the microinjection of purified and cleaved constitutively active RhoA-V14 or inactive RhoA-N19 protein into serum-starved Swiss-3T3 cells. To identify microinjected cells TRITC was injected together with the RhoA proteins, while TRITC microinjected on its own served as control. Purified RhoA proteins were microinjected (section 2.2.2.2) in two concentrations, 0.15 μ g/ μ l and 0.3 μ g/ μ l, and in both cases constitutively active RhoA-V14 induced the formation of stress fibres, while inactive RhoA-N19 injected cells did not differ from control cells (Fig. 3.19). Actin was stained with Alexa Fluor 488 phalloidin and control (Fig. 3.19A and D) and RhoA-N19 (Fig. 3.19B and E) injected cells contained less stress fibres than RhoA-V14 injected cells (Fig. 3.19C and F). To

assess the level of stress fibres objectively the mean fluorescence intensity of each injected cell was measured (section 2.2.11.3) and as cells containing more stress fibres displayed higher mean fluorescence intensity values these could be used to compare control, RhoA-N19 and RhoA-V14 cells (Fig. 3.19G and H). In experiments using 0.15 $\mu\text{g}/\mu\text{l}$ RhoA protein for microinjections the groups' stress fibre levels differed significantly ($P < 0.0001$, one-way ANOVA) and the post-hoc Bonferroni's multiple comparison test detailed that while control (37.1 ± 2.0 mean fluorescence intensity) and RhoA-N19 (39.8 ± 2.3) injected cells did not differ from each other, RhoA-V14 cells (53.0 ± 2.0) were significantly different to both of them (Fig. 3.19G). The same was observed for experiments conducted with 0.3 $\mu\text{g}/\mu\text{l}$ RhoA protein (mean fluorescence intensity 37.1 ± 2.0 (control), 36.8 ± 1.9 (RhoA-N19), 75.0 ± 5.5 (RhoA-V14); $P < 0.0001$, one-way ANOVA; Fig. 3.19H). These results demonstrated that the purified and cleaved mutant RhoA proteins, RhoA-V14 and RhoA-N19, affected the cytoskeleton as expected.

Figure 3.19 **Microinjection of purified constitutively active RhoA-V14, but not purified inactive RhoA-N19, into Swiss-3T3 cells stimulates the formation of stress fibres.** Representative images of serum-starved Swiss-3T3 cells microinjected with 10 $\mu\text{g}/\mu\text{l}$ TRITC alone (control, **A and D**), purified RhoA-N19 (**B and E**) or purified RhoA-V14 (**C and F**). Injected cells were identified by TRITC, which was also microinjected alongside purified RhoA proteins (A–F, lower panels). Actin was labelled using Alexa Fluor 488 phalloidin (0.25 U; A–F, upper panels). Scale bar 20 μm . Microinjections with purified RhoA were performed using a protein concentration of either 0.15 $\mu\text{g}/\mu\text{l}$ or 0.3 $\mu\text{g}/\mu\text{l}$. To compare stress fibre levels between control, RhoA-N19 and RhoA-V14 injected cells the mean fluorescence intensities of each injected cell was measured (section 2.2.11.3). (**G**) Comparison of stress fibre levels between control (37.1 ± 2.0 , $n=30$), 0.15 $\mu\text{g}/\mu\text{l}$ RhoA-N19 (39.8 ± 2.3 , $n=28$) and 0.15 $\mu\text{g}/\mu\text{l}$ RhoA-V14 (53.0 ± 2.0 , $n=72$) ($P<0.0001$, one-way ANOVA). (**H**) Summary of stress fibre level comparison between control (37.1 ± 2.0 , $n=30$), 0.3 $\mu\text{g}/\mu\text{l}$ RhoA-N19 (36.8 ± 1.9 , $n=21$) and 0.3 $\mu\text{g}/\mu\text{l}$ RhoA-V14 (75.0 ± 5.5 , $n=27$) ($P<0.0001$, one-way ANOVA). In both cases (G and H) the post-hoc Bonferroni's multiple comparison test showed that control and RhoA-N19 injected cells did not differ, while RhoA-V14 injected cells differed significantly from control as well as from RhoA-N19. * = $P<0.05$ and n numbers refer to the number of cells analysed from multiple injections. Mean values \pm SEM are presented.



3.2.4 The effect of intracellularly applied mutant RhoA proteins on sI_{AHP} in acute hippocampal slices

Electrophysiological experiments using the purified RhoA proteins have been performed by Anne Boehlen. Purified and cleaved RhoA-V14 or RhoA-N19 proteins (30 $\mu\text{g}/\text{ml}$; section 2.2.7 and 3.2.1) were added to the intracellular solution and introduced into CA1 pyramidal neurons in acute hippocampal slices via the patch pipette. Whole-cell voltage clamp recordings were carried out and the effect of the purified mutant RhoA proteins on sI_{AHP} was assessed. Control recordings were performed with an intracellular solution that contained equal amounts of a mock purification sample (section 2.2.7). It was hypothesised that the presence of RhoA-N19 proteins would not affect sI_{AHP} , while RhoA-V14 would mimic the inhibitory action of cholinergic and glutamatergic agonists. Averaged sI_{AHP} amplitudes of control, RhoA-N19 and RhoA-V14 cells are shown in the time course (Fig. 3.20). In the first 10 min of establishing whole-cell configuration all three groups show the typical increase of current amplitude (Zhang et al., 1995; Pedarzani et al., 1998). However, the maximal steady-state amplitude of sI_{AHP} in cells exposed to constitutively active RhoA-V14 is significantly reduced compared to control and inactive RhoA-N19 ($P < 0.0001$, two-way ANOVA 0.5–20 min). The evaluation of this effect at later time points was complicated by the fact that all three groups showed a run-down of the current from ~20 min onwards.

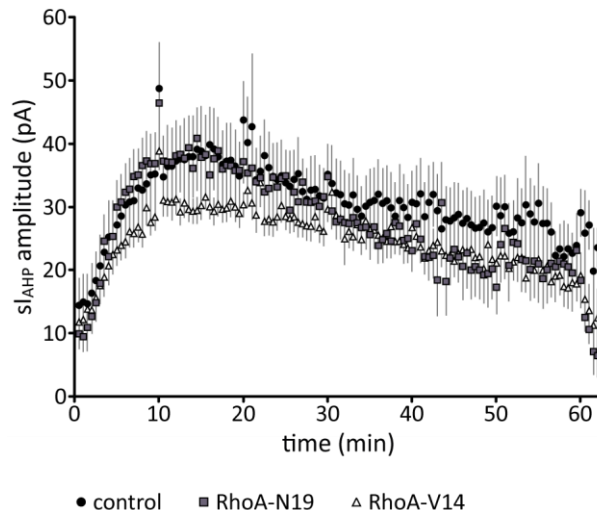


Figure 3.20 sI_{AHP} is partially inhibited by the application of purified constitutively active RhoA-V14, but not by inactive RhoA-N19. Whole-cell voltage clamp recordings of CA1 pyramidal neurons in acute hippocampal slices were performed. The purified and cleaved constitutively active RhoA-V14 or inactive RhoA-N19 was added to the intracellular solution and was introduced into the neurons via the patch pipette. Recordings with intracellular solution containing a mock purification sample served as a control. sI_{AHP} was activated by a depolarisation step to +30 mV for 100 ms. Time courses of sI_{AHP} amplitude in control cells and cells with intracellularly applied RhoA-V14 or RhoA-N19 protein (30 $\mu\text{g}/\text{ml}$); control ($n=13$), RhoA-N19 ($n=13$) and RhoA-V14 ($n=21$), mean values \pm SEM are presented. Comparing the effect of RhoA proteins on amplitude over time showed that sI_{AHP} amplitudes of the three groups are not the same ($P < 0.0001$, two way ANOVA 0.5–20 min and 0.5–62 min). Experiments were performed by A. Boehlen.

3.2.5 Summary

The constitutively active RhoA-V14 and the inactive RhoA-N19 proteins were purified as fusion proteins and their ability to interact with binding partners was shown in pull-down assays with rhophilin and $G\alpha_q$. Besides interaction studies, purified and cleaved mutant RhoA proteins were also tested for their effect on the actin cytoskeleton of cells. Swiss-3T3 cells microinjected with purified RhoA-V14 displayed plenty of stress fibres, while the actin cytoskeleton was not influenced by the injection with purified RhoA-N19. It was concluded that the mutant RhoA proteins are biologically active and were thus used for electrophysiological studies. The role of RhoA in the signalling pathway mediating the suppression of sI_{AHP} by cholinergic and glutamatergic agonists was investigated in electrophysiological experiments by introducing mutant RhoA proteins into neurons via a patch pipette. The intracellular application of purified constitutively active RhoA-V14 protein induced a significant, albeit partial, reduction of sI_{AHP} , which could be due to a low intracellular concentration of RhoA-V14 or a too short exposure to the introduced protein. To establish the role of RhoA in the cholinergic and glutamatergic suppression of sI_{AHP} , electrophysiological experiments were conducted using a different approach, namely the introduction of mutant RhoA into hippocampal neurons by virus infection.

3.3 Assessment of RhoA involvement in the cholinergic modulation of sl_{AHP} in Sindbis virus infected primary hippocampal neurons

RhoA mutants were over-expressed by virus infection in primary hippocampal pyramidal neurons with the ultimate aim of replicating the experiments in acute or organotypic hippocampal slices. The Sindbis virus was chosen to introduce mutant RhoA proteins into hippocampal neurons as it allows fast protein expression and displays high specificity for neurons. Using a modified Sindbis vector (Jeromin et al., 2003) had the additional advantage of containing the nsP2 mutation (S726), which has been shown to markedly reduce cytotoxicity (Dryga et al., 1997), and of simultaneously expressing EGFP allowing for the identification of infected neurons (pSinrep5-EGFP). Primary cultures of hippocampal neurons were infected with recombinant Sindbis virus containing RhoA-V14 or RhoA-N19 and the effect of mutant RhoA protein on sl_{AHP} was investigated by whole-cell voltage clamp recordings.

3.3.1 Sindbis virus production and functionality assay

3.3.1.1 Recombinant Sindbis plasmid construction and RNA synthesis

The RhoA mutants, constitutively active RhoA-V14 and inactive RhoA-N19, were cloned into pSinrep5-EGFP under the control of the Sindbis subgenomic promoter (P_{SG}) to construct the recombinant plasmids pSinrep5-RhoA-V14-EGFP and pSinrep5-RhoA-N19-EGFP (section 2.2.13). The helper plasmid, pHelper-DH-BB (tRNA/TE12) was constructed from the helpers DH-BB and DH-26S (Kim et al., 2004) and thus combined the high replication capacity seen with the DH-BB helper and the ability of DH-26S, a TE12 strain derivative, to infect neurons (Bredenbeek et al., 1993). The Sindbis expression constructs, pSinrep5-EGFP, pSinrep5-RhoA-V14-EGFP and pSinrep5-RhoA-N19-EGFP, were linearized with *PacI* and the helper pHelper-DH-BB (tRNA/TE12) with *XhoI* before *in vitro* transcription (section 2.2.10.1). RNAs were analysed by formaldehyde agarose gel electrophoresis and yielded products of 9 kb (SIN-EGFP, Fig. 3.21A), 9.5 kb (SIN-RhoA-V14-EGFP and SIN-RhoA-N19-EGFP, Fig. 3.21B) and 5 kb (helper, Fig. 3.21B). Isolated RNA of HEK293 (28S, 5 kb and 18S, 1.9 kb) and rat brain type 2 sodium channel α subunit RNA ($Na_v1.2$, 6 kb), which was generated to test the RNA synthesis reaction, were run alongside as size markers (Fig. 3.21). Synthesised RNAs from pSinrep5-EGFP, pSinrep5-RhoA-V14-EGFP, pSinrep5-RhoA-N19-EGFP and pHelper-DH-BB (tRNA/TE12) were used for virus production.

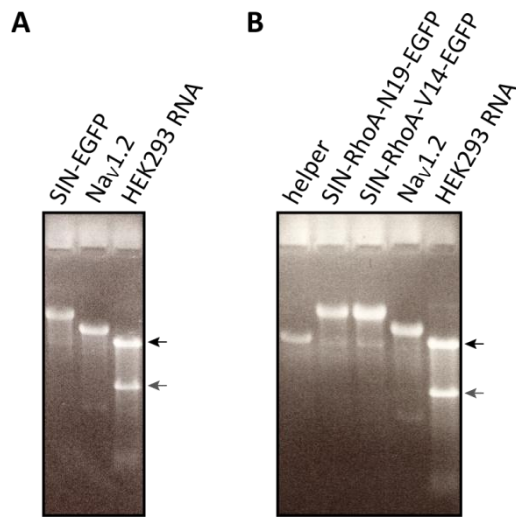


Figure 3.21 RNA synthesis from Sindbis expression and helper constructs. Recombinant Sindbis expression constructs and the helper were linearized and *in vitro* transcribed. Formaldehyde agarose gel electrophoresis of **(A)** SIN-EGFP (9 kb) and **(B)** helper (5 kb), SIN-RhoA-N19-EGFP (9.5 kb) and SIN-RhoA-V14-EGFP (9.5 kb) alongside synthesised Nav_v1.2 (6 kb) RNA and RNA from HEK293 cells (28S, 5 kb, indicated by black arrow; 18S, 1.9 kb, indicated by grey arrow), which were used as size markers.

3.3.1.2 Production of Sindbis virus particles

To produce virus particles, Sindbis expression RNA, together with helper RNA, were electroporated into BHK-21 cells. This co-transfection of helper RNA provides the structural proteins necessary for packaging the recombinant RNA and leads to viral particles being released into the medium, where they can then be harvested and used for infection. Electroporation of Sindbis expression RNA alone (without the structural proteins provided by the helper) will not be packaged and thus expression is limited to the transfected cell. This fact was exploited during the electroporation set-up phase, since electroporation conditions could be tested and the results judged by assessing the number of EGFP expressing cells without producing virus particles. The electroporation of BHK-21 cells with SIN-EGFP RNA was initially tested using the ECM600 electroporation system (BTX) and different electroporation protocols (Invitrogen, manual; Wahlfors and Morgan, 2003; Ehrenguber et al., 2011) and it was determined that pulses of 500 V lasting 7 ms produced the highest transfection efficiency. However, even with these settings the number of EGFP expressing cells varied greatly across experiments (5–50 %; Fig. 3.22A and B) and the ECM600 was considered unsuitable for virus production. The experiment was repeated with a GenePulser II electroporation system (BIO-RAD) using the mentioned optimised settings, but the transfection efficiency achieved was not reproducible between experiments and never high enough to be suitable for the production of viruses with a high-titre (1–10 %; Fig. 3.22C and D). Consistently high transfection efficiencies were only achieved with the GenePulser XCell (BIO-RAD) (40 %; Fig. 3.22E) and it was therefore used for Sindbis virus productions.

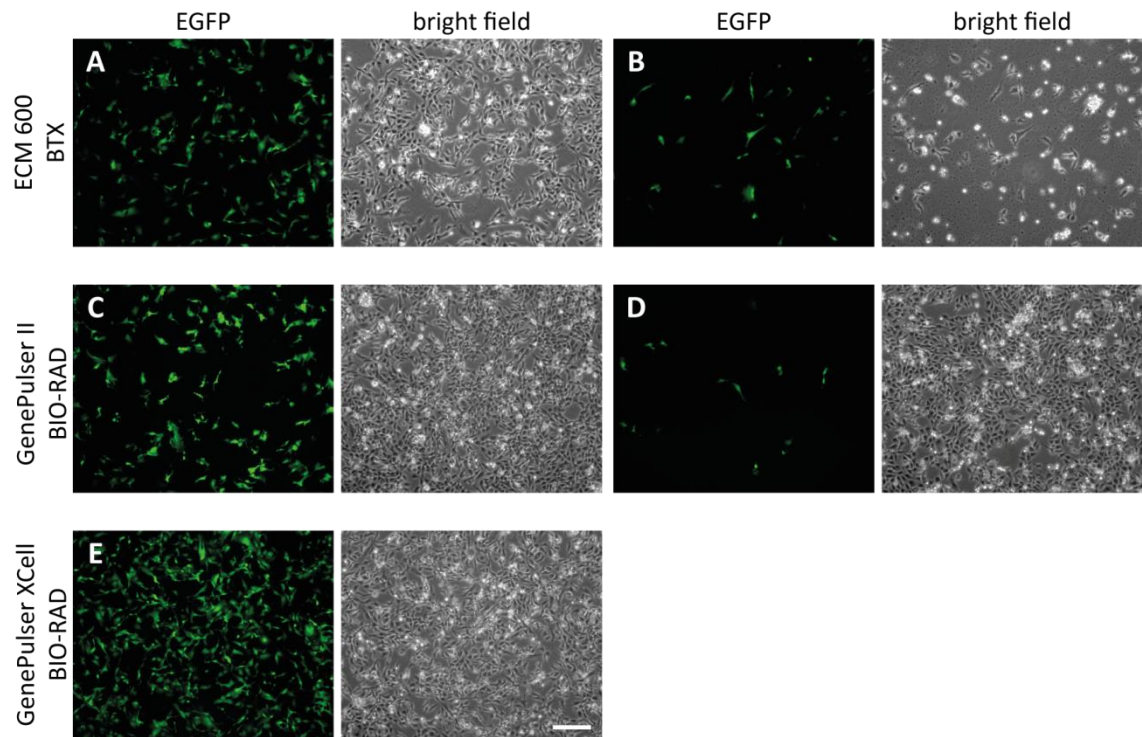


Figure 3.22 Electroporation of BHK-21 cells with SIN-EGFP RNA using different electroporation systems. BHK-21 cells were electroporated with SIN-EGFP RNA using pulses of 500 V lasting 7 ms and the transfection efficiency was examined 24 h later by assessing the number of EGFP expressing cells. Representative EGFP and corresponding bright field images showing electroporation results using the ECM600 electroporation system (BTX) (**A and B**), the GenePulser II (BIO-RAD) (**C and D**) and the GenePulser XCell (BIO-RAD) (**E**). Electroporations performed with the ECM600 electroporation system (BTX) and GenePulser II (BIO-RAD) varied between higher (A and C) and lower (B and D) transfection efficiencies. Electroporations with the GenePulser XCell (BIO-RAD) (E) consistently resulted in high transfection efficiencies and was therefore used for the virus production. Scale bar 200 μ m.

To produce virus particles, BHK-21 cells were electroporated with SIN-EGFP, SIN-RhoA-V14-EGFP or SIN-RhoA-N19-EGFP RNA and helper RNA using the GenePulser XCell (BIO-RAD) protocol (section 2.2.10.2). Electroporated BHK-21 cells were plated and the medium containing the virions was harvested 24 h later.

3.3.1.3 Determining the infection capability of the viral stock and the optimal amount of virus needed for infection

This Sindbis expression system consists of two constructs, which need to be co-transfected to produce virus particles: an expression plasmid containing the nonstructural genes responsible for replication and the genes of interest and a helper plasmid encoding for the structural proteins. The generated viruses are replication-deficient, since only the Sindbis expression RNA is packaged but not the helper RNA, which is defective i.e. does not contain a packaging signal. Therefore the viruses undergo only one round of infection and infected cells express the proteins of interest, but cannot generate new viruses because the structural proteins provided by the helper RNA are missing. Consequently the virus titre cannot be determined by plaque

assays. The infection capability of the Sindbis viruses was therefore assessed empirically by infecting BHK-21 cells with dilutions of Sindbis virus generated from SIN-EGFP (EGFP control), SIN-RhoA-V14-EGFP (RhoA-V14) and SIN-RhoA-N19-EGFP (RhoA-N19) and by counting the number of EGFP expressing cells (Fig. 3.23; section 2.2.10.3). Infecting BHK-21 cells with EGFP control, RhoA-N19 or RhoA-V14 at a dilution of 1:10 resulted in all cells expressing EGFP (Fig. 3.23A, C and E). At higher dilutions for example 1:1000 (Fig. 3.23B, D and F) EGFP control and RhoA-N19 still infected a number of cells, while hardly any EGFP expressing cells could be seen in infections with RhoA-V14. The concentration of viral stock was calculated (section 2.2.10.3) and amounted to 10^8 – 10^9 virions/ml on average; EGFP control being the most potent (1.7×10^9 virions/ml), followed by RhoA-N19 (6.2×10^8 virions/ml) and then RhoA-V14 (1.9×10^8 virions/ml). In addition the assay also determined the optimal dilutions of the viruses (1:5000 for EGFP control, 1:1000–1:2000 for RhoA-N19 and 1:100–1:500 for RhoA-V14) to be used in subsequent experiments in BHK-21 cells and cultured hippocampal neurons.

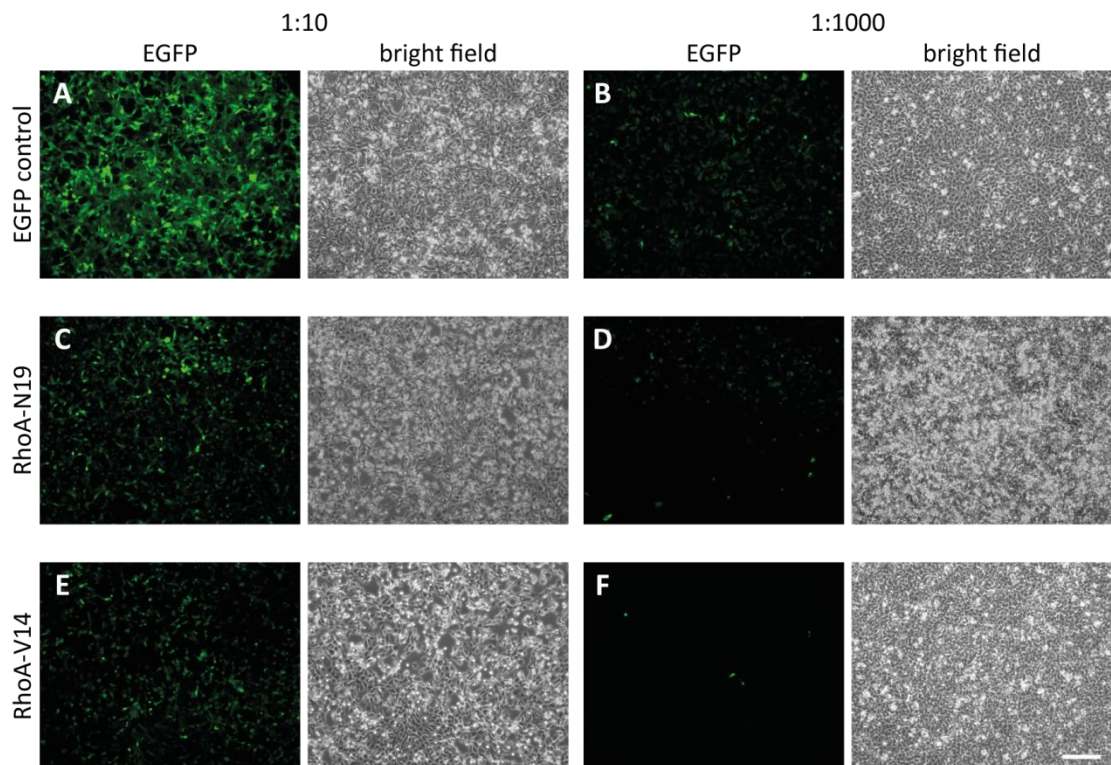


Figure 3.23 Infecting BHK-21 cells with diluted recombinant Sindbis virus to determine the infection capability of the viral stock and the optimal infection conditions for subsequent experiments. BHK-21 cells were infected with Sindbis virus generated from SIN-EGFP (EGFP control), SIN-RhoA-N19-EGFP (RhoA-N19) or SIN-RhoA-V14-EGFP (RhoA-V14) at various dilutions (section 2.2.10; 1:10 (**A, C and E**) and 1:1000 (**B, D and F**) are shown). EGFP expressing cells were counted and used to calculate the concentration of the viral stock (section 2.2.10.3). Optimal dilutions of the virus were determined as 1:5000 for EGFP control, 1:1000–1:2000 for RhoA-N19 and 1:100–1:500 for RhoA-V14. Representative images, EGFP and the corresponding bright field image, are shown. Scale bar 200 μ m.

3.3.1.4 Stress fibres formation in constitutively active RhoA-V14 infected BHK-21 cells, but not in inactive RhoA-N19 infected cells

As described before RhoA is involved in the regulation of the actin cytoskeleton and the expression of constitutively active RhoA-V14 causes the formation of stress fibres, while no changes of the cytoskeleton were observed in cells expressing inactive RhoA-N19 (Ridley and Hall, 1992; section 3.2.3). Hence the effect of the generated RhoA Sindbis viruses on the cytoskeleton was tested by infecting serum-starved BHK-21 cells with diluted EGFP control (1:5000), RhoA-N19 (1:1000) and RhoA-V14 (1:100) virus. Actin was labelled with Alexa Fluor 594 phalloidin and infected cells were identified by their EGFP expression. Cells infected with RhoA-V14 (Fig. 3.24C) contained more stress fibres than RhoA-N19 (Fig. 3.24B) or EGFP control (Fig. 3.24A) infected cells. The mean fluorescence intensity of infected cells was measured and used to compare stress fibre levels between EGFP control (54.7 ± 4.3 mean fluorescence intensity), RhoA-N19 (56.4 ± 6.5) and RhoA-V14 (92.2 ± 6.7 ; Fig. 3.24D). The intensities differed significantly ($P < 0.0001$, one-way ANOVA) and the post-hoc Bonferroni's multiple comparison test showed that while EGFP control and RhoA-N19 did not differ from each other, RhoA-V14 infected cells differed significantly from both. RhoA-V14 and RhoA-N19 Sindbis viruses were affecting the actin cytoskeleton as expected and match the observations made with microinjected purified RhoA-V14 and RhoA-N19 proteins. It can therefore be concluded that the RhoA-V14 and RhoA-N19 viruses are functional and can be used to infect hippocampal neurons to study the involvement of RhoA in the modulation of sI_{AHP} by cholinergic and glutamatergic agonists.

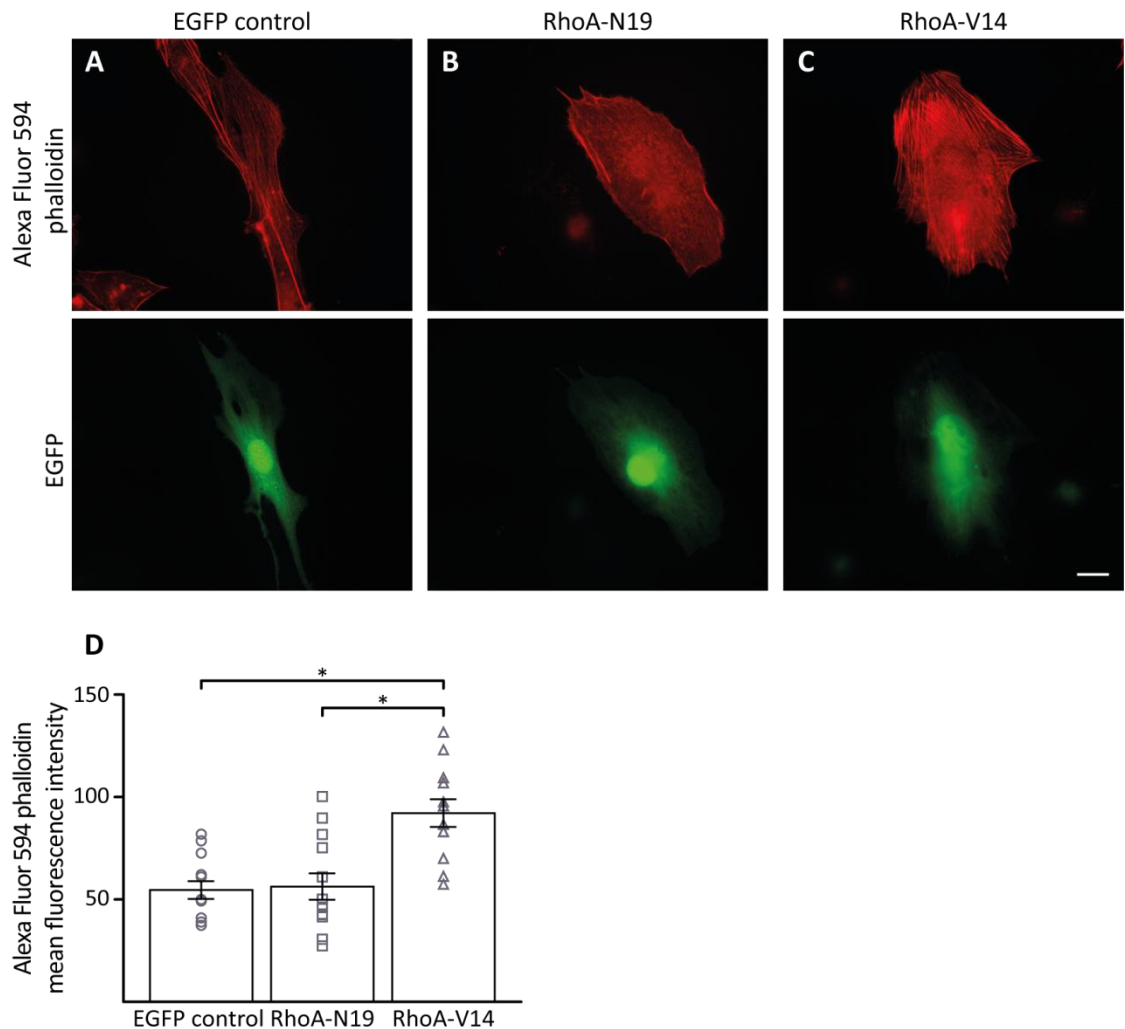


Figure 3.24 Infection with constitutively active RhoA-V14, but not inactive RhoA-N19, Sindbis virus induces stress fibre formation in BHK-21 cells. Representative images of serum-starved BHK-21 cells that were infected with **(A)** EGFP control (1:5000 dilution), **(B)** RhoA-N19 (1:1000) or **(C)** RhoA-V14 (1:100) Sindbis virus. Actin was labelled with Alexa Fluor 594 phalloidin (0.25 U; A–C, upper panels) and infected cells were identified by EGFP expression (A–C, lower panels). Scale bar 20 μ m. **(D)** Stress fibre levels of infected cells were compared by measuring the mean fluorescence intensities of EGFP control (54.7 ± 4.3 , $n=13$), RhoA-N19 (56.4 ± 6.5 , $n=13$) and RhoA-V14 (92.2 ± 6.7 , $n=12$) ($P < 0.0001$, one-way ANOVA). As shown by the post-hoc Bonferroni's multiple comparison test RhoA-V14 infected cells differed significantly from control and RhoA-N19 infected cells, which themselves did not differ from each other. * = $P < 0.05$ and n numbers refer to the number of cells analysed from one infection. Mean values \pm SEM are presented.

3.3.2 sl_{AHP} in primary cultured hippocampal neurons

To assess the role of RhoA in the cholinergic modulation of sl_{AHP} mutant RhoA proteins, the constitutively active RhoA-V14 and the inactive RhoA-N19, were expressed in primary cultured hippocampal neurons by Sindbis virus infection. This preparation was chosen as it presented an accessible environment in which infection can easily be achieved by addition of the virus to the culture medium. sl_{AHP} is known to be present in primary cultures of hippocampal neurons (Shah and Haylett, 2000b; Gallasch, 2008) and its characteristics were examined in control neurons before the effects of mutant RhoA proteins on sl_{AHP} were investigated.

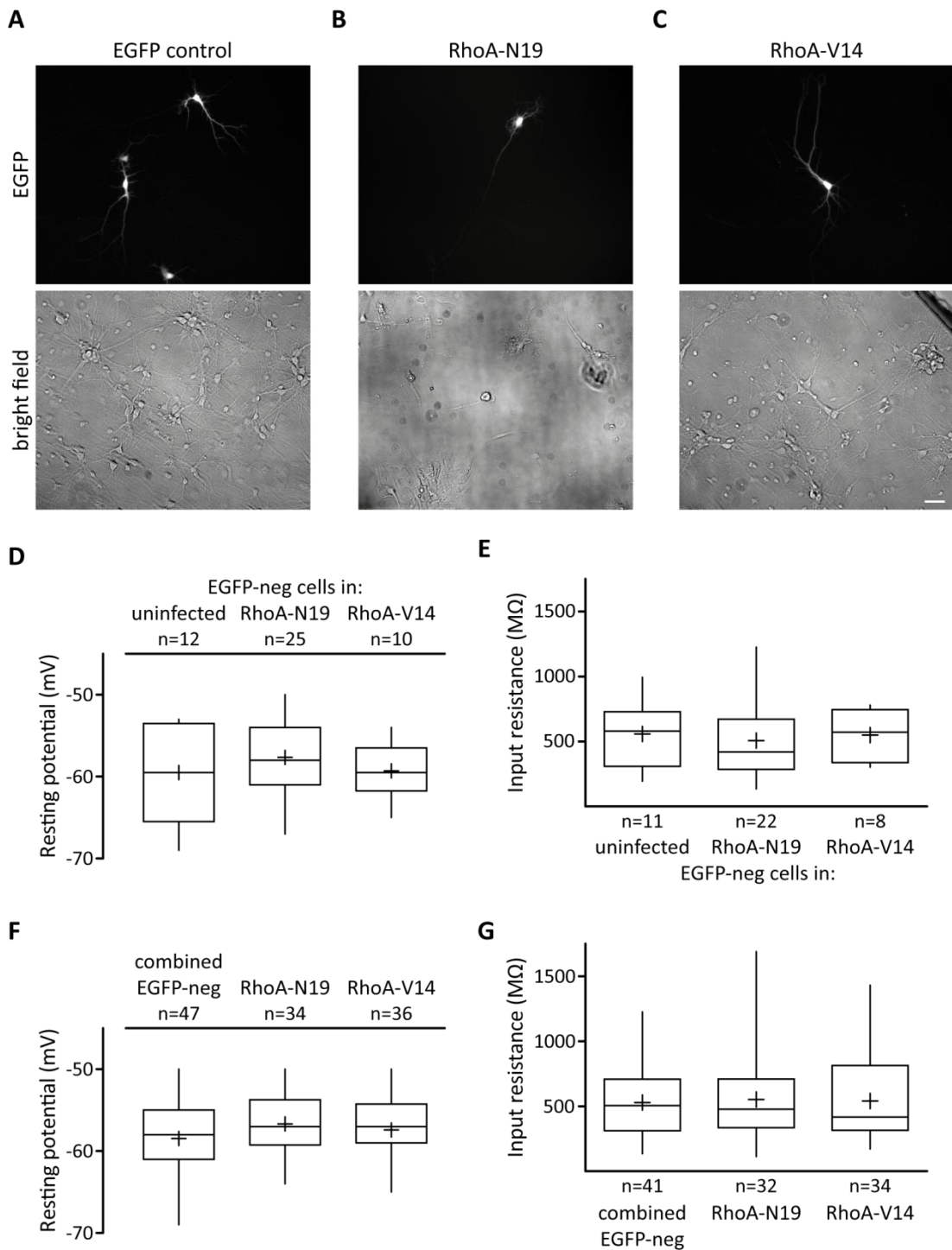
3.3.2.1 Properties of primary cultured hippocampal pyramidal neurons are not affected by Sindbis virus infection

Whole-cell patch clamp recordings of primary cultured hippocampal pyramidal neurons were performed and the effects of a Sindbis virus infection on the properties of hippocampal pyramidal neurons were examined. The morphology of pyramidal neurons with their triangular-shaped soma and distinctive processes was used to select neurons for patching (Fig. 3.25A–C). Infected neurons were identified by their EGFP expression (Fig. 3.25A–C, upper panels) and no morphological differences between control and neurons infected with RhoA-N19 or RhoA-V14 were observed.

Recordings were made from control (EGFP-neg), RhoA-N19 (1:2000 dilutions, occasionally 1:1000) and RhoA-V14 (1:100) infected pyramidal neurons. The control group included EGFP-negative cells recorded from coverslips that had no contact with Sindbis virus (uninfected) and also from coverslips that had undergone infection with RhoA-N19 or RhoA-V14 virus. The membrane resting potential of EGFP-negative cells in uninfected coverslips amounted to -59.5 ± 1.7 mV (n=12), in RhoA-N19 treated coverslips to -57.6 ± 0.9 mV (n=25) and in RhoA-V14 treated coverslips to -59.3 ± 1.2 mV (n=10) and did not differ significantly (P=0.45, one-way ANOVA; Fig. 3.25D). The same was observed for the input resistance of EGFP-negative neurons, which was 558.4 ± 73.8 M Ω (n=11) in uninfected, 506.7 ± 61.8 M Ω (n=22) in RhoA-N19 treated and 548.5 ± 70.4 M Ω (n=8) in RhoA-V14 treated coverslips (P=0.8453, one-way ANOVA; Fig. 3.25E). Since the passive properties of EGFP-negative neurons were not affected by Sindbis virus treatment, they were pooled into one control group. The resting potential of the combined EGFP-negative cells was -58.5 ± 0.7 mV (n=47), of RhoA-N19 infected cells 56.7 ± 0.7 mV (n=34) and of RhoA-V14 infected cells -57.4 ± 0.7 mV (n=36) (P=0.1836, one-way ANOVA; Fig. 3.25F). The input resistance amounted to 528.7 ± 40.3 M Ω (n=41) in EGFP-negative cells, 552.7 ± 60 M Ω (n=32) in RhoA-N19 infected cells and 540.5 ± 54.7 M Ω (n=34) in RhoA-V14 infected cells (P=0.9455, one-way ANOVA; Fig. 3.25G). It can therefore be concluded that the passive properties of hippocampal pyramidal neurons in primary culture were not influenced by the infection with RhoA-N19 or RhoA-V14 Sindbis virus.

All neurons consistently fired overshooting action potentials, although the firing pattern observed for all three groups was variable, ranging from single or irregular spikes, to bursts and regular firing. Regular firing was most commonly observed (90 % of EGFP-negative, 56 % RhoA-N19 and 62 % RhoA-V14 cells). Due to the artificial nature of the pyramidal neuron network in culture, dedicated current clamp experiments to analyse virus induced changes in firing pattern and spike frequency adaptation were not carried out.

Figure 3.25 Properties of hippocampal pyramidal neurons in primary culture. Representative images of pyramidal cultures of hippocampal neurons infected with **(A)** EGFP control (1:5000 dilution), **(B)** RhoA-N19 (1:2000) and **(C)** RhoA-V14 (1:500) Sindbis virus. Scale bar 50 μm . For whole-cell recordings, primary cultures of hippocampal neurons were infected with RhoA-N19 at a dilution of 1:2000 (occasionally 1:1000) or with RhoA-V14 at a 1:100 dilution, while EGFP-negative neurons served as control. **(D)** Comparison of the resting potential of EGFP-negative neurons in uninfected and in RhoA-N19 or RhoA-V14 treated coverslips ($P=0.45$, one-way ANOVA). **(E)** Summary of the input resistance of EGFP-negative cells in uninfected and in RhoA-N19 or RhoA-V14 treated coverslips ($P=0.8453$, one-way ANOVA). **(F)** Comparison of the resting potential of combined EGFP-negative and RhoA-N19 or RhoA-V14 infected cells ($P=0.1836$, one-way ANOVA) and **(G)** of their input resistance ($P=0.9455$, one-way ANOVA). The box plot is made up of the median (horizontal line in the middle of box), 25th and 75th percentile of the data (upper and lower edges of the box), maximum and minimum values of the data (top and bottom of the whiskers) and the mean value (“+” in the box). All recordings were made in the presence of 25 μM D-(-)-2-amino-5-phosphonopentanoic acid and 5 μM 2,3-dioxo-6-nitro-1,2,3,4-tetrahydrobenzo(f)quinoxaline-7-sulfonamide.



3.3.2.2 Unmasking of sI_{AHP} in primary cultured hippocampal neurons

Neurons were voltage-clamped at -50 mV and sI_{AHP} was recorded following a 200 ms-long depolarising step to +30 mV to activate voltage-gated Ca^{2+} channels (Fig.2.11; section 2.2.14.2). After the depolarising step outward tail currents, generated by I_{AHP} and sI_{AHP} , were observed (Fig. 3.26A). Both currents coexist in hippocampal neurons but can be separated pharmacologically because I_{AHP} is inhibited by apamin and dTC, which do not affect sI_{AHP} (Stocker et al., 1999; Shah et al., 2006). The coexistence of I_{AHP} and sI_{AHP} was observed in the

majority of cells recorded (I_{AHP} in 90% and sI_{AHP} in 100% of EGFP-negative cells) and sI_{AHP} could be seen in isolation following the application of 50–100 μM dTC, which blocks $K_{\text{Ca}2}$ channels that underlie I_{AHP} (Fig. 3.26B and D). TTX (0.5 μM ; blocker of voltage-gated Na^+ channels) and TEA (1 mM; blocker of a subset of K_{V} and $K_{\text{Ca}1.1}$ channels, $K_{\text{Ca}2}$ channels are not affected at this concentration) were applied alongside dTC to maximize Ca^{2+} influx and thus sI_{AHP} amplitude. The kinetic features of the sI_{AHP} observed in cultured hippocampal pyramidal neurons matched the ones reported in slices i.e. activating over several hundred milliseconds and decaying over seconds (section 1.2.3; Lancaster and Adams, 1986; Sah, 1996) and sI_{AHP} showed the typical run-up (Zhang et al., 1995; Pedarzani et al., 1998), lasting for 5–10 min, before reaching steady-state amplitude (Fig. 3.26D).

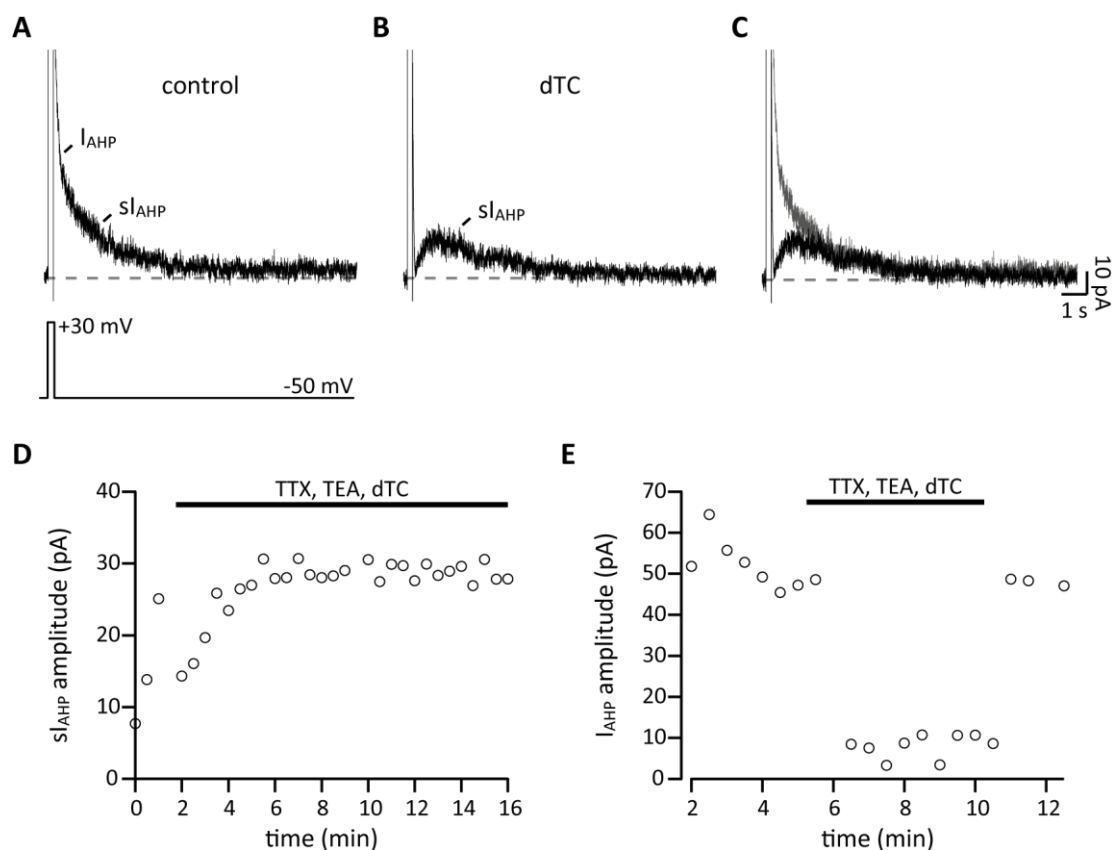


Figure 3.26 Pharmacological isolation of sI_{AHP} in cultured hippocampal neurons. I_{AHP} was selectively blocked by d-Tubocurarine (dTC), while sI_{AHP} was not affected. **(A and B)** Representative whole-cell voltage-clamp recordings of afterhyperpolarizing currents in an EGFP-negative neuron in the absence **(A)** and presence **(B)** of 0.5 μM tetrodotoxin (TTX), 1 mM tetraethylammonium (TEA) and 100 μM dTC. **(C)** Superimposed traces illustrating the coexistence of I_{AHP} and sI_{AHP} in cultured hippocampal neurons. The voltage clamp protocol used to activate the afterhyperpolarizing currents is shown underneath the trace in **(A)**. The dashed grey line indicates zero current **(A–C)**. **(D)** Time course of the run-up and stabilization of the pharmacologically isolated sI_{AHP} . **(E)** Time course of I_{AHP} amplitude in response to application and wash out of the pharmacological blockers used in sI_{AHP} recordings. All recordings were carried out in the presence of synaptic blockers, 25 μM D(-)-2-amino-5-phosphonopentanoic acid and 5 μM 2,3-dioxo-6-nitro-1,2,3,4-tetrahydrobenzo(f)quinoxaline-7-sulfonamide.

3.3.2.3 Regulation of sI_{AHP} in cultured hippocampal neurons

The activation of sI_{AHP} by Ca^{2+} has been shown in various studies (Lancaster and Zucker, 1994; Zhang et al., 1995; Sah, 1996). sI_{AHP} in cultured hippocampal pyramidal neurons was tested for Ca^{2+} dependency by replacing extracellular Ca^{2+} with Mg^{2+} (5 mM; section 2.2.14.1). The removal of Ca^{2+} from the extracellular solution led to the elimination of the unclamped Ca^{2+} currents and sI_{AHP} as seen in the example traces with or without extracellular Ca^{2+} (Fig. 3.27A and B) and the time course of recording (Fig. 3.27D). Once Ca^{2+} levels in the extracellular solutions were restored, sI_{AHP} recovered readily (Fig. 3.27C and D). sI_{AHP} amplitude, which amounted to 22.1 ± 4.2 pA ($n=5$, control), was reduced to 0.2 ± 0.2 pA ($n=5$, 0 Ca^{2+}) by the removal of extracellular Ca^{2+} ($P=0.0062$, paired t-test; Fig. 3.21E); a reduction of 99.1 ± 0.9 %. The effect of 0 Ca^{2+} was reversible and sI_{AHP} recovered to 18.6 ± 3.6 pA ($n=4$, recovery; Fig. 3.27E), which equals a recovery of 78.7 ± 7.0 %.

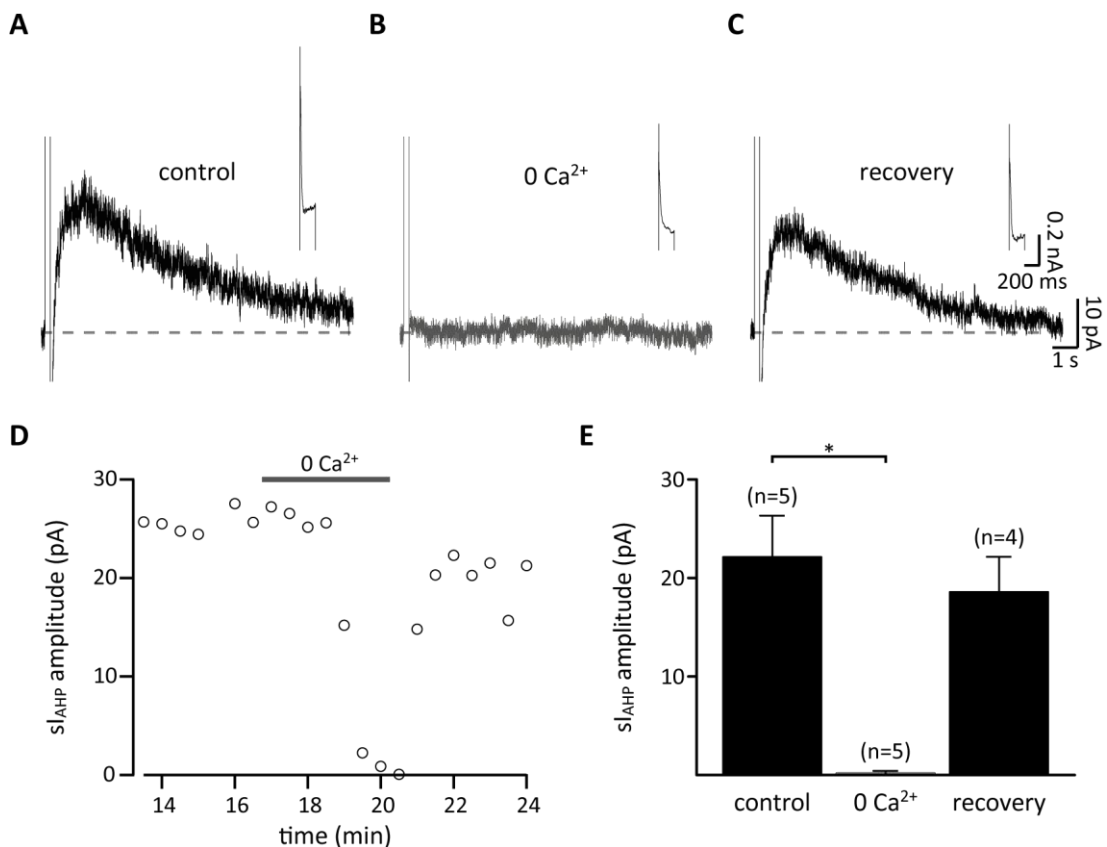


Figure 3.27 Removal of extracellular Ca^{2+} abolishes isolated sI_{AHP} . Representative current traces of sI_{AHP} recorded in an EGFP-negative neuron in the presence of (A) 2 mM Ca^{2+} in the extracellular solution (control) and (B) in its absence (0 Ca^{2+}). sI_{AHP} recovered once the Ca^{2+} level in the extracellular solution was restored to (C) 2 mM Ca^{2+} (recovery). Insets show the corresponding Ca^{2+} spike observed during the depolarisation step that preceded sI_{AHP} recordings. The dashed grey line indicates zero current (A–C). (D) Time course showing sI_{AHP} amplitude in response to the removal of extracellular Ca^{2+} and upon return to original conditions. (E) Bar diagram summarizing the effect of 0 Ca^{2+} on sI_{AHP} ($P=0.0062$, paired t-test). sI_{AHP} recovered to 78.7 ± 7.0 % once 2 mM Ca^{2+} was again present in the extracellular solution. Mean values \pm SEM are presented. * = $P<0.05$. All recordings were performed in the presence of 25 μ M D(-)-2-amino-5-phosphonopentanoic acid, 5 μ M 2,3-dioxo-6-nitro-1,2,3,4-tetrahydrobenzo(f)quinoxaline-7-sulfonamide, 0.5 μ M tetrodotoxin, 1 mM tetraethylammonium and 50 μ M d-Tubocurarine.

sI_{AHP} is suppressed by several neurotransmitters, by monoamines like noradrenaline, dopamine, histamine and serotonin via PKA dependent phosphorylation and also by acetylcholine and glutamate (Stocker et al., 2004). The identity of sI_{AHP} in cultured hippocampal neurons was therefore tested by application of the acetylcholine analogue CCh, which is not hydrolysed by acetylcholinesterase (Cole and Nicoll, 1984) and suppresses sI_{AHP} , and by application of the membrane permeable cAMP analogue 8CPT-cAMP, which activates PKA and inhibits sI_{AHP} (Pedarzani and Storm, 1993). Whole-cell voltage-clamp recordings of sI_{AHP} were performed as described (section 2.2.14.2 and 3.3.2.2) and the current was reversibly suppressed following the addition of 2.5 μ M CCh to the extracellular solution (Fig. 3.28A and C); the overlay of control and CCh traces show the extent of inhibition. In this recording the recovered sI_{AHP} was in one experiment subsequently inhibited to a similar extent by the application of 8CPT-cAMP (Fig. 3.28B and C), consistent with PKA modulation of the underlying conductance. Average sI_{AHP} amplitude before exposure to CCh amounted to 26.4 ± 2.3 pA ($n=9$, control) and was suppressed to 7.3 ± 2.1 pA ($n=9$, CCh; $P=0.0003$, paired t-test; Fig. 3.28D), which is a reduction of sI_{AHP} amplitude to 29.1 ± 8.2 % of the original. Wash out of CCh allowed sI_{AHP} amplitude to return to 18.1 ± 1.8 pA ($n=6$, recovery; Fig. 3.28D), corresponding to a recovery of 71.7 ± 11.3 %. Change of sI_{AHP} was also studied by examining the current charge transfer (Fig. 3.28E). sI_{AHP} charge transfer decreased from 113.5 ± 14.8 pC ($n=9$, control) to 28.6 ± 11.6 pC after CCh application ($n=9$, CCh; $P=0.001$, paired t-test; Fig. 3.28F). This reduction of sI_{AHP} charge transfer to 24.8 ± 9.7 % of the original by CCh was reversible and sI_{AHP} charge transfer recovered to 80.9 ± 13.5 pC ($n=6$, recovery; Fig. 3.28F), which equals a recovery of 86.1 ± 20.5 %. These results agreed with previous observations of sI_{AHP} suppression by CCh and 8CPT-cAMP in cultured hippocampal neurons (Gallasch, 2008) and with results obtained in hippocampal slices (Pedarzani and Storm, 1993).

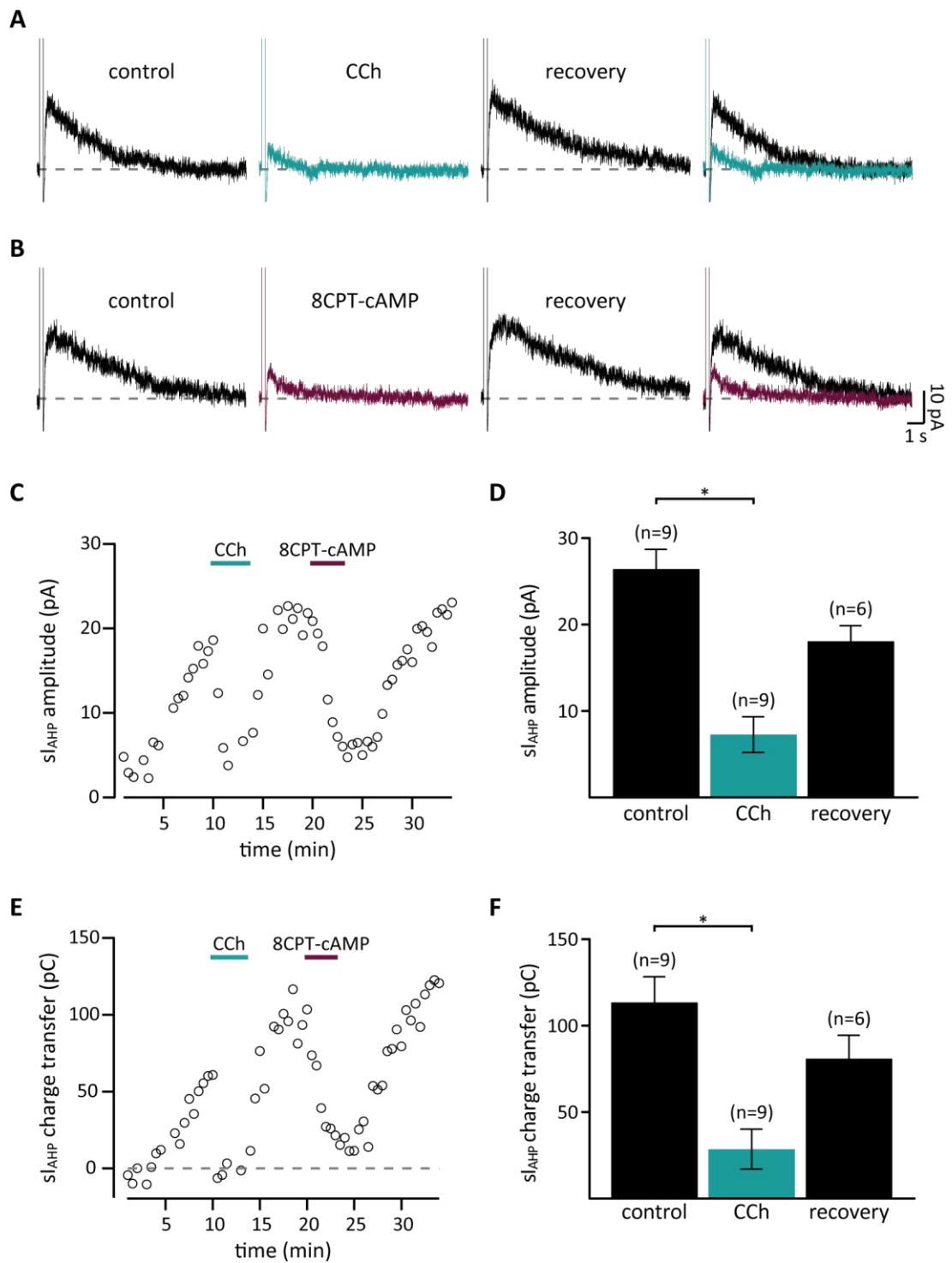


Figure 3.28 **sI_{AHP} is suppressed by CCh and 8CPT-cAMP.** Representative whole-cell voltage-clamp recordings of sI_{AHP} in an EGFP-negative neuron in the presence of 25 μ M D(-)-2-amino-5-phosphonopentanoic acid, 5 μ M 2,3-dioxo-6-nitro-1,2,3,4-tetrahydrobenzo(f)quinoxaline-7-sulfonamide, 0.5 μ M tetrodotoxin, 1 mM tetraethylammonium and 50 μ M d-Tubocurarine. sI_{AHP} was reversibly inhibited by the extracellular application of **(A)** the cholinergic agonist carbachol (CCh; 2.5 μ M) and **(B)** 8CPT-cAMP (100 μ M). The dashed grey line indicates zero current (A and B). **(C)** Example time course of sI_{AHP} amplitude in response to the application of CCh and (in this cell) 8CPT-cAMP. **(D)** Bar diagram summarising the effect of CCh on sI_{AHP} amplitude ($P=0.0003$, paired t-test). sI_{AHP} amplitude recovered to 71.7 ± 11.3 % of control. **(E)** Representative time course showing the effect of CCh and (in this cell) 8CPT-cAMP application on sI_{AHP} charge transfer. **(F)** Summary of the change of sI_{AHP} charge transfer upon CCh application ($P=0.001$, paired t-test). The effect of CCh was reversible and sI_{AHP} charge transfer recovered to 86.1 ± 20.5 % of control. * = $P<0.05$. Mean values \pm SEM are presented.

3.3.3 Effects of mutant RhoA virus infection on sI_{AHP} in cultured hippocampal pyramidal neurons

Examining the passive properties of EGFP-negative, RhoA-V14 and RhoA-N19 infected hippocampal neurons demonstrated that resting potential and input resistance of the cells were not affected by Sindbis virus infection. Furthermore, sI_{AHP} in cultured hippocampal neurons displayed the same properties as described in hippocampal slices (Alger and Nicoll, 1980; Hotson and Prince, 1980; Madison and Nicoll, 1982 and 1984; Lancaster and Adams, 1986; Pedarzani and Storm, 1993). Firstly sI_{AHP} was not affected by dTC, the application of which blocked I_{AHP} present in these cultures. Secondly, sI_{AHP} was Ca^{2+} dependent and thirdly, sI_{AHP} was suppressed by the application of CCh as well as by 8CPT-cAMP. Therefore cultures of hippocampal neurons present a system in which the effect of mutant RhoA infection on sI_{AHP} can be studied. In neurons infected with RhoA-N19 sI_{AHP} is expected to be present just as in EGFP-negative neurons, but might display a lower sensitivity to cholinergic agonists because RhoA-N19 is inactive and its expression might outcompete endogenous RhoA. Infection with constitutively active RhoA-V14 virus on the other hand should mimic the application of cholinergic agonist and thus neurons should show a suppressed sI_{AHP} .

3.3.3.1 sI_{AHP} in RhoA-N19 and RhoA-V14 infected cultured hippocampal neurons

Cultured hippocampal neurons were infected with recombinant Sindbis virus to express either the inactive RhoA-N19 or the constitutively active RhoA-V14 and whole-cell voltage-clamp recordings were performed as described. EGFP-negative pyramidal neurons from uninfected coverslips as well as from coverslips treated with Sindbis virus served as control. sI_{AHP} was observed in EGFP-negative neurons (Fig. 3.29A) as well as in neurons expressing RhoA-N19 (Fig. 3.29B), while sI_{AHP} in RhoA-V14 infected cells was reduced displaying only flat or small sI_{AHP} -shaped traces (Fig. 3.29C). Only once out of eight was a full-size sI_{AHP} detected in cells infected with RhoA-V14 (Fig. 3.29D and E, RhoA-V14). The amplitude of sI_{AHP} detected in EGFP-negative neurons ($n=13$) amounted to 27.1 ± 1.8 pA, in RhoA-N19 infected neurons ($n=9$) to 20.6 ± 1.6 pA and in RhoA-V14 infected neurons ($n=8$) to 6.2 ± 2.7 pA ($P<0.0001$, one-way ANOVA; Fig. 3.29D). The post-hoc Bonferroni's multiple comparison test determined that sI_{AHP} of EGFP-negative and RhoA-N19 infected cells did not differ, while sI_{AHP} of RhoA-V14 infected cells differed significantly from both EGFP-negative and RhoA-N19 infected cells. The same was observed when comparing sI_{AHP} charge transfer, which was 118.4 ± 10.8 pC in EGFP-negative neurons ($n=13$), 113.4 ± 10.9 pC in RhoA-N19 infected cells ($n=9$) and 39.8 ± 19 pC in RhoA-V14 infected cells ($n=8$) ($P=0.0006$, one-way ANOVA; Fig. 3.29E). Additionally, the time to peak of sI_{AHP} was analysed in EGFP-negative (0.7 ± 0.1 s, $n=13$) and RhoA-N19 infected (0.8 ± 0.1 s, $n=9$) neurons and did not differ significantly ($P=0.1932$, unpaired t-test).

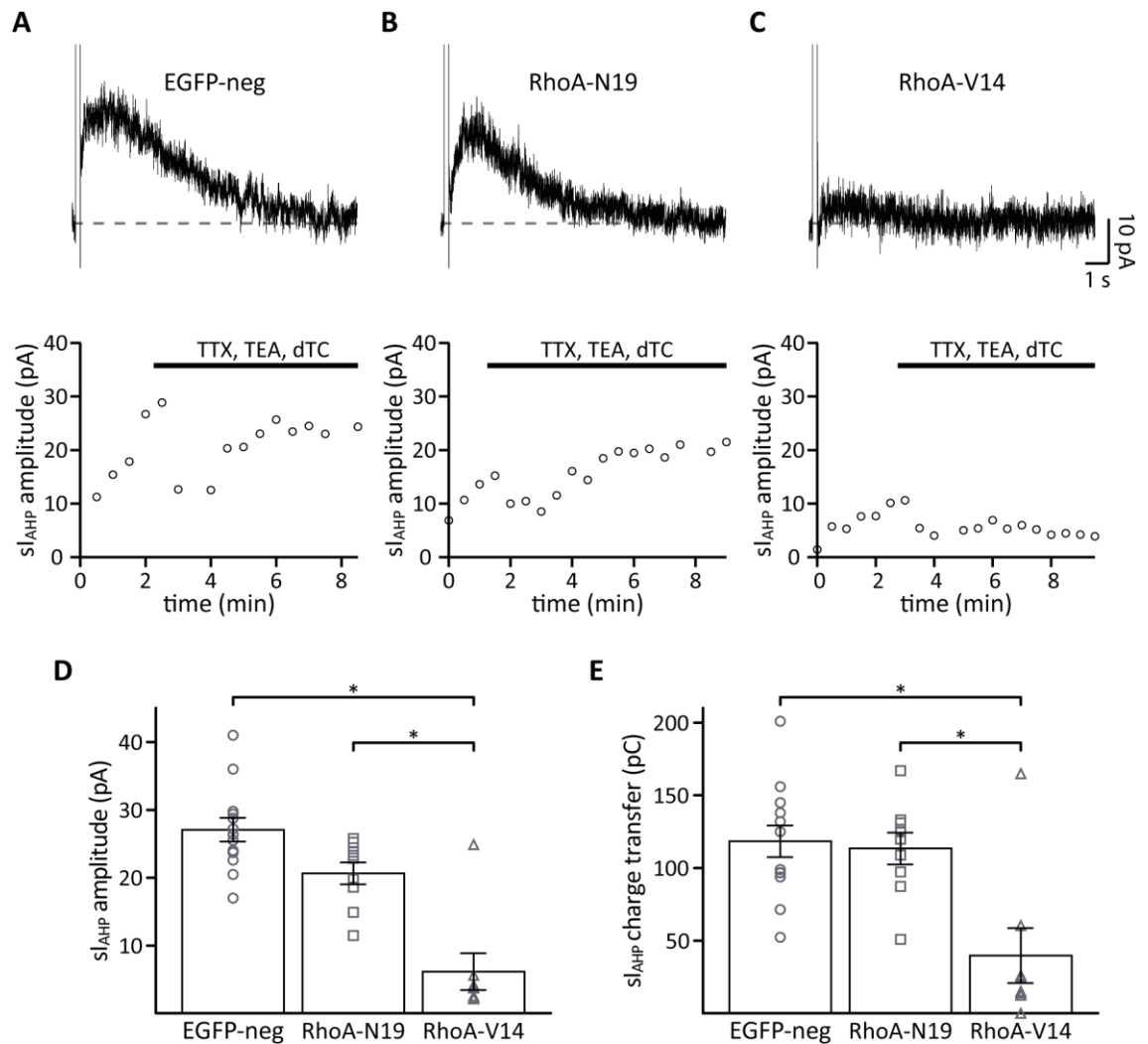


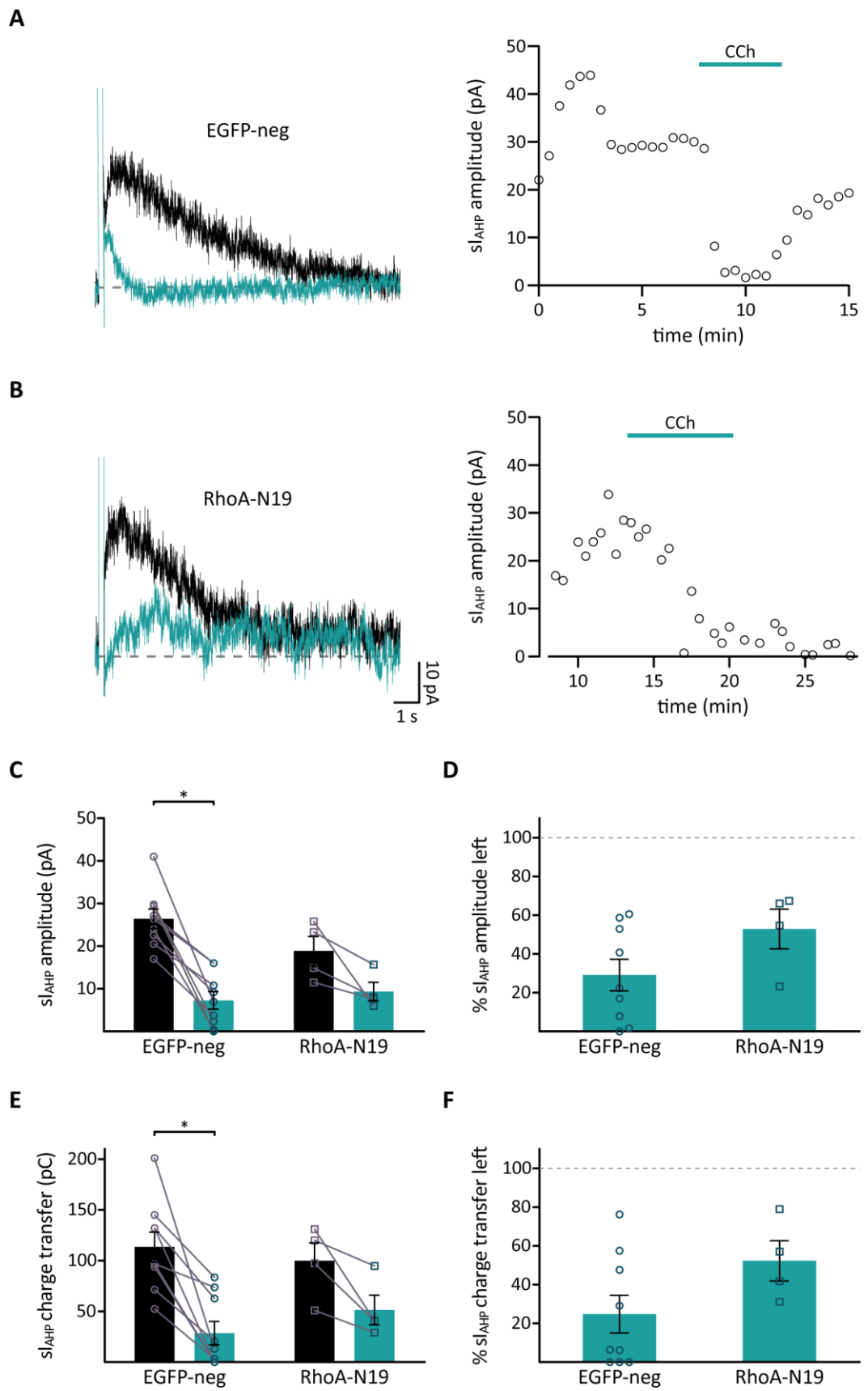
Figure 3.29 sI_{AHP} is present in EGFP-negative and RhoA-N19 infected cultured hippocampal pyramidal neurons, but not in RhoA-V14 infected neurons. Representative current traces and time courses of sI_{AHP} in EGFP-negative (A) and in RhoA-N19 (B) or RhoA-V14 (C) infected neurons. The dashed grey line indicates zero current (A–C). Bar diagrams summarizing (D) sI_{AHP} amplitude in EGFP-negative (27.1 ± 1.8 pA, $n=13$), RhoA-N19 (20.6 ± 1.6 pA, $n=9$) and RhoA-V14 (6.2 ± 2.7 pA, $n=8$) neurons ($P<0.0001$, one-way ANOVA) and (E) sI_{AHP} charge transfer in EGFP-negative (118.4 ± 10.8 pC, $n=13$), RhoA-N19 (113.4 ± 10.9 pC, $n=9$) and RhoA-V14 (39.8 ± 19 pC, $n=8$) infected cells ($P=0.0006$, one-way ANOVA). The post-hoc Bonferroni's multiple comparison tests showed that sI_{AHP} amplitude and charge transfer in RhoA-V14 infected neurons differed significantly from EGFP-negative and RhoA-N19 infected neurons, which themselves did not differ from each other. Amplitude and charge transfer measurements of sI_{AHP} were taken after the current had reached a stable baseline following the application of tetrodotoxin (TTX), tetraethylammonium (TEA) and d-Tubocurarine (dTC) (section 2.2.14.2). All recordings were performed in the presence of $25 \mu\text{M}$ D-(-)-2-amino-5-phosphonopentanoic acid, $5 \mu\text{M}$ 2,3-dioxo-6-nitro-1,2,3,4-tetrahydrobenzo(f)quinoxaline-7-sulfonamide, $0.5 \mu\text{M}$ TTX, 1 mM TEA and $50\text{--}100 \mu\text{M}$ dTC. * = $P<0.05$ and mean values \pm SEM are shown.

3.3.3.2 Cholinergic modulation of sI_{AHP} in EGFP-negative and inactive RhoA-N19 infected cultured hippocampal neurons.

Whole-cell voltage-clamp recordings of sI_{AHP} were performed as described and the cholinergic modulation of sI_{AHP} in EGFP-negative and inactive RhoA-N19 infected neurons was determined by adding $2.5 \mu\text{M}$ CCh to the extracellular solution. The overlay of control traces (black) and

traces under CCh application (blue) display the extent of sI_{AHP} suppression in EGFP-negative and RhoA-N19 infected neurons (Fig. 3.30A and B). In EGFP-negative neurons the effect of CCh on sI_{AHP} was seen to be reversible (Fig. 3.30A, time course; Fig. 3.28D), which was not observed in RhoA-N19 infected cells (Fig. 3.30B, time course). Changes in series resistance were monitored throughout the recordings and did not account for the differences observed in EGFP-negative and RhoA-N19 infected cells. sI_{AHP} amplitude in EGFP-negative cells amounted to 26.4 ± 2.3 pA (n=9, black bar) and was significantly suppressed by CCh to 7.3 ± 2.1 pA (n=9, blue bar; $P=0.0003$, paired t-test; Fig. 3.30C). In RhoA-N19 infected cells sI_{AHP} amplitude was 18.9 ± 3.4 pA (n=4, black bar), which was reduced to 9.4 ± 2.2 pA (n=4, blue bar) by CCh; a suppression that was not significantly different ($P=0.0735$, paired t-test; Fig. 3.30C). The evaluation of sI_{AHP} amplitude left under CCh application also showed a tendency of RhoA-N19 infected cells to be less affected by CCh (52.8 ± 10.3 % sI_{AHP} amplitude left) compared to EGFP-negative cells (29.1 ± 8.2 %), but no significant difference between the two groups was determined ($P=0.1207$, unpaired t-test; Fig. 3.30D). The same was observed when examining sI_{AHP} charge transfer in EGFP-negative and RhoA-N19 infected neurons. In EGFP-negative cells sI_{AHP} charge transfer was 113.5 ± 14.8 pC (n=9, black bar), which was reduced to 28.6 ± 11.6 pC following application of CCh (n=9, blue bar; $P=0.001$, paired t-test; Fig. 3.30E). sI_{AHP} charge transfer in RhoA-N19 infected cells amounted to 99.9 ± 17.7 pC (n=4, black bar) and was reduced by CCh to 51.4 ± 14.7 pC (n=4, blue bar; $P=0.0558$, paired t-test; Fig. 3.30E). Comparing the percentage of sI_{AHP} charge transfer left under CCh application in EGFP-negative, 24.8 ± 9.7 %, and in RhoA-N19 infected cells, 52.3 ± 10.4 %, did not result in a significant difference ($P=0.1197$, unpaired t-test; Fig. 3.30F).

Figure 3.30 **The effect of CCh application on sI_{AHP} in EGFP-negative and inactive RhoA-N19 infected cultured hippocampal pyramidal neurons.** Representative sI_{AHP} current traces and time course in an EGFP-negative (**A**) and a RhoA-N19 (**B**) infected neuron showing the effect of the cholinergic agonist carbachol (CCh; 2.5 μ M, blue) on sI_{AHP} amplitude. The dashed grey line indicates zero current (A and B). (**C**) Bar diagram summarizing sI_{AHP} amplitude in EGFP-negative and RhoA-N19 infected neurons before (black) and after (blue) the application of CCh. In EGFP-negative neurons CCh suppressed sI_{AHP} amplitude significantly ($P=0.0003$, paired t-test; $n=9$), while in RhoA-N19 infected neurons the effect of CCh on sI_{AHP} amplitude was less pronounced ($P=0.0735$, paired t-test; $n=4$). (**D**) Comparison of the percentage of sI_{AHP} amplitude left during CCh application in EGFP-negative and RhoA-N19 infected neurons ($P=0.1207$, unpaired t-test). (**E**) Summary of sI_{AHP} charge transfer in response to CCh application in EGFP-negative and RhoA-N19 infected cells. sI_{AHP} charge transfer was significantly reduced by CCh in EGFP-negative neurons ($P=0.001$, paired t-test; $n=9$), but not in RhoA-N19 infected cells ($P=0.0558$, paired t-test; $n=4$). (**F**) The percentage of sI_{AHP} charge transfer left during CCh application in EGFP-negative and RhoA-N19 infected cells was not significantly different ($P=0.1197$, unpaired t-test). Recordings were performed in the presence of 25 μ M D-(-)-2-amino-5-phosphonopentanoic acid, 5 μ M 2,3-dioxo-6-nitro-1,2,3,4-tetrahydrobenzo(f)quinoxaline-7-sulfonamide, 0.5 μ M tetrodotoxin, 1 mM tetraethylammonium and 50–100 μ M d-Tubocurarine. Mean values \pm SEM are shown and * = $P<0.05$.



3.3.4 Summary

Recombinant Sindbis viruses containing either the inactive RhoA-N19 or the constitutively active RhoA-V14 were used to infect cultured hippocampal neurons and the effect of mutant RhoA protein expression on sI_{AHP} was examined in order to assess the role of RhoA in the signalling pathway mediating the suppression of sI_{AHP} by cholinergic agonists. The functionality of the mutant RhoA proteins has been shown by their ability to regulate the cytoskeleton. Primary cultured hippocampal neurons presented a useful model system, because sI_{AHP} has been demonstrated to have the same properties than in slices. The results show that RhoA is involved in the signalling pathway mediating sI_{AHP} suppression by cholinergic agonists because sI_{AHP} was suppressed in RhoA-V14 infected neurons, but was present in neurons infected with RhoA-N19. Expression of RhoA-V14 thus mimicked the inhibitory effect of cholinergic agonists on sI_{AHP} . The modulation of sI_{AHP} by cholinergic agonists was thought to be diminished in neurons infected with RhoA-N19 and the results show that the suppression of sI_{AHP} by CCh in RhoA-N19 infected neurons was less pronounced, but overall did not differ significantly from EGFP-negative neurons.

4 Discussion

The work presented in this thesis focuses on the signal transduction pathway underlying the regulation of the Ca^{2+} -dependent sI_{AHP} by ACh. Cholinergic agonists suppress sI_{AHP} and enhance the neuronal excitability of hippocampal pyramidal neurons. This regulation of network activity of the hippocampal formation plays a crucial role in learning and memory processes. The main finding of the present study identifies the small GTPase RhoA as a component of this signal transduction pathway and shows that RhoA acts as a binding partner of the G_{q} -protein α subunit ($G\alpha_{\text{q}}$), through which cholinergic agonists have been shown to mediate their inhibitory action on sI_{AHP} (Krause et al., 2002). This reveals a novel pathway for the regulation of sI_{AHP} by neurotransmitters like ACh and glutamate acting on GPCRs coupled to the heterotrimeric G_{q} -protein and an involvement of RhoA in the regulation of membrane excitability of hippocampal neurons presents a novel function. ACh and glutamate suppress sI_{AHP} in hippocampal pyramidal neurons (Cole and Nicoll, 1983; Madison et al., 1987; Charpak et al., 1990), but the details of their signal transduction pathways had not been well identified.

In contrast, the signalling cascade used by monoamine neurotransmitters is better characterised: monoamine neurotransmitters inhibit sI_{AHP} by acting on GPCRs coupled to $G_{\alpha\text{s}}$, which stimulates AC and subsequently results in the production of cAMP and the activation of PKA (Fig. 4.1; Madison and Nicoll, 1986b; Pedarzani and Storm, 1993 and 1995; Torres et al., 1995). This has led to the hypothesis that sI_{AHP} is suppressed through a phosphorylation step, whose ultimate target remains to be identified and could involve intermediate proteins or occur directly at the channel responsible for sI_{AHP} . PIP_2 is involved in the activation of several K^+ channels including K_{ir} and $\text{K}_{\text{v}7}$ channels (Suh and Hille, 2005) and the regulation of sI_{AHP} by PIP_2 has been proposed by one study (Villalobos et al., 2011). PIP_2 synthesis is catalysed by $\text{PIP}5\text{K}$, which itself is prone to phosphorylation by PKA (Park et al., 2001). Hence, the inhibition of sI_{AHP} by monoamine transmitters could be mediated by the inhibition of $\text{PIP}5\text{K}$ by PKA and the subsequent reduction of PIP_2 levels (Fig. 4.1; Andrade et al., 2012).

The suppression of sI_{AHP} by cholinergic and glutamatergic agonists, however, does not involve the described signalling pathway via PKA (Fig. 4.1; Gerber et al., 1992; Pedarzani and Storm, 1993; Blitzler et al., 1994; Pedarzani and Storm, 1996). In contrast, ACh and glutamate regulate sI_{AHP} by activating GPCRs coupled to G-proteins of the G_{q} family (Dutar and Nicoll, 1988; Gerber et al., 1992; Offermanns et al., 1994; Blin et al., 1995; Pin and Duvoisin, 1995; Abdul-Ghani et al., 1996) and studies in knock-out mice have shown that the signalling pathway involves the G-protein α subunit $G\alpha_{\text{q}}$, but not $G\alpha_{11}$ (Fig. 4.1; Krause et al., 2002). However, the suppression of sI_{AHP} by ACh and glutamate is not mediated by the classical pathway of GPCRs coupled to G_{q} -proteins (Fig. 4.1), because neither $\text{PLC}\beta$ (Krause and Pedarzani, 2000; Young et al., 2004), PKC (Gerber et al., 1992; Sim et al., 1992; Engisch et al., 1996) nor IP_3 -sensitive stores (Krause and

Pedarzani, 2000) are involved. The inhibition of CamKII partially reduces the suppression of sI_{AHP} by cholinergic agonists, but how CamKII is activated by mAChRs, in the absence of an involvement of IP_3 , is not established (Müller et al., 1992; Pedarzani and Storm, 1996).

The work presented in this thesis has investigated a novel signalling pathway downstream of $G\alpha_q$ leading to the suppression of sI_{AHP} by ACh and glutamate and the proposed signalling cascade is depicted schematically in Figure 4.1 (highlighted in blue). In order to determine the role of RhoA in the signalling pathway suppressing sI_{AHP} , this study employed RhoA mutants, either constitutively active RhoA-V14 or inactive RhoA-N19. RhoA mutants were introduced into hippocampal pyramidal neurons either by the intracellular application of purified proteins or by Sindbis virus infection. Whole-cell patch clamp recordings have shown that sI_{AHP} is significantly reduced in neurons expressing constitutively active RhoA-V14, hence mimicking the inhibitory effect of ACh and glutamate, while sI_{AHP} is not affected in neurons expressing inactive RhoA-N19. Furthermore, it was investigated whether RhoA and $G\alpha_q$ could act in a common signalling pathway leading to the suppression of sI_{AHP} in hippocampal neurons. The potential protein-protein interaction of $G\alpha_q$ and RhoA was examined by employing various molecular biology and imaging techniques in heterologous expression system and the work presented in this study has established RhoA as a signalling partner of $G\alpha_q$. The proposed signal transduction pathway is initiated by ACh or glutamate acting on GPCRs coupled to $G\alpha_q$, which would activate RhoA and subsequently lead to the suppression of sI_{AHP} (Fig. 4.1).

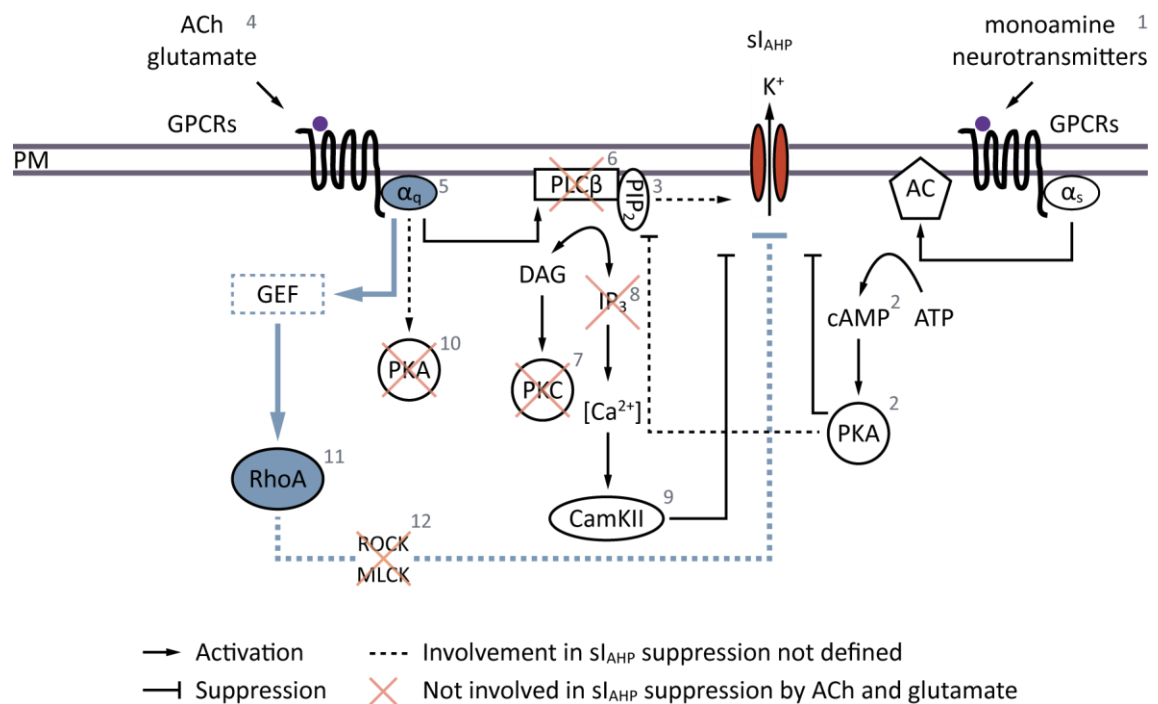


Figure 4.1 **Signal transduction pathways mediating the suppression of sI_{AHP} .** Schematic depiction of established and proposed signal transduction pathways used by various neurotransmitters to suppress sI_{AHP} . The pathway highlighted in blue was the focus of this study. Numbers correspond to a reference list that can be found in Table 4.1.

1	Monoamine NTs	sI_{AHP} suppression	Benardo and Prince, 1982; Pedarzani and Storm, 1995 (dopamine) Haas and Konnerth, 1983; Pedarzani and Storm, 1993 (histamine) Madison and Nicoll, 1982; Haas and Konnerth, 1983; Lancaster and Adams, 1986; Madison and Nicoll, 1986a; Pedarzani and Storm, 1993; Blitzer et al, 1994 (noradrenaline) Andrade and Nicoll, 1987; Colino and Halliwell, 1987; Pedarzani and Storm, 1993; Torres et al, 1995 (serotonin)
2	cAMP and PKA	Monoamine NTs activate GPCRs coupled to $G\alpha_s$ leading to the activation of AC, cAMP production and activation of PKA	Madison and Nicoll, 1986b; Pedarzani and Storm, 1993; Blitzer et al, 1994; Pedarzani and Storm, 1995; Torres et al, 1995
3	PIP ₂	Involved in the activation of several K ⁺ channels. Suggested to enhance Ca ²⁺ sensitivity of sI_{AHP} . PIP5K catalyses the production of PIP ₂ and is inhibited by PKA	Park et al, 2001; Villalobos et al, 2011; Andrade et al, 2012
4	ACh and glutamate	sI_{AHP} suppression	Cole and Nicoll, 1983; Madison et al, 1987 (ACh) Chrapak et al, 1990 (glutamate)
5	$G\alpha_q$	Involvement in sI_{AHP} suppression by ACh and glutamate	Krause et al, 2002
6	PLC β	No involvement in sI_{AHP} suppression by ACh and glutamate	Krause and Pedarzani, 2000; Young et al, 2004
7	PKC	No involvement in sI_{AHP} suppression by ACh and glutamate	Gerber et al, 1992; Sim et al, 1992; Engisch et al, 1996
8	IP ₃	No involvement of IP ₃ -sensitive stores in sI_{AHP} suppression by ACh and glutamate	Krause and Pedarzani, 2000
9	CamKII	sI_{AHP} suppression by ACh (but not by glutamate) is reduced when CamKII is inhibited	Müller et al, 1992; Pedarzani and Storm, 1996
10	PKA	No involvement in sI_{AHP} suppression by ACh and glutamate	Gerber et al, 1992; Pedarzani and Storm, 1993; Blitzer et al, 1994; Pedarzani and Storm, 1996
11	RhoA	Involvement in sI_{AHP} suppression by ACh and glutamate	P. Pedarzani, personal communication; findings of this study
12	ROCK and MLCK	No involvement of ROCK and MLCK in sI_{AHP} suppression by ACh and glutamate	P. Pedarzani, personal communication

Table 4.1 Reference list for the signal transduction pathway diagram (Fig. 4.1.).

4.1 The small GTPase RhoA associates with the heterotrimeric G-protein α subunit $G\alpha_q$

The small GTPase RhoA is best known for its regulation of the actin cytoskeleton and is responsible for the formation of focal adhesion and stress fibres as well as for cell rounding. External stimuli, like the application of lysophosphatidic acid, that activate RhoA affect the cytoskeleton and cause the formation of stress fibres (Paterson et al., 1990; Ridley and Hall, 1992; Naumanen et al., 2008). RhoA contributes to the regulation of the actin cytoskeleton by signalling to mDia, which promotes actin filament polymerization through its interaction with the actin-binding protein profilin (Watanabe et al., 1997). RhoA signalling via ROCK and myosin light chain kinase (MLCK) is responsible for the formation of stress fibres (Kimura et al., 1996; Ridley, 1996 and 1999; Totsukawa et al., 2000; Katoh et al., 2001). Different upstream regulators of RhoA, such as neurotransmitters activating GPCRs coupled to G-proteins of the G_{12} family (Buhl et al., 1995; Fromm et al., 1997; Hart et al., 1998; Fukuhara et al., 1999 and 2000) and the G_q family (Mitchell et al., 1998; Sagi et al., 2001; Booden et al., 2002; Chikumi et al., 2002; Dutt et al., 2002; Lutz et al., 2005), have been identified. Furthermore, targets of small GTPases include ion channels (Pochynyuk et al., 2007) and RhoA is able to modulate ion channel function, for example, inactivating inwardly rectifying K^+ channels (K_{ir2} ; Jones, 2003; Rossignol and Jones, 2006), inhibiting voltage-gated K^+ channels ($K_v1.2$; Cachero et al., 1998; Stirling et al., 2009; ERG ($K_v11.1$); Storey et al., 2002) or stimulating epithelial Na^+ channels (ENaC; Staruschenko et al., 2004) and voltage-gated Ca^{2+} channels (Ca_v1 ; Yatani et al., 2005). The signal transduction pathway mediating the suppression of sl_{AHP} by ACh and glutamate has been shown to include $G\alpha_q$, but not its classical signalling pathway via $PLC\beta$, and the small GTPases RhoA is proposed to be part of this signalling cascade (Fig. 4.1).

The work presented in this thesis investigates the ability of RhoA to interact with $G\alpha_q$ using different molecular biology and imaging techniques. Co-immunoprecipitation experiments in heterologous expression system show that $G\alpha_q$ associates with RhoA (Fig. 3.1), but not with other small GTPases (Fig. 3.2). The interaction of $G\alpha_q$ and RhoA is detected in HEK293 cells expressing unmutated $G\alpha_q$ or constitutively active $G\alpha_q$ -L209, but is prevented in cells expressing the inactive $G\alpha_q$ -L209/N277 mutant, which is unable to bind GTP and thus hindered from binding to downstream effectors (Fig. 3.1). Moreover, unmutated and constitutively active $G\alpha_q$ are able to interact with both constitutively active RhoA-V14 as well as inactive RhoA-N19 (Fig. 3.1B). This is due to the fact that the inactivating mutation leaves RhoA in a nucleotide-free state unable to interact with downstream targets, but not interfering with its binding capability to upstream regulators. The interaction between $G\alpha_q$ and RhoA was not

hindered by the attachment fluorophores to the proteins (Fig. 3.8) and ECFP-tagged $G\alpha_q$ and Venus-tagged RhoA were subsequently used in imaging experiments.

$G\alpha_q$ and RhoA association seems to be independent of $G\alpha_q$ activation, since both unmutated $G\alpha_q$ and constitutively active $G\alpha_q$ -L209 were able to interact with unmutated, constitutively active as well as inactive RhoA. Both $G\alpha_q$ variants had previously been investigated by testing their ability to activate $PLC\beta$ and measuring the subsequent IP_3 formation, and cells transfected with constitutively active $G\alpha_q$ produced higher levels of IP_3 than cells transfected with unmutated $G\alpha_q$ (Wu et al., 1992; Qian et al., 1993). An activation-independent interaction of $G\alpha_q$ and RhoA (Fig. 4.2A) would imply that $G\alpha_q$ sequesters RhoA and that both proteins are constitutively associated with each other. This would mean that the structural conformation of their binding site stays unchanged in the inactive, GDP-bound as well as in the active, GTP-bound state and that $G\alpha_q$ and RhoA complex formation is also possible in the presence of the $G\beta\gamma$ dimer. Moreover, the inability of the inactive, xanthine-bound $G\alpha_q$ to bind RhoA then has to be attributed to its different structural composition and not to its inactive state. However, the classical binding sites of $G\alpha$ subunits as well as RhoA span their switch regions (Vetter and Wittinghofer, 2001) and are thought to be inaccessible in the inactive state, primarily because of the protein's structural conformation and in the case of $G\alpha$ also because of $G\beta\gamma$ binding, which speaks for an activity-dependent interaction (Fig. 4.2C). In order to align an activity-dependent association of $G\alpha_q$ and RhoA (Fig. 4.2C) with the results obtained in the co-immunoprecipitation experiments, the activation of the unmutated $G\alpha_q$ in the cells would have been required. In either case, the co-immunoprecipitation experiments presented in this thesis have established the protein-protein interaction of $G\alpha_q$ and RhoA. In general, successful co-immunoprecipitations in heterologous expression system are regarded as a direct interaction between the expressed proteins. However, the detected association could also be mediated by an endogenously expressed protein that forms part of a multi-protein complex for example a RhoGEFs (Fig. 4.2B and C; Fig. 4.3).

The presented models of $G\alpha_q$ and RhoA interaction (Fig. 4.2) summarize the results of this thesis as well as findings described in the literature. Experiments performed in this thesis identified an interaction between $G\alpha_q$ and RhoA in the unmutated as well as in the constitutively active state, which suggests an activity-independent interaction (Fig. 4.2A and B). However, the literature describes an activation-dependent interaction between $G\alpha$ and small GTPases (Fig. 4.2C), in which the activation of $G\alpha$ leads to the interactions with RhoGEFs, which then serve as activators for small GTPases (Hart et al., 1998; Kozasa et al., 1998; Fukuhara et al., 1999 and 2000; Booden et al., 2002; Lutz et al., 2005). The binding sites of $G\alpha$ subunits as well as small GTPases are thought to only become accessible in the active state and

crystallography has revealed a protein complex $G\alpha_q$ -p63RhoGEF-RhoA (Fig. 4.3) suggesting that the simultaneous binding of $G\alpha_q$ to the $G\beta\gamma$ dimer and to a RhoGEF is not possible (Lutz et al, 2007).

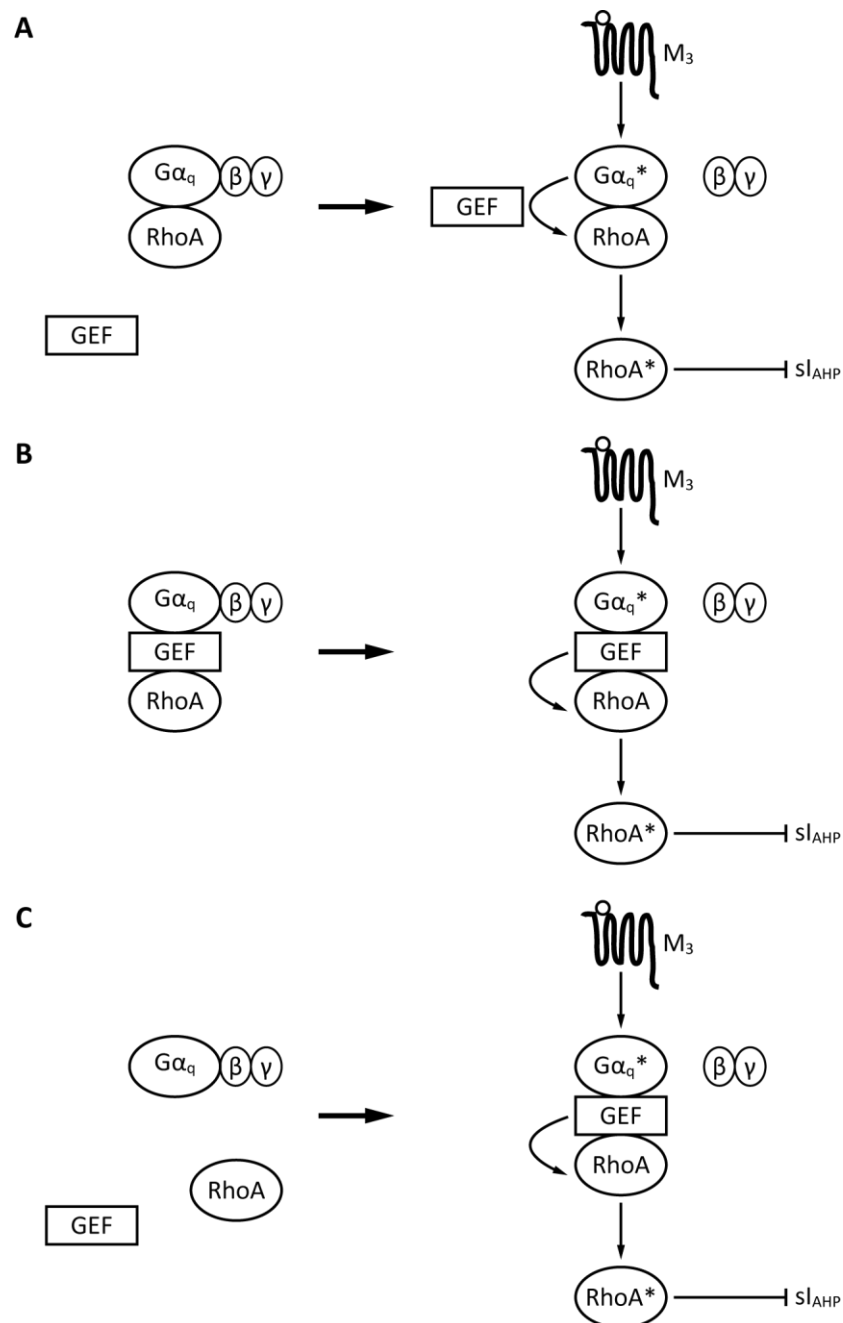


Figure 4.2 Potential models of $G\alpha_q$ and RhoA interaction. (A) In this study $G\alpha_q$ has been shown to associate with RhoA in both its unmutated as well as constitutively active form suggesting an activity-independent interaction. How this can be consolidated with $G\alpha$ being bound to the $G\beta\gamma$ dimer in the inactive state needs to be determined. (B) Whether it is possible for a RhoGEF to be a constitutive part of this protein complex has to be investigated. Information gained from the crystal structure of $G\alpha_q$ -p63RhoGEF-RhoA suggests that the simultaneous binding of $G\alpha_q$ to the $G\beta\gamma$ dimer and to a RhoGEF is not possible (Lutz et al, 2007). (C) Activation-dependent model of $G\alpha_q$ and RhoA interaction based on the literature on the activation of small GTPases (Hart et al., 1998; Kozasa et al., 1998; Fukuhara et al., 1999 and 2000; Booden et al., 2002; Lutz et al., 2005). * indicates active proteins

FRET experiments were performed to investigate the association of $G\alpha_q$ and RhoA by other means and also had the advantage that the direct interaction of proteins can be established, since FRET only takes place when donor and acceptor fluorophores are within 10 nm (100 Å) of each other i.e. over distances the size of proteins (Vogel et al., 2006). FRET efficiency depends on the distance between fluorophores and increases the closer the proximity of the two fluorophores, and FRET only occurs when the fluorophores are not oriented perpendicular to each other (Vogel et al., 2006). FRET has been used to determine $G\alpha_q$ and RhoA functions in other studies, for example, a FRET sensor (RhoA-YFP-linker-CFP-Rho binding domain) was used to investigate RhoA activity during cell migration (Pertz et al., 2006). The interaction of $G\alpha_q$ with downstream targets PLC β (Dowal et al., 2006) and PI3K (Golebiewska and Scarlata, 2008) was also investigated using FRET. The FRET results between $G\alpha_q$ and RhoA obtained in this thesis indicate an interaction of the two proteins and substantiate the findings of co-immunoprecipitation and co-localisation experiments. FRET depends on the distance between two proteins, so the detection of intermediate FRET efficiency values for the ECFP-tagged $G\alpha_q$ and Venus-tagged RhoA ($E = 4\text{--}10\%$; Fig. 3.11 and 3.12) compared to $E = 21\%$ for the positive FRET control CFP-YFP (Fig. 3.10) could imply that the distance between the two fluorophores is only just in the detectable range. FRET would be reduced if the fluorophores happen to be located on opposite ends of the $G\alpha_q$ -RhoA-complex and unable to come into the close proximity necessary for the detection of high FRET efficiency values or if an intermediate protein such as RhoGEFs (Fig. 4.3) causes $G\alpha_q$ and RhoA to be further apart from each other within the protein complex. Furthermore, FRET would also be reduced if the fluorophores were not properly orientated to each other, something that can only be influenced by inserting ECFP and Venus at different sites of the proteins. By performing FRET experiments with ECFP-tagged $G\alpha_q$ that was either carboxyl-terminal or loop-tagged different labelling strategies were tested that could have affected the orientation of the donor and acceptor fluorophores to each other and thus impacted on the FRET signal. However, the results show that the detected FRET signal was not influenced by the different ECFP-tag positions.

This study employed the FRET method of acceptor photobleaching, which measures an increase in donor fluorescence upon the destruction of the acceptor fluorophore if FRET had been occurring. Acceptor photobleaching avoids the disadvantage of sensitized emission, another widely used FRET method. In sensitized emission cross-talk between the two fluorophores is caused by the excitation of the donor fluorophore in order to measure the energy transfer to the acceptor fluorophore and needs to be controlled extensively (Vogel et al., 2006; Piston and Kremers, 2007). Acceptor photobleaching allows for the direct measurement of FRET without needing to remove any cross-talk components necessary when

using sensitized emission to measure FRET. This is also true for FLIM-FRET, which monitors the lifetime of the donor fluorescence in the absence and presence of a donor and which will become shorter when FRET is taking place (Vogel et al., 2006; Piston and Kremers, 2007). Thus FLIM-FRET also prevents the problem of cross-talk and avoids any potential damage to the donor fluorophore that could arise with the acceptor photobleaching method, but specialized equipment to measure the changes in fluorescence lifetime on a nanosecond timescale is needed to perform FLIM (Vogel et al., 2006; Piston and Kremers, 2007). In this study, the FRET measurements performed between ECFP-tagged $G\alpha_q$ and Venus-RhoA have repeatedly resulted in negative FRET efficiency values, an observation that has also been described by others using the method of acceptor photobleaching (Karpova et al., 2003). Negative FRET efficiency values can be caused by the bleaching of the donor ECFP-tagged $G\alpha_q$ itself during image acquisition or by cross-excitation, even though unlikely (section 3.1.7), and damage of ECFP by the 514 nm laser line that was used to excite and bleach the acceptor Venus-RhoA. Negative as well as positive FRET measurements were obtained under the same experimental conditions and on the same day and what exactly caused the bleaching of CFP in this study could not be determined. In addition, the detected FRET efficiency values for any of the investigated ECFP- $G\alpha_q$ variants and Venus-RhoA combinations were rather variable in their strength. In the light of these observations and different advantages and disadvantages of the various FRET methods, repeating the investigation using a different FRET method like FLIM-FRET could enhance our understanding of the nature of the interaction between $G\alpha_q$ and RhoA.

The interaction of $G\alpha_q$ and RhoA with their signalling partners takes place at the plasma membrane to which both proteins are bound through lipid modifications and in the case of $G\alpha_q$ also through its association with the $G\beta\gamma$ dimer (Seabra, 1998; Chen and Manning, 2001; Hughes et al., 2001). In the heterologous expression system used in this study only loop-tagged $G\alpha_q$ -ECFP- $G\alpha_q$ was localised at the plasma membrane of HEK293 cells, while carboxyl-terminally tagged $G\alpha_q$ -ECFP and both constitutively active, looped-tagged $G\alpha_q$ -ECFP- $G\alpha_q$ -C183 or L209 were expressed throughout the cytoplasm (Fig. 3.5). The cytosolic localisation of carboxyl-terminal tagged $G\alpha_q$ has been reported before (Witherow et al., 2003) and loop-tagged $G\alpha_q$ have been developed (Hughes et al., 2001; Witherow et al., 2003) to avoid interference with the functionally important amino- and carboxyl-termini (Conklin and Bourne, 1993; Hepler et al., 1996). On the other hand, Venus-tagged RhoA was localised throughout the cytoplasm (Fig. 3.5), which is in line with previous reports (Adamson et al., 1992b; Michaelson et al., 2001) and with the fact that GDIs sequester inactive Rho-GTPases in the cytoplasm (Boguski and McCormick, 1993). Activated RhoA, upon the separation from GDIs

and the exchange of GDP for GTP, has been described to translocate from the cytoplasm to the plasma membrane (Bokoch et al., 1994; Keller et al., 1997; Kranenburg et al., 1997). The predominantly cytosolic expression of Venus-tagged RhoA and several ECFP-tagged $G\alpha_q$ variants observed in this study made it impossible to differentiate any potential plasma membrane signal. However, a degree of plasma membrane localisation of constitutively active, looped-tagged $G\alpha_q$ -ECFP- $G\alpha_q$ -C183 was revealed when soluble proteins were extracted by Triton X-100 treatment (Hughes et al., 2001). On the other hand, the R183C but not the Q209L mutation has been reported to decrease the ability of $G\alpha_q$ to interact with the $G\beta\gamma$ dimer and would therefore interfere with its membrane targeting (Hughes et al., 2001; Evanko et al., 2005), which could be part of the reason for the observed difference in localisation of the constitutively active, loop-tagged $G\alpha_q$ -ECFP- $G\alpha_q$ -C183 compared to loop-tagged $G\alpha_q$ -ECFP- $G\alpha_q$. That targeting of $G\alpha_q$ to the plasma membrane requires its association with the $G\beta\gamma$ dimer and following GTP binding the switch regions of $G\alpha$ undergo a conformational change that causes dissociation from the $G\beta\gamma$ dimer has been described (section 1.3). Constitutively active $G\alpha_q$ mutants cannot hydrolyse GTP and thus the bound GTP could hinder the association of $G\alpha_q$ with the $G\beta\gamma$ dimer and therefore plasma membrane localisation. Furthermore, the level of endogenous $G\beta\gamma$ might have not been sufficient to aid plasma membrane localisation of the exogenously expressed $G\alpha_q$ variants. But the fact that unmutated $G\alpha_q$ -ECFP- $G\alpha_q$ was able to localise at the plasma membrane (Fig. 3.12) do not support this explanation. Plasma membrane association of $G\alpha_q$ -ECFP- $G\alpha_q$ was also not affected following its activation by the co-expressed mAChR M_3 , which had been activated by the cholinergic agonist CCh (Fig. 3.12). Nevertheless, over-expression of the fusion proteins might influence their localisation as the association of $G\alpha$ proteins with the plasma membrane has been reported to be more easily observed in cells expressing lower amounts of protein (Witherow et al., 2003). On the other hand, the predominantly cytosolic expression of RhoA was preserved in cells stably expressing RhoA at much lower levels than could be achieved with a transient transfection (Michaelson et al., 2001). FRET was measured for all Venus-RhoA and ECFP-tagged $G\alpha_q$ combinations in their respective locations: at the plasma membrane for $G\alpha_q$ -ECFP- $G\alpha_q$ and in the cytoplasm for all other ECFP-tagged $G\alpha_q$ variants. Overall, similar FRET efficiency values were obtained for all of the different ECFP-tagged $G\alpha_q$ variants in combination with Venus-RhoA.

FRET experiments were performed using constitutively active $G\alpha_q$ mutants as well as unmutated $G\alpha_q$, which was either used on its own or in combination with the mAChR M_3 . Since co-immunoprecipitation experiments have shown that $G\alpha_q$ and RhoA interact regardless of whether unmutated or constitutively active proteins were co-expressed, only unmutated RhoA was used in FRET experiments in order to avoid major changes to the actin cytoskeleton by

constitutively active RhoA (Ridley and Hall, 1992; Kranenburg et al., 1997). The expression of unmutated $G\alpha_q$ -ECFP- $G\alpha_q$ and M_3 , which was activated by CCh, in combination with Venus-RhoA did not affect the FRET efficiency values compared to the ones obtained with unmutated $G\alpha_q$ -ECFP- $G\alpha_q$ alone (Fig. 3.12) or with constitutively active ECFP-tagged $G\alpha_q$ variants (Fig. 3.11). This is in agreement with the results obtained from co-immunoprecipitation experiments and indicates that the interaction of $G\alpha_q$ and RhoA is activity-independent (Fig. 4.2A). On the other hand, an activity-dependent interaction of $G\alpha_q$ and RhoA (Fig. 4.2C) would imply that, in the experiments presented in this thesis, unmutated $G\alpha_q$ had been activated in the cell. In this case, the comparable FRET efficiency values, obtained from unmutated $G\alpha_q$, constitutively active $G\alpha_q$ mutants and receptor-activated $G\alpha_q$, would imply that unmutated $G\alpha_q$ was indeed in an active, GTP-bound state during the FRET experiments. In either case, the interaction of $G\alpha_q$ and RhoA that was identified by co-immunoprecipitation was substantiated in the FRET experiments and thus, by definition, indicating their direct interaction. However, since the FRET efficiency values obtained in this study were of intermediate strength, it might be advisable to characterise the interaction of $G\alpha_q$ and RhoA using another FRET method like FLIM as described above or investigate the possibility of an indirect interaction that is mediated by an intermediate protein present in the $G\alpha_q$ -RhoA complex for example a RhoGEF (Fig. 4.2B and C; Fig. 4.3).

The data presented in this thesis identify $G\alpha_q$ and RhoA as interaction partners in heterologous expression systems and indicates that the two proteins could also be part of a common signalling pathway mediating the suppression of sl_{AHP} by ACh and glutamate in hippocampus. RhoA has been established to act as a downstream effector of GPCRs (Seasholtz et al., 1999; Sah et al., 2000) and notably of GPCRs coupled to the heterotrimeric G_q -protein (Mitchell et al., 1998; Sagi et al., 2001; Booden et al., 2002; Chikumi et al., 2002; Dutt et al., 2002; Lutz et al., 2005). Using cell lines, these studies have shown that the activation of GPCRs coupled to G-proteins of the G_q family, or the expression of constitutively active $G\alpha_q$ mutants, enhances GTP-bound RhoA levels as well as serum response factor-dependent gene transcription and induces changes in the actin cytoskeleton as identified by the formation of stress fibres. Furthermore, crystallography has revealed a protein complex that includes $G\alpha_q$ and RhoA as well as a GEF p63RhoGEF (Fig. 4.3; Lutz et al., 2007) and the direct activation of p63RhoGEF by $G\alpha_q$ has also been determined (Shankaranarayanan et al., 2010). Other RhoGEFs have also been shown to be targets of $G\alpha_q$, including Lbc (Sagi et al., 2001) and LARG (Booden et al., 2002).

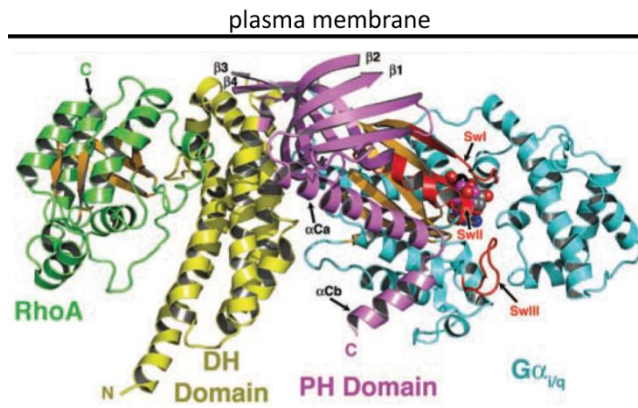


Figure 4.3 Crystal structure of the $G\alpha_q$ -p63RhoGEF-RhoA protein complex. $G\alpha_q$ (blue) was shown to form contacts with p63RhoGEF at its pleckstrin homology (purple) and Dbl homology (yellow) domains, but not with RhoA (green). (from Lutz et al., 2007)

RhoGEFs of the Dbl family are characterised by a Dbl homology (DH) domain, which catalyses GDP to GTP nucleotide exchange of Rho-GTPases, and a pleckstrin homology (PH) domain that is responsible for the correct positioning of the DH domain, for plasma membrane targeting and for the interaction with the $G\alpha$ subunit (Fig. 4.3; Zheng, 2001; Hoffman and Cerione, 2002; Rossman et al., 2005; Aittaleb et al., 2010). $G\alpha_q$ interacts primarily with the PH domain of RhoGEFs of the Dbl family (Fig. 4.3; Lutz et al., 2007; Rojas et al., 2007). The $G\alpha_q$ binding sites for p63RhoGEF and PLC β are almost identical (Waldo et al., 2010) and over-expression of p63RhoGEF reduces PLC β activation (Bodmann et al., 2014), which could explain how sl_{AHP} suppression can be mediated by a signalling pathway comprising p63RhoGEF and RhoA, but be independent of PLC β activation. GEFs like p63RhoGEF are endogenously expressed in HEK293 cells (Lutz et al., 2005) and could have acted as intermediate binding partners of the $G\alpha_q$ -RhoA complex in the co-immunoprecipitation described in this thesis. According to the crystal structure (Fig. 4.3; Lutz et al., 2007) p63RhoGEF links $G\alpha_q$ and RhoA and no contacts are formed between $G\alpha_q$ and RhoA. The presence of p63RhoGEF in the protein complex would increase the distance between the two proteins and might consequently account for the intermediate FRET efficiency values obtained in the FRET experiments. The possibility of RhoGEFs acting as intermediate proteins between $G\alpha_q$ and RhoA can neither be confirmed nor excluded by the experiments undertaken in this study. The crystallography study (Lutz et al., 2007) presents a $G\alpha_q$ -p63RhoGEF-RhoA complex without the direct binding of $G\alpha_q$ and RhoA, but whether RhoGEFs are also involved in the signalling transduction pathway leading to the inhibition of sl_{AHP} by ACh and glutamate needs to be determined by investigating RhoGEFs directly (section 4.4).

4.2 The small GTPase RhoA is involved in the cholinergic suppression of sI_{AHP}

In addition to its characteristic role in the regulation of the actin cytoskeleton, RhoA is also involved in various other cellular processes and contributes to the regulation of cell cycle, gene transcription, microtubule organization, vesicular transport, cell growth and motility, and enzymatic activities (Takai et al., 2001; Jaffe and Hall, 2005). The proposed involvement of RhoA in the suppression of sI_{AHP} by ACh in hippocampal pyramidal neurons, and thus in the regulation of membrane excitability on a relatively fast time-scale, would be a novel function for the small GTPase. The data presented in this and other studies (Krause and Pedarzani, 2000) have shown that the suppression of sI_{AHP} by cholinergic agonists occurs within a few minutes (2.1 ± 0.3 min; Fig. 3.28 and 3.30), which is in agreement with the time course reported for RhoA activation by CCh through GPCRs coupled to G_q -proteins showing (earliest detection at 0.5 min; Chikumi et al., 2002).

In order to identify an involvement of RhoA in this pathway, constitutively active RhoA-V14 or inactive RhoA-N19 protein was purified and introduced into CA1 pyramidal cells of acute hippocampal slices, a system in which sI_{AHP} is well characterised (Alger and Nicoll, 1980; Hotson and Prince, 1980; Madison and Nicoll, 1982 and 1984; Lancaster and Adams, 1986; Pedarzani and Storm, 1993). The strategy of introducing purified proteins into cells through the patch pipette had been used in another study for the intracellular application of Rac1 and RhoA into pituitary cells (Storey et al., 2002). That study demonstrated that, in response to thyrotropin-releasing hormone, the small GTPases regulate $K_V11.1$ (ERG) in opposing fashion, with Rac1 stimulating and RhoA inhibiting the channel. To determine the role of RhoA in the signalling cascade leading to the suppression of sI_{AHP} , whole-cell patch clamp recordings in hippocampal pyramidal neurons in acute slices were performed with either RhoA-V14 or RhoA-N19 protein in the patch pipette and sI_{AHP} was recorded. The data presented suggest an involvement of RhoA, since sI_{AHP} is reduced in cells containing the constitutively active RhoA-V14 protein compared to control and RhoA-N19 cells (Fig. 3.20). At the maximal steady-state level reached by the current, sI_{AHP} amplitude in RhoA-V14 cells was significantly different to sI_{AHP} levels of control and RhoA-N19 cells, but overall the reduction was only partial. Generally, under control condition sI_{AHP} has been reported to be stable throughout the recordings (Pedarzani and Storm, 1993; Pedarzani et al., 1998; but see Villalobos et al., 2011). However, an evaluation of the inhibiting effect of RhoA-V14 on sI_{AHP} after ~20 min of recording was complicated by the run-down of the current in all three groups and a potential increase in the inhibitory effect of RhoA-V14 on sI_{AHP} at later time points could not be determined. The partial reduction of sI_{AHP} in neurons containing RhoA-V14 protein observed at steady-state could be due to the fact that the amount of protein introduced through the patch pipette was

insufficient to suppress sI_{AHP} to levels observed following the application of cholinergic (Cole and Nicoll, 1983; Madison et al., 1987) and glutamatergic (Charpak et al., 1990) agonists. An inadequate diffusion of the protein into the cell could be one reason, and furthermore, whole-cell voltage clamp recordings were performed by patching the cell body and the mutant RhoA proteins might have not reached their site of action if the channels generating sI_{AHP} are located on the dendrites (Sah and Bekkers, 1996; Bekkers, 2000), although their somatic location has also been proposed (Lima and Marrion, 2007). However, sI_{AHP} recordings from hippocampal pyramidal neurons dialyzed with C3-exoenzyme (P. Pedarzani, personal communication), which has a similar molecular weight (25 kDa; Aktories et al., 1988) as RhoA (21 kDa), or the catalytic subunit of PKA (38 kDa; Pedarzani and Storm, 1993) have shown that proteins of this size can diffuse into the neurons and affect sI_{AHP} and its regulation.

To circumvent limitations of the intracellular application of mutant RhoA proteins such as time of exposure of mutant proteins in neurons or diffusion to the correct cellular location and to maximize the effect of exogenous RhoA, Sindbis viruses containing mutant RhoA were generated and used to over-express RhoA-V14 or RhoA-N19 in hippocampal pyramidal cells. The Sindbis virus expression system was chosen, since it enables proteins to be expressed quickly and displays high specificity for neurons. Primary cultured hippocampal neurons were infected with Sindbis virus and the effect of the expressed RhoA mutants on sI_{AHP} was investigated by whole-cell patch clamp recordings. sI_{AHP} is present in hippocampal cultures and has the same features as in acute slices (Shah and Haylett, 2000b; Gallasch, 2008). Furthermore, it was determined that the basic membrane properties of primary hippocampal neurons are not affected by the infection with Sindbis virus (Fig. 3.25). The primary purpose of the Sindbis virus infections of mutant RhoA was to identify whether or not RhoA participates in the suppression of sI_{AHP} in hippocampal neurons and the results clearly demonstrate that RhoA is part of the transduction cascade. In hippocampal neurons that express constitutively active RhoA-V14 sI_{AHP} was almost completely inhibited, whereas in neurons expressing inactive RhoA-N19 sI_{AHP} did not differ from control cells in terms of current amplitude, charge transfer and time to peak (Fig. 3.29). Using Sindbis virus to express mutant RhoA proteins removes the limitations presented by the intracellular application of purified RhoA proteins, which might affect the passage of proteins into the neuron and their diffusion within the cell. However, even this system cannot prevent the possibility of varied RhoA protein expression levels in individual neurons. The residual sI_{AHP} and the single occasion of a full-sized recording of sI_{AHP} in neurons expressing RhoA-V14 can possibly be attributed to this fact.

The cholinergic inhibition of sI_{AHP} is reduced in hippocampal neurons when RhoA was inhibited by a synthetic peptide against its carboxyl-terminus or by the intracellular application of C3-

exoenzyme (P. Pedarzani, personal communication). Thus it was hypothesised that the suppression of sI_{AHP} by cholinergic agonists in hippocampal neurons expressing inactive RhoA-N19 would also be diminished. This was tested by the application of CCh to hippocampal neurons infected with RhoA-N19 and the data presented show that sI_{AHP} in these neurons has the tendency to be less affected by CCh, albeit the effect was not significantly different from control neurons (Fig. 3.30). One explanation why CCh still had an effect on sI_{AHP} in RhoA-N19 expressing neurons could be the RhoA-N19 mutant itself, although its inactivity had been determined in stress fibre formation tests (Fig. 3.24). Another reason, equally to RhoA-V14 expressing neurons, could be a varied protein expression level of RhoA-N19 in individual neurons. This would mean that in neurons expressing low levels of the mutant protein, endogenous RhoA would be able to mediate the inhibitory effect of CCh on sI_{AHP} similar to control cells, whereas the suppression by CCh would be reduced in neurons expressing high levels of exogenous RhoA-N19. Furthermore, a better coupling of endogenous RhoA to mAChRs and the channels generating sI_{AHP} with insufficient turnover and replacement by the RhoA-N19 mutant could be another reason. Insufficient turnover and replacement of mutant RhoA-N19 before recording could be addressed by allowing more time before recording from infected neurons. The data presented in this study were obtained at 24 h, and occasionally 48 h, after infection and the effect of CCh on sI_{AHP} in neurons expressing inactive mutant RhoA-N19 was not changed over this time. Furthermore, constitutively active RhoA-V14 was shown to be able to affect sI_{AHP} in this time frame. A difference between the effect of CCh on sI_{AHP} in EGFP-negative and RhoA-N19 infected neurons was the observed lack of reversibility of the current upon the removal of CCh (Fig. 3.30). The cause of this could not be established. There were no apparent differences in the passive properties of the neurons between the EGFP-negative and RhoA-N19 infected neurons, nor was there in the series resistance that was monitored throughout the recording. A general problem of run-down of sI_{AHP} in RhoA-N19 infected neurons would have to be investigated in long-term recordings without the application of CCh.

The participation of RhoA in the signalling pathway leading to the suppression of sI_{AHP} in primary cultured hippocampal neurons is one of the main findings of this study and a subsequent aim would be to replicate these Sindbis-virus experiments in organotypic or acute brain slices and determine the effect of RhoA mutants on sI_{AHP} in that system and investigate its regulation by cholinergic agonists.

4.3 Signalling downstream of RhoA

The identity of the channel underlying sI_{AHP} has not yet been identified, which makes the identification of the signal transduction pathways leading to its inhibition the more

challenging. As described above, the signalling cascade employed by monoamine transmitters has been determined up to the point of PKA activation and a yet unidentified phosphorylation step is thought to mediate the inhibition of sI_{AHP} (Fig. 4.1). The results of this study, together with other preliminary data from our laboratory, have established the small GTPase RhoA as part of the signalling pathway used by ACh to suppress sI_{AHP} in hippocampal pyramidal neurons. The actual means by which RhoA mediates the inhibition of sI_{AHP} and which downstream effectors might be involved remains elusive.

Classical targets of RhoA such as mDia, ROCK and MLCK participate in the regulation of the actin cytoskeleton and are responsible for actin filament assembly and stress fibre formation. In Swiss-3T3 cells stress fibre formation in response to the application of fetal calf serum or lysophosphatidic acid was observed within a few minutes and within 15 min of injecting constitutively active RhoA-V14 protein (Ridley and Hall, 1992). $G\alpha_q$ has been reported to induce the formation of stress fibres by activating endogenous RhoA in Swiss-3T3 cells (Dutt et al., 2002). In neuronal cells the activation of RhoA by $G\alpha_q$ causes neurite retraction and cell rounding (Kato et al., 1998), which is caused by the formation of contractile actin-myosin filaments (Ridley, 1996; Hall, 1998). ROCK inhibitors hinder the formation of stress fibres caused by $G\alpha_q$ activation of RhoA (Dutt et al., 2002). Whether the suppression of sI_{AHP} also involves ROCK was investigated by the use of ROCK inhibitors in whole-cell patch clamp recordings in acute hippocampal slices and it was determined that ROCK does not participate in the suppression of sI_{AHP} by ACh and glutamate (Fig. 4.1; P. Pedarzani, personal communication). Furthermore, inhibitors of MLCK have also been shown to not affect the inhibitory effect of ACh and glutamate on sI_{AHP} (Fig. 4.1; P. Pedarzani, personal communication). It is therefore unlikely that changes to the cytoskeleton mediated by ROCK and MLCK are the underlying cause for the inhibition of sI_{AHP} following the activation of RhoA by ACh and glutamate, although effects on the cytoskeleton by different downstream effectors of RhoA cannot be excluded. In addition, no clear macroscopic changes in the morphology of the primary cultured hippocampal neurons have been observed in this study, but parameters like neurite retraction or cell rounding have not been quantified. Furthermore, only neurons displaying the morphology of pyramidal neurons i.e. with triangular-shaped soma and distinctive processes were selected for patching.

RhoA has been implicated in the regulation of various ion channels including the inhibition of K^+ channels (Cachero et al., 1998; Storey et al., 2002; Jones, 2003; Rossignol and Jones, 2006; Stirling et al., 2009). These findings give rise to the possibility that RhoA could mediate the suppression of sI_{AHP} by acting directly on the underlying channel or by signalling to intermediate proteins, which in turn affect the channel. In the case of $K_v1.2$, yeast two-hybrid

and co-immunoprecipitation experiments have established the association of RhoA with the amino-terminus of $K_V1.2$ and the over-expression of constitutively active or inactive RhoA mutants or the inhibition of RhoA by C3-exoenzyme has shown that RhoA (Cachero et al., 1998) also mediates the tyrosine kinase-dependent suppression of $K_V1.2$ by the muscarinic acetylcholine receptor M_1 (Huang et al., 1993). Moreover, the suppression of $K_V1.2$ by RhoA involves the endocytosis of the channel via a ROCK-dependent pathway (Stirling et al., 2009). A role of ROCK was also suggested in the inhibition of $K_V11.1$ by RhoA (Storey et al., 2002), whereas the suppression of $K_{ir}2.1$ by RhoA was not affected by the inhibition of ROCK (Jones, 2003). RhoA also enhances the activity of Na^+ channels of the ENaC family; RhoA initiates a signal transduction pathway that activates ROCK, whose stimulation of PIP5K catalyses the production of PIP_2 (Oude Weernink et al., 2000 and 2004) and a PIP_2 increase promotes the expression of ENaC at the plasma membrane (Staruschenko et al., 2004). While the signalling partnership of RhoA and ROCK seems to present a powerful system in the regulation of some ion channels, the cases of $K_{ir}2.1$ and sl_{AHP} , whose regulation does not involve ROCK, show that other downstream effectors of RhoA must also be implicated.

4.4 Future directions

The interaction of $G\alpha_q$ and RhoA has been identified in heterologous expression system and its validation in neuronal tissue has been attempted by performing co-immunoprecipitations of the endogenous proteins. However, the available RhoA antibody merely allowed the detection of endogenous RhoA in brain lysates (Fig. 3.4). Co-immunoprecipitations from brain tissue should therefore be re-attempted once an antibody of sufficient avidity becomes available.

This thesis has established the involvement of RhoA in the signalling pathway leading to the suppression of sl_{AHP} in primary cultured hippocampal neurons. This finding should be validated in brain slices by performing whole-cell patch clamp recordings of sl_{AHP} in slices that have been infected with the Sindbis virus to introduce the RhoA mutants. Initial experiments in organotypic slices have been undertaken (P. Pedarzani, personal communication).

GPCR signalling via $G\alpha_q$ to RhoA has been implicated to involve RhoGEFs, such as p63RhoGEF, Lbc and LARG (Sagi et al., 2001; Booden et al., 2002; Lutz et al., 2005; Shankaranarayanan et al., 2010), and the crystal structure of a $G\alpha_q$ -p63RhoGEF-RhoA complex has been determined (Lutz et al., 2007). The potential involvement of RhoGEFs in the signalling pathways leading to the suppression of sl_{AHP} by ACh and glutamate in hippocampal neurons should thus be examined. The three RhoGEFs named above present a good starting point as they are the only members of the vast RhoGEF family that have been identified to act downstream of $G\alpha_q$. p63RhoGEF, for example, is present mainly in the brain and the heart (Souchet et al., 2002;

Lutz et al., 2004). An antibody for p63RhoGEF is available (Wuertz et al., 2010) and could be used to verify the interaction of endogenous p63RhoGEF with $G\alpha_q$ and RhoA. In order to identify the role of RhoGEFs in the suppression of sI_{AHP} , whole-cell patch clamp recordings could be performed in hippocampal pyramidal neurons, in which candidate RhoGEFs are inhibited, for example, by antibodies directed against them or by the intracellular application of mutant RhoGEFs such as p63RhoGEF-E301 (Souchet et al., 2002). Moreover, candidate RhoGEFs could be downregulated in siRNA experiments or in potential knock-out mice. A reduction in the suppression of sI_{AHP} by ACh and glutamate would indicate the involvement of RhoGEFs in the signalling cascade.

Furthermore, the role of G-proteins of the G_{12} family ($G\alpha_{12}$ and $G\alpha_{13}$) in the suppression of sI_{AHP} by ACh and glutamate should be investigated. The hypothesis arises from the finding that the cholinergic and glutamatergic inhibition of sI_{AHP} in $G\alpha_q$ knock-out mice is only reduced by ~50% (Krause et al., 2002) and from the fact that G-proteins of the G_{12} family are known to signal to Rho-GTPases and can be coupled to mAChRs (Buhl et al., 1995; Fromm et al., 1997; Hart et al., 1998; Fukuhara et al., 1999 and 2000; Siehler, 2009). $G\alpha_{12/13}$ have also been shown to activate RhoA through RhoGEFs (Hart et al., 1998; Fukuhara et al., 1999 and 2000; Suzuki et al., 2003; Kozasa et al., 2011). Mice lacking the G-protein α subunit $G\alpha_{12}$ or $G\alpha_{13}$ (Offermanns et al., 1997; Dettlaff-Swiercz et al., 2005) could be used to perform whole-cell patch clamp recordings in hippocampal pyramidal neurons and the effect of cholinergic and glutamatergic agonists on sI_{AHP} investigated. Their inhibitory action ought to be reduced should $G\alpha_{12}$ or $G\alpha_{13}$ be involved. Thus the suppression of sI_{AHP} by ACh and glutamate could be mediated by two converging pathways onto RhoA.

By determining neuronal excitability and firing patterns of hippocampal pyramidal neurons, sI_{AHP} contributes to the regulation of the network activity of the hippocampal formation that underlies learning and memory processes. sI_{AHP} is responsible for spike frequency adaptation by restricting the repetitive firing of action potentials, thus contributing greatly to the control of neuronal excitability. sI_{AHP} is suppressed by various neurotransmitters including ACh, glutamate and the monoamine neurotransmitters dopamine, histamine, noradrenaline and serotonin (Storm, 1990; Sah, 1996) and its modulation shapes the intrinsic properties of hippocampal pyramidal neurons that are essential in learning and memory processes. sI_{AHP} thus presents a target for multiple pathways aiming to regulate neuronal excitability and firing properties. Irregularity in the control of sI_{AHP} can lead to epileptic activity (Alger and Nicoll, 1980). Establishing the nature of the signalling pathways underlying the suppression of sI_{AHP} is therefore central to our understanding of the regulation of network activity involved in the processes of memory and learning.

References

- Abdul-Ghani MA, Valiante TA, Carlen PL and Pennefather PS (1996). Metabotropic glutamate receptors coupled to IP₃ production mediate inhibition of I_{AHP} in rat dentate granule neurons. *Journal of Neurophysiology*. 76(4):2691–700.
- Abe T, Sugihara H, Nawa H, Shigemoto R, Mizuno N and Nakanishi S (1992). Molecular characterization of a novel metabotropic glutamate receptor mGluR5 coupled to inositol phosphate/Ca²⁺ signal transduction. *The Journal of Biological Chemistry*. 267(19):13361–8.
- Abel HJ, Lee JCF, Callaway JC and Foehring RC (2004). Relationships between intracellular calcium and afterhyperpolarizations in neocortical pyramidal neurons. *Journal of Neurophysiology*. 91(1):324–35.
- Adamson P, Marshall CJ, Hall A and Tilbrook PA (1992a). Post-translational modifications of p21rho proteins. *The Journal of Biological Chemistry*. 267(28):20033–8.
- Adamson P, Paterson HF and Hall A (1992b). Intracellular localization of the P21rho proteins. *The Journal of Cell Biology*. 119(3):617–27.
- Adelman JP, Maylie J and Sah P (2012). Small-conductance Ca²⁺-activated K⁺ channels: form and function. *Annual Review of Physiology*. 74:245–69.
- Adjobo-Hermans MJW, Goedhart J, van Weeren L, Nijmeijer S, Manders EMM, Offermanns S and Gadella TWJ (2011). Real-time visualization of heterotrimeric G protein Gq activation in living cells. *BMC Biology*. 9(1):32.
- Ahmadian MR, Stege P, Scheffzek K and Wittinghofer A (1997). Confirmation of the arginine-finger hypothesis for the GAP-stimulated GTP-hydrolysis reaction of Ras. *Nature Structural Biology*. 4(9):686–9.
- Aittaleb M, Boguth CA and Tesmer JGG (2010). Structure and function of heterotrimeric G protein-regulated Rho guanine nucleotide exchange factors. *Molecular Pharmacology*. 77(2):111–25.
- Aktories K, Rösener S, Blaschke U and Chhatwal GS (1988). Botulinum ADP-ribosyltransferase C3. Purification of the enzyme and characterization of the ADP-ribosylation reaction in platelet membranes. *European Journal of Biochemistry*. 172(2):445–50.
- Aktories K and Hall A (1989). Botulinum ADP-ribosyltransferase C3: a new tool to study low molecular weight GTP-binding proteins. *Trends in Pharmacological Sciences*. 10(10):415–8.
- Alger BE and Nicoll RA (1980). Epileptiform burst afterhyperpolarization: calcium-dependent potassium potential in hippocampal CA1 pyramidal cells. *Science*. 210(4474):1122–4.
- Alkondon M and Albuquerque EX (2004). The nicotinic acetylcholine receptor subtypes and their function in the hippocampus and cerebral cortex. *Progress in Brain Research*. 145:109–20.
- Allen D, Fakler B, Maylie J and Adelman JP (2007). Organization and regulation of small conductance Ca²⁺-activated K⁺ channel multiprotein complexes. *The Journal of Neuroscience*. 27(9):2369–76.
- Amano M, Mukai H, Ono Y, Chihara K, Matsui T, Hamajima Y, Okawa K, Iwamatsu A and Kaibuchi K (1996). Identification of a putative target for Rho as the serine-threonine kinase protein kinase N. *Science*. 271(5249):648–50.

- Amaral D and Witter MP (1989). The three-dimensional organization of the hippocampal formation: a review of anatomical data. *Neuroscience*. 31(3):571–91.
- Amaral D and Lavenex P (2007). Hippocampal Neuroanatomy. In: Andersen P, Morris R, Amaral D, Bliss T and O'Keefe J, ed. *The Hippocampus Book*. Oxford University Press. Oxford:37–114.
- Andrade R and Nicoll RA (1987). Pharmacologically distinct actions of serotonin on single pyramidal neurones of the rat hippocampus recorded in vitro. *The Journal of Physiology*. 394:99–124.
- Andrade R, Foehring RC and Tzingounis AV (2012). The calcium-activated slow AHP: cutting through the Gordian knot. *Frontiers in Cellular Neuroscience*. 6:47.
- Anwyl R (1999). Metabotropic glutamate receptors: electrophysiological properties and role in plasticity. *Brain Research*. 29(1):83–120.
- Anwyl R (2009). Metabotropic glutamate receptor-dependent long-term potentiation. *Neuropharmacology*. 56(4):735–40.
- Arkininstall S, Chabert C, Maundrell K and Peitsch M (1995). Mapping regions of G α_q interacting with PLC β 1 using multiple overlapping synthetic peptides. *FEBS Letters*. 364(1):45–50.
- Aspenström P, Fransson A and Saras J (2004). Rho GTPases have diverse effects on the organization of the actin filament system. *The Biochemical Journal*. 377(2):327–37.
- Bal M, Zhang J, Zaika O, Hernandez CC and Shapiro MS (2008). Homomeric and heteromeric assembly of KCNQ (Kv7) K $^+$ channels assayed by total internal reflection fluorescence/fluorescence resonance energy transfer and patch clamp analysis. *The Journal of Biological Chemistry*. 283(45):30668–76.
- Bao L, Rapin AM, Holmstrand EC and Cox DH (2002). Elimination of the BK $_{Ca}$ channel's high-affinity Ca $^{2+}$ sensitivity. *The Journal of General Physiology*. 120(2):173–89.
- Bao L and Cox DH (2005). Gating and ionic currents reveal how the BK $_{Ca}$ channel's Ca $^{2+}$ sensitivity is enhanced by its β 1 subunit. *The Journal of General Physiology*. 126(4):393–412.
- Barbacid M (1987). ras genes. *Annual Review of Biochemistry*. 56:779–827.
- Barhanin J, Lesage F, Guillemare E, Fink M, Lazdunski M and Romey G (1996). K $_v$ LQT1 and IsK (minK) proteins associate to form the I $_{Ks}$ cardiac potassium current. *Nature*. 384(6604):78–80.
- Bashir ZI, Bortolotto ZA, Davies CH, Berretta N, Irving AJ, Seal AJ, Henley JM, Jane DE, Watkins JC and Collingridge GL (1993). Induction of LTP in the hippocampus needs synaptic activation of glutamate metabotropic receptors. *Nature*. 363(6427):347–50.
- Behrends JC and ten Bruggencate G (1993). Cholinergic modulation of synaptic inhibition in the guinea pig hippocampus in vitro: excitation of GABAergic interneurons and inhibition of GABA-release. *Journal of Neurophysiology*. 69(2):626–9.
- Bekkers JM (2000). Distribution of slow AHP channels on hippocampal CA1 pyramidal neurons. *Journal of Neurophysiology*. 83(3):1756–9.
- Benardo LS and Prince DA (1982). Ionic mechanisms of cholinergic excitation in mammalian hippocampal pyramidal cells. *Brain Research*. 249(2):333–44.
- Benians A, Nobles M, Hosny S and Tinker A (2005). Regulators of G-protein signaling form a quaternary complex with the agonist, receptor, and G-protein. A novel explanation for the acceleration of signaling activation kinetics. *The Journal of Biological Chemistry*. 280(14):13383–94.

- Bentrop D, Beyermann M, Wissmann R and Fakler B (2001). NMR structure of the “ball-and-chain” domain of KCNMB2, the β_2 -subunit of large conductance Ca^{2+} - and voltage-activated potassium channels. *The Journal of Biological Chemistry*. 276(45):42116–21.
- Berkefeld H, Sailer CA, Bildl W, Rohde V, Thumfart J-O, Eble S, Klugbauer N, Reisinger E, Bischofberger J, Oliver D, Knaus H-G, Schulte U and Fakler B (2006). BK_{Ca} -Cav channel complexes mediate rapid and localized Ca^{2+} -activated K^+ signaling. *Science*. 314(5799):615–20.
- Berkefeld H, Fakler B and Schulte U (2010). Ca^{2+} -activated K^+ channels: from protein complexes to function. *Physiological Reviews*. 90(4):1437–59.
- Berman DM, Kozasa T and Gilman AG (1996). The GTPase-activating protein RGS4 stabilizes the transition state for nucleotide hydrolysis. *The Journal of Biological Chemistry*. 271(44):27209–12.
- Berridge MJ, Bootman MD and Roderick HL (2003). Calcium signalling: dynamics, homeostasis and remodelling. *Nature Reviews. Molecular Cell Biology*. 4(7):517–29.
- Berstein G, Blank JL, Smrcka AV, Higashijima T, Sternweis PC, Exton JH and Ross EM (1992). Reconstitution of agonist-stimulated phosphatidylinositol 4,5-bisphosphate hydrolysis using purified m1 muscarinic receptor, $\text{G}_{\text{q}/11}$, and phospholipase C- β 1. *The Journal of Biological Chemistry*. 267(12):8081–8.
- Bhattacharya M, Babwah AV and Ferguson SSG (2004). Small GTP-binding protein-coupled receptors. *Biochemical Society Transactions*. 32(6):1040–4.
- Biel M, Wahl-Schott C, Michalakakis S and Zong X (2009). Hyperpolarization-activated cation channels: from genes to function. *Physiological Reviews*. 89(3):847–85.
- Bildl W, Strassmaier T, Thurm H, Andersen J, Eble S, Oliver D, Knipper M, Mann M, Schulte U, Adelman JP and Fakler B (2004). Protein kinase CK2 is coassembled with small conductance Ca^{2+} -activated K^+ channels and regulates channel gating. *Neuron*. 43(6):847–58.
- Biou V and Cherfils J (2004). Structural principles for the multispecificity of small GTP-binding proteins. *Biochemistry*. 43(22):6833–40.
- Blin N, Yun J and Wess J (1995). Mapping of single amino acid residues required for selective activation of $\text{G}_{\text{q}/11}$ by the m3 muscarinic acetylcholine receptor. *The Journal of Biological Chemistry*. 270(30):17741–8.
- Bliss TV and Collingridge GL (1993). A synaptic model of memory: long-term potentiation in the hippocampus. *Nature*. 361(6407):31–9.
- Blitzer RD, Wong T, Nouranifar R and Landau EM (1994). The cholinergic inhibition of afterhyperpolarization in rat hippocampus is independent of cAMP-dependent protein kinase. *Brain Research*. 646(2):312–4.
- Bodmann E-L, Rinne A, Brandt D, Lutz S, Wieland T, Grosse R and Bünemann M (2014). Dynamics of $\text{G}\alpha_{\text{q}}$ -protein-p63RhoGEF interaction and its regulation by RGS2. *The Biochemical Journal*. 458(1):131–40.
- Boguski MS and McCormick F (1993). Proteins regulating Ras and its relatives. *Nature*. 366(6456):643–54.
- Bokoch GM, Bohl BP and Chuang TH (1994). Guanine nucleotide exchange regulates membrane translocation of Rac/Rho GTP-binding proteins. *The Journal of Biological Chemistry*. 269(50):31674–9.

- Bolte S and Cordelières FP (2006). A guided tour into subcellular colocalization analysis in light microscopy. *Journal of Microscopy*. 224(3):213–32.
- Bond CT, Herson PS, Strassmaier T, Hammond R, Stackman R, Maylie J and Adelman JP (2004). Small conductance Ca^{2+} -activated K^+ channel knock-out mice reveal the identity of calcium-dependent afterhyperpolarization currents. *The Journal of Neuroscience*. 24(23):5301–6.
- Booden MA, Siderovski DP and Der CJ (2002). Leukemia-associated Rho guanine nucleotide exchange factor promotes G α_q -coupled activation of RhoA. *Molecular and Cellular Biology*. 22(12):4053–61.
- Bourne HR, Sanders DA and McCormick F (1991). The GTPase superfamily: conserved structure and molecular mechanism. *Nature*. 349(6305):117–27.
- Bourne HR (1997). How receptors talk to trimeric G proteins. *Current Opinion in Cell Biology*. 9(2):134–42.
- Bowden SE, Fletcher S, Loane DJ and Marrion NV (2001). Somatic colocalization of rat SK1 and D class ($\text{Ca}_v1.2$) L-type calcium channels in rat CA1 hippocampal pyramidal neurons. *The Journal of Neuroscience*. 21(20):rc175.
- Bredenbeek PJ, Frolov I, Rice CM and Schlesinger S (1993). Sindbis virus expression vectors: packaging of RNA replicons by using defective helper RNAs. *Journal of Virology*. 67(11):6439–46.
- Brenner R, Jegla TJ, Wickenden A, Liu Y and Aldrich RW (2000). Cloning and functional characterization of novel large conductance calcium-activated potassium channel β subunits, hKCNMB3 and hKCNMB4. *The Journal of Biological Chemistry*. 275(9):6453–61.
- Brown DA and Adams PR (1980). Muscarinic suppression of a novel voltage-sensitive K^+ current in a vertebrate neurone. *Nature*. 283(5748):673–6.
- Brown DA and Griffith WH (1983). Calcium-activated outward current in voltage-clamped hippocampal neurones of the guinea-pig. *The Journal of Physiology*. 337:287–301.
- Brown DA, Gähwiler BH, Griffith WH and Halliwell JV (1990). Membrane currents in hippocampal neurons. *Progress in Brain Research*. 83:141–60.
- Brown DA, Hughes SA, Marsh SJ and Tinker A (2007). Regulation of M(Kv7.2/7.3) channels in neurons by PIP_2 and products of PIP_2 hydrolysis: significance for receptor-mediated inhibition. *The Journal of Physiology*. 582(3):917–25.
- Brown DA and Passmore GM (2009). Neural KCNQ (Kv7) channels. *British Journal of Pharmacology*. 156(8):1185–95.
- Buchanan KA, Petrovic MM, Chamberlain SEL, Marrion NV and Mellor JR (2010). Facilitation of long-term potentiation by muscarinic M1 receptors is mediated by inhibition of SK channels. *Neuron*. 68(5):948–63.
- Bünemann M, Frank M and Lohse MJ (2003). Gi protein activation in intact cells involves subunit rearrangement rather than dissociation. *Proceedings of the National Academy of Sciences of the United States of America*. 100(26):16077–82.
- Buhl AM, Johnson NL, Dhanasekaran N and Johnson GL (1995). $\text{G}\alpha_{12}$ and $\text{G}\alpha_{13}$ stimulate Rho-dependent stress fiber formation and focal adhesion assembly. *The Journal of Biological Chemistry*. 270(42):24631–4.

- Buhl E and Whittington M (2007). Local Circuits. In: Andersen P, Morris R, Amaral D, Bliss T and O'Keefe J, ed. *The Hippocampus Book*. Oxford University Press. Oxford:297–319.
- Buzsáki G (2002). Theta oscillations in the hippocampus. *Neuron*. 33(3):325–40.
- Cachero TG, Morielli AD and Peralta EG (1998). The small GTP-binding protein RhoA regulates a delayed rectifier potassium channel. *Cell*. 93(6):1077–85.
- Cartmell J and Schoepp DD (2000). Regulation of neurotransmitter release by metabotropic glutamate receptors. *Journal of Neurochemistry*. 75(3):889–907.
- Castillo PE, Malenka RC and Nicoll RA (1997). Kainate receptors mediate a slow postsynaptic current in hippocampal CA3 neurons. *Nature*. 388(6638):182–6.
- Caulfield M, Jones S, Vallis Y, Buckley N, Kim G, Milligan G and Brown D (1994). Muscarinic M-current inhibition via $G_{\alpha q/11}$ and α -adrenoceptor inhibition of Ca^{2+} current via $G_{\alpha o}$ in rat sympathetic neurones. *The Journal of Physiology*. 477(3):415–22.
- Caulfield MP and Birdsall NJ (1998). International Union of Pharmacology. XVII. Classification of muscarinic acetylcholine receptors. *Pharmacological Reviews*. 50(2):279–90.
- Cerione RA and Zheng Y (1996). The Dbl family of oncogenes. *Current Opinion in Cell Biology*. 8(2):216–22.
- Chardin P, Camonis JH, Gale NW, van Aelst L, Schlessinger J, Wigler MH and Bar-Sagi D (1993). Human Sos1: a guanine nucleotide exchange factor for Ras that binds to GRB2. *Science*. 260(5112):1338–43.
- Charpak S, Gähwiler BH, Do KQ and Knöpfel T (1990). Potassium conductances in hippocampal neurons blocked by excitatory amino-acid transmitters. *Nature*. 347(6295):765–7.
- Chen CA and Manning DR (2001). Regulation of G proteins by covalent modification. *Oncogene*. 20(13):1643–52.
- Chen H, Kim LA, Rajan S, Xu S and Goldstein SAN (2003). Charybdotoxin binding in the I_{Ks} pore demonstrates two MinK subunits in each channel complex. *Neuron*. 40(1):15–23.
- Chikumi H, Vázquez-Prado J, Servitja J-M, Miyazaki H and Gutkind JS (2002). Potent activation of RhoA by $G_{\alpha q}$ and $G_{\alpha q}$ -coupled receptors. *The Journal of Biological Chemistry*. 277(30):27130–4.
- Clapham DE and Neer EJ (1997). G protein $\beta\gamma$ subunits. *Annual Review of Pharmacology and Toxicology*. 37:167–203.
- Cloues RK, Tavalin SJ and Marrion NV (1997). B-adrenergic stimulation selectively inhibits long-lasting L-type calcium channel facilitation in hippocampal pyramidal neurons. *The Journal of Neuroscience*. 17(17):6493–503.
- Cobb SR and Davies CH (2005). Cholinergic modulation of hippocampal cells and circuits. *The Journal of Physiology*. 562(1):81–8.
- Cole AE and Nicoll RA (1983). Acetylcholine mediates a slow synaptic potential in hippocampal pyramidal cells. *Science*. 221(4617):1299–301.
- Cole AE and Nicoll RA (1984). Characterization of a slow cholinergic post-synaptic potential recorded in vitro from rat hippocampal pyramidal cells. *The Journal of Physiology*. 352:173–88.

- Coleman DE, Berghuis AM, Lee E, Linder ME, Gilman AG and Sprang SR (1994). Structures of active conformations of $G_{i\alpha 1}$ and the mechanism of GTP hydrolysis. *Science*. 265(5177):1405–12.
- Colino A and Halliwell JV (1987). Differential modulation of three separate K-conductances in hippocampal CA1 neurons by serotonin. *Nature*. 328(6125):73–7.
- Collingridge GL, Olsen RW, Peters J and Spedding M (2009). A nomenclature for ligand-gated ion channels. *Neuropharmacology*. 56(1):2–5.
- Conklin BR, Chabre O, Wong YH, Federman AD and Bourne HR (1992). Recombinant $G_q\alpha$. Mutational activation and coupling to receptors and phospholipase C. *The Journal of Biological Chemistry*. 267(1):31–4.
- Conklin BR and Bourne HR (1993). Structural elements of $G\alpha$ subunits that interact with $G\beta\gamma$, receptors, and effectors. *Cell*. 73(4):631–41.
- Corbett KD and Alber T (2001). The many faces of Ras: recognition of small GTP-binding proteins. *Trends in Biochemical Sciences*. 26(12):710–6.
- Côté J-F and Vuori K (2002). Identification of an evolutionarily conserved superfamily of DOCK180-related proteins with guanine nucleotide exchange activity. *Journal of Cell Science*. 115(24):4901–13.
- Crépel V, Aniksztejn L, Ben-Ari Y and Hammond C (1994). Glutamate metabotropic receptors increase a Ca^{2+} -activated nonspecific cationic current in CA1 hippocampal neurons. *Journal of Neurophysiology*. 72(4):1561–9.
- Cui J, Yang H and Lee US (2009). Molecular mechanisms of BK channel activation. *Cellular and Molecular Life Sciences*. 66(5):852–75.
- Davies CH, Clarke VR, Jane DE and Collingridge GL (1995). Pharmacology of postsynaptic metabotropic glutamate receptors in rat hippocampal CA1 pyramidal neurones. *British Journal of Pharmacology*. 116(2):1859–69.
- De Vivo M, Chen J, Codina J and Iyengar R (1992). Enhanced phospholipase C stimulation and transformation in NIH-3T3 cells expressing Q209LG $_q$ - α -subunits. *The Journal of Biological Chemistry*. 267(26):18263–6.
- Delmas P and Brown DA (2005). Pathways modulating neural KCNQ/M (Kv7) potassium channels. *Nature Reviews. Neuroscience*. 6(11):850–62.
- Der CJ, Finkel T and Cooper GM (1986). Biological and biochemical properties of human ras^H genes mutated at codon 61. *Cell*. 44(1):167–76.
- Dettlaff-Swiercz DA, Wettschureck N, Moers A, Huber K and Offermanns S (2005). Characteristic defects in neural crest cell-specific $G\alpha_q/G\alpha_{11}$ - and $G\alpha_{12}/G\alpha_{13}$ -deficient mice. *Developmental Biology*. 282(1):174–82.
- Dowal L, Provitera P and Scarlata S (2006). Stable association between $G\alpha_q$ and phospholipase $C\beta_1$ in living cells. *The Journal of Biological Chemistry*. 281(33):23999–4014.
- Drever BD, Riedel G and Platt B (2011). The cholinergic system and hippocampal plasticity. *Behavioural Brain Research*. 221(2):505–14.
- Druey KM, Blumer KJ, Kang VH and Kehrl JH (1996). Inhibition of G-protein-mediated MAP kinase activation by a new mammalian gene family. *Nature*. 379(6567):742–6.

- Dryga SA, Dryga OA and Schlesinger S (1997). Identification of mutations in a Sindbis virus variant able to establish persistent infection in BHK cells: the importance of a mutation in the nsP2 gene. *Virology*. 228(1):74–83.
- Dutar P and Nicoll RA (1988). Classification of muscarinic responses in hippocampus in terms of receptor subtypes and second-messenger systems: electrophysiological studies in vitro. *The Journal of Neuroscience*. 8(11):4214–24.
- Dutar P, Bassant MH, Senut MC and Lamour Y (1995). The septohippocampal pathway: structure and function of a central cholinergic system. *Physiological Reviews*. 75(2):393–427.
- Dutt P, Kjoller L, Giel M, Hall A and Toksoz D (2002). Activated Gαq family members induce Rho GTPase activation and Rho-dependent actin filament assembly. *FEBS Letters*. 531(3):565–9.
- Ehrengruber MU, Schlesinger S and Lundstrom K (2011). Alphaviruses: Semliki forest virus and Sindbis virus vectors for gene transfer into neurons. *Current Protocols in Neuroscience*. 4:4.22.1–4.22.27.
- Engisch KL, Wagner JJ and Alger BE (1996). Whole-cell voltage-clamp investigation of the role of PKC in muscarinic inhibition of I_{AHP} in rat CA1 hippocampal neurons. *Hippocampus*. 6(2):183–91.
- Evanko DS, Thiyagarajan MM and Wedegaertner PB (2000). Interaction with Gβγ is required for membrane targeting and palmitoylation of Gα_s and Gα_q. *The Journal of Biological Chemistry*. 275(2):1327–36.
- Evanko DS, Thiyagarajan MM, Siderovski DP and Wedegaertner PB (2001). Gβγ isoforms selectively rescue plasma membrane localization and palmitoylation of mutant Gα_s and Gα_q. *The Journal of Biological Chemistry*. 276(26):23945–53.
- Evanko DS, Thiyagarajan MM, Takida S and Wedegaertner PB (2005). Loss of association between activated Gαq and Gβγ disrupts receptor-dependent and receptor-independent signaling. *Cellular Signalling*. 17(10):1218–28.
- Fabian-Fine R, Skehel P, Errington ML, Davies HA, Sher E, Stewart MG and Fine A (2001). Ultrastructural distribution of the α7 nicotinic acetylcholine receptor subunit in rat hippocampus. *The Journal of Neuroscience*. 21(20):7993–8003.
- Farrens DL, Altenbach C, Yang K, Hubbell WL and Khorana HG (1996). Requirement of rigid-body motion of transmembrane helices for light activation of rhodopsin. *Science*. 274(5288):768–70.
- Feig LA and Cooper GM (1988). Inhibition of NIH 3T3 cell proliferation by a mutant ras protein with preferential affinity for GDP. *Molecular and Cellular Biology*. 8(8):3235–43.
- Feig LA (1999). Tools of the trade: use of dominant-inhibitory mutants of Ras-family GTPases. *Nature Cell Biology*. 1(2):E25–7.
- Ferguson KM, Higashijima T, Smigel MD and Gilman a G (1986). The influence of bound GDP on the kinetics of guanine nucleotide binding to G proteins. *The Journal of Biological Chemistry*. 261(16):7393–9.
- Ford CE, Skiba NP, Bae H, Daaka Y, Reuveny E, Shekter LR, Rosal R, Weng G, Yang CS, Iyengar R, Miller RJ, Jan LY, Lefkowitz RJ and Hamm HE (1998). Molecular basis for interactions of G protein βγ subunits with effectors. *Science*. 280(5367):1271–4.
- Fotuhi M, Standaert DG, Testa CM, Penney JB and Young AB (1994). Differential expression of metabotropic glutamate receptors in the hippocampus and entorhinal cortex of the rat. *Brain Research. Molecular Brain Research*. 21(3-4):283–92.

- Freund TF and Buzsáki G (1996). Interneurons of the hippocampus. *Hippocampus*. 6(4):347–470.
- Fromm C, Coso OA, Montaner S, Xu N and Gutkind JS (1997). The small GTP-binding protein Rho links G protein-coupled receptors and $G\alpha_{12}$ to the serum response element and to cellular transformation. *Proceedings of the National Academy of Sciences of the United States of America*. 94(19):10098–103.
- Frotscher M and Léránth C (1985). Cholinergic innervation of the rat hippocampus as revealed by choline acetyltransferase immunocytochemistry: a combined light and electron microscopic study. *The Journal of Comparative Neurology*. 239(2):237–46.
- Fukuhara S, Murga C, Zohar M, Igishi T and Gutkind JS (1999). A novel PDZ domain containing guanine nucleotide exchange factor links heterotrimeric G proteins to Rho. *The Journal of Biological Chemistry*. 274(9):5868–79.
- Fukuhara S, Chikumi H and Gutkind JS (2000). Leukemia-associated Rho guanine nucleotide exchange factor (LARG) links heterotrimeric G proteins of the G_{12} family to Rho. *FEBS Letters*. 485(2-3):183–8.
- Fung BK, Hurley JB and Stryer L (1981). Flow of information in the light-triggered cyclic nucleotide cascade of vision. *Proceedings of the National Academy of Sciences of the United States of America*. 78(1):152–6.
- Galés C, Rebois R V, Hogue M, Trieu P, Breit A, Hébert TE and Bouvier M (2005). Real-time monitoring of receptor and G-protein interactions in living cells. *Nature Methods*. 2(3):177–84.
- Galés C, Van Durm JJJ, Schaak S, Pontier S, Percherancier Y, Audet M, Paris H and Bouvier M (2006). Probing the activation-promoted structural rearrangements in preassembled receptor-G protein complexes. *Nature Structural & Molecular Biology*. 13(9):778–86.
- Gallasch L (2008). Characterisation of sI_{AHP} in primary cultures of hippocampal neurons and development of FRET constructs to visualize the signalling pathway underlying the modulation of sI_{AHP} by acetylcholine. MSc thesis, UCL.
- Gamblin SJ and Smerdon SJ (1998). GTPase-activating proteins and their complexes. *Current Opinion in Structural Biology*. 8(2):195–201.
- Gamelli AE, McKinney BC, White JA and Murphy GG (2011). Deletion of the L-type calcium channel $Ca_v1.3$ but not $Ca_v1.2$ results in a diminished sAHP in mouse CA1 pyramidal neurons. *Hippocampus*. 21(2):133–41.
- Gamper N and Shapiro MS (2003). Calmodulin mediates Ca^{2+} -dependent modulation of M-type K^+ channels. *The Journal of General Physiology*. 122(1):17–31.
- Gamper N, Li Y and Shapiro MS (2005). Structural requirements for differential sensitivity of KCNQ K^+ channels to modulation by Ca^{2+} /calmodulin. *Molecular Biology of the Cell*. 16(8):3538–51.
- Garrett MD, Self AJ, van Oers C and Hall A (1989). Identification of distinct cytoplasmic targets for ras/R-ras and rho regulatory proteins. *The Journal of Biological Chemistry*. 264(1):10–3.
- Gehlert DR and Gackenheimer SL (1993). Comparison of the distribution of binding sites for the potassium channel ligands [^{125}I]apamin, [^{125}I]charybdotoxin and [^{125}I]iodoglyburide in the rat brain. *Neuroscience*. 52(1):191–205.
- Gerber U, Sim JA and Gähwiler BH (1992). Reduction of Potassium Conductances Mediated by Metabotropic Glutamate Receptors in Rat CA3 Pyramidal Cells Does Not Require Protein Kinase C or Protein Kinase A. *The European Journal of Neuroscience*. 4(9):792–797.

- Gereau RW and Conn PJ (1995). Roles of specific metabotropic glutamate receptor subtypes in regulation of hippocampal CA1 pyramidal cell excitability. *Journal of Neurophysiology*. 74(1):122–9.
- Gerlach AC, Maylie J and Adelman JP (2004). Activation kinetics of the slow afterhyperpolarization in hippocampal CA1 neurons. *Pflügers Archiv*. 448(2):187–96.
- Gether U, Lin S and Kobilka BK (1995). Fluorescent labeling of purified β_2 adrenergic receptor. Evidence for ligand-specific conformational changes. *The Journal of Biological Chemistry*. 270(47):28268–75.
- Giessel AJ and Sabatini BL (2010). M1 muscarinic receptors boost synaptic potentials and calcium influx in dendritic spines by inhibiting postsynaptic SK channels. *Neuron*. 68(5):936–47.
- Gohla A, Harhammer R and Schultz G (1998). The G-protein G_{13} but not G_{12} mediates signaling from lysophosphatidic acid receptor via epidermal growth factor receptor to Rho. *The Journal of Biological Chemistry*. 273(8):4653–9.
- Golebiewska U and Scarlata S (2008). $G\alpha_q$ binds two effectors separately in cells: evidence for predetermined signaling pathways. *Biophysical Journal*. 95(5):2575–82.
- Gosser YQ, Nomanbhoy TK, Aghazadeh B, Manor D, Combs C, Cerione RA and Rosen MK (1997). C-terminal binding domain of Rho GDP-dissociation inhibitor directs N-terminal inhibitory peptide to GTPases. *Nature*. 387(6635):814–9.
- Graziano MP and Gilman AG (1989). Synthesis in Escherichia coli of GTPase-deficient mutants of G_{sa} . *The Journal of Biological Chemistry*. 264(26):15475–82.
- Gribkoff VK, Starrett JE and Dworetzky SI (2001). Maxi-K Potassium Channels: Form, Function, and Modulation of a Class of Endogenous Regulators of Intracellular Calcium. *The Neuroscientist*. 7(2):166–177.
- Gu N, Vervaeke K, Hu H and Storm JF (2005). Kv7/KCNQ/M and HCN/h, but not K_{Ca2} /SK channels, contribute to the somatic medium after-hyperpolarization and excitability control in CA1 hippocampal pyramidal cells. *The Journal of Physiology*. 566(3):689–715.
- Gu N, Hu H, Vervaeke K and Storm JF (2008). SK (K_{Ca2}) channels do not control somatic excitability in CA1 pyramidal neurons but can be activated by dendritic excitatory synapses and regulate their impact. *Journal of Neurophysiology*. 100(5):2589–604.
- Guérineau NC, Bossu JL, Gähwiler BH and Gerber U (1995). Activation of a nonselective cationic conductance by metabotropic glutamatergic and muscarinic agonists in CA3 pyramidal neurons of the rat hippocampus. *The Journal of Neuroscience*. 15(6):4395–407.
- Gupta SK, Gallego C, Lowndes JM, Pleiman CM, Sable C, Eisfelder BJ and Johnson GL (1992). Analysis of the fibroblast transformation potential of GTPase-deficient *gip2* oncogenes. *Molecular and Cellular Biology*. 12(1):190–7.
- Gustafsson B and Wigström H (1981). Evidence for two types of afterhyperpolarization in CA1 pyramidal cells in the hippocampus. *Brain Research*. 206(2):462–8.
- Ha TS, Heo M-S and Park C-S (2004). Functional effects of auxiliary β_4 -subunit on rat large-conductance Ca^{2+} -activated K^+ channel. *Biophysical Journal*. 86(5):2871–82.
- Haas HL and Konnerth A (1983). Histamine and noradrenaline decrease calcium-activated potassium conductance in hippocampal pyramidal cells. *Nature*. 302(5907):432–4.

- Hadley JK, Noda M, Selyanko AA, Wood IC, Abogadie FC and Brown DA (2000). Differential tetraethylammonium sensitivity of KCNQ1-4 potassium channels. *British Journal of Pharmacology*. 129(3):413–5.
- Hadley JK, Passmore GM, Tatulian L, Al-Qatari M, Ye F, Wickenden AD and Brown DA (2003). Stoichiometry of expressed KCNQ2/KCNQ3 potassium channels and subunit composition of native ganglionic M channels deduced from block by tetraethylammonium. *The Journal of Neuroscience*. 23(12):5012–9.
- Haitin Y and Attali B (2008). The C-terminus of Kv7 channels: a multifunctional module. *The Journal of Physiology*. 586(7):1803–10.
- Hall A (1998). Rho GTPases and the actin cytoskeleton. *Science*. 279(5350):509–14.
- Halling DB, Kenrick SA, Riggs AF and Aldrich RW (2014). Calcium-dependent stoichiometries of the KCa_{2.2} (SK) intracellular domain/calmodulin complex in solution. *The Journal of General Physiology*. 143(2):231–52.
- Halliwel JV and Adams PR (1982). Voltage-clamp analysis of muscarinic excitation in hippocampal neurons. *Brain Research*. 250(1):71–92.
- Hamill OP, Marty A, Neher E, Sakmann B and Sigworth FJ (1981). Improved patch-clamp techniques for high-resolution current recording from cells and cell-free membrane patches. *Pflügers Archiv*. 391(2):85–100.
- Hamm HE, Deretic D, Arendt A, Hargrave PA, Koenig B and Hofmann KP (1988). Site of G protein binding to rhodopsin mapped with synthetic peptides from the α subunit. *Science*. 241(4867):832–5.
- Hamm HE and Gilchrist A (1996). Heterotrimeric G proteins. *Current Opinion in Cell Biology*. 8(2):189–96.
- Hanner M, Schmalhofer WA, Munujos P, Knaus HG, Kaczorowski GJ and Garcia ML (1997). The β subunit of the high-conductance calcium-activated potassium channel contributes to the high-affinity receptor for charybdotoxin. *Proceedings of the National Academy of Sciences of the United States of America*. 94(7):2853–8.
- Hamm HE (1998). The many faces of G protein signaling. *The Journal of Biological Chemistry*. 273(2):669–72.
- Hart MJ, Jiang X, Kozasa T, Roscoe W, Singer WD, Gilman AG, Sternweis PC and Bollag G (1998). Direct stimulation of the guanine nucleotide exchange activity of p115 RhoGEF by G α_{13} . *Science*. 280(5372):2112–4.
- Hein P, Frank M, Hoffmann C, Lohse MJ and Bünemann M (2005). Dynamics of receptor/G protein coupling in living cells. *The EMBO Journal*. 24(23):4106–14.
- Hein P, Rochais F, Hoffmann C, Dorsch S, Nikolaev VO, Engelhardt S, Berlot CH, Lohse MJ and Bünemann M (2006). G_s activation is time-limiting in initiating receptor-mediated signaling. *The Journal of Biological Chemistry*. 281(44):33345–51.
- Hepler JR, Biddlecome GH, Kleuss C, Camp LA, Hofmann SL, Ross EM and Gilman AG (1996). Functional importance of the amino terminus of G_q. *The Journal of Biological Chemistry*. 271(1):496–504.
- Hernandez CC, Zaika O and Shapiro MS (2008). A carboxy-terminal inter-helix linker as the site of phosphatidylinositol 4,5-bisphosphate action on Kv7 (M-type) K⁺ channels. *The Journal of General Physiology*. 132(3):361–81.

- Hirschberg B, Maylie J, Adelman JP and Marrion NV (1998). Gating of recombinant small-conductance Ca-activated K⁺ channels by calcium. *The Journal of General Physiology*. 111(4):565–81.
- Hirschberg B, Maylie J, Adelman JP and Marrion NV (1999). Gating properties of single SK channels in hippocampal CA1 pyramidal neurons. *Biophysical Journal*. 77(4):1905–13.
- Hoffman GR, Nassar N and Cerione RA (2000). Structure of the Rho family GTP-binding protein Cdc42 in complex with the multifunctional regulator RhoGDI. *Cell*. 100(3):345–56.
- Hoffman GR and Cerione RA (2002). Signaling to the Rho GTPases: networking with the DH domain. *FEBS Letters*. 513(1):85–91.
- Hotson JR and Prince DA (1980). A calcium-activated hyperpolarization follows repetitive firing in hippocampal neurons. *Journal of Neurophysiology*. 43(2):409–19.
- Hou Y, Azpiazu I, Smrcka A and Gautam N (2000). Selective role of G protein γ subunits in receptor interaction. *The Journal of Biological Chemistry*. 275(50):38961–4.
- Hou Y, Chang V, Capper AB, Taussig R and Gautam N (2001). G Protein β subunit types differentially interact with a muscarinic receptor but not adenylyl cyclase type II or phospholipase C- β 2/3. *The Journal of Biological Chemistry*. 276(23):19982–8.
- Howard RJ, Clark KA, Holton JM and Minor DL (2007). Structural insight into KCNQ (Kv7) channel assembly and channelopathy. *Neuron*. 53(5):663–75.
- Hu J, Wang Y, Zhang X, Lloyd JR, Li JH, Karpiak J, Costanzi S and Wess J (2010). Structural basis of G protein-coupled receptor-G protein interactions. *Nature Chemical Biology*. 6(7):541–8, Nature Publishing Group.
- Huang XY, Morielli AD and Peralta EG (1993). Tyrosine kinase-dependent suppression of a potassium channel by the G protein-coupled m1 muscarinic acetylcholine receptor. *Cell*. 75(6):1145–56.
- Huerta PT and Lisman JE (1995). Bidirectional synaptic plasticity induced by a single burst during cholinergic theta oscillation in CA1 in vitro. *Neuron*. 15(5):1053–63.
- Hughes TE, Zhang H, Logothetis DE and Berlot CH (2001). Visualization of a functional G α_q -green fluorescent protein fusion in living cells. *The Journal of Biological Chemistry*. 276(6):4227–35.
- Hutchinson JP and Eccleston JF (2000). Mechanism of nucleotide release from Rho by the GDP dissociation stimulator protein. *Biochemistry*. 39(37):11348–59.
- Ihara K, Muraguchi S, Kato M, Shimizu T, Shirakawa M, Kuroda S, Kaibuchi K and Hakoshima T (1998). Crystal structure of human RhoA in a dominantly active form complexed with a GTP analogue. *The Journal of Biological Chemistry*. 273(16):9656–66.
- Invitrogen. Sindbis Expression System. *Invitrogen Manual*.
- Ishii TM, Maylie J and Adelman JP (1997). Determinants of apamin and d-tubocurarine block in SK potassium channels. *The Journal of Biological Chemistry*. 272(37):23195–200.
- Ito I, Kohda A, Tanabe S, Hirose E, Hayashi M, Mitsunaga S and Sugiyama H (1992). 3,5-Dihydroxyphenylglycine: a potent agonist of metabotropic glutamate receptors. *Neuroreport*. 3(11):1013–6.
- Jaffe AB and Hall A (2005). Rho GTPases: biochemistry and biology. *Annual Review of Cell and Developmental Biology*. 21:247–69.

- Janz JM and Farrens DL (2004). Rhodopsin activation exposes a key hydrophobic binding site for the transducin α -subunit C terminus. *The Journal of Biological Chemistry*. 279(28):29767–73.
- Jentsch TJ (2000). Neuronal KCNQ potassium channels: physiology and role in disease. *Nature Reviews. Neuroscience*. 1(1):21–30.
- Jeromin A, Yuan L-L, Frick A, Pfaffinger P and Johnston D (2003). A modified Sindbis vector for prolonged gene expression in neurons. *Journal of Neurophysiology*. 90(4):2741–5.
- Ji D, Lape R and Dani JA (2001). Timing and location of nicotinic activity enhances or depresses hippocampal synaptic plasticity. *Neuron*. 31(1):131–41.
- Johnston CA and Siderovski DP (2007). Receptor-mediated activation of heterotrimeric G-proteins: current structural insights. *Molecular Pharmacology*. 72(2):219–30.
- Jonas P, Bischofberger J, Fricker D and Miles R (2004). Interneuron Diversity series: Fast in, fast out - temporal and spatial signal processing in hippocampal interneurons. *Trends in Neurosciences*. 27(1):30–40.
- Jones SVP (2003). Role of the small GTPase Rho in modulation of the inwardly rectifying potassium channel Kir2.1. *Molecular Pharmacology*. 64(4):987–93.
- Kaczorowski GJ, Knaus HG, Leonard RJ, McManus OB and Garcia ML (1996). High-conductance calcium-activated potassium channels; structure, pharmacology, and function. *Journal of Bioenergetics and Biomembranes*. 28(3):255–67.
- Kalinec G, Nazarali AJ, Hermouet S, Xu N and Gutkind JS (1992). Mutated α subunit of the G_q protein induces malignant transformation in NIH 3T3 cells. *Molecular and Cellular Biology*. 12(10):4687–93.
- Karpova TS, Baumann CT, He L, Wu X, Grammer A, Lipsky P, Hager GL and McNally JG (2003). Fluorescence resonance energy transfer from cyan to yellow fluorescent protein detected by acceptor photobleaching using confocal microscopy and a single laser. *Journal of Microscopy*. 209(1):56–70.
- Katoh H, Aoki J, Yamaguchi Y, Kitano Y, Ichikawa A and Negishi M (1998). Constitutively active $G\alpha_{12}$, $G\alpha_{13}$, and $G\alpha_q$ induce Rho-dependent neurite retraction through different signaling pathways. *The Journal of Biological Chemistry*. 273(44):28700–7.
- Katoh K, Kano Y, Amano M, Kaibuchi K and Fujiwara K (2001). Stress fiber organization regulated by MLCK and Rho-kinase in cultured human fibroblasts. *American Journal of Physiology. Cell Physiology*. 280(6):C1669–79.
- Keen JE, Khawaled R, Farrens DL, Neelands T, Rivard A, Bond CT, Janowsky A, Fakler B, Adelman JP and Maylie J (1999). Domains responsible for constitutive and Ca^{2+} -dependent interactions between calmodulin and small conductance Ca^{2+} -activated potassium channels. *The Journal of Neuroscience*. 19(20):8830–8.
- Keller J, Schmidt M, Hussein B, Rumenapp U and Jakobs KH (1997). Muscarinic receptor-stimulated cytosol-membrane translocation of RhoA. *FEBS Letters*. 403(3):299–302.
- Kerschensteiner D, Soto F and Stocker M (2005). Fluorescence measurements reveal stoichiometry of K^+ channels formed by modulatory and delayed rectifier α -subunits. *Proceedings of the National Academy of Sciences of the United States of America*. 102(17):6160–5.

- Khanna R, Li Q, Sun L, Collins TJ and Stanley EF (2006). N type Ca^{2+} channels and RIM scaffold protein covary at the presynaptic transmitter release face but are components of independent protein complexes. *Neuroscience*. 140(4):1201–8.
- Kim J, Dittgen T, Nimmerjahn A, Waters J, Pawlak V, Helmchen F, Schlesinger S, Seeburg PH and Osten P (2004). Sindbis vector SINrep(nsP2S⁷²⁵): a tool for rapid heterologous expression with attenuated cytotoxicity in neurons. *Journal of Neuroscience Methods*. 133(1-2):81–90.
- Kim KS, Kobayashi M, Takamatsu K and Tzingounis AV (2012). Hippocalcin and KCNQ channels contribute to the kinetics of the slow afterhyperpolarization. *Biophysical Journal*. 103(12):2446–54.
- Kimura K, Ito M, Amano M, Chihara K, Fukata Y, Nakafuku M, Yamamori B, Feng J, Nakano T, Okawa K, Iwamatsu A and Kaibuchi K (1996). Regulation of myosin phosphatase by Rho and Rho-associated kinase (Rho-kinase). *Science*. 273(5272):245–8.
- Kimura K, Fukata Y, Matsuoka Y, Bennett V, Matsuura Y, Okawa K, Iwamatsu A and Kaibuchi K (1998). Regulation of the association of adducin with actin filaments by Rho-associated kinase (Rho-kinase) and myosin phosphatase. *The Journal of Biological Chemistry*. 273(10):5542–8.
- Kisselev OG, Kao J, Ponder JW, Fann YC, Gautam N and Marshall GR (1998). Light-activated rhodopsin induces structural binding motif in G protein α subunit. *Proceedings of the National Academy of Sciences of the United States of America*. 95(8):4270–5.
- Kjøller L and Hall A (1999). Signaling to Rho GTPases. *Experimental Cell Research*. 253(1):166–79.
- Klebe C, Prinz H, Wittinghofer a and Goody RS (1995). The kinetic mechanism of Ran—nucleotide exchange catalyzed by RCC1. *Biochemistry*. 34(39):12543–52.
- Knaus HG, Garcia-Calvo M, Kaczorowski GJ and Garcia ML (1994). Subunit composition of the high conductance calcium-activated potassium channel from smooth muscle, a representative of the mSlo and slowpoke family of potassium channels. *The Journal of Biological Chemistry*. 269(6):3921–4.
- Knöpfel T, Vranesic I, Gähwiler BH and Brown DA (1990). Muscarinic and β -adrenergic depression of the slow Ca^{2+} -activated potassium conductance in hippocampal CA3 pyramidal cells is not mediated by a reduction of depolarization-induced cytosolic Ca^{2+} transients. *Proceedings of the National Academy of Sciences of the United States of America*. 87(11):4083–7.
- Kobayashi Y and Amaral DG (1999). Chemical neuroanatomy of the hippocampal formation and the perirhinal and parahippocampal cortices. In: Bloom A, Björklund FE and Hökfelt T, ed. *The Primate Nervous System Part 3, Handbook of Chemical Neuroanatomy, Vol 15*. Elsevier. Oxford:285–401.
- Kogo N, Dalezios Y, Capogna M, Ferraguti F, Shigemoto R and Somogyi P (2004). Depression of GABAergic input to identified hippocampal neurons by group III metabotropic glutamate receptors in the rat. *The European Journal of Neuroscience*. 19(10):2727–40.
- Köhler M, Hirschberg B, Bond CT, Kinzie JM, Marrion NV, Maylie J and Adelman JP (1996). Small-conductance, calcium-activated potassium channels from mammalian brain. *Science*. 273(5282):1709–14.
- Kostenis E, Conklin BR and Wess J (1997). Molecular basis of receptor/G protein coupling selectivity studied by coexpression of wild type and mutant m2 muscarinic receptors with mutant $\text{G}\alpha_q$ subunits. *Biochemistry*. 36(6):1487–95.
- Kozasa T, Jiang X, Hart MJ, Sternweis PM, Singer WD, Gilman AG, Bollag G and Sternweis PC (1998). p115 RhoGEF, a GTPase activating protein for $\text{G}\alpha_{12}$ and $\text{G}\alpha_{13}$. *Science*. 280(5372):2109–11.

- Kozasa T, Hajicek N, Chow CR and Suzuki N (2011). Signalling mechanisms of RhoGTPase regulation by the heterotrimeric G proteins G12 and G13. *Journal of Biochemistry*. 150(4):357–69.
- Kozma R, Ahmed S, Best A and Lim L (1995). The Ras-related protein Cdc42Hs and bradykinin promote formation of peripheral actin microspikes and filopodia in Swiss 3T3 fibroblasts. *Molecular and Cellular Biology*. 15(4):1942–52.
- Kranenburg O, Poland M, Gebbink M, Oomen L and Moolenaar WH (1997). Dissociation of LPA-induced cytoskeletal contraction from stress fiber formation by differential localization of RhoA. *Journal of Cell Science*. 110(19):2417–27.
- Krause M and Pedarzani P (2000). A protein phosphatase is involved in the cholinergic suppression of the Ca²⁺-activated K⁺ current *I*_{AHP} in hippocampal pyramidal neurons. *Neuropharmacology*. 39(7):1274–83.
- Krause M, Offermanns S, Stocker M and Pedarzani P (2002). Functional specificity of Gα_q and Gα₁₁ in the cholinergic and glutamatergic modulation of potassium currents and excitability in hippocampal neurons. *The Journal of Neuroscience*. 22(3):666–73.
- Krengel U, Schlichting I, Scherer a, Schumann R, Frech M, John J, Kabsch W, Pai EF and Wittinghofer a (1990). Three-dimensional structures of H-ras p21 mutants: molecular basis for their inability to function as signal switch molecules. *Cell*. 62(3):539–48.
- Kubisch C, Schroeder BC, Friedrich T, Lütjohann B, El-Amraoui a, Marlin S, Petit C and Jentsch TJ (1999). KCNQ4, a novel potassium channel expressed in sensory outer hair cells, is mutated in dominant deafness. *Cell*. 96(3):437–46.
- Lambright DG, Noel JP, Hamm HE and Sigler PB (1994). Structural determinants for activation of the α-subunit of a heterotrimeric G protein. *Nature*. 369(6482):621–8.
- Lambright DG, Sondek J, Bohm A, Skiba NP, Hamm HE and Sigler PB (1996). The 2.0 Å crystal structure of a heterotrimeric G protein. *Nature*. 379(6563):311–9.
- Lancaster B and Adams PR (1986). Calcium-dependent current generating the afterhyperpolarization of hippocampal neurons. *Journal of Neurophysiology*. 55(6):1268–82.
- Lancaster B and Nicoll RA (1987). Properties of two calcium-activated hyperpolarizations in rat hippocampal neurones. *The Journal of Physiology*. 389:187–203.
- Lancaster B, Nicoll RA and Perkel DJ (1991). Calcium activates two types of potassium channels in rat hippocampal neurons in culture. *The Journal of Neuroscience*. 11(1):23–30.
- Lancaster B and Zucker RS (1994). Photolytic manipulation of Ca²⁺ and the time course of slow, Ca²⁺-activated K⁺ current in rat hippocampal neurones. *The Journal of Physiology*. 475(2):229–39.
- Landis CA, Masters SB, Spada A, Pace AM, Bourne HR and Vallar L (1989). GTPase inhibiting mutations activate the α chain of G_s and stimulate adenylyl cyclase in human pituitary tumours. *Nature*. 340(6236):692–6.
- Latorre R and Brauchi S (2006). Large conductance Ca²⁺-activated K⁺ (BK) channel: activation by Ca²⁺ and voltage. *Biological Research*. 39(3):385–401.
- Latorre R, Morera FJ and Zaelzer C (2010). Allosteric interactions and the modular nature of the voltage- and Ca²⁺-activated (BK) channel. *The Journal of Physiology*. 588(17):3141–8.

- Lee JCF, Callaway JC and Foehring RC (2005). Effects of temperature on calcium transients and Ca²⁺-dependent afterhyperpolarizations in neocortical pyramidal neurons. *Journal of Neurophysiology*. 93(4):2012–20.
- Lee W-S, Ngo-Anh TJ, Bruening-Wright A, Maylie J and Adelman JP (2003). Small conductance Ca²⁺-activated K⁺ channels and calmodulin: cell surface expression and gating. *The Journal of Biological Chemistry*. 278(28):25940–6.
- Lenzen C, Cool RH, Prinz H, Kuhlmann J and Wittinghofer A (1998). Kinetic analysis by fluorescence of the interaction between Ras and the catalytic domain of the guanine nucleotide exchange factor Cdc25Mm. *Biochemistry*. 37(20):7420–30.
- Lerche C, Scherer CR, Seeböhm G, Derst C, Wei a D, Busch a E and Steinmeyer K (2000). Molecular cloning and functional expression of KCNQ5, a potassium channel subunit that may contribute to neuronal M-current diversity. *The Journal of Biological Chemistry*. 275(29):22395–400.
- Leung T, Manser E, Tan L and Lim L (1995). A novel serine/threonine kinase binding the Ras-related RhoA GTPase which translocates the kinase to peripheral membranes. *The Journal of Biological Chemistry*. 270(49):29051–4.
- Levey AI, Kitt CA, Simonds WF, Price DL and Brann MR (1991). Identification and localization of muscarinic acetylcholine receptor proteins in brain with subtype-specific antibodies. *The Journal of Neuroscience*. 11(10):3218–26.
- Levey AI, Edmunds SM, Koliatsos V, Wiley RG and Heilman CJ (1995). Expression of m1-m4 muscarinic acetylcholine receptor proteins in rat hippocampus and regulation by cholinergic innervation. *The Journal of Neuroscience*. 15(5):4077–92.
- Li R, Zhang B and Zheng Y (1997). Structural determinants required for the interaction between Rho GTPase and the GTPase-activating domain of p190. *The Journal of Biological Chemistry*. 272(52):32830–5.
- Li Q, Lau A, Morris TJ, Guo L, Fordyce CB and Stanley EF (2004). A syntaxin 1, Gα_o, and N-type calcium channel complex at a presynaptic nerve terminal: analysis by quantitative immunocolocalization. *The Journal of Neuroscience*. 24(16):4070–81.
- Lima PA and Marrion NV (2007). Mechanisms underlying activation of the slow AHP in rat hippocampal neurons. *Brain Research*. 1150:74–82.
- Lingle CJ, Zeng XH, Ding JP and Xia XM (2001). Inactivation of BK channels mediated by the NH2 terminus of the β3b auxiliary subunit involves a two-step mechanism: possible separation of binding and blockade. *The Journal of General Physiology*. 117(6):583–606.
- Liu G, Niu X, Wu RS, Chudasama N, Yao Y, Jin X, Weinberg R, Zakharov SI, Motoike H, Marx SO and Karlin A (2010). Location of modulatory β subunits in BK potassium channels. *The Journal of General Physiology*. 135(5):449–59.
- Lohse MJ, Hein P, Hoffmann C, Nikolaev VO, Vilardaga J-P and Bünemann M (2008). Kinetics of G-protein-coupled receptor signals in intact cells. *British Journal of Pharmacology*. 153 Suppl(December 2007):S125–32.
- Lujan R, Nusser Z, Roberts JD, Shigemoto R and Somogyi P (1996). Perisynaptic location of metabotropic glutamate receptors mGluR1 and mGluR5 on dendrites and dendritic spines in the rat hippocampus. *The European Journal of Neuroscience*. 8(7):1488–500.

- Luján R, Roberts JD, Shigemoto R, Ohishi H and Somogyi P (1997). Differential plasma membrane distribution of metabotropic glutamate receptors mGluR1 α , mGluR2 and mGluR5, relative to neurotransmitter release sites. *Journal of Chemical Neuroanatomy*. 13(4):219–41.
- Luo L (2000). Rho GTPases in neuronal morphogenesis. *Nature Reviews. Neuroscience*. 1(3):173–80.
- Lutz S, Freichel-Blomquist A, Rügenapp U, Schmidt M, Jakobs KH and Wieland T (2004). p63RhoGEF and GEFT are Rho-specific guanine nucleotide exchange factors encoded by the same gene. *Naunyn-Schmiedeberg's Archives of Pharmacology*. 369(5):540–6.
- Lutz S, Freichel-Blomquist A, Yang Y, Rügenapp U, Jakobs KH, Schmidt M and Wieland T (2005). The guanine nucleotide exchange factor p63RhoGEF, a specific link between G_{q/11}-coupled receptor signaling and RhoA. *The Journal of Biological Chemistry*. 280(12):11134–9.
- Lutz S, Shankaranarayanan A, Coco C, Ridilla M, Nance MR, Vettel C, Baltus D, Evelyn CR, Neubig RR, Wieland T and Tesmer JJG (2007). Structure of G α_q -p63RhoGEF-RhoA complex reveals a pathway for the activation of RhoA by GPCRs. *Science*. 318(5858):1923–7.
- Ma Z, Lou XJ and Horrigan FT (2006). Role of charged residues in the S1-S4 voltage sensor of BK channels. *The Journal of General Physiology*. 127(3):309–28.
- Machesky LM and Hall A (1996). Rho: a connection between membrane receptor signalling and the cytoskeleton. *Trends in Cell Biology*. 6(8):304–10.
- Madaule P, Furuyashiki T, Reid T, Ishizaki T, Watanabe G, Morii N and Narumiya S (1995). A novel partner for the GTP-bound forms of rho and rac. *FEBS Letters*. 377(2):243–8.
- Madison DV and Nicoll RA (1982). Noradrenaline blocks accommodation of pyramidal cell discharge in the hippocampus. *Nature*. 299(5884):636–8.
- Madison DV and Nicoll RA (1984). Control of the repetitive discharge of rat CA1 pyramidal neurones in vitro. *The Journal of Physiology*. 354:319–31.
- Madison DV and Nicoll RA (1986a). Actions of noradrenaline recorded intracellularly in rat hippocampal CA1 pyramidal neurones, in vitro. *The Journal of Physiology*. 372:221–44.
- Madison DV and Nicoll RA (1986b). Cyclic adenosine 3',5'-monophosphate mediates β -receptor actions of noradrenaline in rat hippocampal pyramidal cells. *The Journal of Physiology*. 372:245–59.
- Madison DV, Lancaster B and Nicoll RA (1987). Voltage clamp analysis of cholinergic action in the hippocampus. *The Journal of Neuroscience*. 7(3):733–41.
- Mahon MJ, Bonacci TM, Divieti P and Smrcka AV (2006). A docking site for G protein $\beta\gamma$ subunits on the parathyroid hormone 1 receptor supports signaling through multiple pathways. *Molecular Endocrinology*. 20(1):136–46.
- Maingret F, Coste B, Hao J, Giamarchi A, Allen D, Crest M, Litchfield DW, Adelman JP and Delmas P (2008). Neurotransmitter modulation of small-conductance Ca²⁺-activated K⁺ channels by regulation of Ca²⁺ gating. *Neuron*. 59(3):439–49.
- Maljevic S, Lerche C, Seebohm G, Alekov AK, Busch AE and Lerche H (2003). C-terminal interaction of KCNQ2 and KCNQ3 K⁺ channels. *The Journal of Physiology*. 548(2):353–60.
- Manders EM, Stap J, Brakenhoff GJ, van Driel R and Aten JA (1992). Dynamics of three-dimensional replication patterns during the S-phase, analysed by double labelling of DNA and confocal microscopy. *Journal of Cell Science*. 103(3):857–62.

- Manders EMM, Verbeek FJ and Aten JA (1993). Measurement of co-localization in objects of dual-colour confocal images. *Journal of Microscopy*. 169(3):375–382.
- Mannaioni G, Marino MJ, Valenti O, Traynelis SF and Conn PJ (2001). Metabotropic glutamate receptors 1 and 5 differentially regulate CA1 pyramidal cell function. *The Journal of Neuroscience*. 21(16):5925–34.
- Marinissen MJ and Gutkind JS (2001). G-protein-coupled receptors and signaling networks: emerging paradigms. *Trends in Pharmacological Sciences*. 22(7):368–76.
- Marino MJ, Rouse ST, Levey AI, Potter LT and Conn PJ (1998). Activation of the genetically defined m1 muscarinic receptor potentiates N-methyl-D-aspartate (NMDA) receptor currents in hippocampal pyramidal cells. *Proceedings of the National Academy of Sciences of the United States of America*. 95(19):11465–70.
- Markova O, Fitzgerald D, Stepanyuk A, Dovgan A, Cherkas V, Tepikin A, Burgoyne RD and Belan P (2008). Hippocampal signaling via site-specific translocation in hippocampal neurons. *Neuroscience Letters*. 442(2):152–7.
- Markram H and Segal M (1990). Acetylcholine potentiates responses to N-methyl-D-aspartate in the rat hippocampus. *Neuroscience Letters*. 113(1):62–5.
- Marrion NV and Tavalin SJ (1998). Selective activation of Ca²⁺-activated K⁺ channels by co-localized Ca²⁺ channels in hippocampal neurons. *Nature*. 395(6705):900–5.
- Martin EL, Rens-Domiano S, Schatz PJ and Hamm HE (1996). Potent peptide analogues of a G protein receptor-binding region obtained with a combinatorial library. *The Journal of Biological Chemistry*. 271(1):361–6.
- Matsui T, Amano M, Yamamoto T, Chihara K, Nakafuku M, Ito M, Nakano T, Okawa K, Iwamatsu A and Kaibuchi K (1996). Rho-associated kinase, a novel serine/threonine kinase, as a putative target for small GTP binding protein Rho. *The EMBO Journal*. 15(9):2208–16.
- McCrossan ZA and Abbott GW (2004). The Mink-related peptides. *Neuropharmacology*. 47(6):787–821.
- McCudden CR, Hains MD, Kimple RJ, Siderovski DP and Willard FS (2005). G-protein signaling: back to the future. *Cellular and Molecular Life Sciences*. 62(5):551–77.
- McLaughlin S, Wang J, Gambhir A and Murray D (2002). PIP₂ and proteins: interactions, organization, and information flow. *Annual Review of Biophysics and Biomolecular Structure*. 31:151–75.
- McManus OB (1991). Calcium-activated potassium channels: regulation by calcium. *Journal of Bioenergetics and Biomembranes*. 23(4):537–60.
- Meera P, Wallner M, Song M and Toro L (1997). Large conductance voltage- and calcium-dependent K⁺ channel, a distinct member of voltage-dependent ion channels with seven N-terminal transmembrane segments (S0-S6), an extracellular N terminus, and an intracellular (S9-S10) C terminus. *Proceedings of the National Academy of Sciences of the United States of America*. 94(25):14066–71.
- Meera P, Wallner M and Toro L (2000). A neuronal β subunit (KCNMB4) makes the large conductance, voltage- and Ca²⁺-activated K⁺ channel resistant to charybdotoxin and iberiotoxin. *Proceedings of the National Academy of Sciences of the United States of America*. 97(10):5562–7.
- Michaelson D, Silletti J, Murphy G, D'Eustachio P, Rush M and Philips MR (2001). Differential localization of Rho GTPases in live cells: regulation by hypervariable regions and RhoGDI binding. *The Journal of Cell Biology*. 152(1):111–26.

- Milburn MV, Tong L, DeVos AM, Brünger A, Yamaizumi Z, Nishimura S and Kim SH (1990). Molecular switch for signal transduction: structural differences between active and inactive forms of protooncogenic ras proteins. *Science*. 247(4945):939–45.
- Mitchell R, McCulloch D, Lutz E, Johnson M, MacKenzie C, Fennell M, Fink G, Zhou W and Sealfon SC (1998). Rhodopsin-family receptors associate with small G proteins to activate phospholipase D. *Nature*. 392(6674):411–4.
- Monaghan AS, Benton DCH, Bahia PK, Hosseini R, Shah YA, Haylett DG and Moss GWJ (2004). The SK3 subunit of small conductance Ca^{2+} -activated K^{+} channels interacts with both SK1 and SK2 subunits in a heterologous expression system. *The Journal of Biological Chemistry*. 279(2):1003–9.
- Moon SY and Zheng Y (2003). Rho GTPase-activating proteins in cell regulation. *Trends in Cell Biology*. 13(1):13–22.
- Morin TJ and Kobertz WR (2008). Counting membrane-embedded KCNE β -subunits in functioning K^{+} channel complexes. *Proceedings of the National Academy of Sciences of the United States of America*. 105(5):1478–82.
- Mourre C, Hugues M and Lazdunski M (1986). Quantitative autoradiographic mapping in rat brain of the receptor of apamin, a polypeptide toxin specific for one class of Ca^{2+} -dependent K^{+} channels. *Brain Research*. 382(2):239–49.
- Müller W, Petrozzino JJ, Griffith LC, Danho W and Connor JA (1992). Specific involvement of Ca^{2+} -calmodulin kinase II in cholinergic modulation of neuronal responsiveness. *Journal of Neurophysiology*. 68(6):2264–9.
- Mukhopadhyay S and Ross EM (1999). Rapid GTP binding and hydrolysis by Gq promoted by receptor and GTPase-activating proteins. *Proceedings of the National Academy of Sciences of the United States of America*. 96(17):9539–44.
- Muntz KH, Sternweis PC, Gilman AG and Mumby SM (1992). Influence of γ subunit prenylation on association of guanine nucleotide-binding regulatory proteins with membranes. *Molecular Biology of the Cell*. 3(1):49–61.
- Nakajo K, Ulbrich MH, Kubo Y and Isacoff EY (2010). Stoichiometry of the KCNQ1 – KCNE1 ion channel complex. *Proceedings of the National Academy of Sciences of the United States of America*. 107(44):18862–7.
- Nakayama AY, Harms MB and Luo L (2000). Small GTPases Rac and Rho in the maintenance of dendritic spines and branches in hippocampal pyramidal neurons. *The Journal of Neuroscience*. 20(14):5329–38.
- Narumiya S, Sekine A and Fujiwara M (1988). Substrate for botulinum ADP-ribosyltransferase, Gb, has an amino acid sequence homologous to a putative rho gene product. *The Journal of Biological Chemistry*. 263(33):17255–7.
- Nassar N, Hoffman GR, Manor D, Clardy JC and Cerione RA (1998). Structures of Cdc42 bound to the active and catalytically compromised forms of Cdc42GAP. *Nature Structural Biology*. 5(12):1047–52.
- Naumanen P, Lappalainen P and Hotulainen P (2008). Mechanisms of actin stress fibre assembly. *Journal of Microscopy*. 231(3):446–54.
- Neer EJ, Pulsifer L and Wolf LG (1988). The amino terminus of G protein α subunits is required for interaction with $\beta\gamma$. *The Journal of Biological Chemistry*. 263(18):8996–70.

- Nicoll RA (1988). The coupling of neurotransmitter receptors to ion channels in the brain. *Science*. 241(4865):545–51.
- Nikolaev V, Hoffmann C, Bünemann M, Lohse MJ and Vilardaga J-P (2006). Molecular basis of partial agonism at the neurotransmitter α_{2A} -adrenergic receptor and G_i-protein heterotrimer. *The Journal of Biological Chemistry*. 281(34):24506–11.
- Niswender CM and Conn PJ (2010). Metabotropic glutamate receptors: physiology, pharmacology, and disease. *Annual Review of Pharmacology and Toxicology*. 50:295–322.
- Nobes CD and Hall A (1995). Rho, rac, and cdc42 GTPases regulate the assembly of multimolecular focal complexes associated with actin stress fibers, lamellipodia, and filopodia. *Cell*. 81(1):53–62.
- Nobles M, Benians A and Tinker A (2005). Heterotrimeric G proteins precouple with G protein-coupled receptors in living cells. *Proceedings of the National Academy of Sciences of the United States of America*. 102(51):18706–11.
- Noel JP, Hamm HE and Sigler PB (1993). The 2.2 Å crystal structure of transducin- α complexed with GTP γ S. *Nature*. 366(6456):654–63.
- O’Kane EM, Stone TW and Morris BJ (2003). Distribution of Rho family GTPases in the adult rat hippocampus and cerebellum. *Brain Research. Molecular Brain Research*. 114(1):1–8.
- O’Keefe J and Dostrovsky J (1971). The hippocampus as a spatial map. Preliminary evidence from unit activity in the freely-moving rat. *Brain Research*. 34(1):171–5.
- O’Keefe J and Nadel L (1978). *The Hippocampus as a Cognitive Map*. Oxford University Press. Oxford.
- Offermanns S, Wieland T, Homann D, Sandmann J, Bombien E, Spicher K, Schultz G and Jakobs KH (1994). Transfected muscarinic acetylcholine receptors selectively couple to G_i-type G proteins and G_{q/11}. *Molecular Pharmacology*. 45(5):890–8.
- Offermanns S, Mancino V, Revel JP and Simon MI (1997). Vascular system defects and impaired cell chemokinesis as a result of G α_{13} deficiency. *Science*. 275(5299):533–6.
- Oldham WM, Van Eps N, Preininger AM, Hubbell WL and Hamm HE (2006). Mechanism of the receptor-catalyzed activation of heterotrimeric G proteins. *Nature Structural & Molecular Biology*. 13(9):772–7.
- Oldham WM and Hamm HE (2008). Heterotrimeric G protein activation by G-protein-coupled receptors. *Nature Reviews. Molecular Cell Biology*. 9(1):60–71.
- Olenik C, Barth H, Just I, Aktories K and Meyer DK (1997). Gene expression of the small GTP-binding proteins RhoA, RhoB, Rac1, and Cdc42 in adult rat brain. *Brain Research. Molecular Brain Research*. 52(2):263–9.
- Onrust R, Herzmark P, Chi P, Garcia PD, Lichtarge O, Kingsley C and Bourne HR (1997). Receptor and β binding sites in the α subunit of the retinal G protein transducin. *Science*. 275(5298):381–4.
- Orio P, Rojas P, Ferreira G and Latorre R (2002). New disguises for an old channel: MaxiK channel β -subunits. *News in Physiological Sciences*. 17:156–61.
- Oude Weernink PA, Schulte P, Guo Y, Wetzel J, Amano M, Kaibuchi K, Haverland S, Voss M, Schmidt M, Mayr GW and Jakobs KH (2000). Stimulation of phosphatidylinositol-4-phosphate 5-kinase by Rho-kinase. *The Journal of Biological Chemistry*. 275(14):10168–74.

- Oude Weernink PA, Meletiadis K, Hommeltenberg S, Hinz M, Ishihara H, Schmidt M and Jakobs KH (2004). Activation of type I phosphatidylinositol 4-phosphate 5-kinase isoforms by the Rho GTPases, RhoA, Rac1, and Cdc42. *The Journal of Biological Chemistry*. 279(9):7840–9.
- Paduch M, Jeleń F and Otlewski J (2001). Structure of small G proteins and their regulators. *Acta Biochimica Polonica*. 48(4):829–50.
- Pai EF, Krengel U, Petsko GA, Goody RS, Kabsch W and Wittinghofer A (1990). Refined crystal structure of the triphosphate conformation of H-ras p21 at 1.35 Å resolution: implications for the mechanism of GTP hydrolysis. *The EMBO Journal*. 9(8):2351–9.
- Pantazis A, Gudzenko V, Savalli N, Sigg D and Olcese R (2010). Operation of the voltage sensor of a human voltage- and Ca²⁺-activated K⁺ channel. *Proceedings of the National Academy of Sciences of the United States of America*. 107(9):4459–64.
- Park SJ, Itoh T and Takenawa T (2001). Phosphatidylinositol 4-phosphate 5-kinase type I is regulated through phosphorylation response by extracellular stimuli. *The Journal of Biological Chemistry*. 276(7):4781–7.
- Park JH, Scheerer P, Hofmann KP, Choe H-W and Ernst OP (2008). Crystal structure of the ligand-free G-protein-coupled receptor opsin. *Nature*. 454(7201):183–7.
- Paterlini M, Revilla V, Grant AL and Wisden W (2000). Expression of the neuronal calcium sensor protein family in the rat brain. *Neuroscience*. 99(2):205–16.
- Paterson HF, Self AJ, Garrett MD, Just I, Aktories K and Hall A (1990). Microinjection of recombinant p21rho induces rapid changes in cell morphology. *The Journal of Cell Biology*. 111(3):1001–7.
- Pedarzani P and Storm JF (1993). PKA mediates the effects of monoamine transmitters on the K⁺ current underlying the slow spike frequency adaptation in hippocampal neurons. *Neuron*. 11(6):1023–35.
- Pedarzani P and Storm JF (1995). Dopamine modulates the slow Ca²⁺-activated K⁺ current I_{AHP} via cyclic AMP-dependent protein kinase in hippocampal neurons. *Journal of Neurophysiology*. 74(6):2749–53.
- Pedarzani P and Storm JF (1996). Evidence that Ca/calmodulin-dependent protein kinase mediates the modulation of the Ca²⁺-dependent K⁺ current, I_{AHP}, by acetylcholine, but not by glutamate, in hippocampal neurons. *Pflügers Archiv*. 431(5):723–8.
- Pedarzani P, Krause M, Haug T, Storm JF and Stühmer W (1998). Modulation of the Ca²⁺-activated K⁺ current I_{AHP} by a phosphatase-kinase balance under basal conditions in rat CA1 pyramidal neurons. *Journal of Neurophysiology*. 79(6):3252–6.
- Pedarzani P and Stocker M (2008). Molecular and cellular basis of small-and intermediate-conductance, calcium-activated potassium channel function in the brain. *Cellular and Molecular Life Sciences*. 65(20):3196–217.
- Peralta EG, Ashkenazi A, Winslow JW, Ramachandran J and Capon DJ (1988). Differential regulation of PI hydrolysis and adenylyl cyclase by muscarinic receptor subtypes. *Nature*. 334(6181):434–7.
- Pertz O, Hodgson L, Klemke RL and Hahn KM (2006). Spatiotemporal dynamics of RhoA activity in migrating cells. *Nature*. 440(7087):1069–72.
- Peters HC, Hu H, Pongs O, Storm JF and Isbrandt D (2005). Conditional transgenic suppression of M channels in mouse brain reveals functions in neuronal excitability, resonance and behavior. *Nature Neuroscience*. 8(1):51–60.

- Pin JP and Duvoisin R (1995). The metabotropic glutamate receptors: structure and functions. *Neuropharmacology*. 34(1):1–26.
- Piston DW and Kremers G-J (2007). Fluorescent protein FRET: the good, the bad and the ugly. *Trends in Biochemical Sciences*. 32(9):407–14.
- Pitcher JA, Freedman NJ and Lefkowitz RJ (1998). G protein-coupled receptor kinases. *Annual Review of Biochemistry*. 67:653–92.
- Pitler TA and Alger BE (1990). Activation of the pharmacologically defined M₃ muscarinic receptor depolarizes hippocampal pyramidal cells. *Brain Research*. 534(1-2):257–62.
- Pitler TA and Alger BE (1992). Cholinergic excitation of GABAergic interneurons in the rat hippocampal slice. *The Journal of Physiology*. 450:127–42.
- Pochynyuk O, Stockand JD and Staruschenko A (2007). Ion channel regulation by Ras, Rho, and Rab small GTPases. *Experimental Biology and Medicine*. 232(10):1258–65.
- Preininger AM and Hamm HE (2004). G protein signaling: insights from new structures. *Science's STKE*. 2004(218):re3.
- Qian NX, Winitz S and Johnson GL (1993). Epitope-tagged G_q α subunits: expression of GTPase-deficient α subunits persistently stimulates phosphatidylinositol-specific phospholipase C but not mitogen-activated protein kinase activity regulated by the M₁ muscarinic acetylcholine receptor. *Proceedings of the National Academy of Sciences of the United States of America*. 90(9):4077–81.
- Qiu RG, Chen J, McCormick F and Symons M (1995). A role for Rho in Ras transformation. *Proceedings of the National Academy of Sciences of the United States of America*. 92(25):11781–5.
- Raiteri M, Marchi M and Paudice P (1990). Presynaptic muscarinic receptors in the central nervous system. *Annals of the New York Academy of Sciences*. 604:113–29.
- Ray K, Kunsch C, Bonner LM and Robishaw JD (1995). Isolation of cDNA clones encoding eight different human G protein γ subunits, including three novel forms designated the γ₄, γ₁₀, and γ₁₁ subunits. *The Journal of Biological Chemistry*. 270(37):21765–71.
- Reever CM, Ferrari-DiLeo G and Flynn DD (1997). The M5 (m5) receptor subtype: fact or fiction? *Life sciences*. 60(13-14):1105–12.
- Reid T, Furuyashiki T, Ishizaki T, Watanabe G, Watanabe N, Fujisawa K, Morii N, Madaule P and Narumiya S (1996). Rhotekin, a new putative target for Rho bearing homology to a serine/threonine kinase, PKN, and rhophilin in the rho-binding domain. *The Journal of Biological Chemistry*. 271(23):13556–60.
- Renault L, Kuhlmann J, Henkel a and Wittinghofer a (2001). Structural basis for guanine nucleotide exchange on Ran by the regulator of chromosome condensation (RCC1). *Cell*. 105(2):245–55.
- Resat H, Straatsma TP, Dixon DA and Miller JH (2001). The arginine finger of RasGAP helps Gln-61 align the nucleophilic water in GAP-stimulated hydrolysis of GTP. *Proceedings of the National Academy of Sciences of the United States of America*. 98(11):6033–8.
- Rhee SG (2001). Regulation of phosphoinositide-specific phospholipase C. *Annual Review of Biochemistry*. 70:281–312.
- Ridley AJ and Hall A (1992). The small GTP-binding protein rho regulates the assembly of focal adhesions and actin stress fibers in response to growth factors. *Cell*. 70(3):389–99.

- Ridley AJ, Paterson HF, Johnston CL, Diekmann D and Hall A (1992). The small GTP-binding protein rac regulates growth factor-induced membrane ruffling. *Cell*. 70(3):401–10.
- Ridley AJ (1996). Rho: theme and variations. *Current Biology*. 6(10):1256–64.
- Ridley AJ (1999). Stress fibres take shape. *Nature Cell Biology*. 1(3):E64–6.
- Robbins J (2001). KCNQ potassium channels: physiology, pathophysiology, and pharmacology. *Pharmacology & Therapeutics*. 90(1):1–19.
- Robertson D, Paterson HF, Adamson P, Hall A and Monaghan P (1995). Ultrastructural localization of ras-related proteins using epitope-tagged plasmids. *The Journal of Histochemistry and Cytochemistry*. 43(5):471–80.
- Rojas RJ, Yohe ME, Gershburg S, Kawano T, Kozasa T and Sondek J (2007). $G\alpha_q$ directly activates p63RhoGEF and Trio via a conserved extension of the Dbl homology-associated pleckstrin homology domain. *The Journal of Biological Chemistry*. 282(40):29201–10.
- Romano C, Sesma MA, McDonald CT, O'Malley K, van den Pol AN and Olney JW (1995). Distribution of metabotropic glutamate receptor mGluR5 immunoreactivity in rat brain. *The Journal of Comparative Neurology*. 355(3):455–69.
- Ross EM and Wilkie TM (2000). GTPase-activating proteins for heterotrimeric G proteins: regulators of G protein signaling (RGS) and RGS-like proteins. *Annual Review of Biochemistry*. 69:795–827.
- Rosignol TM and Jones SVP (2006). Regulation of a family of inwardly rectifying potassium channels (Kir2) by the m1 muscarinic receptor and the small GTPase Rho. *Pflügers Archiv*. 452(2):164–74.
- Rossmann KL, Der CJ and Sondek J (2005). GEF means go: turning on RHO GTPases with guanine nucleotide-exchange factors. *Nature Reviews. Molecular Cell Biology*. 6(2):167–80.
- Roszik J, Szöllosi J and Vereb G (2008). AccPbFRET: an ImageJ plugin for semi-automatic, fully corrected analysis of acceptor photobleaching FRET images. *BMC Bioinformatics*. 9:346.
- Rouse ST, Marino MJ, Potter LT, Conn PJ and Levey AI (1999). Muscarinic receptor subtypes involved in hippocampal circuits. *Life Sciences*. 64(6-7):501–9.
- Rouse ST, Hamilton SE, Potter LT, Nathanson NM and Conn PJ (2000). Muscarinic-induced modulation of potassium conductances is unchanged in mouse hippocampal pyramidal cells that lack functional M1 receptors. *Neuroscience Letters*. 278(1-2):61–4.
- Sagi SA, Seasholtz TM, Kobiashvili M, Wilson BA, Toksoz D and Brown JH (2001). Physical and functional interactions of $G\alpha_q$ with Rho and its exchange factors. *The Journal of Biological Chemistry*. 276(18):15445–52.
- Sah P (1996). Ca^{2+} -activated K^+ currents in neurones: types, physiological roles and modulation. *Trends in Neurosciences*. 19(4):150–4.
- Sah P and Bekkers JM (1996). Apical dendritic location of slow afterhyperpolarization current in hippocampal pyramidal neurons: implications for the integration of long-term potentiation. *The Journal of Neuroscience*. 16(15):4537–42.
- Sah P and Isaacson JS (1995). Channels underlying the slow afterhyperpolarization in hippocampal pyramidal neurons: neurotransmitters modulate the open probability. *Neuron*. 15(2):435–41.

- Sah P and Clements JD (1999). Photolytic manipulation of $[Ca^{2+}]_i$ reveals slow kinetics of potassium channels underlying the afterhyperpolarization in hippocampal pyramidal neurons. *The Journal of Neuroscience*. 19(10):3657–64.
- Sah VP, Seasholtz TM, Sagi SA and Brown JH (2000). The role of Rho in G protein-coupled receptor signal transduction. *Annual Review of Pharmacology and Toxicology*. 40:459–89.
- Sahara Y and Westbrook GL (1993). Modulation of calcium currents by a metabotropic glutamate receptor involves fast and slow kinetic components in cultured hippocampal neurons. *The Journal of Neuroscience*. 13(7):3041–50.
- Sailer CA, Hu H, Kaufmann WA, Trieb M, Schwarzer C, Storm JF and Knaus H-G (2002). Regional differences in distribution and functional expression of small-conductance Ca^{2+} -activated K^+ channels in rat brain. *The Journal of Neuroscience*. 22(22):9698–707.
- Saitoh S, Takamatsu K, Kobayashi M and Noguchi T (1994). Expression of hippocalcin in the developing rat brain. *Brain Research. Developmental Brain Research*. 80(1-2):199–208.
- Sanchez-Fernandes G, Cabezudo S, Garcia-Hoz C, Beninca C, Aragay AM, Mayor F Jr and Ribas C (2014). Gαq signalling: the new and the old. *Cell Signalling*. 26(5):833-48.
- Sanguinetti MC, Curran ME, Zou A, Shen J, Spector PS, Atkinson DL and Keating MT (1996). Coassembly of K_vLQT1 and $minK$ (IsK) proteins to form cardiac I_{Ks} potassium channel. *Nature*. 384(6604):80–3.
- Scanziani M, Gahwiler BH and Thompson SM (1995). Presynaptic inhibition of excitatory synaptic transmission by muscarinic and metabotropic glutamate receptor activation in the hippocampus: are Ca^{2+} channels involved? *Neuropharmacology*. 34(11):1549–57.
- Scanziani M, Salin PA, Vogt KE, Malenka RC and Nicoll RA (1997). Use-dependent increases in glutamate concentration activate presynaptic metabotropic glutamate receptors. *Nature*. 385(6617):630–4.
- Scheerer P, Park JH, Hildebrand PW, Kim YJ, Krauss N, Choe H-W, Hofmann KP and Ernst OP (2008). Crystal structure of opsin in its G-protein-interacting conformation. *Nature*. 455(7212):497–502.
- Scheffzek K, Ahmadian MR, Kabsch W, Wiesmüller L, Lautwein A, Schmitz F and Wittinghofer A (1997). The Ras-RasGAP complex: structural basis for GTPase activation and its loss in oncogenic Ras mutants. *Science*. 277(5324):333–8.
- Scheffzek K, Ahmadian MR and Wittinghofer A (1998). GTPase-activating proteins: helping hands to complement an active site. *Trends in Biochemical Sciences*. 23(7):257–62.
- Scheffzek K, Stephan I, Jensen ON, Illenberger D and Gierschik P (2000). The Rac-RhoGDI complex and the structural basis for the regulation of Rho proteins by RhoGDI. *Nature Structural Biology*. 7(2):122–6.
- Schmidt A and Hall A (2002). Guanine nucleotide exchange factors for Rho GTPases: turning on the switch. *Genes & Development*. 16(13):1587–609.
- Schmitt N, Schwarz M, Peretz A, Abitbol I, Attali B and Pongs O (2000). A recessive C-terminal Jervell and Lange-Nielsen mutation of the KCNQ1 channel impairs subunit assembly. *The EMBO Journal*. 19(3):332–40.
- Schoepp DD, Jane DE and Monn JA (1999). Pharmacological agents acting at subtypes of metabotropic glutamate receptors. *Neuropharmacology*. 38(10):1431–76.

- Schreiber M and Salkoff L (1997). A novel calcium-sensing domain in the BK channel. *Biophysical Journal*. 73(3):1355–63.
- Schroeder BC, Hechenberger M, Weinreich F, Kubisch C and Jentsch TJ (2000). KCNQ5, a novel potassium channel broadly expressed in brain, mediates M-type currents. *The Journal of Biological Chemistry*. 275(31):24089–95.
- Schumacher MA, Rivard AF, Bächinger HP and Adelman JP (2001). Structure of the gating domain of a Ca^{2+} -activated K^+ channel complexed with Ca^{2+} /calmodulin. *Nature*. 410(6832):1120–4.
- Schwake M, Pusch M, Kharkovets T and Jentsch TJ (2000). Surface expression and single channel properties of KCNQ2/KCNQ3, M-type K^+ channels involved in epilepsy. *The Journal of Biological Chemistry*. 275(18):13343–8.
- Schwake M, Jentsch TJ and Friedrich T (2003). A carboxy-terminal domain determines the subunit specificity of KCNQ K^+ channel assembly. *EMBO Reports*. 4(1):76–81.
- Schwartzkroin PA and Stafstrom CE (1980). Effects of EGTA on the calcium-activated afterhyperpolarization in hippocampal CA3 pyramidal cells. *Science*. 210(4474):1125–6.
- Seabra MC (1998). Membrane association and targeting of prenylated Ras-like GTPases. *Cellular Signalling*. 10(3):167–72.
- Seasholtz TM, Majumdar M and Brown JH (1999). Rho as a mediator of G protein-coupled receptor signaling. *Molecular Pharmacology*. 55(6):949–56.
- Seeburg PH, Colby WW, Capon DJ, Goeddel D V and Levinson AD (1984). Biological properties of human c-Ha-ras1 genes mutated at codon 12. *Nature*. 312(5989):71–5.
- Séguéla P, Wadiche J, Dineley-Miller K, Dani JA and Patrick JW (1993). Molecular cloning, functional properties, and distribution of rat brain α_7 : a nicotinic cation channel highly permeable to calcium. *The Journal of Neuroscience*. 13(2):596–604.
- Sekine A, Fujiwara M and Narumiya S (1989). Asparagine residue in the rho gene product is the modification site for botulinum ADP-ribosyltransferase. *The Journal of Biological Chemistry*. 264(15):8602–5.
- Selyanko AA, Hadley JK, Wood IC, Abogadie FC, Jentsch TJ and Brown DA (2000). Inhibition of KCNQ1-4 potassium channels expressed in mammalian cells via M1 muscarinic acetylcholine receptors. *The Journal of Physiology*. 522(3):349–55.
- Semyanov A and Kullmann DM (2000). Modulation of GABAergic signaling among interneurons by metabotropic glutamate receptors. *Neuron*. 25(3):663–72.
- Shah M and Haylett DG (2000a). The pharmacology of hSK1 Ca^{2+} -activated K^+ channels expressed in mammalian cell lines. *British Journal of Pharmacology*. 129(4):627–30.
- Shah M and Haylett DG (2000b). Ca^{2+} channels involved in the generation of the slow afterhyperpolarization in cultured rat hippocampal pyramidal neurons. *Journal of Neurophysiology*. 83(5):2554–61.
- Shah MM, Miscony Z, Javadzadeh-Tabatabaie M, Ganellin CR and Haylett DG (2001). Clotrimazole analogues: effective blockers of the slow afterhyperpolarization in cultured rat hippocampal pyramidal neurones. *British Journal of Pharmacology*. 132(4):889–98.

- Shah MM, Mistry M, Marsh SJ, Brown DA and Delmas P (2002). Molecular correlates of the M-current in cultured rat hippocampal neurons. *The Journal of Physiology*. 544(1):29–37.
- Shah MM, Javadzadeh-Tabatabaie M, Benton DCH, Ganellin CR and Haylett DG (2006). Enhancement of hippocampal pyramidal cell excitability by the novel selective slow-afterhyperpolarization channel blocker 3-(triphenylmethylaminomethyl)pyridine (UCL2077). *Molecular Pharmacology*. 70(5):1494–502.
- Shamgar L, Ma L, Schmitt N, Haitin Y, Peretz A, Wiener R, Hirsch J, Pongs O and Attali B (2006). Calmodulin is essential for cardiac I_{KS} channel gating and assembly: impaired function in long-QT mutations. *Circulation Research*. 98(8):1055–63.
- Shankaranarayanan A, Boguth CA, Lutz S, Vettel C, Uhlemann F, Aittaleb M, Wieland T and Tesmer JGG (2010). $G\alpha_q$ allosterically activates and relieves autoinhibition of p63RhoGEF. *Cellular Signalling*. 22(7):1114–23.
- Shen KZ, Lagrutta A, Davies NW, Standen NB, Adelman JP and North RA (1994). Tetraethylammonium block of Slowpoke calcium-activated potassium channels expressed in *Xenopus* oocytes: evidence for tetrameric channel formation. *Pflügers Archiv*. 426(5):440–5.
- Shigemoto R, Nakanishi S and Mizuno N (1992). Distribution of the mRNA for a metabotropic glutamate receptor (mGluR1) in the central nervous system: an in situ hybridization study in adult and developing rat. *The Journal of Comparative Neurology*. 322(1):121–35.
- Shigemoto R, Kinoshita A, Wada E, Nomura S, Ohishi H, Takada M, Flor PJ, Neki A, Abe T, Nakanishi S and Mizuno N (1997). Differential presynaptic localization of metabotropic glutamate receptor subtypes in the rat hippocampus. *The Journal of Neuroscience*. 17(19):7503–22.
- Siehler S (2009). Regulation of RhoGEF proteins by $G_{12/13}$ -coupled receptors. *British Journal of Pharmacology*. 158(1):41–9.
- Sim JA, Gerber U, Knöpfel T and Brown DA (1992). Evidence Against a Role for Protein Kinase C in the Inhibition of the Calcium-activated Potassium Current I_{AHP} by Muscarinic Stimulants in Rat Hippocampal Neurons. *The European Journal of Neuroscience*. 4(9):785–791.
- Simon MI, Strathmann MP and Gautam N (1991). Diversity of G proteins in signal transduction. *Science*. 252(5007):802–8.
- Simonds WF, Butrynski JE, Gautam N, Unson CG and Spiegel AM (1991). G-protein $\beta\gamma$ dimers. Membrane targeting requires subunit coexpression and intact γ C-A-A-X domain. *The Journal of Biological Chemistry*. 266(9):5363–6.
- Smrcka AV, Hepler JR, Brown KO and Sternweis PC (1991). Regulation of polyphosphoinositide-specific phospholipase C activity by purified G_q . *Science*. 251(4995):804–7.
- Soh H and Tzingounis AV (2010). The specific slow afterhyperpolarization inhibitor UCL2077 is a subtype-selective blocker of the epilepsy associated KCNQ channels. *Molecular Pharmacology*. 78(6):1088–95.
- Sondek J, Lambright DG, Noel JP, Hamm HE and Sigler PB (1994). GTPase mechanism of Gproteins from the 1.7-Å crystal structure of transducin α -GDP-AIF₄. *Nature*. 372(6503):276–9.
- Sondek J, Bohm A, Lambright DG, Hamm HE and Sigler PB (1996). Crystal structure of a G-protein $\beta\gamma$ dimer at 2.1Å resolution. *Nature*. 379(6563):369–74.
- Souchet M, Portales-Casamar E, Mazurais D, Schmidt S, Léger I, Javré J-L, Robert P, Berrebi-Bertrand I, Bril A, Gout B, Debant A and Calmels TPG (2002). Human p63RhoGEF, a novel RhoA-specific

- guanine nucleotide exchange factor, is localized in cardiac sarcomere. *Journal of Cell Science*. 115(3):629–40.
- Sprang SR (1997). G protein mechanisms: insights from structural analysis. *Annual Review of Biochemistry*. 66:639–78.
- Spruston N and McBain C (2007). Structural and Functional Properties of Hippocampus Neurons. In: Andersen P, Morris R, Amaral D, Bliss T and O'Keefe J, ed. *The Hippocampus Book*. Oxford University Press. Oxford:133–201.
- Squire LR and Zola-Morgan S (1991). The medial temporal lobe memory system. *Science*. 253(5026):1380–6.
- Squire LR, Stark CEL and Clark RE (2004). The medial temporal lobe. *Annual Review of Neuroscience*. 27:279–306.
- Staruschenko A, Nichols A, Medina JL, Camacho P, Zheleznova NN and Stockand JD (2004). Rho small GTPases activate the epithelial Na⁺ channel. *The Journal of Biological Chemistry*. 279(48):49989–94.
- Sternweis PC and Robishaw JD (1984). Isolation of two proteins with high affinity for guanine nucleotides from membranes of bovine brain. *The Journal of Biological Chemistry*. 259(22):13806–13.
- Stewart M and Fox SE (1990). Do septal neurons pace the hippocampal theta rhythm? *Trends in Neurosciences*. 13(5):163–8.
- Stirling L, Williams MR and Morielli AD (2009). Dual roles for RHOA/RHO-kinase in the regulated trafficking of a voltage-sensitive potassium channel. *Molecular Biology of the Cell*. 20(12):2991–3002.
- Stocker M, Krause M and Pedarzani P (1999). An apamin-sensitive Ca²⁺-activated K⁺ current in hippocampal pyramidal neurons. *Proceedings of the National Academy of Sciences of the United States of America*. 96(8):4662–7.
- Stocker M and Pedarzani P (2000). Differential distribution of three Ca²⁺-activated K⁺ channel subunits, SK1, SK2, and SK3, in the adult rat central nervous system. *Molecular and Cellular Neurosciences*. 15(5):476–93.
- Stocker M (2004). Ca²⁺-activated K⁺ channels: molecular determinants and function of the SK family. *Nature Reviews. Neuroscience*. 5(10):758–70.
- Stocker M, Hirzel K, D'hoedt D and Pedarzani P (2004). Matching molecules to function: neuronal Ca²⁺-activated K⁺ channels and afterhyperpolarizations. *Toxicon*. 43(8):933–49.
- Storey NM, O'Bryan JP and Armstrong DL (2002). Rac and Rho mediate opposing hormonal regulation of the ether-a-go-go-related potassium channel. *Current Biology*. 12(1):27–33.
- Storm JF (1987a). Action potential repolarization and a fast after-hyperpolarization in rat hippocampal pyramidal cells. *The Journal of Physiology*. 385(1):733–59.
- Storm JF (1987b). Intracellular injection of a Ca²⁺ chelator inhibits spike repolarization in hippocampal neurons. *Brain Research*. 435(1-2):387–92.
- Storm JF (1989). An after-hyperpolarization of medium duration in rat hippocampal pyramidal cells. *The Journal of Physiology*. 409:171–90.

- Storm JF (1990). Potassium currents in hippocampal pyramidal cells. *Progress in Brain Research*. 83:161–87.
- Strassheim D, Porter RA, Phelps SH and Williams CL (2000). Unique in vivo associations with SmgGDS and RhoGDI and different guanine nucleotide exchange activities exhibited by RhoA, dominant negative RhoA^{Asn-19}, and activated RhoA^{Val-14}. *The Journal of Biological Chemistry*. 275(10):6699–702.
- Strøbaek D, Jørgensen TD, Christophersen P, Ahring PK and Olesen SP (2000). Pharmacological characterization of small-conductance Ca²⁺-activated K⁺ channels stably expressed in HEK 293 cells. *British Journal of Pharmacology*. 129(5):991–9.
- Suh B-C and Hille B (2005). Regulation of ion channels by phosphatidylinositol 4,5-bisphosphate. *Current Opinion in Neurobiology*. 15(3):370–8.
- Suzuki N, Nakamura S, Mano H and Kozasa T (2003). Gα12 activates Rho GTPase through tyrosine-phosphorylated leukemia-associated RhoGEF. *Proceedings of the National Academy of Sciences of the United States of America*. 100(2):733–8.
- Swartz KJ and Bean BP (1992). Inhibition of calcium channels in rat CA3 pyramidal neurons by a metabotropic glutamate receptor. *The Journal of Neuroscience*. 12(11):4358–71.
- Takahashi T, Forsythe ID, Tsujimoto T, Barnes-Davies M and Onodera K (1996). Presynaptic calcium current modulation by a metabotropic glutamate receptor. *Science*. 274(5287):594–7.
- Takai Y, Sasaki T and Matozaki T (2001). Small GTP-binding proteins. *Physiological Reviews*. 81(1):153–208.
- Tanabe M, Gähwiler BH and Gerber U (1998). L-Type Ca²⁺ channels mediate the slow Ca²⁺-dependent afterhyperpolarization current in rat CA3 pyramidal cells in vitro. *Journal of Neurophysiology*. 80(5):2268–73.
- Taylor JM, Jacob-Mosier GG, Lawton RG, Remmers AE and Neubig RR (1994). Binding of an α₂ adrenergic receptor third intracellular loop peptide to Gβ and the amino terminus of Gα. *The Journal of Biological Chemistry*. 269(44):27618–24.
- Taylor JM, Jacob-Mosier GG, Lawton RG, VanDort M and Neubig RR (1996). Receptor and membrane interaction sites on Gβ. A receptor-derived peptide binds to the carboxyl terminus. *The Journal of Biological Chemistry*. 271(7):3336–9.
- Tesmer JJ, Berman DM, Gilman AG and Sprang SR (1997). Structure of RGS4 bound to AlF₄⁻-activated G_{iα1}: stabilization of the transition state for GTP hydrolysis. *Cell*. 89(2):251–61.
- Thomas TC, Schmidt CJ and Neer EJ (1993). G-protein α_o subunit: mutation of conserved cysteines identifies a subunit contact surface and alters GDP affinity. *Proceedings of the National Academy of Sciences of the United States of America*. 90(21):10295–9.
- Thompson SM, Masukawa LM and Prince DA (1985). Temperature dependence of intrinsic membrane properties and synaptic potentials in hippocampal CA1 neurons in vitro. *The Journal of Neuroscience*. 5(3):817–24.
- Torres GE, Chaput Y and Andrade R (1995). Cyclic AMP and protein kinase A mediate 5-hydroxytryptamine type 4 receptor regulation of calcium-activated potassium current in adult hippocampal neurons. *Molecular Pharmacology*. 47(1):191–7.

- Totsukawa G, Yamakita Y, Yamashiro S, Hartshorne DJ, Sasaki Y and Matsumura F (2000). Distinct roles of ROCK (Rho-kinase) and MLCK in spatial regulation of MLC phosphorylation for assembly of stress fibers and focal adhesions in 3T3 fibroblasts. *The Journal of Cell Biology*. 150(4):797–806.
- Trahey M and McCormick F (1987). A cytoplasmic protein stimulates normal N-ras p21 GTPase, but does not affect oncogenic mutants. *Science*. 238(4826):542–5.
- Tsien JZ, Huerta PT and Tonegawa S (1996). The essential role of hippocampal CA1 NMDA receptor-dependent synaptic plasticity in spatial memory. *Cell*. 87(7):1327–38.
- Tzingounis AV, Kobayashi M, Takamatsu K and Nicoll RA (2007). Hippocalcin gates the calcium activation of the slow afterhyperpolarization in hippocampal pyramidal cells. *Neuron*. 53(4):487–93.
- Tzingounis AV and Nicoll RA (2008). Contribution of KCNQ2 and KCNQ3 to the medium and slow afterhyperpolarization currents. *Proceedings of the National Academy of Sciences of the United States of America*. 105(50):19974–9.
- Tzingounis AV, Heidenreich M, Kharkovets T, Spitzmaul G, Jensen HS, Nicoll RA and Jentsch TJ (2010). The KCNQ5 potassium channel mediates a component of the afterhyperpolarization current in mouse hippocampus. *Proceedings of the National Academy of Sciences of the United States of America*. 107(22):10232–7.
- van Biesen T, Luttrell LM, Hawes BE and Lefkowitz RJ (1996). Mitogenic signaling via G protein-coupled receptors. *Endocrine Reviews*. 17(6):698–714.
- van de Vrede Y, Fossier P, Baux G, Joels M and Chameau P (2007). Control of IsAHP in mouse hippocampus CA1 pyramidal neurons by RyR3-mediated calcium-induced calcium release. *Pflügers Archiv*. 455(2):297–308.
- van der Zee EA and Luiten PG (1999). Muscarinic acetylcholine receptors in the hippocampus, neocortex and amygdala: a review of immunocytochemical localization in relation to learning and memory. *Progress in Neurobiology*. 58(5):409–71.
- Vetter IR and Wittinghofer A (2001). The guanine nucleotide-binding switch in three dimensions. *Science*. 294(5545):1299–304.
- Villardaga J-P, Bünemann M, Krasel C, Castro M and Lohse MJ (2003). Measurement of the millisecond activation switch of G protein-coupled receptors in living cells. *Nature Biotechnology*. 21(7):807–12.
- Villalobos C and Andrade R (2010). Visinin-like neuronal calcium sensor proteins regulate the slow calcium-activated afterhyperpolarizing current in the rat cerebral cortex. *The Journal of Neuroscience*. 30(43):14361–5.
- Villalobos C, Foehring RC, Lee JC and Andrade R (2011). Essential role for phosphatidylinositol 4,5-bisphosphate in the expression, regulation, and gating of the slow afterhyperpolarization current in the cerebral cortex. *The Journal of Neuroscience*. 31(50):18303–12.
- Vizi ES and Kiss JP (1998). Neurochemistry and pharmacology of the major hippocampal transmitter systems: synaptic and nonsynaptic interactions. *Hippocampus*. 8(6):566–607.
- Vogel SS, Thaler C and Koushik SV (2006). Fanciful FRET. *Science's STKE*. 2006(331):re2.
- Volpicelli LA and Levey AI (2004). Muscarinic acetylcholine receptor subtypes in cerebral cortex and hippocampus. *Progress in Brain Research*. 145:59–66.

- Wahlfors J and Morgan RA (2003). Semliki Forest Viral Vectors for Gene Transfer. In: Machida C A, ed. *Viral Vectors for Gene Therapy*. Humana Press. New Jersey:493–502.
- Waldo GL, Ricks TK, Hicks SN, Cheever ML, Kawano T, Tsuboi K, Wang X, Montell C, Kozasa T, Sondek J and Harden T (2010). Kinetic scaffolding mediated by a phospholipase C- β and G_q signaling complex. *Science*. 330(6006):974–80.
- Walker M, Chan D and Thom M (2007). Hippocampus and Human Disease. In: Andersen P, Morris R, Amaral D, Bliss T and O’Keefe J, ed. *The Hippocampus Book*. Oxford University Press. Oxford:769–812.
- Wall MA, Coleman DE, Lee E, Iñiguez-Lluhi JA, Posner BA, Gilman AG and Sprang SR (1995). The structure of the G protein heterotrimer G_{i α 1 β 1 γ 2}. *Cell*. 83(6):1047–58.
- Wang Q, Curran ME, Splawski I, Burn TC, Millholland JM, VanRaay TJ, Shen J, Timothy KW, Vincent GM, de Jager T, Schwartz PJ, Toubin JA, Moss AJ, Atkinson DL, Landes GM, Connors TD and Keating MT (1996). Positional cloning of a novel potassium channel gene: KVLQT1 mutations cause cardiac arrhythmias. *Nature Genetics*. 12(1):17–23.
- Wang H-S, Pan Z, Shi W, Brown BS, Wymore RS, Cohen IS, Dixon JE and McKinnon D (1998). KCNQ2 and KCNQ3 potassium channel subunits: molecular correlates of the M-channel. *Science*. 282(5395):1890–3.
- Wang W, Xia J and Kass RS (1998). MinK-KvLQT1 fusion proteins, evidence for multiple stoichiometries of the assembled I_{sk} channel. *The Journal of Biological Chemistry*. 273(51):34069–74.
- Watanabe G, Saito Y, Madaule P, Ishizaki T, Fujisawa K, Morii N, Mukai H, Ono Y, Kakizuka A and Narumiya S (1996). Protein kinase N (PKN) and PKN-related protein rhotaxilin as targets of small GTPase Rho. *Science*. 271(5249):645–8.
- Watanabe N, Madaule P, Reid T, Ishizaki T, Watanabe G, Kakizuka A, Saito Y, Nakao K, Jockusch BM and Narumiya S (1997). p140mDia, a mammalian homolog of Drosophila diaphanous, is a target protein for Rho small GTPase and is a ligand for profilin. *The EMBO Journal*. 16(11):3044–56.
- Watson N, Linder ME, Druey KM, Kehrl JH and Blumberg PM (1996). RGS family members: GTPase-activating proteins for heterotrimeric G-protein α -subunits. *Nature*. 383(6596):172–5.
- Wei Y, Zhang Y, Derewenda U, Liu X, Minor W, Nakamoto RK, Somlyo A V, Somlyo AP and Derewenda ZS (1997). Crystal structure of RhoA-GDP and its functional implications. *Nature Structural Biology*. 4(9):699–703.
- Wen H and Levitan IB (2002). Calmodulin is an auxiliary subunit of KCNQ2/3 potassium channels. *The Journal of Neuroscience*. 22(18):7991–8001.
- Wennerberg K and Der CJ (2004). Rho-family GTPases: it’s not only Rac and Rho (and I like it). *Journal of Cell Science*. 117(8):1301–12.
- Wennerberg K, Rossman KL and Der CJ (2005). The Ras superfamily at a glance. *Journal of Cell Science*. 118(5):843–6.
- Wilk-Blaszczak MA, Singer WD, Quill T, Miller B, Frost JA, Sternweis PC and Belardetti F (1997). The monomeric G-proteins Rac1 and/or Cdc42 are required for the inhibition of voltage-dependent calcium current by bradykinin. *The Journal of Neuroscience*. 17(11):4094–100.
- Wilkie TM, Gilbert DJ, Olsen AS, Chen XN, Amatruda TT, Korenberg JR, Trask BJ, de Jong P, Reed RR and Simon MI (1992). Evolution of the mammalian G protein α subunit multigene family. *Nature Genetics*. 1(2):85–91.

- Willard FS, Kimple RJ and Siderovski DP (2004). Return of the GDI: the GoLoco motif in cell division. *Annual Review of Biochemistry*. 73:925–51.
- Witherow DS, Tovey SC, Wang Q, Willars GB and Slepak VZ (2003). Gβ5.RGS7 inhibits Gα_q-mediated signaling via a direct protein-protein interaction. *The Journal of Biological Chemistry*. 278(23):21307–13.
- Witter MP and Amaral DG (2004). Hippocampal Formation. In: Paxinos G, ed. *The Rat Nervous System*. Elsevier Academic Press. London:635–704.
- Wong YH, Federman A, Pace AM, Zachary I, Evans T, Pouyssegur J and Bourne HR (1991). Mutant α subunits of G_{i2} inhibit cyclic AMP accumulation. *Nature*. 351(6321):63–5.
- Wonnacott S (1997). Presynaptic nicotinic ACh receptors. *Trends in Neurosciences*. 20(2):92–8.
- Wu DQ, Lee CH, Rhee SG and Simon MI (1992). Activation of phospholipase C by the α subunits of the G_q and G₁₁ proteins in transfected Cos-7 cells. *The Journal of Biological Chemistry*. 267(3):1811–7.
- Wu G, Benovic JL, Hildebrandt JD and Lanier SM (1998). Receptor docking sites for G-protein βγ subunits. Implications for signal regulation. *The Journal of Biological Chemistry*. 273(13):7197–200.
- Wu G, Bogatkevich GS, Mukhin Y V, Benovic JL, Hildebrandt JD and Lanier SM (2000). Identification of Gβγ binding sites in the third intracellular loop of the M₃-muscarinic receptor and their role in receptor regulation. *The Journal of Biological Chemistry*. 275(12):9026–34.
- Wu RS, Liu G, Zakharov SI, Chudasama N, Motoike H, Karlin A and Marx SO (2013). Positions of β2 and β3 subunits in the large-conductance calcium- and voltage-activated BK potassium channel. *The Journal of General Physiology*. 141(1):105–17.
- Wuertz CM, Lorincz A, Vettel C, Thomas MA, Wieland T and Lutz S (2010). p63RhoGEF—a key mediator of angiotensin II-dependent signaling and processes in vascular smooth muscle cells. *The FASEB Journal*. 24(12):4865–76.
- Xia X-M, Fakler B, Rivard A, Wayman G, Johnson-Pais T, Keen JE, Ishii T, Hirschberg B, Bond CT, Lutsenko S, Maylie J and Adelman JP (1998). Mechanism of calcium gating in small-conductance calcium-activated potassium channels. *Nature*. 395(6701):503–7.
- Xia X-M, Zeng X and Lingle CJ (2002). Multiple regulatory sites in large-conductance calcium-activated potassium channels. *Nature*. 418(6900):880–4.
- Yasuda H, Lindorfer MA, Woodfork KA, Fletcher JE and Garrison JC (1996). Role of the prenyl group on the G protein γ subunit in coupling trimeric G proteins to A1 adenosine receptors. *The Journal of Biological Chemistry*. 271(31):18588–95.
- Yatani A, Irie K, Otani T, Abdellatif M and Wei L (2005). RhoA GTPase regulates L-type Ca²⁺ currents in cardiac myocytes. *American Journal of Physiology. Heart and Circulatory Physiology*. 288(2):H650–9.
- Yoder RM and Pang KCH (2005). Involvement of GABAergic and cholinergic medial septal neurons in hippocampal theta rhythm. *Hippocampus*. 15(3):381–92.
- Young SR, Chuang S-C and Wong RKS (2004). Modulation of afterpotentials and firing pattern in guinea pig CA3 neurones by group I metabotropic glutamate receptors. *The Journal of Physiology*. 554(2):371–85.

- Yu B, Slepak VZ and Simon MI (1997). Characterization of a Go α mutant that binds xanthine nucleotides. *The Journal of Biological Chemistry*. 272(29):18015–9.
- Yu B and Simon MI (1998). Interaction of the xanthine nucleotide binding Go α mutant with G protein-coupled receptors. *The Journal of Biological Chemistry*. 273(46):30183–8.
- Yuan P, Leonetti MD, Pico AR, Hsiung Y and MacKinnon R (2010). Structure of the human BK channel Ca²⁺-activation apparatus at 3.0 Å resolution. *Science*. 329(5988):182–6.
- Yus-Najera E, Santana-Castro I and Villarroel A (2002). The identification and characterization of a noncontinuous calmodulin-binding site in noninactivating voltage-dependent KCNQ potassium channels. *The Journal of Biological Chemistry*. 277(32):28545–53.
- Zhang L, Pennefather P, Velumian A, Tymianski M, Charlton M and Carlen PL (1995). Potentiation of a slow Ca²⁺-dependent K⁺ current by intracellular Ca²⁺ chelators in hippocampal CA1 neurons of rat brain slices. *Journal of Neurophysiology*. 74(6):2225–41.
- Zhang B, Chernoff J and Zheng Y (1998). Interaction of Rac1 with GTPase-activating proteins and putative effectors. A comparison with Cdc42 and RhoA. *The Journal of Biological Chemistry*. 273(15):8776–82.
- Zhang H, Craciun LC, Mirshahi T, Rohács T, Lopes CMB, Jin T and Logothetis DE (2003). PIP₂ activates KCNQ channels, and its hydrolysis underlies receptor-mediated inhibition of M currents. *Neuron*. 37(6):963–75.
- Zheng Y (2001). Dbl family guanine nucleotide exchange factors. *Trends in Biochemical Sciences*. 26(12):724–32.

Abbreviations

4-AP	4-aminopyridine
8-Br cAMP	8-bromoadenosine 3',5'-monophosphate
8CPT-cAMP	8-(4-chlorophenylthio) adenosine 3',5'-cyclic monophosphate
AA/BA	Acrylamide/Bisacrylamide
AC	Adenylyl Cyclase
ACh	Acetylcholine
AMPA	α -amino-3-hydroxy-5-methyl-isoxazole-propionic acid
APS	Ammonium Persulfate
APV	D-(-)-2-Amino-5-phosphonopentanoic acid
ATP	Adenosine Triphosphate
BHK	Baby Hamster Kidney
BSA	Bovine Serum Albumin
CA	Cornu Ammonis
CaM	Calmodulin
cAMP	Cyclic Adenosine Monophosphate
cGMP	Cyclic Guanosine Monophosphate
CCh	Carbachol
CFP	Cyan Fluorescent Protein
CTP	Cytidine Triphosphate
DAG	Diacylglycerol
DEPC	Diethyl Pyrocarbonate
dH ₂ O	Deionised H ₂ O
DH	Dbl Homology
DIV	Day <i>in vitro</i>
DMEM	Dulbecco's Modified Eagle Medium
DMSO	Dimethyl Sulfoxide
dTC	d-Tubocurarine
DTT	Dithiothreitol
ECFP	Enhanced Cyan Fluorescent Protein
EDTA	Ethylenediaminetetraacetic Acid
EE-tag	Glu Glu epitope-tag
EGFP	Enhanced Green Fluorescent Protein
EYFP	Enhanced Yellow Fluorescent Protein
fAHP	Fast Afterhyperpolarization
FBS	Fetal Bovine Serum
FLIM	Fluorescence Lifetime Imaging Microscopy
FRET	Fluorescence Resonance Energy Transfer
GAP	GTPase Accelerating Protein
GDI	Guanine Nucleotide Dissociation Inhibitor
GDP	Guanosine Diphosphate
GEF	Guanine Nucleotide Exchange Factor
GFP	Green Fluorescent Protein

GPCR	G-protein Coupled Receptor
GRK	G-protein-coupled Receptor Kinase
GST	Glutathione-S-Transferase
GTP	Guanosine Triphosphate
HBSS	Hank's Buffered Salt Solution
HEK	Human Embryonic Kidney
HEPES	4-(2-hydroxyethyl)-1-piperazineethanesulfonic Acid
HRP	Horseradish Peroxidase
ICQ	Intensity Correlation Quotient
IMS	Industrial Methylated Spirit
IP ₃	Inositol 1,4,5-Triphosphate
IPTG	Isopropyl β-D-Thiogalactopyranoside
KGluc	Potassium Gluconate
KMeSO ₄	Potassium Methylsulphate
LB	Luria Broth
LTP	Long-Term Potentiation
mAHP	Medium Afterhyperpolarisation
mGluR	Metabotropic Glutamate Receptor
mAChR	Muscarinic Acetylcholine Receptor
MAPK	Mitogen-Activated Protein Kinase
MEM	Minimum Essential Medium
MLCK	Myosin Light Chain Kinase
MOPS	3-(N-Morpholino)propanesulfonic Acid
mRFP	Monomeric Red Fluorescent Protein
nAChR	Nicotinic Acetylcholine Receptor
NGS	Normal Goat Serum
NBQX	2,3-Dioxo-6-nitro-1,2,3,4-tetrahydrobenzo(f)quinoxaline-7-sulfonamide
NMDA	N-methyl-D-aspartate
NMDAR	N-methyl-D-aspartate Receptor
nsP	Nonstructural Protein
OD	Optical Density
PBS	Phosphate Buffered Saline
PCR	Polymerase Chain Reaction
PDM	Product of the Difference of the Mean
PFA	Paraformaldehyde
PH	Pleckstrin Homology
P _i	Inorganic Phosphate
PIP ₂	Phosphatidylinositol 4,5-bisphosphate
PIP5K	Phosphatidylinositol 4 phosphate 5-Kinase
PKA	Protein Kinase A
PKC	Protein Kinase C
PKI	Walsh Peptide PKA Inhibitor
PKN	Protein Kinase N
PLC	Phospholipase C

PMSF	Phenylmethylsulfonyl Fluoride
PMT	Photomultiplier Tube
P _{SG}	Subgenomic Promoter
RGS	Regulator of G-protein signalling
ROCK	Rho-Kinase
ROI	Region of Interest
Rp-cAMP	Rp-adenosine-3',5'-cyclic monophosphorothioate
sAHP	Slow Afterhyperpolarization
SDS	Sodium Dodecyl Sulfate
SDS-PAGE	Sodium Dodecyl Sulfate Polyacrylamide Gel Electrophoresis
SEM	Standard Error of the Mean
SOB	Super Optimum Broth
SOC	Super Optimum Broth with Catabolite Repression
TAE	Tris Acetate EDTA
TBE	Tris Borate EDTA
TBS	Tris Buffered Saline
TBST	Tris Buffered Saline with Tween-20
TEA	Tetraethylammonium
TEMED	N,N,N',N'-tetramethylethylenediamine
TRITC	Tetramethylrhodamine Isothiocyanate
TTX	Tetrodotoxin
UTP	Uridine Triphosphate
Venus	YFP derivative
YFP	Yellow Fluorescent Protein

A Appendix

A.1 List of Materials

A.1.1 Consumables

Item		Company	Cat.-No.
Cellophane Sheets		Novex	NC2380
Centrifuge Tubes	12 ml	Greiner	163270
	10 ml, polycarbonate	Beckman	355630
Coverslips	24 x 60 mm	BDH	406.0181.02
	22 x 22mm	Menzel-Glaeser	406.0187.35
	10 mm Ø	Menzel-Glaeser	CB00100RA1
Cryotube		Nunc	343958
Cuvettes		Sarstedt	67.742
Electroporation Cuvettes	4 mm, BTX model 640	Harvard Apparatus	45-0126
	1 mm, BTX model 610	Harvard Apparatus	45-0124
Films	BioMax MR-1	Kodak	873-6936
	Hyperfilm ECL	GE	28-9068-40
Filters	Syringe filter, 0.22 µm	Millipore	SLGP033RS
	Stericup 150, 0.22 µm	Millipore	SCGPU01RE
	Stericup 500, 0.22 µm	Millipore	SCGPU05RE
	VectaSpin Micro, 0.2 µm	Whatman	6830-0203
Glass Capillaries	Borosilicate	Harvard	300044
	1.2 mm OD, 0.69 mm ID, 100 mm L		
	Borosilicate	Kimble Chase	34500-99
	1.5–1.8 mm OD, 1.3–1.6 mm ID, 100 mm L		
Microcentrifuge Tubes	0.5 ml	Sarstedt	72.699
	1.5 ml		72.690
	2 ml		72.695
Nitrocellulose Membranes	Protran BA83, 0.2 µm	Whatman	10401396
	Hybond ECL, 0.2 µm	GE	RPN3032D
PCR Reaction Tube	0.2 ml	Applied Biosystems	N8010540
Plastic Tubes	15 ml	Sarstedt	62.553.001
	50 ml		62.547.004
Plastic Tube with Snap-Cap	14 ml	Falcon	352059
Serological Pipettes	5 ml	Sarstedt	86.1253.001
	10 ml		86.1254.001
	25 ml		86.1685.001
Tissue Culture Flasks	T25	Sarstedt	83.1810.002
	T75	Nunc	156499
	T225	Nunc	159933
Tissue Culture Dishes	Ø 3.5 cm	Nunc	153066
	Ø 6 cm		150288
	Ø 10 cm		150350
	6-well dish	Nunc	140675
	4-well dish	Nunc	176740
Transfer Pipettes	3.5 ml	Sarstedt	86.1171.001

A.1.2 Equipment

Item		Company
Anti-vibration Table		TCM
Centrifuges	5415R/5424/5702R Megafuge 1.0 & 1.0R J2-M1	Eppendorf Heraeus Beckman
Electrophoresis Cell	mini-PROTEAN II SE 600	BIO-RAD Hoefer
Electroporation Systems	GenePulser XCell ECM 600	BIO-RAD BTX
Gel Dryer	Model 583	BIO-RAD
Glass Homogeniser		Glas-Col
Heat Block	Thermomixer compact	Eppendorf
Hoods	BioMAT2 Class II MSC	CAS Walker Envair
ImageQuant	LAS4000 mini	GE
Incubators		Heraeus
Microelectrode Puller	L/M-3P-A P-97 Flaming/Brown	List Medical Sutter
Microinjector	FemtoJet	Eppendorf
Micromanipulator	5171	Eppendorf
Mixer		IKA
Osmometer	Vapro 5520	Wescor
Patch Clamp Amplifier	EPC10	HEKA
pH Meter	RL150 766	Russell Knick
Power Supply	EV261 PowerPac 300 PowerPac 3000	Consort BIO-RAD BIO-RAD
Pressure Control Unit	MPCU-3	Lorenz
Pump	Dymax 30	Charles Austen KNF Neuberger
Rotors	JA-14/JA-17	Beckman
Scales		Delta Range
Sequencer	3100-Avant	Applied Biosystems
Semi-Dry Transfer Cell	V20-SDB	Scie-Plas
Shaker, orbital	3005	GFL
Shaker, incubator	Innova4230 G25	New Brunswick Scientific Brunswick Scientific
Sonicator	SonoPuls	Bandelin
Spectrophotometer	NanoDrop 1000	Labtech International

	SmartSpec Plus	BIO-RAD
Tank Transfer Cell	mini Trans-Blot	BIO-RAD
Thermal Cycler	2720	Applied Biosystems
Thermal Printer	P91	Mitsubishi
UV lamp	UV (254 nm)	IBI
	UVL-24 (4 W, 365 nm)	UVP
X-Ray Film Processor	RG II	Fuji

A.1.3 Microscopes

Item	Company
Axiophot	Zeiss
Filter Set 10 (GFP, Alexa Fluor 488) Excitation: BP 450-490, Beam Splitter: FT 510, Emission: BP 515-565	Zeiss
Filter Set 15 (TRITC, mRFP, Alexa Fluor 594) Excitation: BP 546/12, Beam Splitter: FT 580, Emission: LP 590	Zeiss
HBO Mercury Short-Arc Lamp, 103W/2	Osram
Micropublisher CCD Camera	QImaging
Objectives (Plan Neofluar) 10x/0.3NA, 20x/0.5NA, air-immersion 40x/1.3NA, 63x/1.25NA, oil-immersion	Zeiss
QCapture Software	QImaging
Axiovert 135M	Zeiss
Objectives (Plan Neofluar and AchroStigmat) 5x/0.5NA, 20x/0.3NA, 32x/0.4NA air-immersion	Zeiss
Axiovert 200	Zeiss
HBO Mercury Short-Arc Lamp, 103W/2	Osram
Longpass Filter (EGFP) Excitation: HQ 480/40, Beam Splitter: DCLPQ505, Emission: HQ510LP	Chroma
Objective (Epiplan Neofluar) 20x/0.5NA, air-immersion	Zeiss
DM IBR	Leica
Filter Set L5 (GFP) Excitation: BP 480/40, Beam Splitter: 505, Emission: BP 527/30	Leica
Filter Set N2.1 (Cy3, TRITC) Excitation: BP 515-560, Beam Splitter: RKP580, Emission: LP 590	Leica
HBO Mercury Short-Arc Lamp, 103W/2	Osram
Objectives (N Plan and N Plan L) 10x/0.25 NA, 20x/0.4 NA, 40x/0.55 NA air-immersion	Leica
OpenLab software, v.5.5.2	Improvision
ORCA-HR CCD camera, C4742-95	Hamamatsu

TCS SP5 Confocal	Leica
Argon laser, 100 mW	
Acquisition settings	
CFP; Excitation: 458 nm, Emission: 462–500 nm	
YFP; Excitation: 514 nm, Emission: 520–600 nm	
Cy5; Excitation: 633 nm, Emission: 650–750 nm	
LAS AF software	Leica
Objective (HCX Plan Apochromat)	Leica
63x/1.4 NA, oil-immersion	

A.1.4 Kits, reagents and chemicals

A.1.4.1 Kits

Item	Company	Cat.-No.
BigDye Terminator v2.0	Applied Biosystems	4314414
ECL Western Blotting Detection Reagents	GE	RPN2106
Bradford Protein Assay Dye Reagent Concentrate	BIO-RAD	500-0006
mMESSAGE mMACHINE SP6	Ambion	AM1340
Nucleobond PC 100/500	Macherey-Nagel	740573/4
NucleoSpin Extract-II	Macherey-Nagel	740609.50
NucleoSpin Plasmid	Macherey-Nagel	740588.50
ProLong Antifade	Molecular Probes	P7481
SP6 TNT Coupled Reticulocyte Lysate System	Promega	L4600
SuperSignal West Pico Chemiluminescent Substrate	Pierce	34079
T7 TNT Quick Coupled Transcription/Translation System	Promega	L1171

A.1.4.2 Reagents and chemicals

Item	Company	Cat.-No.
8CPT-cAMP-Na	Sigma	C3912
30 % Acrylamide/Bisacrylamide (AA/BA)	BIO-RAD	161-0158
Acetic Acid	VWR	20104.334
Agar Select	Gibco	30391-023
Agarose, Ultra Pure	Invitrogen	15510-027
Ammonium Persulfate (APS)	Sigma	A3678
Ampicillin	Boehringer Mannheim	835269
APV	Ascent Scientific	ASC-004
Aprotinin	Sigma	A1153
ATP-Na	Sigma	A2383
Autofluor	National Diagnostics	LS-315
B27, 50x	Gibco	17504-044
Benzamidine	Sigma	B6506
β-Mercaptoethanol	BDH	436022A

2-Butanol	BDH	27500
Boric Acid	BDH	44390
Bovine Serum Albumin (BSA)	Sigma	A3294
Bovine Serum Albumin (BSA) (protein standards)	Pierce First Link UK Ltd	23209 40-00-410
Bromphenol Blue	Sigma	B5525
Carbenicillin	Melford	C0109
Carbachol (CCh)	Sigma	C4382
Chloroform	BDH	100776B
Coomassie Brilliant Blue R250	Biomol	03285
Diethyl Pyrocarbonate (DEPC)	Sigma	D5758
DMEM	Gibco	21969-035
DMEM/F-12	Gibco	21331-020
Dimethyl Sulfoxide (DMSO)	Sigma	D2650
d-Tubocurarine-Cl (dTC)	Sigma	93750
Dithiothreitol (DTT)	Biomol	04010.100
Ethylenediaminetetraacetic Acid (EDTA)	IBI Technical	IB70180
Ethanol	BDH	101074F
Ethidium Bromide (10mg/ml)	Sigma	E1510
Fetal Bovine Serum (FBS)	Gibco	10500-064
Ficoll 400	GE	17-0300-10
Formaldehyde	Calbiochem	344198
Formamid	Fluka	47671
FuGene 6	Roche	11814443001
Glucose	Fisher Scientific Merck	10141520 1.08337.1000
Glucose (tissue culture, 45 %)	Sigma	G8769
Glutathione Agarose	Sigma	G4510
Glycerol	Sigma	G7893
Glycine	BIO-RAD SIGMA	161-0724 G8898
GTP-Na	Sigma	G8877
H ₂ O (cell culture)	Baxter	UKF7113
H ₂ O (intracellular solution)	Romil	H951
HBSS, 10x	Gibco	14180-046
HEPES	Fluka	54461
HEPES (tissue culture, 1 M)	Gibco	15630-049
Horse Serum	Gibco	26050-070
Industrial Methylated Spirit (IMS)	VWR	302444E
Isopropanol	BDH	102245K

Isopropyl β -D-Thiogalactopyranoside (IPTG)	Biomol	05684.1
Kanamycin	Sigma	K4000
Potassium Gluconate (KGluc)	SIGMA	G4500
Potassium Methylsulphate (KMeSO ₄)	ICN	215481
L-Glutamine	Gibco	25030-024
Leupeptin	Calbiochem	108975
Lipofectamine 2000	Invitrogen	11668-019
MEM	Gibco	21090-022
MEM alpha (with Ultraglutamine and nucleosides)	Lonza	BE02-002F
MEM alpha (without L-Glutamine)	Lonza	BE12-169F
Methanol	VWR	20846.326
[³⁵ S] methionine, 1000 Ci/mMol	PerkinElmer	NEG009T001MC
Miller's Luria Broth (LB) Base	Invitrogen	12795-027
Mowiol 4-88 (polyvinyl alcohol)	Calbiochem	475904
Milk Powder	Marvel	
	Merck	1153630500
MOPS	Sigma	M3183
NBQX	Ascent Scientific	ASC-046
Neurobasal	Gibco	21103-049
Normal Goat Serum (NGS)	Gibco	16210-072
NP-40	Sigma	N0896
Opti-MEM	Gibco	51985-034
Paraformaldehyde (PFA)	SIGMA	P6148
	EMS	19208
PBS, pH 7.2	Gibco	20012-019
Penicillin/Streptomycin	Gibco	15140-148
Pepstatin	Calbiochem	516481
Phenol f. RNA (buffered pH 7.5)	Gibco-BRL	15513-013
Phenylmethylsulfonyl Fluoride (PMSF)	Sigma	P7626
Poly-D-Lysine	Sigma	P0899
Protein A/G Plus Agarose	Santa Cruz	SC-2003
Protein A Sepharose Fast Flow	GE	17-5138-01
Protein G Sepharose Fast Flow	GE	17-0618-01
SeaKem LE Agarose	Lonza	50009
Sodium Dodecyl Sulfate (SDS)	USB	US75819
Sodium Pyruvate	Gibco	11360-039
Streptomycin Sulphate	Melford	S0148
Sucrose	Sigma	S7903
TAE	National Diagnostics	EC-872
TEA	Sigma	T2265

N,N,N',N'-tetramethylethylenediamine (TEMED)	BDH	443083G
Tris Base	Sigma BIO-RAD	T1503 161-0716
Triton X-100	Fluka	93426
Trypan Blue	Sigma	T8154
Trypsin 0.05 %/EDTA (cell culture)	Gibco	25300-054
Trypsin 2.5 % (tissue culture)	Gibco	15090-046
Tryptone	Difco	0123-01-1
TTX	Latoxan	L8503
Tween-20	Calbiochem	655205
Yeast Extract	Difco	0127-01-1

All other chemicals were purchased from BDH, Fluka, Merck, Sigma and VWR.

A.1.5 Enzymes

Item	Company	Cat.-No.
Alkaline Phosphatase	Roche	10713023001
KOD Hot Start DNA polymerase	Novagen	71316
Lysozyme	Boehringer Mannheim	1243004
PreScission Protease	GE	27-0843-01
T4 DNA Ligase	Roche	10481220001
Tag Polymerase	Invitrogen	10342-020

All restriction enzymes, aside from *PacI* (New England Biolabs) and *NdeI* (GE) were purchased from Roche.

A.1.6 Antibodies and dyes

Item	Company	Cat.-No.	
RhoA	Mouse Monoclonal, Clone 26C4 Rabbit Polyclonal	Santa Cruz Santa Cruz	SC-418 SC-179
G α_q	Rabbit Polyclonal	Santa Cruz	SC-393
G $\alpha_{q/11}$	Rabbit Polyclonal	Santa Cruz	SC-392
Myc	Mouse Monoclonal, Clone 9E10 Mouse Monoclonal, Clone 4A6 Rabbit Polyclonal	Roche Millipore Santa Cruz	11667149001 05-724 SC-789
HA	Mouse Monoclonal, Clone 12CA5	Roche	11583816001
EE	Rabbit Polyclonal	Abcam	18585
Mouse Cy5 conjugated (source: goat)	Jackson IR	115-175-003	
Mouse HRP conjugated (source: goat)	BIO-RAD	170-6516	
Mouse HRP conjugated (source: sheep)	GE	NA931	
Rabbit HRP conjugated (source: goat)	BIO-RAD	170-6515	
Rabbit HRP conjugated (source: donkey)	GE	NA934	

Alexa Fluor 488 Phalloidin conjugated	Molecular Probes	A12379
Alexa Fluor 594 Phalloidin conjugated	Molecular Probes	A12381
Tetramethylrhodamine Isothiocyanate (TRITC) Dextran	Sigma	T1287

A.1.7 DNA and protein molecular weight ladders

Item	Company	Cat.-No.
100 bp DNA Ladder 2072, 1500, 1400, 1300, 1200, 1100, 1000, 900, 800, 700, 600, 500, 400, 300, 200, 100 bp	Invitrogen	15628-019
1 kb DNA Ladder 12216, 11198, 10180, 9162, 8144, 7126, 6108, 5090, 4072, 3054, 2036, 1636, 1018, 506/517, 396, 344, 298, 220, 201, 154, 134, 75 bp	Invitrogen	15615-016
All Blue PrecisionPlus Protein Marker 250, 150, 100, 75, 50, 37, 25, 20, 15, 10 kDa	BIO-RAD	161-0373
Low Range Marker 97, 66, 45, 31, 21, 14 kDa	BIO-RAD	161-0304

A.1.8 Primers

M13	GTAAAACGACGGCCAGT
P5	GATCGATCCAGACATGATAAGATACATTGATG
SP6	GATTTAGGTGACACTATAG
T3	ATTAACCCTCACTAAAGGGA
T7	TAATACGACTCACTATAGGG
P1417	CTTCCACAGGCAACATCACCAACAATCAC
P1496	TAGAAGGCACAGTCGAGG
P2014	CCGGGAGCTGCATGTGTCAGAGG
P2135	TAGGCGTGTACGGTGGGAGGTC
P2136	ATGTGGTATGGCTGATTATG
P2137	CGTCGCCGTCCAGCTCGACCAG
P2139	CGGCGGGGTCTTGTAGTTGC
P2187	GCATGGGATCCAAGGGCGAGGAGCTGTTTAC
P2188	TCCATGCCGAGAGTGATCCCGGCGGGTCCAGAACTCCAGC
P2189	CTGGTGGATCCCTTGACAGCTCGTCCATGCCGAGAGTGATCCCG
P2191	GGGTATTCGATGATCCCTGT
P2222	CGCGGGTCTAGACCACCATGGCTGCCATCCGGAAGAAACTG

All primers were purchased from Eurofins MWG Operon.